Doctoral theses at NTNU, 2019:226

Hamideh Kaffash

Dissolution kinetics of carbon materials in FeMn

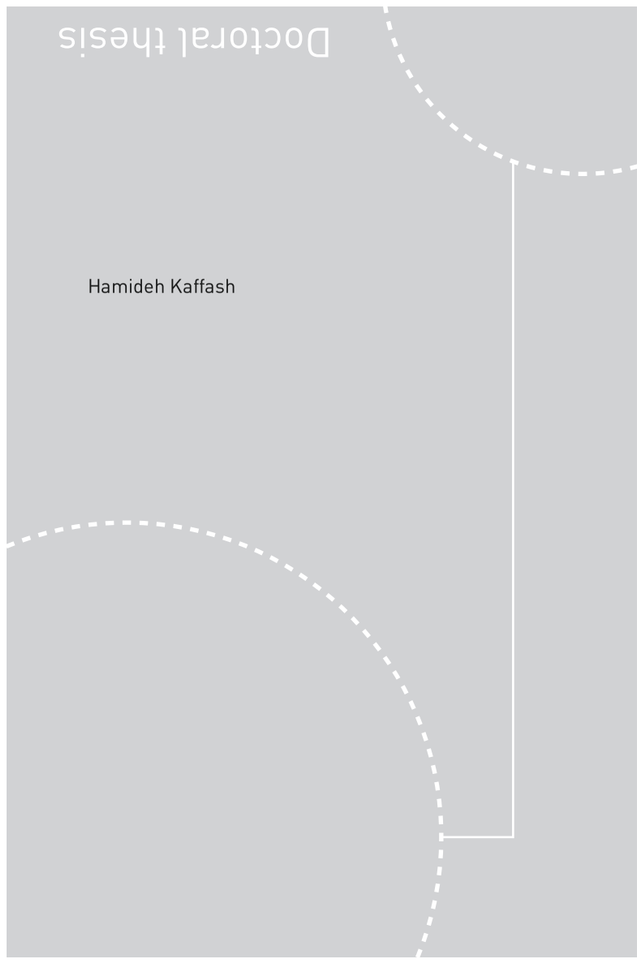

ISBN 978-82-326-4048-5 (printed ver.)
ISBN 978-82-326-4049-2 (electronic ver.)
ISSN 1503-8181

NTNU
Norwegian University of
Science and Technology

NTNU
Norwegian University of Science and Technology
Thesis for the Degree of
Philosophiae Doctor
Faculty of Natural Sciences
Department of Materials Science and
Engineering

Doctoral theses at NTNU, 2019:226

NTNU
Norwegian University of
Science and Technology

Hamideh Kaffash

Dissolution kinetics of carbon materials in FeMn

Thesis for the Degree of Philosophiae Doctor

Trondheim, August 2019

Norwegian University of Science and Technology
Faculty of Natural Sciences
Department of Materials Science and Engineering

NTNU
Norwegian University of
Science and Technology

NTNU
Norwegian University of Science and Technology

Thesis for the Degree of Philosophiae Doctor

Faculty of Natural Sciences
Department of Materials Science and Engineering

ISBN 978-82-326-4048-5 (printed ver.)
ISBN 978-82-326-4049-2 (electronic ver.)
ISSN 1503-8181

Doctoral theses at NTNU, 2019:226

Printed by NTNU Grafisk senter

Preface

The present doctoral thesis is submitted to the Norwegian University of Science and Technology (NTNU) as a partial fulfillment of the requirements for the Ph.D degree.

The work presented in this thesis has been carried out at the Department of Materials Science and Engineering at NTNU in the period of July 2016 to June 2019 with Prof. Merete Tangstad as advisor. This Ph.D project was funded by NTNU in cooperation with the SFI Metal production (NRC 237738).

The main aim of the present research work was to investigate the dissolution kinetic of different carbonaceous materials in FeMn metal. The raw materials were provided by ELKEM and SINTEF and the experiments were done by the author.

Hamideh Kaffash
Trondheim, June 17, 2019

Acknowledgment

I arrived in Norway in 2013. My heart was filled with hope and my head filled with bright ideas about furthering materials science and engineering. However, things didn't turn out the way I expected. Instead, I was turned away by the authorities and I had to return to my beloved country for a period of time. I was determined to be back and worked hard towards achieving this goal. Without getting into too many details about what transpired later, I was successful in returning to beautiful Trondheim and pursue my degree here. This success wouldn't have been possible without the involvement of many people. A special mention to thank Jostein Mårdalen and Merete Tangstad for their continued support during my most difficult period. and I would also like to thank all the people in the Material department for their warm support. I will never forget each of their warm hugs, the shaking voice and the touching tears when I had to say goodbye in 2014. I would also like to thank all my Iranian friends in SEDAI (Stop Education Discrimination Against Iranians in Norway) campaign who supported me with their heartful thoughts and efforts.

My return to NTNU in 2016 was warmly welcomed by many in Trondheim, which was very touching for me. Subsequently, I restarted my Ph.D. program under the supervision of Prof. Merete Tangstad. It is worth mentioning that I regard Prof. Tangstad as not just my thesis supervisor but more as a maternal figure who cares about the welfare of each and every student, as I seek her advice on a wide variety of topics. I would like to express my sincere gratitude for her guidance and helpful advice during all stages of my research work.

I am also very grateful to my friends Dr.Vincent Yves Canaguier, Raghed Saadieh, Jian Meng Jiao, Dr. Kei Erik Ekstrøm and Trygve storm Aarnæs for precious discussions. I would like to also thank Prof. Jafar Safarian for very useful discussions.

Many thanks to Prof. Ostrovski and Dr. Xing Xing as they helped during my experimental work at UNSW.

I am grateful to NTNU for providing the support and resources to complete this work. As well as SFI Metal Production Center for providing supports for the experimental works and participating in conferences.

I would like to thank my family for their constant love and support. Although they were far away from Trondheim, their love and supports were encouraging me throughout my study.

Lastly but not least, I thank my husband, Arvand, for the love and patience. His endless support has been very valuable for the completion of this study.

Abstract

Submerged electric arc furnace (SAF) is the main process for industrial production of ferroalloys, in which metal oxides are reduced by carbon. To decrease the production cost and reduce the CO_2 emissions, a variety of carbonaceous materials is used including metallurgical cokes, charcoals and coals. The dissolution of carbon in metal in the coke bed area of the EAF is one of the important reactions and must be better understood. By understanding how carbon materials properties influence the rate at which carbon dissolves in metal we can predict the carbon's performance. The carbon dissolution rate may also be an important factor when new processes with lower energy and CO_2 emissions is developed.

As carbon dissolution rates have mainly been determined in iron, a systematic and comprehensive study was conducted on the dissolution of carbon from six cokes, charcoal and graphite into liquid Fe-Mn. The kinetics of carbon dissolution from cokes A to F was measured and a range of experimental techniques were used to elucidate the dominant factors affecting the dissolution rate. The role of carbon microstructure and macrostructure, coke inorganic matter composition and yield and temperature were investigated. Furthermore, the influence of interfacial products and dynamic wettability studies were also conducted.

The immersion rod method was used to measure carbon dissolution as a function of time at two different temperatures, 1450 and 1550°C. Fundamental data on the total carbon dissolution rate constant (k_t) in molten Fe-85wt%Mn at 1550°C for cokes A to F were obtained and ranged from k_t ($\times 10^3$ m/s) = 48.9 to k_t ($\times 10^3$ m/s) = 67.3. For charcoal, k_t ($\times 10^3$ m/s) = 14.7 and for graphite k_t ($\times 10^3$ m/s) = 35.2. The wide variation in k_t showed that not all carbon materials dissolve at similar rates.

Thermal annealing of carbonaceous materials above 1250 ºC significantly increased the degree of graphitization. This conclusion follows from a reduction of the interlayer spacing (d_{002}) between aromatic planes, an increase of the stack height (L_c) of graphite crystallites, and an increased G fraction in the Raman spectra. Since the crystallite size of cokes at

1550°C were quite close, the difference in their dissolution rate cannot be explained on the basis of different microstructure. Within poorly ordered carbon materials like cokes and charcoal, with increasing crystallite size the dissolution rate increased

Increasing surface roughness, porosity and BET of different cokes, slightly increased the dissolution rate. Surface roughness of carbon materials also affected the wettability between cokes and Fe-Mn metal. With increasing roughness of non-wetting system, that is the cokes, the wettability decreased and with increasing surface roughness of wetting systems, that is graphite and charcoal, wettability increased.

Wettability experiments were carried out using the sessile drop technique. The wettability of cokes C, D, E and F and charcoal with liquid Fe-85wt%Mn was measured as a function of time from the melting point (1300°C). All coke samples showed wetting behavior with contact angles ranging between 60-65° in the initial stages (at the time of melting) and between 95-110° after 30 minutes of contact. Wettability of cokes with Fe-Mn at the initial stage can explain the high dissolution rate of the cokes.

The sessile drop technique was also used to study the interfacial products formed at the coke/metal interface. Interfacial products formed between the coke and the metal, after contact with cokes C and E. The cokes were initially different in regard to the morphology and chemical composition. The interfacial product formed with coke E had a network or mesh like structure that seemed to cover the metal droplet much better than the interfacial product formed with coke C. In contrast, globules and discrete interfacial products were observed in coke C. It was suggested that this was due to differences in inorganic matter content, especially in sulfur (S) content in the coke.

Dissolution mechanism was believed to be both interfacial reactions and carbon mass transfer in boundary layer. As the carbon microstructure and macrostructure affected the dissolution rate, the interfacial reactions are affecting the dissolution rate limiting step. Some indications such as metal composition and temperature dependence supported the carbon mass transfer to affect the dissolution rate limiting step.

List of Publications

1. Kaffash H, Tangstad M., “Dissolution kinetics of carbon in Fe-Mn alloys”, INFACON XV, February 2018, Cape town, South Africa.
2. Kaffash H, Tangstad M., “Dissolution of graphite in iron manganese alloys”, Extraction 2018, August 2018, Ottawa, Canada, pp.971-979.
3. Kaffash H, Tangstad M., “Dissolution rate of carbon in liquid metal”, LMPC 2019, September 2019, Birmingham, UK.
4. Kaffash H, Tangstad M., “Factors influencing dissolution of carbonaceous materials in liquid Fe-Mn”, submitted to Journal of Iron and Steel Research International.
5. Kaffash H, Xing X, Tangstad M., “Wettability of cokes by Fe-Mn melt”, submitted to Journal of Dispersion Science and Technology.

Contents

List of Figures

List of Tables

1 Introduction

Submerged electric arc furnace (SAF) is the major method in the manganese alloys production. In this process, manganese oxides in manganese ores are reduced to manganese (ferromanganese) by carbonaceous materials, including metallurgical cokes, chars and variety of coals with the heat supplied by the electric power in SAF. A cross section of an SAF around one electrode is shown schematically in **Figure 1.1**. The furnace charge, which consists of ore, fluxes and reducing agents, is fed from the top, and the electrodes are buried in the charge. Thus, the charge becomes a part of the electric circuit and the resistive heating of the charge provides the necessary energy. For the production of ferroalloys, such furnaces operate at low secondary voltages and high secondary currents, and these electric requirements are provided by transformers[1]. The process is often carried out by using a high manganese slag practice. The tapped slag will then contain 30-40% MnO. Because of its high manganese value, the slag is recycled as feed for the production of manganese metal by electrolytic process or for the production of silicomanganese alloy.

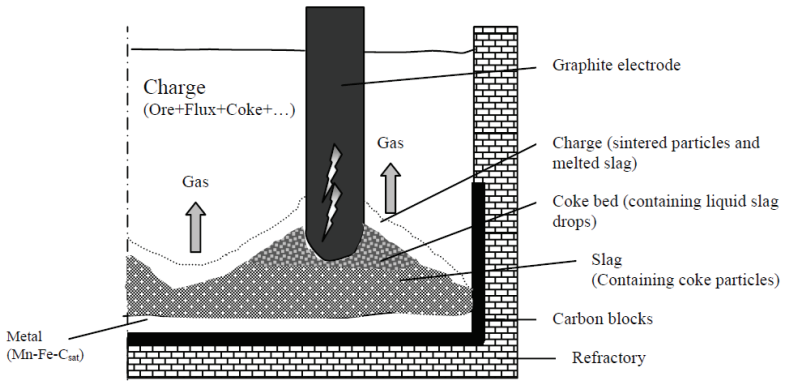

Figure 1.1: A schematic of the submerged arc furnace around one electrode[1].

The raw materials undergo various reactions on their pathway to the bottom of the furnace, from where the liquid metal and the slag are periodically tapped. Due to the temperature gradient, and thus the distribution of reactions, the furnace shaft is often divided into specific

zones. The reduction of MnO is taking place by solid carbon in the coke bed area which is the lowest zone of the furnace with the highest temperature.

The coke bed area is a very important area in the furnace. The coke bed is the resistance element of the furnace where heat is developed. The main reactions such as slag formation reactions and the reactions between carbon and slag are also mainly taking place in this area. The resistivity of the coke bed is very important parameter for furnace operation. On the other hand, the slag-reactivity of carbon in the coke bed area is important as it determines the temperature in the high temperature zone. The electrical resistivity and the slag reactivity of carbon in the coke bed area are affected by many parameters such as temperature, type of carbon material, particle size etc. The metal producing reaction is described in **Reaction 1.1** and as **Reaction 2.2** describes, some carbon is dissolved into the produced metal up to about saturation.

$$MnO_{(l)} + C = Mn_{(l)} + CO_{(g)} \qquad \textbf{1.1}$$

$$C = \underline{C} \qquad \textbf{1.2}$$

Carbon which is charged to the furnace together with other raw materials is mainly consumed through the reduction of metal oxides. However, it is also consumed through its reaction with CO_2 gas in the burden following **Reaction 1.3** (Boudouard reaction).

$$CO_2 + C = 2CO \qquad \textbf{1.3}$$

Production of 1 tonne high carbon FeMn in a ferroalloy submerged electric arc furnace (SAF) requires approximately 2 tonnes manganese ore and sinter, 330 – 380 kg coke and 2,400 – 3,400 kWh electrical energy[2]. Fluxes are also added in production of manganese alloys. In average, CO_2 emission only in the ferroalloy furnace amounts to ~3,800 kg/t HC FeMn.

There is a continuous goal to reduce energy and carbon consumption in the production of Mn-ferroalloys. One research path is to improve the current process, however new process concept has also been suggested. In order to produce ferroalloys and related products with lower energy consumption and/or lower CO_2 emission, the Norwegian Gassferrosil project introduced a new concept for producing FeMn in combination with SG (Synthetic gas)

where the gas is split into one H_2-rich (2 in **Figure 1.2**), and one CO-rich stream (4 in **Figure 1.2**). Earlier work at NTNU/SINTEF e.g. part of the National Gas Research Program "SPUNG" (1987-1993), showed that NG (Natural gas) can be effectively converted to SG using an iron bath as reaction medium [3]. Further theoretical development, involving transport of C between two reaction vessels also showed promising results. The reactor to the right on **Figure 1.2** closely resembles the process concept called "Manganese Oxygen Refining" (MOR) used industrially.

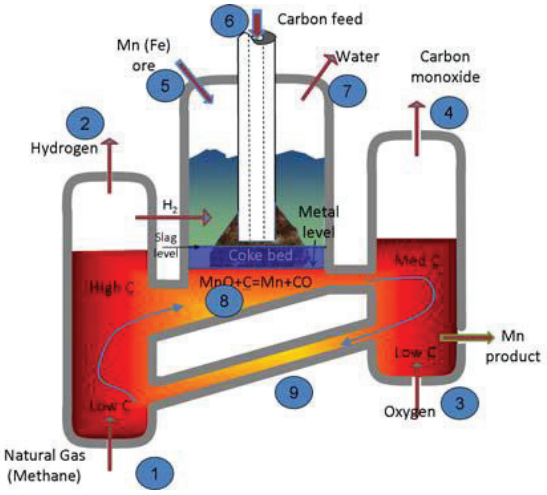

Figure 1.2: New process for Mn-alloy production.

One of the important sub-process in this process is the dissolution of C from the natural gas into the metal and subsequently the use of dissolved carbon as the reductant for the MnO reduction as shown in **Reaction 1.1**. Also, in the traditional SAF the slag can be reduced with dissolved carbon in the metal as well as solid carbon as described above. The relative contribution of solid and dissolved carbon in MnO reduction, is not well established and contradictory observations have been reported. Skjervheim[4] found that the rate of MnO reduction by solid carbon is about 2.3 times higher than that by dissolved carbon. However, in previous PhD work by Safarian[1], it was shown that reduction of slag with carbon dissolved in the metal was kinetically more favorable than with solid carbon. A study by Lee and Kolbinesen[5] showed that the dissolution rate of C into the metal was fast.

Both in future and present processes the dissolution of carbon into Fe-Mn alloy is an important sub-process. There were however no studies published in the literature on the dissolution reaction kinetics of carbonaceous materials in Fe-Mn. The kinetic of carbon dissolution in Fe and Fe-C and also Fe-C-S which is a key process in iron-making processes has however been studied for a long time. There is hence a gap in the fundamental knowledge regarding the rate of carbon dissolution from various carbon sources.

Using carbon dissolved in metal as reducing agent in ferromanganese production can have decisive advantages. Firstly, the Boudouard reaction, which is a highly endothermic reaction, would be avoided. Secondly, other carbon sources could be used, possibly lowering costs or CO_2 emissions. Biocarbon such as charcoal could be an option. Other carbon materials with low quality such as coal can also be used.

The present Ph.D. work is aimed at improving fundamental understanding of the mechanism of carbon dissolution in metal as a supplementary study of the Gassferrosil project. We investigated the dissolution of different carbon materials in Fe-Mn metal. Pure graphite was chosen as a reference material because it contains low ash, low impurities and it has the most graphitic structure and also low porosity. Charcoal will be included as bio-carbon is one of the ways man can reduce CO_2 emissions drastically. Metallurgical coke will be investigated as this is the material that is most typically used today as reductant. The goal was also to find a model describing the dissolution rate and determine the kinetic parameters for each individual carbon material. Since it is believed that wetting properties will affect the dissolution rate, and hence the wettability of the Mn-ferroalloy towards the different carbon materials will also be investigated.

The organization of the thesis will be according to the typical report layout. Chapter 2 will present the theoretical background and previous studies related to this work. Details regarding dissolution kinetics of different carbon materials in iron melts and factors influencing the dissolution rate are reviewed. Wetting behavior between different carbon materials and iron droplet is also included. The various mechanisms of carbon dissolution found in literature are analyzed.

In chapter 3 the experimental procedures are described. The selected carbonaceous materials and the characterization techniques used are detailed. The stationary rod technique was used

to investigate the dissolution rate of different carbon materials in Fe-Mn melt. The sessile drop wettability technique, which was used to study the interaction between Fe-Mn melts and carbon materials are explained.

Chapter 4 presents the obtained experimental results of the three main research topics: dissolution behavior of different carbon materials in Fe-Mn melt and factors affecting that, characterization of different carbon materials and how heat treatment can influence the microstructure and wetting behavior of different carbon materials with Fe-Mn melts and also factors influencing wettability.

Chapter 5 discusses the experimental methods and results of this work. The main objective of this chapter is finding the relationship between the carbon material properties and their effects on the rate of carbon dissolution. In this chapter, some mechanisms for the dissolution of carbon in Fe-Mn melts are suggested.

Chapter 6 presents the conclusions of this study. Some recommendations for the future work based on the obtained results from the present work are also included.

2 Theoretical background

2.1 Carbonaceous materials

Carbon as a reductant, fuel or additive is used in the production of metals and alloys. Carbonaceous materials are complex systems, which are generally heterogeneous in nature. Based on the costs, availability, required properties and so on, each metallurgical process use different kinds of carbon material or a mix of carbon materials. The most important carbon reductants for ferroalloy industry are charcoal, metallurgical coke, petroleum coke, coal, char and anthracite. In this report charcoal, coke and graphite are studied. Coke is used in the Norwegian industry, charcoal can replace fossil carbon[6] and graphite is used as a reference material. The properties of these carbon materials will be further discussed below.

Charcoal is produced from plant-derived biomass material. Charcoal properties depend on the type of wood from which it is obtained as well as the carbonization process. As compared to coal and coke, charcoal has lower sulfur and ash content and higher fixed carbon content and reactivity towards CO_2. The amount of volatile matter in charcoal is an important factor affecting charcoal properties. Charcoal has been used as a reducing agent in open submerged arc furnaces for a number of years, especially in Brazil. Charcoal applications in metallurgy are considered as clean technology due to reduced levels of CO_2 and SO_2 emissions[7].

Coke is produced by heating coal blend in the absence of oxygen to about 1100ºC. As temperature increases inside the coal mass, it melts and becomes plastic, fusing together as devitalization occurs, and ultimately re-solidifies and condenses into particles large enough for metallurgical use. During this process, much of the hydrogen, nitrogen, oxygen and sulfur are released as volatile by-products, leaving behind a poorly crystalline and porous product. Quality and properties of coke are affected by the coal-rank, fluidity, coal-macerals and mineral matter composition as well as processing conditions. Traditionally, chemistry, particle size, reactivity and strength after reaction are considered as the most important properties of metallurgical coke for blast furnace operations. Electric furnace coke, however, requires higher reactivity, lower strength and proper electrical resistivity [7, 8].

Graphite is one of the natural crystalline allotropic forms of carbon. Synthetic and natural graphite represent highly ordered form of carbonaceous materials. Natural graphite is a mineral consisting of graphitic carbon. Most commercial graphites are mined (natural graphite) and often contain other minerals. Graphite is a refractory material with a high melting point (3650°C). Synthetic graphite can be produced from coke and pitch. It tends to be of higher purity though not as crystalline as natural graphite. Mainly, due to cost and availability considerations, graphite are not used as reductants but are used in special applications such as electrodes for the arc furnace[1].

Carbon structure

Microstructure of carbonaceous materials has been extensively studied using X-ray diffraction (XRD) and Raman spectroscopy [9-14]. These methods can provide better understanding of the structure at the atomic level. Graphite structure can be described by a regular, vertical stacking of hexagonal aromatic layers with the degree of ordering characterized by the vertical dimension of the L_c (**Figure 2.1a**)[7]. Within each plane the carbon atom is covalently bonded to three other carbon atoms to form infinite two-dimensional sheets of aromatic rings. The fourth valence electron forms a much weaker van der Waals bond with a carbon atom in the adjacent plane, i.e. perpendicular to the basal plane. The most common stacking sequence of graphite is with -ABABAB- stacking order[15] as shown in **Figure 2.1b**. Natural graphite has also highly ordered structure like synthetic graphite but contains high level of impurities.

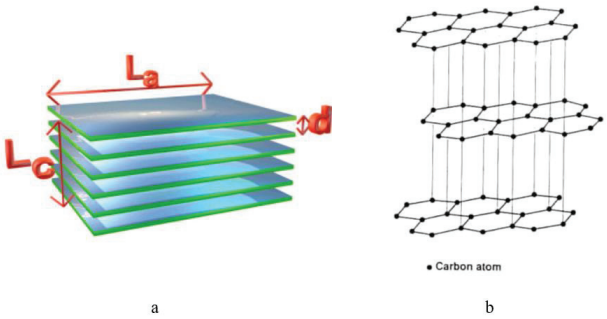

Figure 2.1: A schematic of crystal structure of graphite a)[7] b)[15].

Coals are considered to have some carbon atoms arranged in small clusters resembling the graphite structure [7]. Main difference is in their crystallite size and the degree of ordering (L_c and L_a). L_a values are difficult to quantify for coals due to small crystallite sizes. Inter-layer spacing are fairly similar for all carbonaceous materials typically ranging between 0.3-0.4 nm and will be smaller in more ordered structures. In graphite the d_{002} is 0.0335 nm. The bonding of carbon atoms in coals is highly complex as compared to that in graphite.

When producing metallurgical coke, coal is thermally pyrolysed and dehydrogenated through heating at 300-490°C to form a pitch-like material. On further heat treatment (510-1300°C) additional dehydrogenation occurs and a semi-solid green coke forms (510°C) followed by an increasingly more refractory coke as the temperature is increased to at least 1300°C during calcination. For some specialty cokes, calcination may be performed at 1450°C. At this stage, the green coke has been completely transferred into a solid carbon called coke with a limited three-dimensional order. Heat treatment in excess of 2100°C is required to obtain crystallite growth and the long range three-dimensional ordering typical of graphite. This microscopic process is shown graphically in **Figure 2.2**[1].

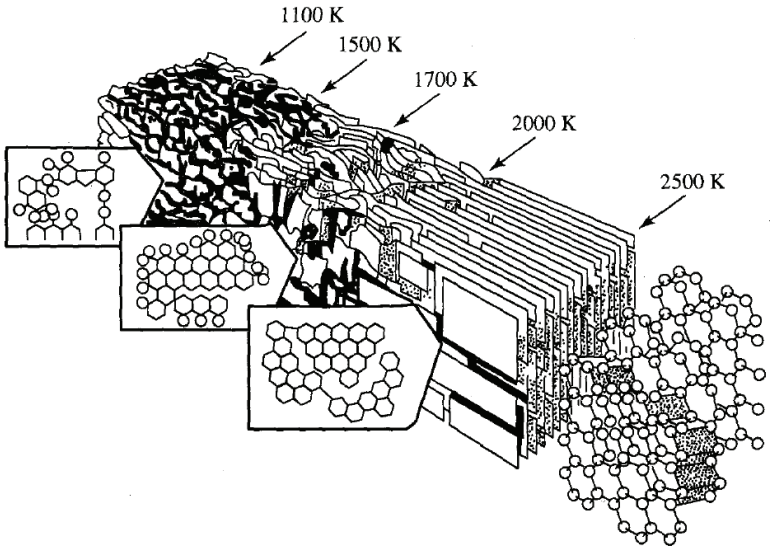

Figure 2.2: Development of crystallite alignment during graphitization[1].

When carbonaceous materials such as coal, char or coke are exposed to X-ray radiation the small crystalline regions diffract the beam causing (00l) and (hk) interferences from the prismatic plane (3D arrangement) and basal plane (2D arrangement) respectively. These interference patterns produce two main peaks in a carbonaceous spectrum that correspond to the (002) and (001) planes of the ideal graphite lattice. If the small graphite like clusters are considered as crystallite particles as shown in **Figure 2.1a**, then the extent of carbon ordering can be determined. The crystallite height (L_c) can be calculated by using Scherrer's equation (**Equation 2.1**)[16]:

$$L_c = 0.89\lambda / B \cos\theta_{B(002)} \qquad \textbf{2.1}$$

Where L_c is the crystallite size (angstroms, Å), λ is the wavelength of incident X-ray (Å), B is the angular width at half-maximum intensity of the (002) peak (radians, rad) and $\theta_{B(002)}$ is the Bragg angle of the (002) peak (degrees, °). The horizontal size of the crystallites (L_a) can be similarly obtained by **Equation 2.2**[16]:

$$L_a = 1.84\lambda / B \cos\theta_{B(001)} \qquad \textbf{2.2}$$

Where $\theta_{B(001)}$ is the Bragg angle of the (01) peak (degrees, °) and B is the broadening of this peak at half its maximum intensity.

Heating of cokes was shown to have a significant impact on the growth of crystallite size, L_c, by demonstrating the correlation between crystallite size and annealing temperature[9, 10]. Correspondingly, the proportion of graphite-like structure increased during the thermal heating process [10, 11]. Legin–Kolar et al.[14] studied the crystallographic parameters (crystallite height, L_c, and interlayer spacing, d_{002}) of petroleum coke, pitch coke and metallurgical coke after heat treatment at 1200, 1600, 2000 and 2400 °C and found that the crystal height, L_c, increases linearly between 1200 and 2400 °C; The interlayer spacing starts decreasing at 1200 °C as well (**Figure 2.3**).

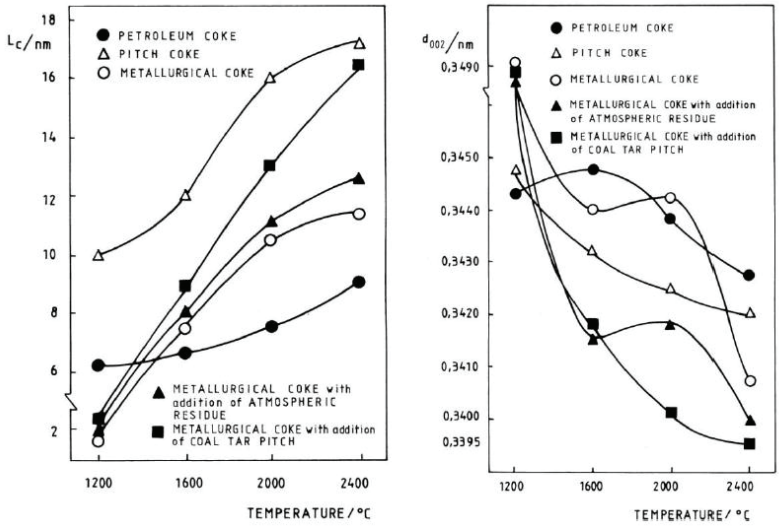

Figure 2.3: Influence of temperature on the crystallographic parameters of carbonaceous materials[14].

Gruber et al.[17] studied the heat treatment from room temperature to 2727°C on the microstructural properties of carbon black using Raman spectra analysis, and found that the G peak which is assigned to the E_{2g} symmetric vibrational mode, shifts toward lower frequency with increasing heat treatment temperature. Kawakami et al.[11] found that the increase of graphitization degree of coke, represented by G fraction, starts at 1100 °C, and this increase becomes significant from 1800 °C.

One of the important macroscopic properties is the pore structure of the carbon materials. This will affect a number of different properties e.g. reactivity and mechanical strength [2, 18]. The pore structure of carbonaceous materials has been intensively studied with a focus on its evolution during carbonization of coals.

Gomez-Serrano et al.[19] examined the effect of heat treatment of chars in the temperature range of 350°C to 850°C using gas absorption and found that total porosity and microporosity developed with increasing heat treatment temperature in the temperature range of 350°C to 750°C. At higher temperature, total porosity and microporosity was reduced with further increase of temperature due to micropore narrowing and pore closing.

Porosity of chars and coals at elevated temperatures was also studied using image analysis software [2, 20, 21]. It was found that the porosity significantly increased in the annealing at temperature below 1100 °C due to volatile matter release. Further increasing annealing temperature from 1100 – 1500 °C caused marginal porosity evolution in coals and chars by the reduction of oxides of mineral phases. Porosity of cokes increased slightly in the temperature range of 1300 – 1500 °C as result of reactions with the mineral phases.

Porosity and roughness of different types of graphite was studied by Safarian[1]. For porosity measurements, Mercury porosimetry (Carlo Erba Porosimeter) was used. This method cannot be used for cokes due to the existence of large pores. For roughness studies, a standard roughness instrument with a sharp diamond needle (Mitutoyo SJ. 201 P/M) was used. Porosity and roughness of the carbon materials was used to better understand its effects on the reduction rate of slags. In his study, the porosity of cokes ranged from 38.6% to 48.4% and the porosity of graphite ranged from 12.1% to 22.9%. Porosity of charcoal was found to be 27.3% which is far from expectations. The roughness of different cut graphite ranged from 0.53µm to 3.41µm. Ciftja [22] also used the same instrument to measure the roughness of different types of graphite and for the same reason. The roughness of different graphite ranged from 0.1 to 1.32 µm in his study.

Tomeczek et al.[23] studied the effect of coking temperature, heating rate and holding time on the porosity evolution. The porosity of coke produced under different conditions varied in the range of 32.46 % to 62.47 %. The porosity of different types of charcoal and coke was studied using Helium Pycnometry by Ramos [24]. The porosity of charcoals was ranging from 70% to 77.2%. The coke had the lowest porosity, at 43% lower than the average of the other charcoals. The high porosity and, hence, the low apparent density were related to higher friability of charcoal.

Roughness and porosity of different carbon materials (coke, graphite, anthracite and carbon black) was studied using white light interferometry (non-contact technique that uses light to determine the surface profile) by Nadir [25]. Coke showed the highest porosity (45%) followed by carbon black (18%) and graphite (10.8%), Anthracite showed the lowest porosity (1.7%). The surface roughness of coke, graphite, carbon black and anthracite found to be 1.13µm, 4.35µm, 1.19 µm and 0.75µm respectively.

2.2 Carbon dissolution in molten metal

2.2.1 Carbon saturation

Chipman et al.[26], Turkdogan et al.[27] and Tuset and Sandvik [28] investigated the saturation solubility of carbon in Fe, Mn and Fe- Mn melts. They found that the solubility is described by the following equation developed by linear regression analysis.

$$\boldsymbol{log\%C = \left(1.065 - \frac{614}{T(K)}\right) + 0.181\frac{\%Mn}{\%Mn + \%Fe}} \qquad \textbf{2.3}$$

The carbon solubility in the mentioned melts have the same temperature dependency and increases with temperature as shown by **Equation 2.3**.

Tangstad [29] did a comprehensive comparison of experimental and calculated carbon solubility data (**Equation 2.3)** in liquid Mn, Fe and Mn-Fe alloys from different investigators. The data are collected in **Figure 2.4**.

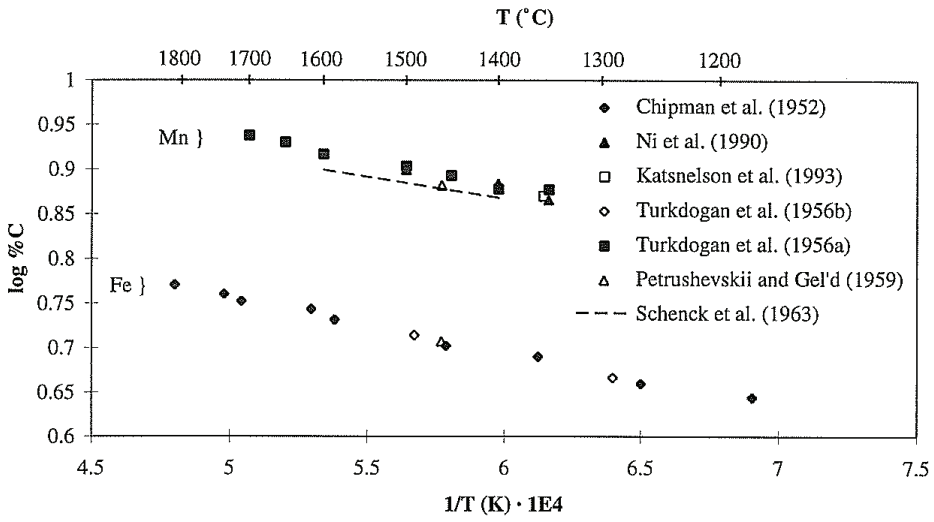

Figure 2.4: Solubility of carbon in liquid Mn and Fe melts versus temperature [29].

The calculated data fits well with the solubilities in pure Mn and Fe, but a small deviation of +0.3% for Tuset and Sandvik[28] and -0.3% for Turkdogan et al.[27]for Mn-Fe alloys was seen (**Figure 2.5**).

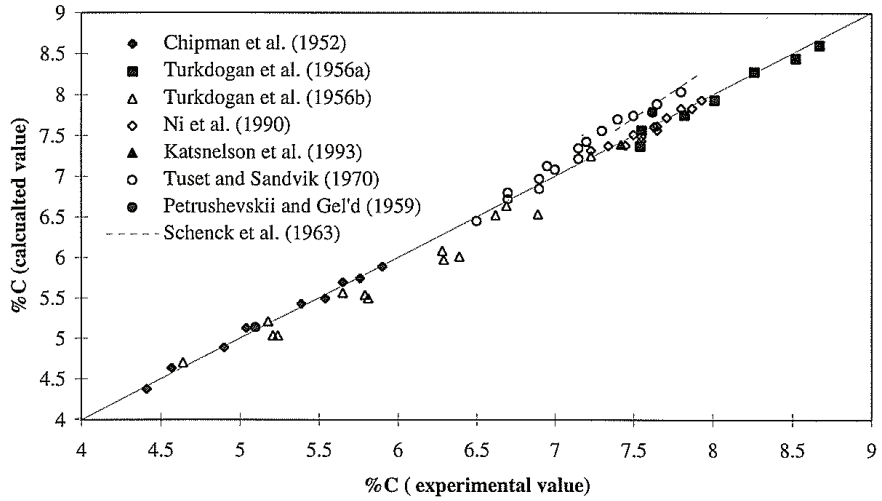

Figure 2.5: Comparison of calculated carbon solubility (Equation 2.3) and experimental results for the Mn-C, Fe-C and Mn-Fe-C systems [29].

High carbon ferromanganese contains typically about 80%Mn. Carbon solubilities in the temperature range from 1330-1630°C and manganese from 75 to 83% can be expressed by **Equation 2.4**. This equation is developed by linear regression analysis based on data from Tuset and Sandvik [28].

$$\boldsymbol{log\%C = \left(1.005 - \frac{478}{T(K)}\right) + 0.147\ \frac{\%Mn}{\%Mn + \%Fe}} \qquad \textbf{2.4}$$

Figure 2.6 shows the deviation between results of Tuset and Sandvik [28] and Ni et al.[30] and Turkdogan et al. [31] in the same composition and temperature. The deviation between experimental and calculated values from **Equation 2.4** is about 0.05% with a max deviation of 0.1%.

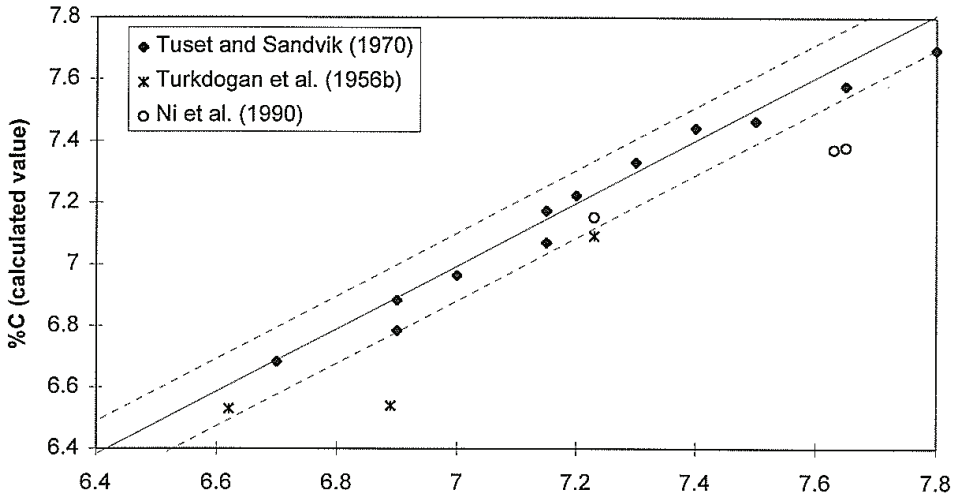

Figure 2.6: Comparison of carbon solubility calculated by Equation 2.4 and experimental results for Mn-Fe-C alloys between 74 and 94%Mn [29].

2.2.2 Experimental techniques for carbon dissolution studies

Experimental approaches in carbon dissolution studies can be under the following four categories:

- Rotating carbon block method
- Immersion rod method
- Carbonaceous material injection
- Carburizer cover method

Rotating carbon block was used by researchers, e.g. Olsson [32] and Kosaka [33]. In this method, a carbon block was formed mechanically as a cylinder or disk with well defined geometric size or shape. The advantage of this method was that carbon dissolution from carbon block to molten iron could be determined by the change of geometric size or weight of the carbon block before and after the dissolution experiment. The fluid dynamic situation can also be easily estimated from the peripheral velocity of rotating carbon block. Because of difficulty in shaping carbonaceous materials with high porosity or poor strength such as coke or coal, this method was best suited to a study dissolution of graphite**. Figure 2.7** shows a schematic diagram of rotating cylinder method and rotating disc method.

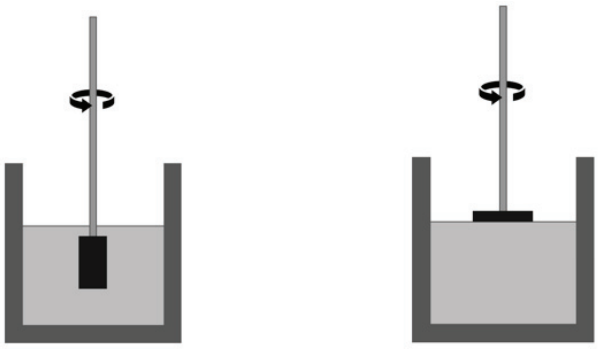

Figure 2.7: Schematic diagram of rotating cylinder method and rotating disk method in carbon dissolution studies.

Carbonaceous injection approach was used for studying coal dissolution in hot melts [34]. Coal particles with selected size range were introduced into hot melts via a tube from the top or bottom of the bath. With this technique the rate of carbon supply can be controlled quite accurately, and the bath fluid dynamic situation also can be controlled through flow rate of carrying gas. The disadvantage is that the rate of carbon supply will not be necessarily fast enough to obtain maximum dissolution rate in hot melt. Hence, rate of carbon supply will be a special parameter that should be taken into account in the investigation. A schematic diagram of carbon injection technique in carbon dissolution is shown in **Figure 2.8**.

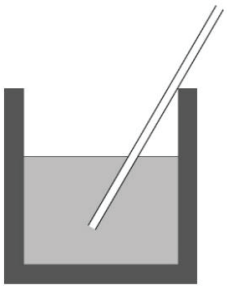

Figure 2.8: Schematic diagram of carbon injection technique in carbon dissolution studies.

Carburizer cover method is suitable for all carbonaceous materials with different physical properties [35, 36]. This procedure involves addition of small lump material onto the top of a molten metal bath and monitoring the change in bath composition with time. An induction furnace is usually used as heating source in this method. Induction stirring established bath movement, which is strong enough to improve mass flow dynamics within the molten bath. The results obtained from the carburizer cover method were shown to be comparable to those obtained from the rotation method.

Immersion rod method was also applied in previous graphite dissolution studies in an induction stirred bath [33, 37]. The mass transport phenomena in immersion rod method could also be determined by the change of geometric size or weight of the carbon rod before and after the dissolution experiment. However, the fluid dynamic condition determined by induction stirring could not be handled as easy as in rotating cylinder method. Carburizer cover method and immersion rod method are schematically shown in **Figure 2.9.**

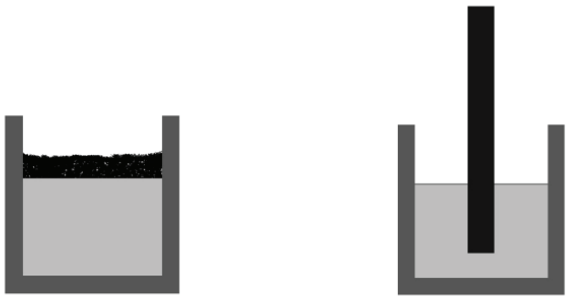

Figure 2.9: Schematic diagram of carburizer cover method (left) and immersion rod method (right) in carbon dissolution study.

2.2.3 Kinetics of carbon dissolution

A first order reaction rate is generally accepted as the carbon dissolution rate as shown in **Equation 2.5** [32, 33, 35-43].

$$\frac{dC}{dt} = \frac{kA}{V}(Cs - Ct) \qquad \textbf{2.5}$$

Where C_s and C_t are the saturation carbon solubility (wt%) and the carbon content at time t, respectively. A is the interfacial contact area (m^2), V is the volume of molten metal (m^3) and k is the rate constant (m/s).

By integrating **Equation 2.5**, one may obtain **Equation 2.6**.

$$ln\left(\frac{Cs - Ct}{Cs - C_{\circ}}\right) = -k't \qquad \textbf{2.6}$$

Where C_s, C_t, and C_0 are the melt carbon saturation level, the instantaneous melt carbon content, and the initial carbon content, respectively. k′ is apparent dissolution-rate constant. k′ can be expressed as **Equation 2.7**:

$$k' = \frac{k\,A}{V} \quad (s^{-1}) \qquad \textbf{2.7}$$

Figure 2.10 shows an example [44] which confirms the validity of using first order reaction rate for dissolution of coke in molten iron at 1550°C.

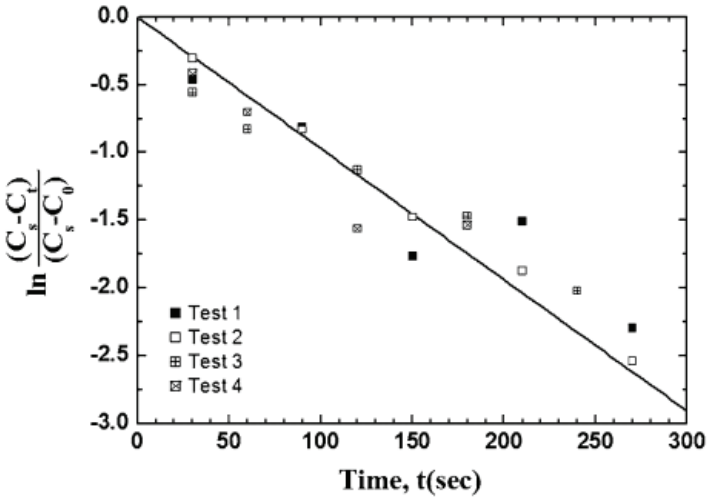

Figure 2.10: A plot of ln[(Cs- Ct)/(Cs- C0)] with respect to time for dissolution of coke in iron at 1550°C [44].

The apparent activation energy of carburization reaction is calculated by Arrhenius formula (**Equations 2.8** and **2.9)**.

$$k = k_{\circ}\, exp(\frac{E_a}{RT}) \qquad \textbf{2.8}$$

$$ln(k) = ln(k_{\circ}) - \frac{E_a}{RT} \qquad \textbf{2.9}$$

The apparent activation energy for the previous example in **Figure 2.10** was estimated to be 442 kJ/mol[44].

2.2.4 Dissolution mechanism

For carbon dissolution from its source into iron, possible reaction controlling mechanisms could be:

1. Liquid side mass transfer control of the carbon away from the interface.
2. Chemical reaction control at the interface.
3. A third condition involving a combination of mass transfer control and chemical reaction control (mixed control).

2.2.4.1 Mass transfer control

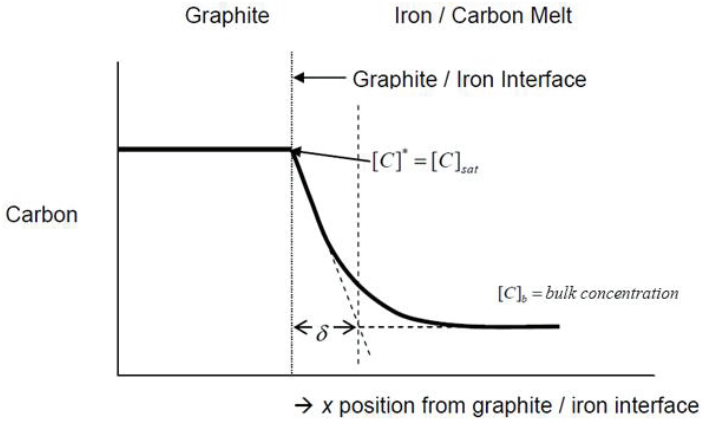

Figure 2.11: Schematic illustration of mass transfer kinetic control being the limiting case for carbon dissolution in liquid iron[45].

For the kinetics of carbon dissolution into iron to be controlled by mass transfer, the rate limiting step of the dissolution reaction is the movement of carbon away from the reaction interface into the melt. Under such conditions, as shown in **Figure 2.11**, a local equilibrium condition is established where the metal on the melt side of the interface is at carbon saturation and is in equilibrium with the solid carbonaceous material. In this case the flux can be represented as:

$$J = -D \frac{dc}{dx} \qquad \textbf{2.10}$$

Or as mass transfer is assumed to be controlling step, the flux can be represented as:

$$J = \frac{D}{\delta} (C_{sat} - C_{bulk}) \qquad \textbf{2.11}$$

Or:

$$J = k_m (C_{sat} - C_{bulk}) \qquad \textbf{2.12}$$

For a given volume of material (V) reacting over an area (A) this **Equation 2.12** can be represented as **Equation 2.13**:

$$V\frac{dc}{dt} = A\,k_m(C_{sat} - C_{bulk}) \qquad \textbf{2.13}$$

Which can be integrated as (assuming A,V and k_m are all time independent) as:

$$\frac{V}{A}ln(\frac{C_{sat} - C_0}{C_{sat} - C_{bulk}}) = k_m t \qquad \textbf{2.14}$$

Where C_{sat} is carbon concentration at carbon saturation, C_0 is initial carbon concentration of bulk at t=0, C_{bulk} is bulk carbon concentration in melt, k_m is mass transfer coefficient and D is diffusion coefficient of carbon in liquid metal.

2.2.4.2 Chemical reaction control

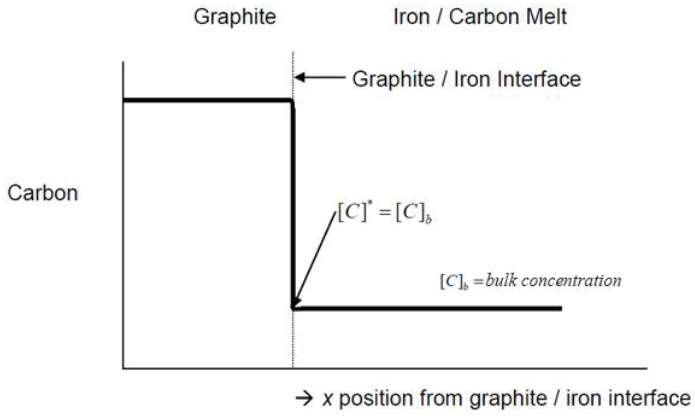

Figure 2.12: Schematic illustration of chemical reaction kinetic control being the limiting case for carbon dissolution in liquid metal[45].

In the case where the chemical reaction at the carbon/metal interface is the rate limiting step in the kinetics of carbon dissolution in liquid iron (**Figure 2.12**), carbon transport away from the interface is very fast. The carbon concentration and the rate at which the reaction

proceeds, is proportional to the activities of carbonaceous material and the solute carbon. Thus, the rate of the forward reaction is given by:

$$A\frac{dc}{dt} = k_{r1}a_{(c)} \quad \textbf{2.15}$$

And the reverse reaction rate by:

$$A\frac{dc}{dt} = k_{r2}a_c \quad \textbf{2.16}$$

At equilibrium the 2 rates must be equal but opposite, and the ration of k_{r1} and k_{r2} is equal to the equilibrium constant K.

$$A\frac{dc}{dt} = k_{r1}a_{(c)} - k_{r2}a_c \quad \textbf{2.17}$$

$$K = \frac{k_{r1}}{k_{r2}} \quad \textbf{2.18}$$

Or in terms of flux:

$$J = Ak_r(a_{(c)} - \frac{a_c}{K_r}) \quad \textbf{2.19}$$

$$K_r = \frac{a_c^{sat}}{a_{solid}} \quad \textbf{2.20}$$

Where:

k_{r1}= Rate constant for forward chemical reaction

k_{r2}= Rate constant for backwards chemical reaction

k_r = Rate constant for the overall chemical reaction

K_r= Equilibrium constant for the dissolution reaction

$a_{(c)}$= Activity of carbon in carbon material

a = Activity of carbon in liquid metal

2.2.4.3 Mixed control

In the situation where the carbon flux generated from the dissolution reaction is similar to the carbon flux away from the interface by mass transfer, no mechanism is dominant, and the control of the carbon dissolution reaction is mixed. Sun [46] derived an expression for the flux:

$$J = Ak_t(a_{(c)} - \frac{f[C]}{K_r}) \quad \textbf{2.21}$$

Where f is carbon activity coefficient at the liquid side of the interface and k_t is the overall rate constant of carbon dissolution and is given by:

$$\frac{1}{k_t} = \frac{1}{k_r} + \frac{100f}{k_m \rho K_r} \quad \textbf{2.22}$$

Equation 2.21 is the carbon dissolution rate equation involving interfacial dissociation reaction and mass transfer process. The total resistance R_t , the resistance of dissociation reaction R_r and the resistance of mass transfer R_m to the carbon dissolution process are given by **Equations 2.23**, **2.24** and **2.25**[46].

$$R_t = \frac{1}{k_t} = R_r + R_m \quad \textbf{2.23}$$

$$R_r = \frac{1}{k_r} \quad \textbf{2.24}$$

$$R_m = \frac{100\, f}{k_m \rho_m K_r} \quad \textbf{2.25}$$

It is noted that, the resistance of the mass transfer to the carbon dissolution, R_m, is a function of interfacial carbon activity coefficient, f, which is a dependence of interfacial carbon content, [C]. It indicates that R_m and k_t vary with time during carbon dissolution process [46]. If $R_m >> R_r$ the carbon dissolution is limited by mass transfer because the interfacial dissociation reaction is much faster than that of the mass transfer. If $R_r >> R_m$, the carbon dissolution is limited by the dissociation reaction at the interface because the dissociation is much lower than the mass transfer process[46].

Table 2.1 summarizes the dissolution rate equations for the carbon dissolution process for three possible mechanisms[46]. Case A, Case B and Case C represent the rate is limited by the mass transfer, interfacial dissociation reaction and by both of them respectively. As it is shown in **Table 2.1**, the dissolution rate is strongly influenced by the contact area A in all three cases. The dissolution rates for Case A and Case C vary with k_m, those for Case B and Case C vary with K_r and k_r, and that for Case A varies with carbon saturation content, C_{sat}. C_{sat} depends on temperature and alloying element in the liquid, while K_r solely depends on temperature for a given solid.

Table 2.1: Limiting steps, rate equation and kinetic and thermodynamic parameters for carbon dissolution [46].

Case	Limiting steps	Rate equation	Parameters				
			A	k_m	k_r	K_r	C_{sat}
A	Mass transfer	$\frac{V}{A}\ln(\frac{C_{sat}-C_0}{C_{sat}-C_{bulk}}) = k_m t$	Y	Y	N	N	Y
B	Interfacial reaction	$J = Ak_r(a_{(c)} - \frac{a_c}{K_r})$	Y	N	Y	Y	N
C	Mass transfer& interfacial reaction	$J = \frac{A(a_{(c)} - \frac{f[C]}{K_r})}{\frac{1}{k_r} + \frac{100\,f}{k_m \rho_m K_r}}$	Y	Y	Y	Y	N

Y: Involves N: Not involves

Mass transfer coefficient, k_m, is active in both the mass transfer and mixed control cases. Changes in the mass transfer coefficient with respect to diffusivity, temperature and viscosity can be represented by the Sutherland Einstein equation (**Equation 2.26** [45]) where η is the dynamic viscosity, R is the radius of the spherical particle.

$$\boldsymbol{D = \frac{k_m T}{4\pi R \eta}} \qquad \textbf{2.26}$$

The rate constant for the dissociation reaction, k_r, is present in both the mixed and interfacial reaction control cases. The influence of temperature is more significant on k_r than on k_m as chemical based reactions usually have a higher activation energy than mass transfer based reactions [46]. As the k_r value describes the rate of the reaction involving carbon atoms being removed from their lattice positions at the interface, the structure of carbonaceous source will have a significant impact on the reaction, but only if the reaction kinetics are truly reaction controlled. As in the case of contact area, the presence of surface active elements at the interface will have an impact on the value of k_r. As well as reducing the effective available contact area, the presence of a surface active element may block atomic sites at the surface, preventing some of carbon atoms from reacting with the liquid interface, and retarding the dissociation reaction [45].

Wettability between solid carbon and liquid affects the contact area when porous or small particles of solid are in contact with the liquid. This is because good wetting will allow liquid to penetrate into pores of the solid or interstitial space between particles to increase the contact area. Wettability can affect k_r since good wetting means higher work of adherence (strength of bonds between two media) that may help to dissociate carbon atoms from solid lattice and this may give a higher k_r . The factors that can affect the interfacial tension between solid and liquid will also affect the wettability. These factors include temperature, solid structure, interfacial active elements and metal compositions [46].

2.2.5 Carbon dissolution from graphite

The dissolution rate of various carbonaceous materials into iron melts has been studied for a long time [32, 33, 47] and the majority of the previous investigations used graphite in their studies [32, 33, 35, 38, 47-49]. More details will be explained below:

2.2.5.1 The carbon dissolution mechanism

The goal of the following studies [33, 38, 39, 47-49] on carbon dissolution from graphite was to establish an understanding of the mechanism that controls the transfer of carbon from graphite into molten iron. The dissolution of carbon from graphite is thought to be a two-step process [32, 33, 50] where the first step involves dissociation of carbon atoms from its crystal site in the graphite into the carbon/melt interface. The second step is the mass transfer of carbon atoms through the adjacent boundary layer into the bulk liquid iron as depicted in **Figure 2.13**. The dissolution of carbon into liquid iron was traditionally considered to be limited by the mass transfer in liquid iron [32, 51, 52]. This was mainly evidenced by the strong dependency of the dissolution rate on the liquid agitation and weak dependency of the rate on the temperature and sulfur in liquid.

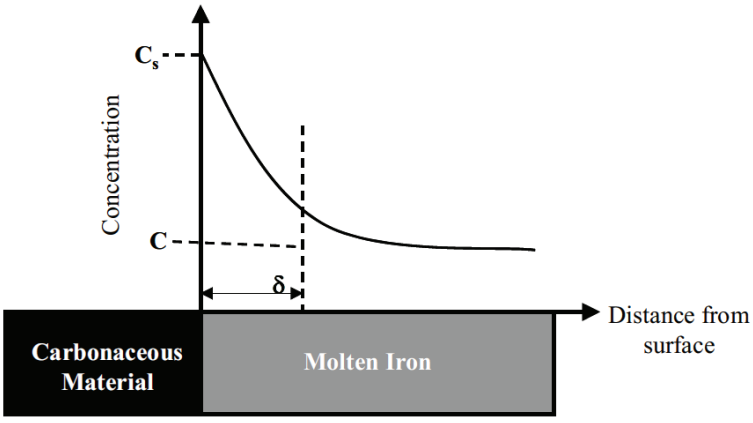

Figure 2.13: Variations in carbon concentration at the graphite / molten iron interface when diffusion through boundary layer is rate determining. (C_s is the carbon saturation level at the interface, C is the bulk carbon concentration and δ is the thickness of the boundary layer)[16].

Olsson et al. [32] studied the rate of carbon dissolution from graphite in molten Fe-C alloys in the temperature range of 1470-1640ºC. Rotating graphite rods placed in the liquid iron bath was used in this study. The equation of continuity was applied to determine the rate of carbon diffusion from the graphite/melt interface, based on their assumption that the resistance to mass transfer resides in a laminar boundary layer adjacent to the interface and that the diffusion coefficient is independent of concentration. It was found that the mass-transfer coefficient for carbon dissolution from graphite to Fe-C melt is a function of the peripheral velocity (υ) of the rotating cylinder and can be described by **Equation 2.27**.

$$\boldsymbol{k = (const)\upsilon_i^{0.7}} \qquad \textbf{2.27}$$

They proposed that the rate of carbon dissolution from graphite to the Fe-C melt is controlled by carbon diffusion (mass transfer) from the interface between the solid graphite and bulk liquid when the Reynolds number is in the range from 790 to 18000.

Kosaka and Minowa [33] used a stationary immersion graphite cylinder as well as the rotating graphite rod to investigate the dissolution rate of graphite in Fe-C melts in the temperature range 1270-1550ºC. A first order kinetic equation was applied, based on the assumption that the dissolution of carbon was controlled by liquid side mass transfer. A non-dimensional fluid-dynamics correlation of mass transfer was also applied to calculate the mass-transfer coefficient in the investigation. It was found that the mass transfer coefficient obtained from a first-order kinetic equation was between 0.8 to 3.6 m/s at a stirring velocity of 48 to 52 cm/s in a rotating cylinder apparatus and between 0.22 and 1.8 m/s at a stirring velocity of 4.5 to 33 cm/s in an induction furnace. Those are in reasonable agreement with the mass transfer coefficients evaluated by the use of non-dimensional correlation. On this evidence, it was concluded that carbon dissolution from graphite to Fe-C melts is controlled by mass transfer in the liquid.

Sahajwalla and Khanna [50] used Monte Carlo simulation to model carbon dissolution from graphite into molten iron. It was seen that due to the weak bonding between carbon in each graphene layer, the carbon atoms dissociate easily across the prismatic planes compared to carbon atoms in the basal planes. The simulation showed that the rate of mass transfer of carbon atoms in the melt is slower than the corresponding dissociation rate at the interface. Hence, results from this study also confirmed the findings of previously mentioned authors.

2.2.5.2 Influence of sulfur

Grigoryan and Karshin [48] studied the effect of sulfur and oxygen on the dissolution kinetics of rotating discs of graphite in liquid iron at1580°C. It was found that the addition of sulfur and oxygen to the melt decreased the dissolution rate. It was suggested that the addition of sulfur changed the surface properties of metal/graphite at the interface. However, when the dissolution was controlled by diffusion mechanisms, sulfur had no effect and different rate limiting steps may be valid dependent on experimental conditions.

Analogous experiments using rotating graphite cylinders were conducted by Ericsson and Melberg [53]. In this study the addition of sulfur to melt was found to decrease the rate of carbon dissolution in liquid iron, due to the decrease in carbon solubility. Results also indicated that in high sulfur melts the rate of carbon dissolution was limited by mass transfer. It was proposed that this was partly due to the decreasing carbon diffusivity at higher sulfur contents. They suggested that the effect of sulfur maybe due to its influence on the interfacial kinetics of the dissolution process.

Influence of sulfur and phosphorus on the dissolution of two types of electrodes, graphitic and non-graphitic, in Fe-C melt in the temperature range of 1300-1500ºC was investigated by Shigeno et al.[38]. A decrease of the carbon dissolution-rate coefficient with increasing sulfur in melt was found. It was explained in terms of sulfur selectively absorbing onto the prism plane of the graphite and it retarded the dissolution of graphite from this plane and consequently the mass transfer in the presence of sulfur decreased. The planes of non-graphitic carbon are more exposed than those of graphitic carbon. The reduction of the effective area available for dissolution was hence greater.

Wright and Baldock [47] also studied the effect of sulfur on the dissolution rate of graphite in Fe-C melt in the temperature range 1400-1500ºC. The results were in agreement with previous investigations. Authors suggested that the decrease in k value was due to a decrease in carbon diffusivity with an increase in sulfur content. They also suggested that at higher levels, sulfur may affect the dissolution rates by influencing the interfacial kinetics of the process. They also found that sulfur decreased the carbon solubility in iron, thus reducing the driving force for carbon dissolution. This was in agreement with experiments conducted by other research group [27].

Wu and Sahajwalla [35] studied the effect of initial sulfur content (0.1-0.4 wt%) of Fe-C-S bath on the dissolution of synthetic graphite and coal. It was again found that an increase in sulfur content decreased the overall carbon dissolution rate constant using synthetic graphite. The retarding effect of sulfur was greater with coal rather than with graphite dissolution. The retarding effect of sulfur, however, decreased with further increases.

Dissolution rate of graphite in molten iron and the effect of sulfur content on the dissolution rate at the temperature range 1450-1550ºC was studied by Zhang et al.[43]. In contradiction to previous results they found that an increasing sulfur content, increased the dissolution rate when the concentration of sulfur in molten iron varied in the range of 0.02-0.06 wt%. The sulfur concentration was very low compared to other studies.

Jang et al.[44] studied the kinetics of carbon from coke in molten iron in the temperature range of 1450-1550ºC and the effect of sulfur on the dissolution rate. It was found that the sulfur dissolution did not affect the carbon dissolution rates in molten iron and it was considered that the sulfur adsorption at the metal/coke interface was not so significant.

Sun et al.[51] investigated the dissolution reaction of graphite in molten iron in a resistance furnace at 1500°C. It was found that with adding 1 wt% sulfur to the melt, a decrease in carbon dissolution rate was observed. A decrease in the carbon dissolution rate with increasing sulfur content in the melt was considered to occur because a portion of the boundary reaction sites is occupied by the sulfur atoms.

Cham[16] investigated the sulfur and carbon dissolution from coke simultaneously. It was found that sulfur content followed a pattern similar to carbon dissolution. It was found that there was a direct correlation between carbon and sulfur pick-up from the coke, i.e. the dissolution of sulfur occurs simultaneously with carbon dissolution, as if dissolution of carbon from coke somehow made it easier for sulfur from coke to dissolve. This pattern was observed for all the coke samples and as a typical example, one of the cokes is illustrated in **Figure 2.14**. This figure indicates that there is a strong and direct connection between sulfur and carbon dissolution.

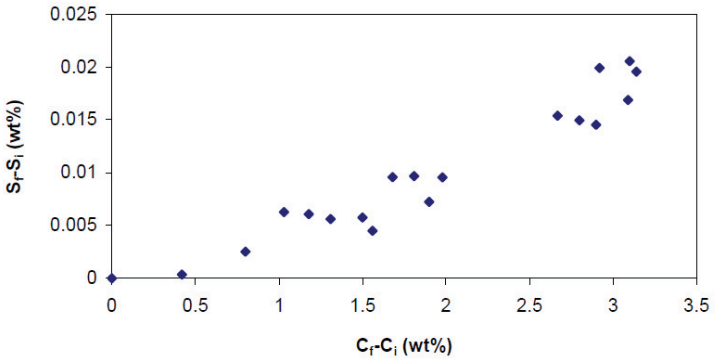

Figure 2.14: Change in S and C content in the iron bath for coke at 1550°C[16].

This pattern was also observed by Jones [54] who conducted an investigation on the kinetics of carbon dissolution in Fe-C alloy at 1550°C using commercial calcined petroleum coke. Jones [54] concluded that the pick-up of sulfur by the molten alloy increased proportionately to the dissolution of carbon.

Wu [55] found that with increasing sulfur content of iron up to 1.2 wt%, the rate constant of carbon dissolution from graphite was decreased by approximately 60%. The retarding effect was remarkable with initial increase of sulfur content. However, the influence becomes relatively minor with further increase of sulfur as it is shown in **Figure 2.15**. It is worth mentioning that in his study, induction furnace was used for dissolution experiments. The decrease of carbon dissolution rate by increase of sulfur content was attributed to the decrease of carbon diffusion coefficient with presence of sulfur.

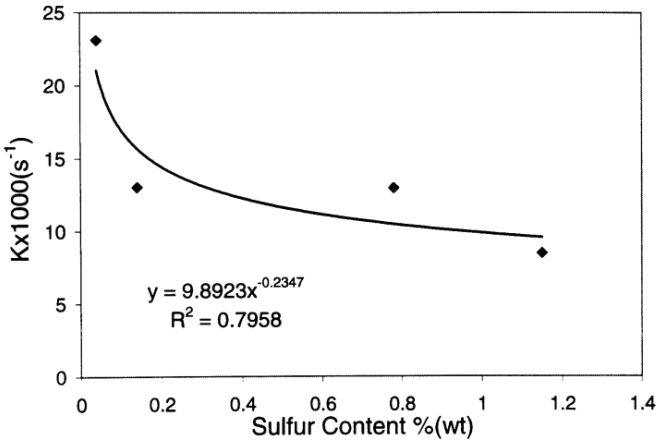

Figure 2.15: Influence of iron bath sulfur content on carbon dissolution from graphite[55].

2.2.5.3 Influence of temperature

Dissolution rate of graphite in molten iron and effect of temperature on the dissolution rate was studied by Zhang et al.[43]. The carburization of molten iron was studied at three different temperatures,1450,1500 and 1550ºC. It was found that the dissolution rate increased with increasing temperature as it is shown in **Figure 2.16** with an apparent activation energy of 51.4 kJ/mol.

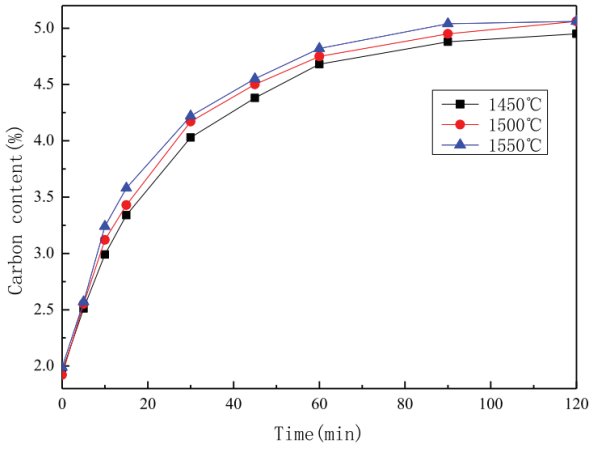

Figure 2.16: Carbon content in metal versus time at different temperatures [43].

Sun et al.[51] studied the dissolution of carbon from graphite into liquid iron using an electric resistance furnace from 1300-1500°C. It was found that there were small increases in carbon dissolution rate with temperature from 1.82×10^3 cm/s at 1300°C to 2.54×10^3 cm/s at 1500ºC. The activation energy for diffusion of carbon were found to be 40 kJ/mol.

Bandyopadhyay et al.[41] investigated the effect of temperature on the dissolution rate of graphite in liquid iron. It was noticed that increase in temperature helps to promote the dissolution rate as it is shown in **Figure 2.17**. The apparent activation energy for the dissolution process was found to be 42 kJ/mol.

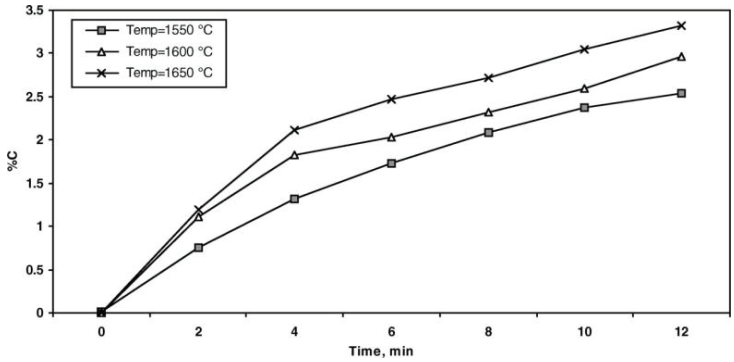

Figure 2.17: Effect of temperature on dissolution of graphite in electrolytic iron bath[41].

Wright and Baldock [47] studied the effect of Fe-C bath temperature on the dissolution rate of graphite. It was found that the bath temperature over the range of 1400 to 1500°C does not appear to have a major effect on the graphite dissolution rate, however they are not providing the activation energy.

Olivares [56] examined the effect of temperature on the dissolution of high purity spectrographic grade graphite discs in sulfur-free and sulfur-containing melts from 1350 – 1650°C. The author determined the apparent activation energy for carbon dissolution to be 70.7 kJ/mol and 78.9 kJ/mol for sulfur-free and sulfur-containing melts, respectively, which were in good agreement with previous graphite studies. The effect of temperature on the dissolution of industrial carbons, such as coke (with an ash yield of 12 wt%) and blast furnace carbon refractory brick (with an ash yield of 20 wt%), from 1400 – 1600°C was also

investigated. The experimental results showed that carbon dissolution increased as the temperature increased. However, due to the poor dissolution of the coke sample, the author could not determine the dissolution rate constant and hence the apparent activation energy.

Kosaka and Minowa [33] studied the dissolution of synthetic graphite electrodes into molten Fe-C alloy over the temperature range 1270-1550ºC. They observed that there was a slight increase in k with increasing temperature. Similar findings were made by Wright and Denholm [57] during their investigation on carbon dissolution from graphite, char and petroleum coke particles between 1300 – 1500°C. However, Kosaka and Minowa [33] found that the mass transfer coefficient, k , was greatly influenced by stirring conditions.

A study by Orsten and Oeters [58] on the dissolution of graphite cylinders rotating in liquid iron from 1470°C to 1625°C, determined the activation energy to be 78 kJ/mol. The authors found in their literature review, the activation energy for carbon dissolution of graphitic sources to be in the range of 65-90 kJ/mol.

2.2.6 Carbon dissolution from Non-graphitic sources

Non-graphitic sources include coke, coal, char and glassy carbon. Few studies concentrated on coke while most of them have used a combination of carbon sources in the dissolution experiments. The researchers claimed that the crystal structure, porosity of carbonaceous material and composition of molten iron have a strong influence on carbon dissolution.

2.2.6.1 The carbon dissolution mechanism

Investigations were carried out on carbon dissolution from graphite and coke into liquid Fe-C alloy using induction furnace at 1300-1600ºC by Sun [46]. As mentioned earlier, three mathematical models were used for analyzing the reaction rate between solid carbon and molten iron. These models were developed in terms of three possible rate limiting steps for carbon dissolution in molten iron. The kinetic parameters describing carbon dissolution rate were obtained from the comparison of observed carbon dissolution rates and model calculations. The rate influencing factors suggested by the model discussion were

temperature, solid structure, interfacial active elements, metal composition, liquid agitation, wettability between solid and liquid, solid particle size, ash and side reactions. It was found that the mass transfer in the liquid was the major limiting step for the carbon dissolution. However, there was no evidence to rule out the possibility of a mixed limiting mechanism.

Investigations by Khanna et al.[36] on the dissolution of carbon from coal-chars into liquid iron at 1550°C also discussed the possibility of other rate limiting factors. The authors highlighted the importance of reactions at the carbon/iron interface and their effect on carbon dissolution rates. They found that the consumption of dissolved carbon through silica reduction and deposition of reaction products, such as CaS, at the interface strongly inhibited carbon dissolution in chars. Khanna et al.[36] also developed a theoretical model to estimate the solid/liquid contact area. This was used in conjunction with the overall apparent dissolution rate constant (K) to calculate the first order dissolution rate constant (k).

2.2.6.2 Influence of bath sulfur content

Shigeno et al.[38] studied the effect of sulfur and phosphorus on the rate of carbon dissolution from non-graphite sources into molten iron. It was reported that the rate of carbon dissolution from a non-graphitic electrode could be retarded significantly by surface-active elements such as sulfur and phosphorus in the bath. They proposed that the reduction of effective surface area for dissolution due to sulfur absorption at carbon/iron interface was greater for non-graphite carbon than for graphite.

A model was developed by Wright and Taylor [34] to predict the dissolution behavior of carbon particles into iron bath. The model predictions were consistent with laboratory studies of high purity graphite injected to iron bath when mass transport limitation was dominant. However, when they substituted graphite with petroleum coke, results deviated from model predictions. This showed that the rate of dissolution from pet coke was limited by factors other than mass transport from solid to liquid. It was found that the model could predict the change of carbon concentration in Fe-C melts with time by graphite dissolution with or without presence of sulfur. As applied to poorly graphitic carburizer however, the model results were found to deviate from laboratory experiments. As shown in **Figure 2.18**, it can be implied that the model is not applicable to dissolution of non-graphite carburizer

in Fe-C melts especially at high sulfur concentration. The reduction in dissolution rate due to the presence of sulfur were much greater than that could be accounted for on the basis of liquid side mass transport, especially at high sulfur concentration.

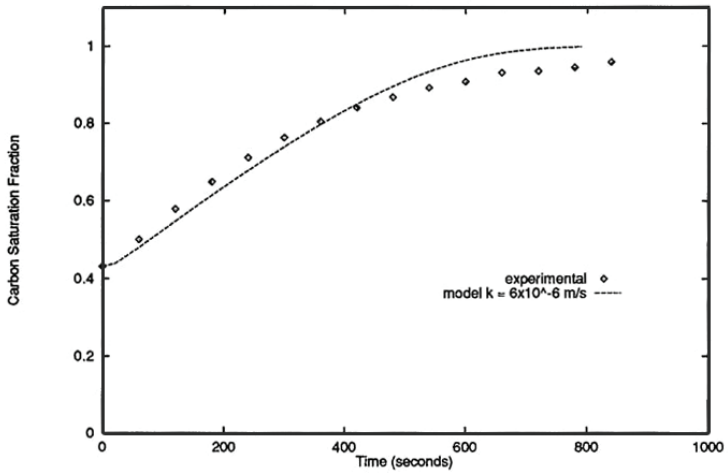

Figure 2.18: The deviations between model prediction and experimental results for dissolution of carbon from petroleum coke in bath with 0.4% sulfur[34].

Studies conducted by Sahajwalla et al.[59] on injected anthracites and brown coal char into liquid Fe-C-S melts found that increasing the bath sulfur content decreased the dissolution rate. Each carbon source behaved differently with respect to bath sulfur levels and dissolution rate. It was proposed that the differences in behavior were due to the structural arrangement of each carbon sample.

Wu [55] found that with increasing initial sulfur contents of the molten iron, the dissolution rate of coal would decrease. The results are plotted in **Figure 2.19**. Upon comparing **Figure 2.15** and **Figure 2.19**, it could be seen that the influence of sulfur content on the rate of carbon dissolution for coal was similar in trend to that for graphite. However, with increasing initial bath sulfur content from 0.06% to 0.79%, the carbon dissolution rate constant for coal decreased about 70% of initial value. This number is a little larger than that found in graphite dissolution.

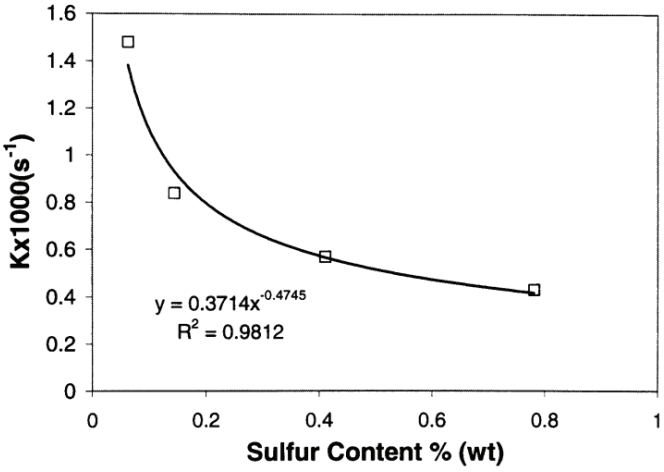

Figure 2.19: Influence of iron bath sulfur on carbon dissolution from coal[55].

Mourao et al. [39] investigated the dissolution of spectroscopic graphite and industrial cokes in Fe-C melts at temperatures ranging from 1350-1662ºC. Sulfur was found to have a retarding effect on the dissolution rate and this effect was greater on coke in compare with graphite. Authors suggested that this behavior might be because of the graphitization degree of graphite which offers fewer active sites for sulfur adsorption.

2.2.6.3 Effect of carbon crystal structure

Wu and Sahajwalla [49] developed correlations between dissolution rate and the carbon structure of various coals, showing that the rate of dissolution from coal increased with increasing crystallite size as it is shown in **Figure 2.20**. The authors suggested that increased L_c value indicates an improvement in the ordering in the carbon atom arrangement, and that this increased ordering in turn leads to increased carbon atom dissociation and hence has the effect of enhancing the carbon dissolution rate from coals with higher L_c values.

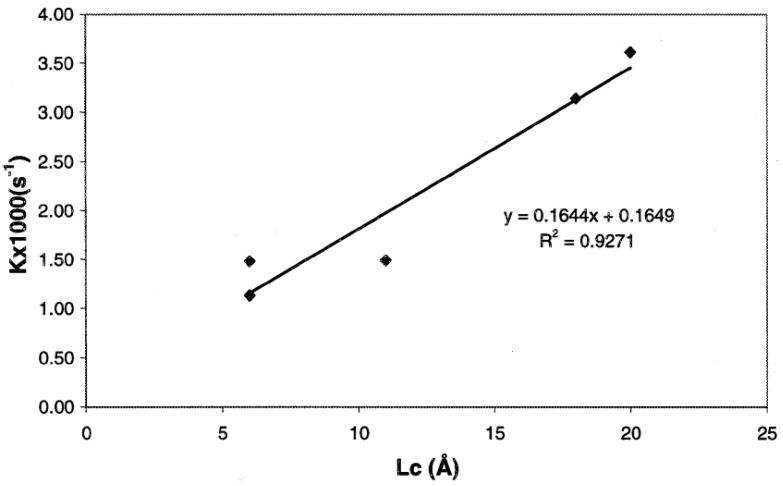

Figure 2.20: The dependence of carbon dissolution rate constant on crystallite size L_c for coals[49].

In a latter studies focused on carbon dissolution from graphite and Australian cokes, Cham et al. [40, 60, 61] in contrast to above study, found no obvious effect of crystallite size on the rate of dissolution into liquid iron at 1550ºC. It is seen from **Figure 2.21** that the crystallites are more ordered after the reaction since the L_c values have doubled in comparison to raw cokes, however, there is a little difference in L_c between the two cokes. The high dissolution rate of coke 1 cannot be explained on the basis of the crystallite size according to **Figure 2.22**. It was found that the difference in crystallite size does not appear to be a dominant factor in influencing the overall carbon dissolution rate for relatively high ordered material such as graphite and cokes at high temperatures. However, no attempt was made in this study to determine the coke porosity and its influence on the relative contact areas and thus reaction rates between the different cokes and iron used.

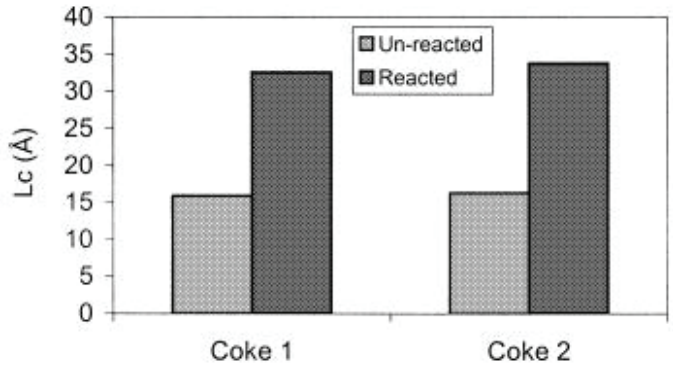

Figure 2.21: Average crystallite size, L_c, before and after reaction for two cokes [60].

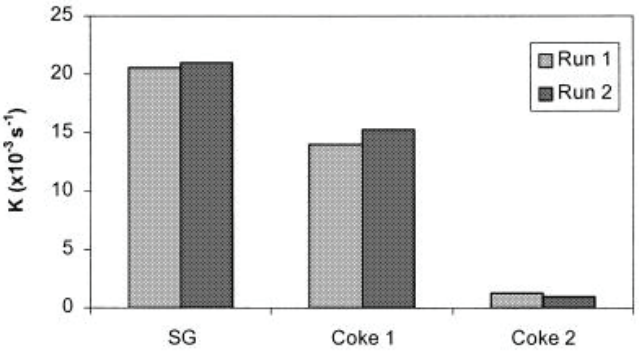

Figure 2.22: Average rate constant, k, for the 3 carbonaceous materials at 1550°C, SG stands for synthetic graphite [60].

Ohno et al.[62] investigated the effect of carbon structure crystallinity on initial stage of iron carburization. It was studied by in-situ observation of primary Fe-C liquid formation and diffusion couple method. Carbon structures of samples were analyzed by Raman spectroscopy. It was found that using carbonaceous material with lower crystallization degree, (lower I_V/I_G, see **Figure 2.23**), the initial iron carburization reaction was enhanced.

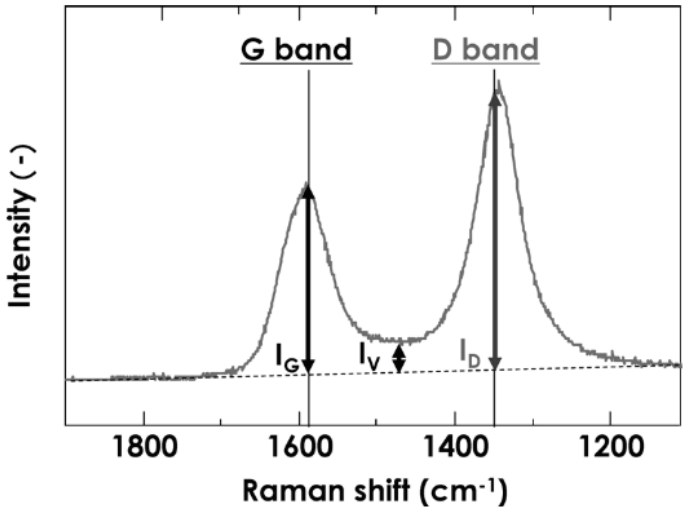

Figure 2.23: Schematic procedure of estimation of I_D, I_V and I_G from Raman spectrum [62].

In another study, Ohno et al.[63] studied the effects of carbon crystallinity of different types of charcoal on carbon dissolution in molten iron. Charcoal was heat treated at three different temperatures, 1000, 1500 and 2000ºC to control the carbon crystallinity. As shown in **Figure 2.24**, charcoal heat treated at lower temperature increased the carbon dissolution in molten iron. It means that carbonaceous material with lower crystallinity of carbon have an obvious advantage from the point of view of carbon dissolution in molten iron which was opposite to the finding of Wu and Sahajwalla [49].

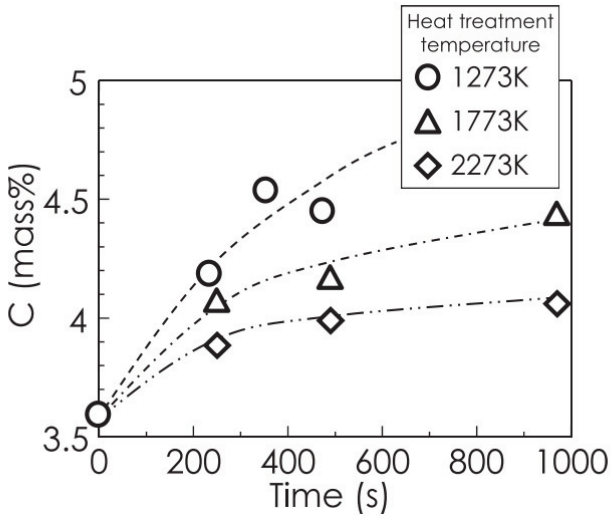

Figure 2.24: Carbon dissolution behavior at 1200°C using charcoal [63].

Wu [55] studied the dependence between carbon dissolution rate constant and crystallite size of different carbonaceous materials. It can be seen from **Figure 2.25** that apparent rate constant, K′, increases with increasing L_c value. At relatively lower L_c value, there was a reasonable increase in K′, whereas at higher values the slope changes significantly and the rate slows down. It means that with initial increase of L_c value, it could possibly result in a quick increase in the rate of carbon dissolution. On the other hand, if L_c value is relatively high, increase of L_c value has negligible influence on carbon dissolution. Therefore, for materials with poorly ordered carbon atom arrangement such as coal or coke, the crystallite size (L_c) plays an important role in determining the carbon dissolution behavior. For materials with highly ordered carbon atom arrangement such as graphite, crystallite size is not an important factor in determining the rate of carbon dissolution.

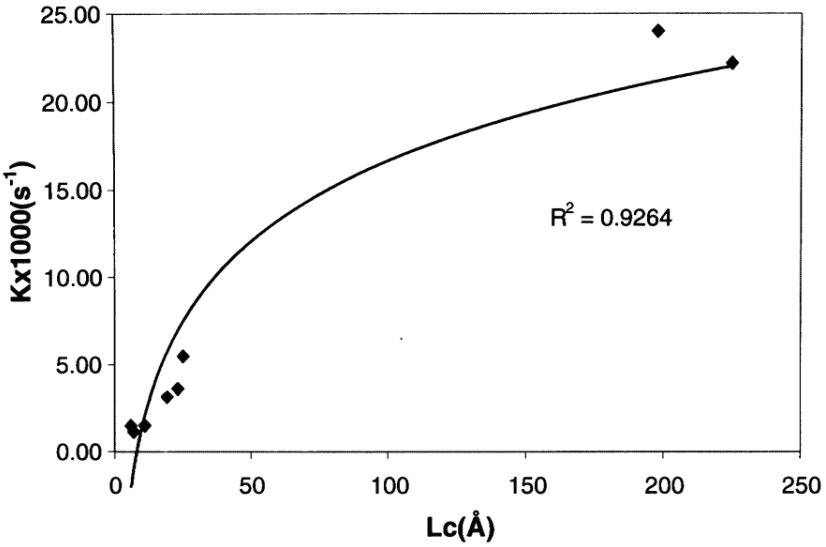

Figure 2.25: Dependence of carbon dissolution rate constant on the crystallite size (L_c) obtained from XRD for carbonaceous materials used in the investigation [55].

It was also mentioned by Wu [55] that the dependence of dissolution rates of coke and coals can be increased linearly with increasing L_c value. The relationship was shown in **Figure 2.26**.

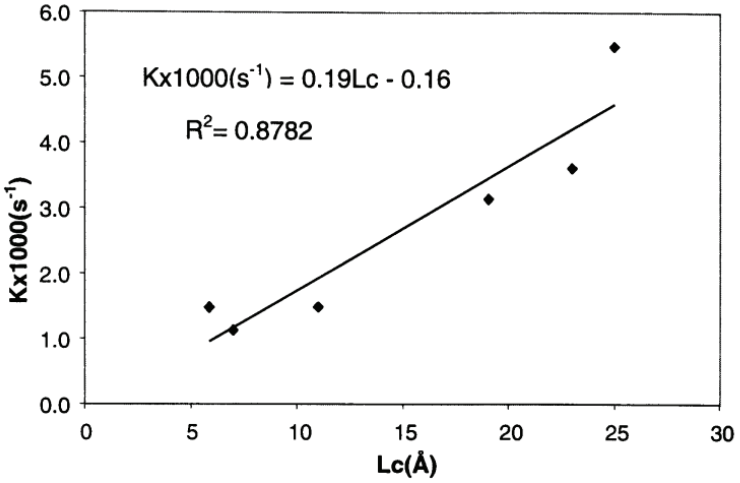

Figure 2.26: The dependence of carbon dissolution rate constant on crystallite size (L_c) for coals and coke[55].

Pistorius [64] measured the dissolution rates of coal by placing a cover of relevant reductant on molten iron (initially containing 2%C) in an induction furnace at 1550°C. It was found that the coal property affecting the dissolution rate most strongly is the degree of crystallinity. One model of the complex structure of coal is that it consists of small regions which have the graphite crystal structure, with complex three-dimensional bonds between these ordered regions. A measure of the degree of crystallinity of the coal is then the average thickness of the ordered regions (crystallites). It was concluded that, the more crystalline coals or chars exhibited more rapid dissolution, perhaps because the complex three-dimensional bonds in poorly ordered coal are more difficult to break.

2.2.6.4 Influence of temperature

Cham et al.[40] studied the effect of temperature on the rate of carbon dissolution from two Australian cokes and compared them with results from synthetic graphite. It was found that the temperature has a strong effect on dissolution rates of cokes, as temperature increases, the rate of carbon dissolution increases (see **Figure 2.27**). The apparent activation energies of dissolution for synthetic graphite was 54 kJ/mol while for the two cokes was 479 and 313 kJ/mol. It was found that the activation energy obtained for the dissolution of two cokes was far larger than for graphite. The apparent dissolution rate constant for synthetic graphite was 16.68×10^{-3} s^{-1} at 1450°C and 20.74×10^{-3} s^{-1} at 1550°C and the apparent rate constant for two types of coke was significantly lower than that for graphite.

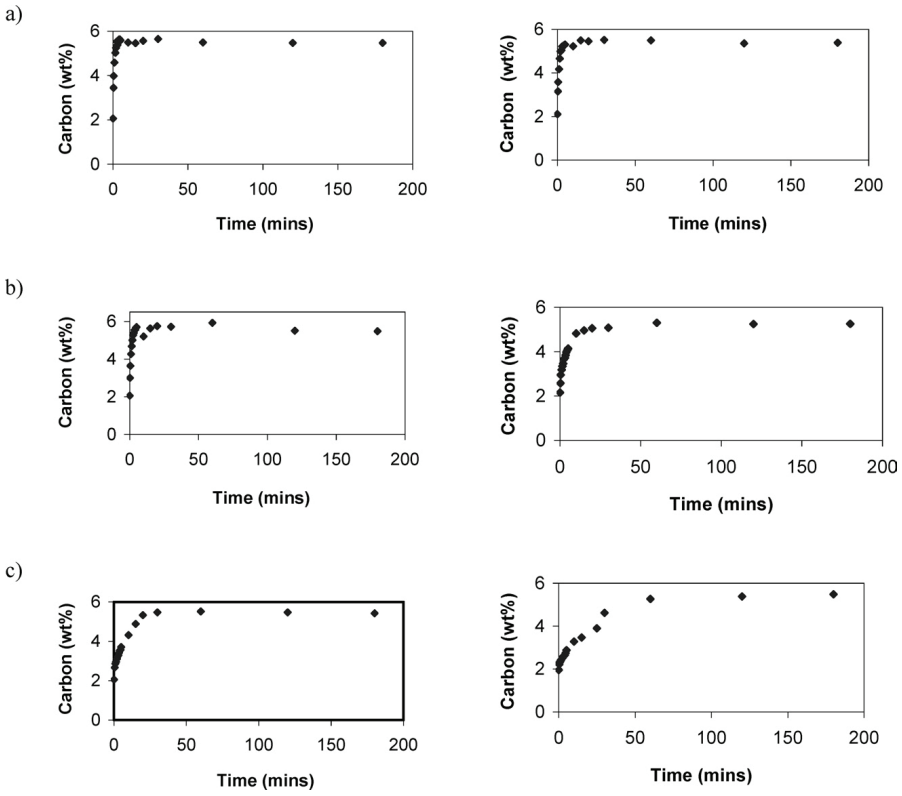

Figure 2.27: Change in carbon content at 1550°C(left) and 1450°C(right) for (a) synthetic graphite, (b) coke 1 and (c) coke 2 [40].

Jang et al.[44] studied the effect of temperature on the dissolution rate of coke in molten iron in the temperature range of 1450-1650°C. It was found that the dissolution rate of cokes increased as temperature increased. The apparent activation energy of the carbon dissolution of coke in iron was estimated to be 442 kJ/mol.

2.2.6.5 Influence of carbon porosity

Contradictory observations have been reported in the literature on the effect of carbon porosity on dissolution rate. Kayama et al.[65] observed that coke with lower porosity has a higher rate of dissolution. On the contrary, Mourao et al.[39] reported that coke with high porosity exhibit higher dissolution and further suggested that higher porosity offers more

surface area for reaction and its effect seems to be more significant in the initial period of dissolution. Depending on the hydrodynamic condition of the bath, liquid metal penetrates the pores and thus, a larger surface area will participate in the reaction. At the later stage, the liquid metal may be trapped in the pores and tend to get saturated by carbon. This will make the inner surface area relatively ineffective.

2.2.6.6 Influence of inorganic matter

Coke and coal generally contain ash, which is composed of different oxide or mineral materials. The existence of these components will affect, to some extent, carbon transfer from the solid surface into molten iron.

Gudenau et al.[52] investigated the dissolution rates of different cokes in the iron carbon melts. It was found that the dissolution rates of cokes were less than of pure graphite and it was because of the ash content of the cokes. Ash formed a film on the coke surface, reducing the total surface area for carbon dissolution. The presence of Fe_2O_3 was found to be favorable for dissolution. CaO, SiO_2, MgO and Al_2O_3 was found to reduce the dissolution of carbon. It was also noted that by controlling the ash composition of the coking coal, the ash fusion temperature and the carburizing ability of cokes could be modified.

Major constituents of the inorganic matter in coke are alumina and silica [66]. Iron oxides, calcia and other oxides are the rest of inorganic component. Ash in carbonaceous materials can affect the dissolution of carbon in liquid iron by blocking the surface [39, 52]. It was also found that calcium oxide (CaO), aluminum oxide (Al_2O_3), silicon oxide (SiO_2) and magnesium oxide (MgO) reduced the rate of coke dissolution in iron by forming an interfacial slag layer [39, 52, 67, 68].

Wu et al.[69] studied the dissolution reaction of natural and pure graphite with electrolytic pure iron. It was found that iron interacts differently with natural and pure graphite and the cause of this behavior was the presence of ash in natural graphite. It formed an interfacial layer which partially blocked the contact area between natural graphite and iron and decreased the dissolution rate of carbon as shown in **Figure 2.28**.

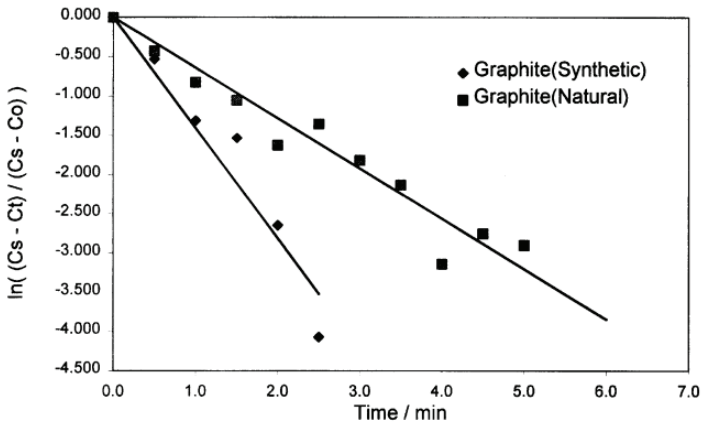

Figure2.28: Influence of ash content on dissolution of carbon from synthetic graphite [69].

McCarthy et al.[70] investigated the interfacial reactions occurring between coke and liquid iron at a temperature of 1550°C. Results showed that the transfer of carbon and sulfur were limited because of the presence of ash in coke. It was suggested that the combination of carbon consumption and poor transfer rates were the most important factors. It was also found that the iron oxide and silica reduction took place in the interface decreasing the carbon dissolved in metal.

Wu[55], found from **Figure 2.29** that the carbon dissolution rate constant decreased with increase of ash content for graphite and coal. The apparent rate constant (K′) was altered significantly for graphite but not for coal. It was also mentioned that the significant difference in dissolution rate constants between graphite and coals could not be simply interpreted by the "surface ash blockage" mechanism since regardless of higher solid ash percentage in natural graphite, carbon can dissolve about 4 times faster from natural graphite than from coke with the same amount of ash.

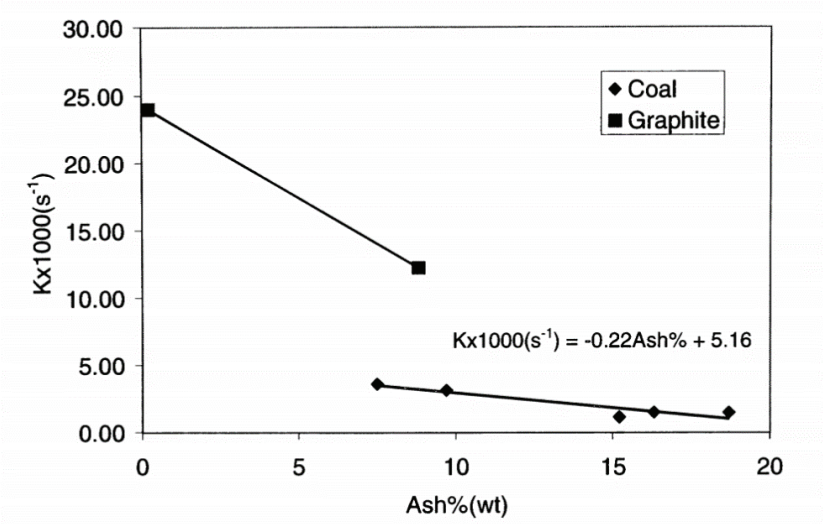

Figure 2.29: Dependence of overall carbon dissolution rate constants of coal and graphite on their ash content[55].

Cham et al.[71] also studied the influence of mineral matter of two types of coke (one with 9.7 wt% ash and the other with 12.3 wt% ash) on carburization rate in molten iron at two different temperatures, 1450ºC and 1550°C. The coke with lower ash content showed a much higher dissolution rate ($K'=14.7\times10^{-3}$ s^{-1} in compare with the other coke with $K'=1.1\times10^{-3}$ s^{-1}). X-ray analyses for low ash content coke identified iron to be in close association with sulfur. Fe/S species have atomic ratio similar to pyrrhotite ($Fe_{1-x}S$) or troilite (FeS). Pyrrhotite in coke can decompose to produce gaseous sulfur and metallic iron which can be carburized to form Fe-C particles. These Fe-C particles would lead to carburization of molten iron. It was concluded that the fine details of mineral matter can play an important role and influence the kinetics of carbon dissolution from cokes.

Bandyopadhyay et al.[41] studied the effect of different physical and chemical characteristics of five types of carbon sources on dissolution kinetics in liquid iron bath at the temperatures range from 1550-1650ºC. It was found that the ash content in the carbon material plays an important role on the dissolution kinetics, but volatile matter did not show any effect on the dissolution process. It was also found that the pet coke with the lowest amount of ash (0.24%) showed the highest dissolution rate while the dissolution rate for nut

coke, with the highest amount of ash, was the lowest as shown in **Figure 2.30**. Dissolution rate of graphite, charcoal and coal fall in between in decreasing order.

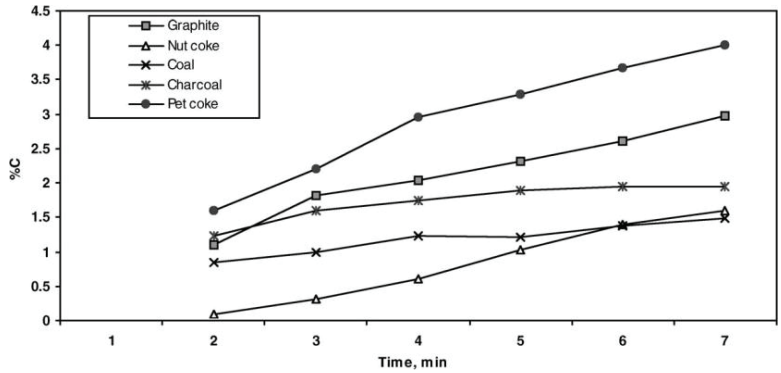

Figure 2.30: Carbon concentration of bath against time for different forms of carbon at 1600°C [41].

Ohno et al.[63] investigated the dissolution rate of four different types of charcoal (Japanese oak, Japanese bamboo, German oak bark and German oak trunk) with different ash content in molten iron at a temperature ranging 1300-1450°C. It was found that the charcoal with higher amount of ash content (German oak bark) showed a lower dissolution rate. Existence of ash in charcoal would prevent the contact between carbon and iron.

In a study of Cham et al.[60] carbon dissolution rates of two different cokes from coals of similar rank, ash yield and carbon crystallite structural parameters were determined. It was found that the apparent carbon dissolution rates were 14.7×10^{-3} s^{-1} and 1.1×10^{-3} s^{-1} and the significant difference was because of the mineral matter and the variation in its composition. It was found that the iron oxide available in coke, would be reduced with the solute carbon in melt and consequently reduces the carbon amount in the melt. It can also be converted to metallic iron and it would be difficult for iron oxide to be a fluxing agent because the iron is not present as iron oxide. Iron can also be in the form of FeS which may influence chemical reactions occurring at the coke/metal interface.

Jang et al.[44] studied the dissolution rate of coke in molten iron at three different temperatures, 1450, 1550 and 1650°C. As it is shown in **Figure 2.31**, it was found that there were two reaction stages at 1450°C. Initially there was a sudden increase of carbon content, and then the dissolution rate suddenly decreased and had a constant value. It was believed that the formation of ash layer on the surface of coke reduced the free surface for reaction. It was stated that at 1450°C, the rate-determining step changed from the mass transfer to the interfacial chemical reaction as the reaction proceeded.

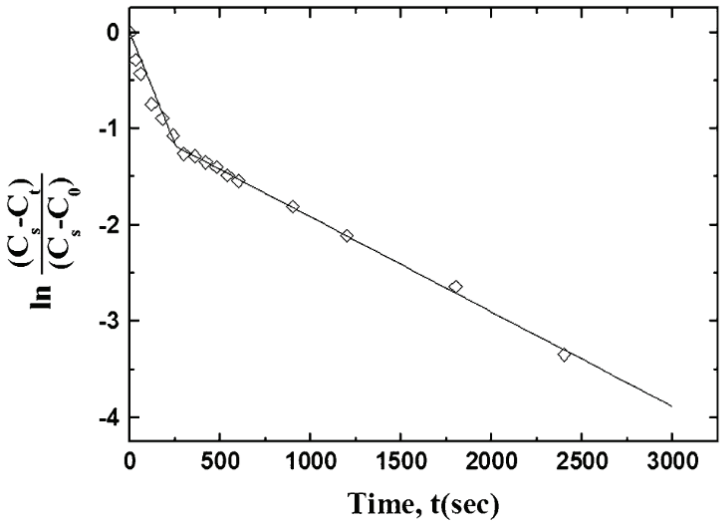

Figure 2.31: Plots of $\ln[(C_s - C_t)/(C_s - C_0)]$ with respect to time for the carburization from coke to molten Fe-2%wt C alloy at 1450°C[44].

Khanna et al.[36] in a study of char dissolution in liquid iron identified similar trends as Jang et al.[44] in the dissolution rate and divided the data into two periods covering the initial period of carbon dissolution and a latter period. It was proposed that the two stages behavior was caused by the deposition of CaO at the char-iron interface, blocking metal contact and subsequent carbon dissolution from the char. Chapman [45] also found that dissolution of cokes in the iron melt have two stages at three different temperatures, 1450,1500 and 1550°C. The dissolution rate of coke at the first stage (<40 minutes) was

higher compared to second stage and the reason was forming ash mineral layer after 60 minutes.

The above mentioned investigations show that ash, i.e. inorganic matter, influences carbon dissolution rates. This suggests that the rate limiting step for carbon dissolution from non-graphitic materials may be different to the rate limiting step that governs carbon dissolution from pure graphite. That is to say, the rate controlling step for carbon dissolution from non-graphitic materials, such as cokes, may not necessarily be mass transport of dissolved carbon from the interface to the bulk liquid iron.

The role of the inorganic matter in coke on coke dissolution rates is still ambiguous and has not been fully investigated. The knowledge that coke inorganic matter composition can appreciably alter the carburizing ability of the coke adds complexity to the role of ash during carbon dissolution. For example, the interfacial products formed at the carbon/iron interface and its chemical and physical properties (such as the interfacial tension and viscosity) depends on the bulk inorganic matter composition.

2.3 Wetting

In the dissolution process, the interaction of metal and carbon materials is important, because a large part of the dissolution reactions take place between liquid metal and solid carbon. It is believed that the interaction depends on the contact angle between the metal and carbon, and overall a good wetting between them is needed.

2.3.1 Principle of wettability

Figure 2.32a and **Figure 2.32b** show a sessile drop of liquid (L) resting in equilibrium on a flat horizontal solid surface (S) in a gaseous environment (G). The profile adopted by the liquid drop is a consequence of the balance between surface forces and the gravitational forces. The surface forces tend to minimize the free surface energy of the system by forming a sphere while gravitational forces tend to flatten the drop. The contact angle, θ, can be

defined as the angle between the liquid phase and the solid surface. It is hence the tangent to the liquid surface at point A i.e. the point of the three phases contact. When $\theta > 90°$, the system is non-wetting. However, wetting of the solid by liquid is said to be achieved when $\theta < 90°$. At $\theta = 0°$, complete wetting is achieved. According to young's **Equation 2.28**, the tension forces at point A are related to the contact angle by:

$$\boldsymbol{cos\,\theta = \frac{(\gamma SG - \gamma LS)}{\gamma LS}} \qquad \textbf{2.28}$$

Where

- θ is the contact angle.
- γSG is the surface tension between solid and gas phases.
- γLG is the surface tension between liquid and gas phases.
- γLS is the interfacial tension between liquid and solid phases.

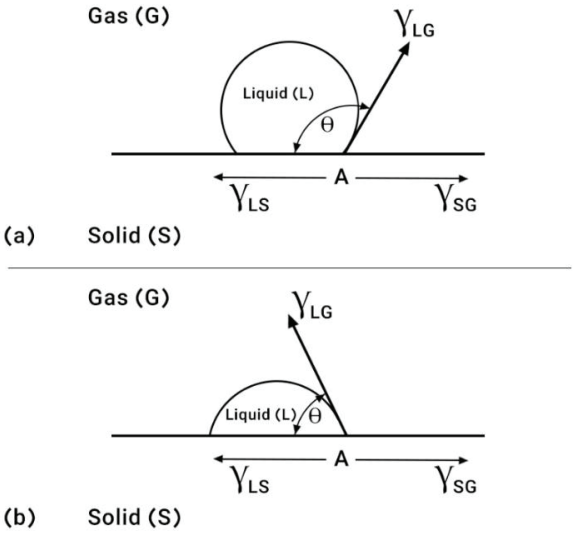

Figure 2.32: The relation at equilibrium between the respective surface tensions and the contact angle (a) Liquid on solid (Non-wetting condition), (b) Liquid on solid (Wetting condition)[1].

It is important to note that the Young's equation was derived under the assumption that the solid to liquid contact is perfectly smooth, flat and rigid.

In non-reactive wetting systems [72], the nature of the solid surface is not significantly changed by its contact with the liquid phase. Such systems are characterized by rapid kinetics of wetting and the contact angle's weak dependence on temperature. In contrast, chemical reactions at the solid/liquid interface can occur in reactive systems. The reactive system's wetting behavior can vary with both time and temperature as a result of the new phase/product formed at the interface. The interfacial product can influence the wettability as a result of the associated free energy change.

It is clear from the above discussion that the wettability of a solid by a liquid is governed by the interfacial energies and Gibb's free energy change, in the case of reactive systems. Interfacial energies are sensitive to environmental factors and small changes in temperature, chemistry of the wetting system and gaseous atmosphere can lead to changes in contact angle. Some of these factors are discussed below.

2.3.2 Chemical reactions

Two chemical interactions can take place during wettability, namely adsorption and chemical reaction [16]. During any chemical interactions at the solid/liquid interface, the system is in non-equilibrium state. The contact angle will change in accordance with changing interfacial energies until equilibrium is attained [73].

If the nature of the chemical interaction in the system is solely adsorption, then surface active species migrate to the two-phase interface. There is no mass transfer of the surface active species across the interface [74]. The time to attain equilibrium depends on the diffusion rates of the active species to the surface.

The chemical potentials of the solid, liquid and gaseous phases are not equal in systems where chemical reactions occur. Chemical reactions at the solid/liquid interface involve mass transfer of components across the interface. This can result in the formation of a new phase at the interface, dissolution of the substrate (or some component in the substrate) or dissolution of the liquid (or some component of the liquid) into the substrate. The interfacial

reactions contribute to the system free energy change and therefore affect the dynamic contact angle [75].

2.3.3 Influence of interfacial tension

The contact angle generally decreases with increasing temperature [76], that is a higher temperature gives a better wetting. The magnitude of the change in wetting is dependent on the type of system under consideration. For example, in non-reactive systems, wettability is mainly due to the changes in surface tension of the liquid as it varies with temperature. In reactive systems, the temperature dependence may be of greater significance as it can influence chemical interactions and free energy changes as well as surface tension.

Temperature has a strong effect on the surface tension of the liquid phase and on surface active species. In general, the surface tension of pure materials decrease with increasing temperature [77]. The surface tension of pure Fe is high, about 1.8 Nm^{-1} at 1550°C which is 25 times larger than that of water [78] and decreases with increasing temperature.

The presence of surface active elements such as S and O alter the energy at the interface and hence contact angle [76-78]. Surface active elements would change the surface tension with increasing surface activity. In general, the surface activity of surface active specious decreases with increasing temperature [76]. Takiuchi et al.[79] showed that the surface activity of oxygen decreases with an increase in temperature. Non-metal elements such as those from the VIA group in the periodic table, are highly surface active in liquid iron and their addition causes a large decrease in surface tension [78]. Jimbo et al.[80] summarized the data obtained from prior investigators. It was shown that all the authors found that with increasing activity of sulfur, the surface tension decreased.

The density and surface tension of liquid Fe-Mn alloys were studied using sessile drop method at 1550°C by many researchers, e.g. Lee [81] and Lida [82]. It was found that the density and surface tension of liquid Fe-Mn alloys decreased with increasing Mn content.

2.3.4 Influence of surface topography

As it was mentioned earlier in the current section, Young's equation was derived under the assumption that the solid to liquid contact is perfectly smooth, flat and rigid. In many practical situations, the surface cannot be completely smooth. It can result in a deviation in the contact angles obtained from experiments and that obtained from Young's equation. If it is assumed that true surface area is α_T and apparent area is α_A, then usually $\alpha_T > \alpha_A$ without gas trapped in interface. Wenzel [83] derived a simple relation based on the consideration of the effect of change in surface energy due to different surface roughness.

$$\cos\theta_R = R\ \cos\theta_S \qquad \textbf{2.29}$$

Here R (R≥l) is the roughness factor, defined as α_T/α_A; θ_R and θ_s are contact angles on rough surface and on a perfectly smooth surface. The contact angles will decrease with an increase in the roughness for a wetting system. For non-wetting systems, the contact angle will increase with increasing roughness. This simple model has been found to be useful in capturing experimentally observed influence on the contact angle for simple roughness topography and for well wetting surface where the practical range of the contact angle, θ, is $0^o<\theta<90°$. The more complex case is that where the contact angle lies in the range $90^o<\theta<180^o$. In this case, roughness increase transforms a non-wetting surface into an even more non-wetting one. In practice, however, this model is only used for wetting surfaces ($\theta<90°$), because, by the rough non-wetting surfaces the liquid cannot wet all the surface due to the presence of air pockets; then the main requirement of the Wenzel model, the complete wetting, would not be fulfilled [84].

Cassie Baxter model [85] is shown as **Equation 2.30** where φ is the area fractions of solid and air under a drop on the substrate. θ_R and θ_S are contact angles on rough surface and smooth surface respectively. Porous surfaces in contact with liquids are formed by a solid fraction and air filled pores. One can say that the surface roughness is saturated with air [84]. This equation simply indicates the contact angle can be increased even when the intrinsic contact angle of a liquid on the original smooth surface is less than 90°.

$$\cos\theta_R = \varphi(\cos\theta_S + 1) - 1 \qquad \textbf{2.30}$$

Besides the Wenzel roughness R and the solid fraction φ, the theories of Wenzel and Cassie-Baxter are essentially independent of the geometric characteristics of roughness, i.e. the shape of the pores. While the liquid penetration into a porous surface by capillary forces does not occur, wetting is usually associated with the regimes of Wenzel or Cassie-Baxter. Normally it is assumed that if $\theta < 90°$ Wenzel model is met, while if $\theta > 90°$ the Cassie-Baxter model is met. The experimental results, however, sometimes show that this criterion is not completely correct [84].

Ciftja [22] studied the wetting behavior of molten silicon with graphite materials with different surface roughness. Here the graphite will be transformed to SiC at the surface. As depicted in **Figure 2.33**, when the surface is smooth (R_a<0.1µm), the final contact angle for all the graphites is about 30°. As the surface becomes rougher, the final contact angle decreases, and it can reach even zero. In that case the silicon is absorbed completely by the graphite materials.

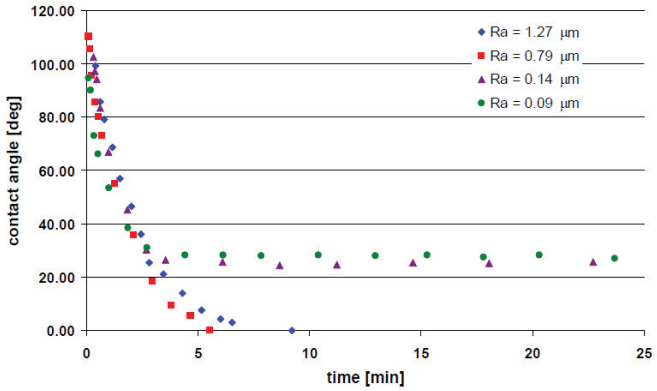

Figure 2.33: Contact angles of molten silicon versus time graphite substrates with different surface roughness[22].

2.3.5 Influence of crystallite size

There is little literature on the influence of crystallite size of carbon materials on the wettability. Khanna et al.[86] studied the effect of structure on the initial wettability of carbons by liquid iron at 1550°C. No well-defined trends were observed with L_c values. Wide variations were observed in contact angles for chars possessing very similar L_c values.

Due to the likelihood of structure evolution and changes in particle morphologies, no comments however were made regarding the influence of structure on contact angles over prolonged periods of contact.

Cham [16] did not observed any correlation between the crystallite size of the cokes and their wettability with iron at 1550°C. It was also stated that the crystallite size of nine cokes tested, were similar and therefore the effect of L_c could not be established.

2.3.6 Wettability of carbonaceous materials by liquid iron

Wettability of several carbonaceous materials, e.g., synthetic graphite, natural graphite, coke and coal-chars with molten iron at 1550°C were carried out using sessile drop method by Khanna et al.[86]. It was found that the formation of an ash interfacial layer between carbonaceous material and liquid iron had a strong effect on the mass transfer and interfacial reaction. Wetting results of pure liquid iron with three types of cokes at 1550°C showed a non-wetting behavior for all cokes at the beginning and then a slight decrease in contact angles which was attributed to the transfer of carbon from coke to liquid iron. No correlation was observed between the initial char structure, ash composition and contact angles in the initial stages of contact, but the contact angles were affected by the presence of reaction products and impurity deposits in the interfacial region.

Ohno et al.[87] studied the wetting of liquid iron on synthetic coke (made from graphite and different amount of Al_2O_3 powders) at 1400ºC. As indicated in **Figure 2.34**, the contact angle increased with increasing Al_2O_3 content in the coke. The alumina powder had not only effects on the wettability but also on the reaction between carbonaceous materials and iron as it changed the effective contact area.

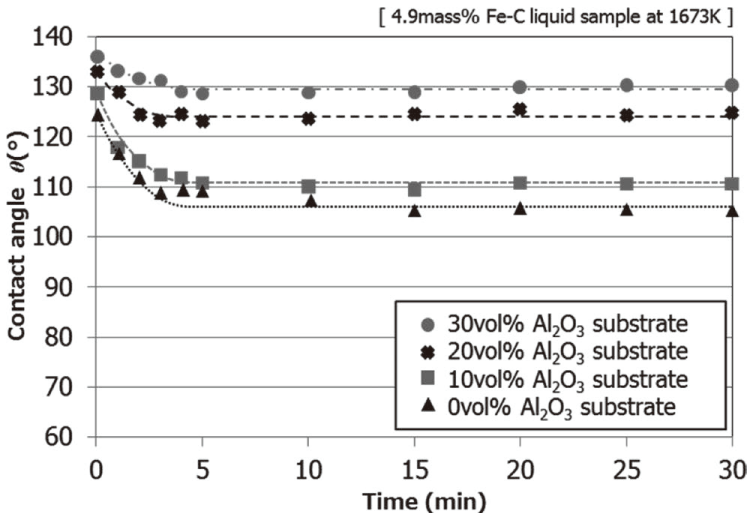

Figure 2.34: Effect of Al_2O_3 content in the simulant coke substrate on wetting of Fe-C liquid sample at 1400°C[87].

Findings from Ohno et al.[87] was in agreement with the results from Zhao and Sahajwalla [88]. The contact angle variations with time of electrolytic iron on the composite substrates are shown in **Figure 2.35** and it can also be seen that with adding alumina to the graphite substrates, the wetting decreased. It was found that the dissolution of carbon in iron is very quick and the carbon content reached 5.62 % after 2.5 minutes which is the saturation content of carbon in this system (**Figure 2.36**).

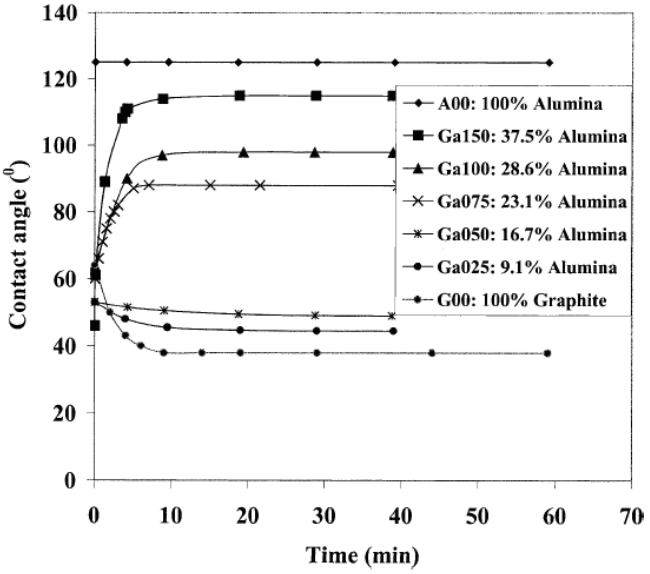

Figure 2.35: Variation of contact angle of iron with time on different substrates at 1600°C[87].

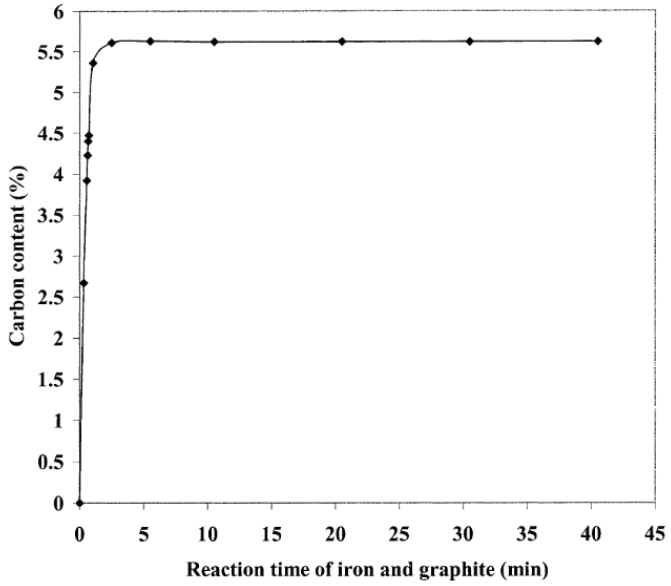

Figure 2.36: Variation of carbon content of iron with reaction time at 1600°C[87].

Monaghan et al.[89] studied wetting of iron on alumina, CA_6($CaO \cdot 6Al_2O_3$),CA_2($CaO \cdot 2Al_2O_3$) and CA($CaO.Al_2O_3$) minerals over the temperature range 1450 to 1550°C. It was found that the effect of temperature was not as significant as the type of mineral in the layer and that the contact angle decreased with increasing calcium content of this mineral as shown in **Figure 2.37a**. It was found that the increased temperature resulted in a slight lowering of the contact angle, indicating an increase in the wetting of the substrate (**Figure 2.37b**). They found it consistent with the expected decrease in surface tension with increasing temperature. It was also believed that it may represent the increased substrate interaction with the droplet.

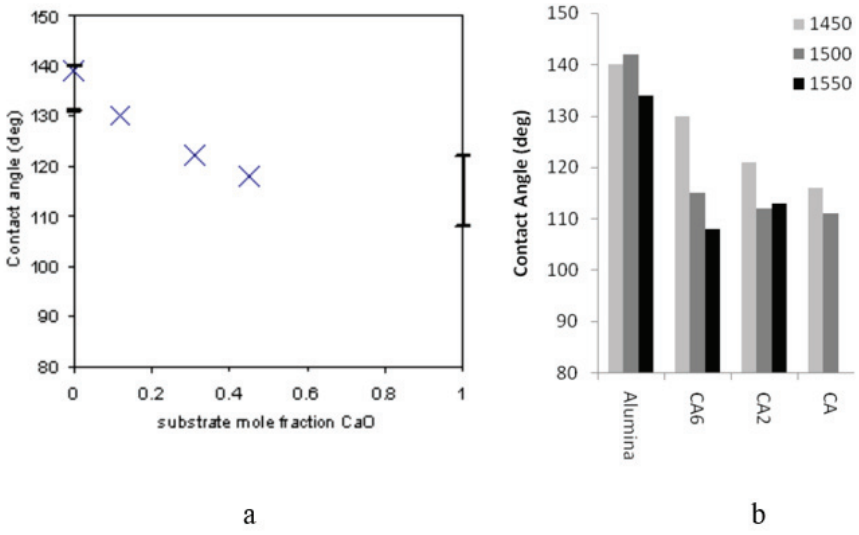

Figure 2.37: a) The influence of substrate on contact angle at 1450°C(vertical bar shows the range of contact angle in different literature) b) Contact angle measurements of Fe-5%[C] melt on different substrates at different temperatures [89].

Wu and Sahajwalla [90] studied the influence of carbon and sulfur content of the melt on the wettability of pure graphite using sessile drop technique. **Figure 2.38** shows how contact angle changes with time.

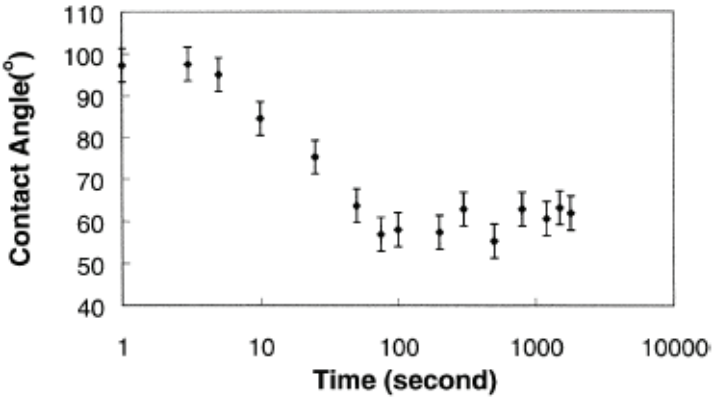

Figure 2.38: The variation of the contact angle with time in the sessile drop experiment for a melt/graphite assembly [90].

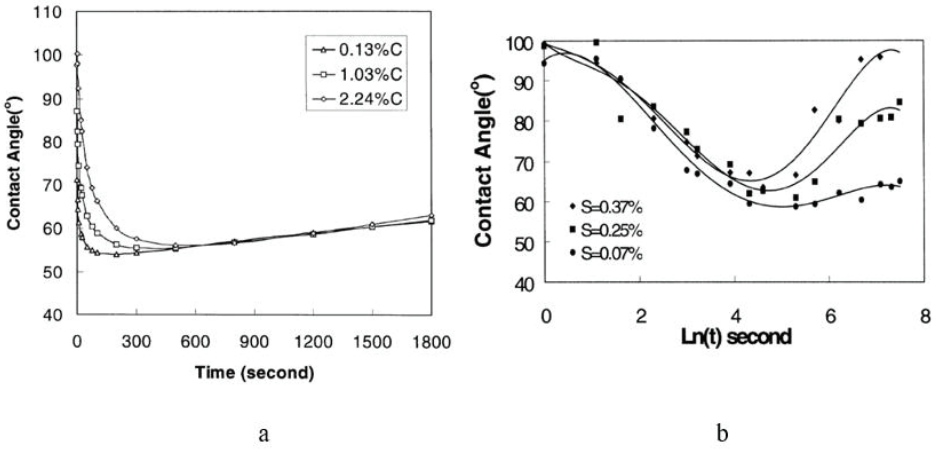

a b

Figure 2.39: The dynamic wetting process for the Fe-C-S melt on the graphite substrate a) (sulfur < 0.02 pct) b)with different sulfur concentration(C pct=2.0) [90].

It was found that the mass transfer between the liquid drop and solid graphite has a significant influence on wettability. As indicated in **Figure 2.39a**, with decreasing the initial carbon content of metal, wettability increased. It was suggested that the increase in chemical potential difference could be directly responsible for the decrease in initial interfacial energy and therefore, the increased wettability. As **Figure 2.39b** shows, it was also found that the

adsorption of sulfur from the melt to the melt/carbon interface increased the contact angle and decreased the wettability. Wu and Sahajwalla [90] attributed this trend to sulfur adsorption at the interface and its effect on the iron/graphite interfacial tension. However, the influence of sulfur on the melt/graphite can only be seen after the potential difference becomes negligible and the system approaches equilibrium.

In another study, Wu et al.[69] investigated the wettability of natural graphite containing 8.8 pct ash with electrolytic iron at 1600°C. It was found that the formation of interfacial layer (which was observed by a field emission scanning electron microscope (FESEM)) blocked the contact between the droplet and natural graphite and caused a decrease in the rate of carbon and sulfur transfer, and subsequently decrease the wettability at the interface as shown in **Figure 2.40**. Comparing **Figure 2.38** and **Figure 2.40** indicates that the wetting behavior of graphite/iron system and natural graphite/iron is completely different which indicates that the interactions involved in the two systems are very different.

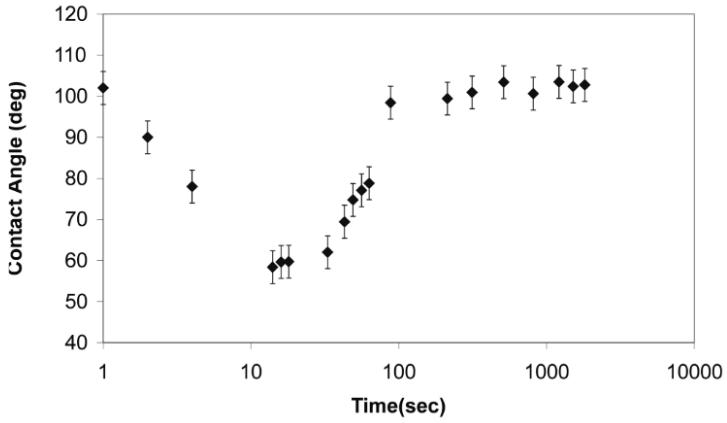

Figure 2.40: Change of contact angle with time for iron on natural graphite substrate [69].

As shown in **Figure 2.41**, Wu et al. [69] investigated the surface of carbon after reaction with molten iron, and found that alumina and calcium oxide layer were initially formed, after 10 minutes, Fe-Ca and S complex phases were formed and 30-60 minutes later, 50% of the carbon surface was covered by an ash layer.

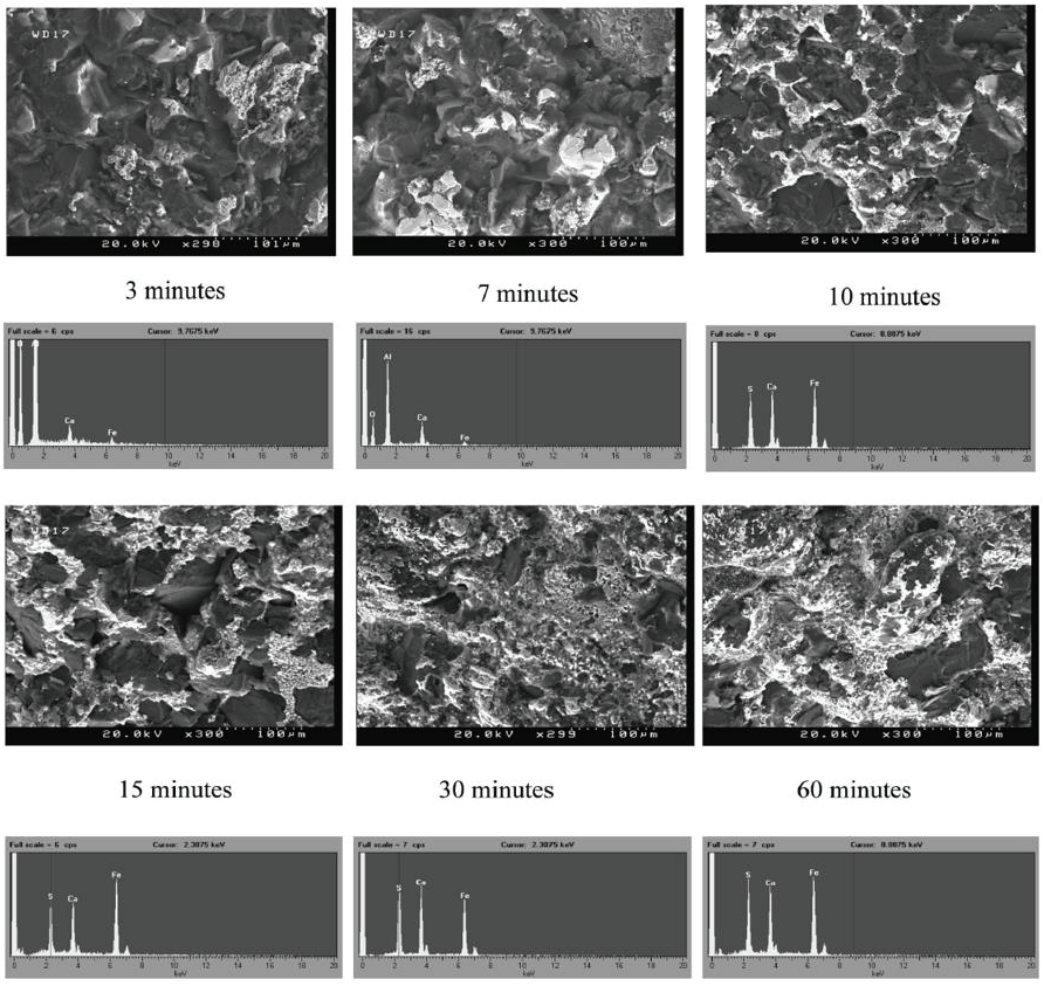

Figure 2.41: Image shows the formation of interfacial layers between electrolytic iron (99.8 pct Fe) and natural graphite (8.8 pct ash) at 1600°C after contacting for different time intervals [69].

Cham [16] investigated the wettability of different types of coke with iron at 1550°C. All cokes showed non-wetting behavior, although improvements in wetting occurred over time. Authors suggested that it is possible for a number of reactions to occur simultaneously at the interfacial region that could affect the wettability of coke by molten iron. The two main factors identified were:

1- Transfer of carbon and sulfur across the interface: The initial decrease in contact angles was likely due to carbon transfer into the liquid iron and sulfur is a surface active element.
2- Formation of an interfacial layer: The formation of an interfacial layer changes the chemistry of the substrate locally and an interfacial layer rich in certain products, such as CaS, may act to reduce the contact angle.

Cham[16] compared the interfacial products which was formed at the underside of the iron drop after contact with two different cokes after 30 minutes. One coke contained more S and Mn at the interface compared to other coke. As shown in **Figure 2.42**, the interfacial product formed with coke with lower Mn and S content had a network or mesh like structure that seemed to wet the iron droplet much better than the interfacial product formed with the one with higher amount of Mn and S. The slow carbon dissolution rate observed for coke with lower S and Mn content could be caused to some extent by this mesh like structure, which would block liquid iron from coming into contact with carbon. The interfacial product formed with higher amount of Mn and S lacked the mesh or network like structure. Instead, there were Fe globules and discrete interfacial products, which would allow liquid iron to freely come into contact with carbon. However, it was found that after 2 hours of contact the interfacial products observed were similar in morphology and composition.

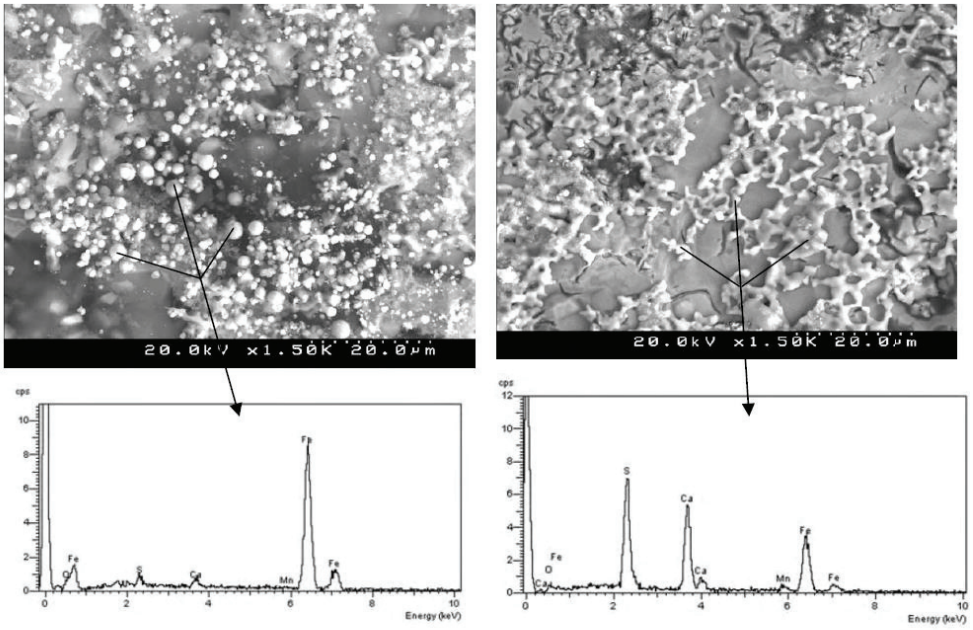

Figure 2.42: Comparison of the interfacial products formed after 30 minutes of contact with a) Coke with higher amount of S and Mn and b) Coke with lower amount of S and Mn at 1550°C[16].

Khanna et al.[36] studied the wettability of four chars with liquid iron at 1550°C. The behavior of chars seemed to be very different compared to graphite. Chars showed very high contact angle (~120°) and thus less wettability in comparison with graphite. They stated that carbon and sulfur which transfer to the interface, participate in the formation of interfacial layer. Accumulation of alumina was also found for all chars and it decreased the dynamic wettability of chars with molten iron due to the reduction of contact area between them.

Sun et al. [51] studied the wetting behavior of iron droplet with and without initial carbon content and graphite. It was found that the contact angle of iron on carbon with 0% initial carbon was 59° at 1500°C, while that of sample with 4.8 wt% carbon was 118° which is about twice as large as that for a 0% carbon content.

Wu et al.[35] investigated the wetting behavior of natural graphite with liquid iron at 1600°C using the sessile drop technique. They observed a decrease in contact angles (from ~100° to ~60°) along with a rapid increase in the carbon content in the metal droplet within the first

10 seconds of reaction. Thereafter, the carbon content in the melt was observed to slightly decrease and the contact angles were observed to increase from ~60° to ~100° within approximately 2 minutes of contact and then stabilize for the rest of the reaction times.

In another study of Wu et al.[35], the influence of wettability on carbon dissolution for coal was investigated. It can be seen from **Figure 2.43** that the dissolution rate constant of coal chars shows a relatively minor dependence on their wettability. On the other hand, a stronger dependence of the carbon dissolution rate constant on wettability was found for graphite. Authors suggested that the rate of carbon dissolution from graphite depends more on the area available for the carbon transfer, however, rate of carbon dissolution from coal char depends less on the area available for the carbon dissolution. This implies that carbon dissolution from graphite is controlled by mass transfer in liquid. On the other hand, they found it reasonable to assume that coal char dissolution is controlled by a more complex mechanism in addition to liquid mass transfer.

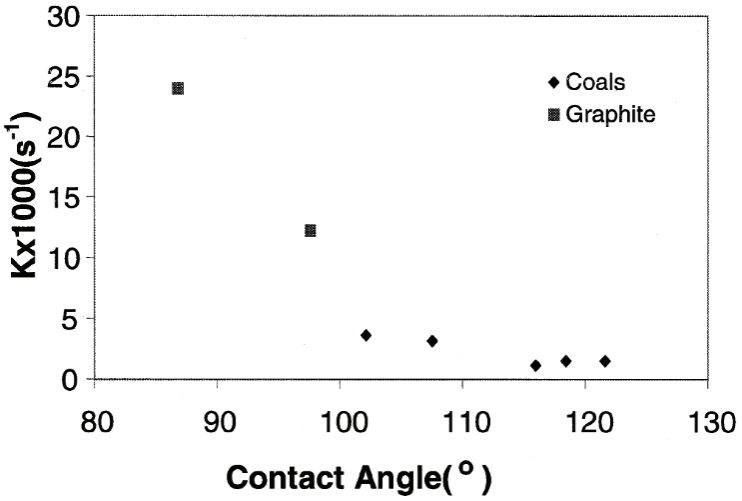

Figure 2.43: The relationship between wettability and carbon dissolution rate constant of different carbonaceous materials [35].

From the above investigations, it is clear that reactions taking place at the interface can significantly influence the wettability of the system. The system of interest in this study is rather complex since coke is a heterogeneous material. Aspects such as coke inorganic matter composition and yield, the non-graphitic nature of carbon in coke and the sulfur

content in coke need to be considered. All this in combination with liquid iron can lead to the possibility of many reactions occurring at the interface and could explain the greater contact angle in cokes. Apart from carbon dissolution, reactions with coke inorganic matter and mass transfer of sulfur across the interface can occur.

2.4 Summary of literature review

Table 2.2 shows a summary of previous studies on the dissolution rate of different carbon materials in metal.

Table 2.2: Summary of studies on the dissolution rate of different carbon materials in metal (*MT is mass transfer control and **IR is Interfacial reaction control).

Reference	**Metal**	**Carbon material**	**T (°C)**	**k cm/s**	**E_a kJ/mol**	**K´ 1/s**	**Rate controlling mechanism**
Olsson et al.[32]	Fe-C	Graphite	1470 1640	1.30×10^{-2} 3.40×10^{-2}			MT*
Kosaka and minowa[33]	Fe-C	Graphite	1270 1550	1.06×10^{-3} 8.45×10^{-3}			MT
Wright and Baldock [47]	Fe-C	Graphite	1450 1550	12×10^{-2}			MT
Wu and Sahajwalla[35]	Fe-C-S	Graphite Coals	1550			2×10^{-2} 1×10^{-3}- 4×10^{-3}	MT Mixed
Zhang et al.[43]	Fe	Graphite	1450 1500		51.4	4.3×10^{-4} 4.8×10^{-4}	MT

			1550			5.2×10^{-4}	
Jang et al.[44]	Fe	Coke	1450 1550 1650		442		At 1650: MT At 1450: IR**
Mourao et al.[39]	Fe-C	Graphite Coke	1580 1572	1.82×10^{-2} 2.31×10^{-2}			MT Mixed
Wright and Taylor[34]	Fe-C	Graphite Pet coke	1450	1×10^{-1} 3×10^{-3}			
Khanna et al.[36]	Fe	Coal char	1550	1.8×10^{-3}- 2.8×10^{-4}			Mixed
Sun[46]	Fe-C	Graphite Coke	1500 1600	2.9×10^{-3} 1.43×10^{-2}	40		MT
Cham et al.[60]	Fe	Graphite Coke	1550		313,479	2.1×10^{-3} 1.5×10^{-2}	
Bandyopadhyay[41]	Electrolytic iron	Graphite Charcoal Pet coke	1600	4.96×10^{-3} 2.5×10^{-3} 1.08×10^{-4}	42		MT
Wu[55]	Fe-C-S	Graphite Coke	1550			24×10^{-3} 6.89×10^{-3}	MT

Olivares[56]	Fe-C-S	Graphite Coke	1350-1650		78.9	7.8×10^{-3} 2.3×10^{-4}	
Orsten and Oeters[58]	Fe-S	Graphite	1470-1625		78		

There is no data on the dissolution kinetics of different carbon materials in Fe-Mn alloys. The main literature used is hence for other metals and alloys, specifically iron, which is close to the Mn/Fe alloys. It is clear from previous studies that two steps could be the rate limitation for carbon dissolution from carbonaceous materials into molten iron:

- Liquid side mass transfer
- Interaction at the solid/liquid interface

It is generally agreed that the dissolution of graphite into molten iron is controlled by rate of mass transfer in liquid side in all situations. However, the dissolution of non-graphite sources into molten iron was assumed to also be influenced by interaction at the solid/liquid interface. Several hypotheses have been proposed including the influence of structure, the influence of inorganic matter and changes in wetting properties of the carbonaceous material.

The influence of coke structure on the dissolution rate in hot metal, both on an atomic and macro-scale, has been studied. On the atomic scale, the influence of crystallite size on carbon dissolution has been mainly focused on cokes[49, 91]. There is little in the literature on the influence of carbon porosity and roughness in the coke and even less on their effects on dissolution rates.

Graphite dissolution rates show a slight increase with increases in temperature and its activation energy ranges from 38 kJ/mol to 90 kJ/mol. The variations are likely to be a consequence of the different experimental techniques employed by the different research groups. In addition, the small activation energy value for graphite dissolution is in agreement with a diffusion limited mechanism. This may not be the case for other carbonaceous materials such as cokes.

Sulfur could retard the carbon dissolution rate of both graphite and non-graphite sources in molten iron by different mechanisms. For graphite sources, the decrease in dissolution rate is due to the decrease in dissolution coefficient and solubility of carbon in liquid iron. For non-graphite sources, it was suggested that the decrease of dissolution rate was not only affected by depression of carbon dissolution coefficient in liquid iron, it was also due to the reduction of interfacial area by either surface blockage or poor wetting for melts containing sulfur.

Carbon dissolution research from coke shows that inorganic matter affects the dissolution rate by forming a physical barrier at the carbon / iron interface. There are different opinions on how mineral matter in cokes may affect the dissolution rates. The melting point of ash in non-graphite carbon sources was seen to have significant influence on carbon dissolution.

While taking into account influence of wettability on carbon dissolution, it could be assumed that the wetting of the solid carbon by liquid iron plays an important role in determining the rate of carbon dissolution since wetting is the first step for the melt to obtain carbon atoms for dissolution. There is very little data on the effect of wettability on the dissolution rate of carbon in metal.

Wettability could be characterized by the contact angle. An increase in carbon content, a decrease in sulfur concentration and a decrease in temperature are reported to increase surface tension of molten iron, which in turn influences wettability. Previous researchers are generally agreed that wetting in based on the three forces balance along the solid liquid interface. Interfacial reactions, surface tension and surface topography seemed to have some effects on the wettability.

3 Experimental apparatus, procedures and model description

In the current investigation, carbon dissolution experiments and wettability experiments were conducted in parallel in order to establish an understanding of the mechanisms which influence carbon dissolution from carbonaceous materials into molten Fe-Mn alloys. For the carbon dissolution study, immersion rod method was used in a resistance furnace. Wett ability experiments were conducted in a horizontal tube furnace using sessile drop approach with live wetting image capturing and recording system. X-ray diffraction and Raman spectroscopy were applied to quantitatively determine the ordering in crystal structure of carbonaceous materials. Scanning Electron Microscopy (SEM) and X-ray Energy Dispersive Spectrometer (EDS) were used to study carbon/iron interaction on a microscopic scale. Roughness, porosity and Brunauer–Emmett–Teller (BET, specific surface area) of carbon materials were measured to study how these parameters affect wettability and dissolution rate.

This chapter describes the materials, equipment and procedures used in this study. Results from various characterization techniques of raw materials are also presented.

3.1 Materials

3.1.1 Metallic materials

100 grams of iron manganese alloys with a Mn/Fe ratio of 5.6 and 1.5 were used as solutions made from 99% high purity manganese chips and 99.8% high purity iron, both from Aldrich Chemical Company Ltd. The chips were mixed in an alumina crucible manually. Then the crucible was placed in a resistance furnace and was heated to the defined temperatures. Sulfur was added in the form of iron sulfide, which was also from Aldrich Chemical Company Ltd.

The alloy used in the wetting experiments was heated to 1550ºC at a rate of 20°C/min under continuous argon in alumina crucibles. After the metal melted, time was allowed for thermal stabilization of the bath for 30 minutes and then the furnace was shut down. The crucible

was pulled down to the bottom of the furnace, after cooling to room temperature. A small cylinder was cut from both the alloy (Fe-85%Mn) and pure iron to the weight of 0.35-0.37 g and used as metal droplet in sessile drop experiments.

3.1.2 Carbonaceous materials

Various carbonaceous materials supplied by industry were used for investigating their dissolution and wetting behaviors:

- Graphite (Synthetic graphite, IG-15, manufacturer: Toyo Tanso)
- 6 cokes (Commercial cokes and supplied by industry)
- Charcoal (Eucalyptus charcoal supplied by industry)

In dissolution studies, six different cokes, charcoal and graphite were used as sources of carbon. These are named graphite, charcoal, cokes A to F. Graphite bars were cut from a graphite bulk into 10×15×80 mm rectangular prism. Charcoal rods, 20 mm diameter and 40 mm length and coke rods, 15mm diameter and 30 mm length were prepared. The initial surface area of carbon materials used were hence different. This is due to the fact that for charcoal and cokes, it was difficult to find big enough particles to cut in a defined shape. Hence, large particle size charcoal and cokes were obtained and cut into uniform cylinder shape rods. For graphite, the initial shape was rectangular bulk.

For the sessile drop experiment a substrate of carbon materials with a flat surface is needed to be in contact with the liquid metal drop. The received graphite materials were in the form of blocks and appropriate sections flat surfaces of them were prepared by cutting. The received cokes and charcoals were in the form of lumps and since the physical and even chemical properties of coke and charcoal are not distributed uniformly in the structure, several samples from different lumps were chosen. The carbon materials were cut into slices with 2-3 mm thickness using a diamond wheel with 2 mm thickness at a speed of 10 mm/sec (cutter 1). Then, discs with a diameter of 10 mm were cut with a core drill from the slices. The sessile drop experiments are performed using six carbon materials as substrate materials. These include graphite, charcoal, cokes C, D, E and F.

There are two commonly used ways for reporting the chemical composition of carbon materials; namely ultimate analysis and proximate analysis. An ultimate analysis shows the quantities of carbon, hydrogen, oxygen, nitrogen, sulfur, chlorine and ash in dry carbon. A proximate analysis, which is mostly used, shows the fixed carbon, volatile matter, moisture, and ash contents. Fixed carbon is the quantity of carbon remaining after removing the volatiles and moisture by heating and subtracting the remaining ash. The reported proximate analysis of the cokes and charcoal and graphite is shown in **Table 3.1**.

Table 3.1: Proximate analyses of different carbon materials used (analyzed at SINTEF Molab.).

Property(unit)	Coke A	Coke B	Coke C	Coke D	Coke E	Coke F	Charcoal	Graphite
Fix C (wt%)	88.62	87.49	85.28	89.34	85.57	87.93	83.4	98.6
Ash (wt%)	10.39	11.25	11.82	9.61	13.68	11.42	2.6	0.3
VM (wt%)	0.94	1.26	1.43	1.05	1.35	1.15	14	0.8

The ash residue of the proximate analysis in the coke may originate either from minerals trapped in the coal or minerals that are present as a result of the mining of the coal. The ash analyses of the carbon materials are shown in **Table 3.2**. It can be noted from the two tables that the cokes are quite similar.

Table 3.2: Bulk chemical composition of ash content (dry basis(db)), (analyzed at SINTEF Molab. by XRF).

Carbonaceous material	Ash(%db)							
	SiO_2	Al_2O_3	Fe_2O_3	CaO	MgO	MnO	K_2O	S
Coke A	6.38	3.18	0.8	0.11	0.04	0.01	0.13	0.4
Coke B	5.6	2.79	0.6	0.42	0.22	0.04	0.18	0.48
Coke C	6.97	3.07	0.87	0.66	0.24	0.08	0.03	0.44
Coke D	4.22	2.84	0.83	0.42	0.19	0.1	0.22	0.50

Coke E	7.35	3.96	0.95	0.43	0.09	0.01	0.11	0.63
Coke F	6.29	2.87	0.68	0.39	0.18	0.01	0.23	0.50
Charcoal	0.48	0.09	0.04	0.84	0.26	0.01	0.44	0.05
Graphite*	-	-	-	-	-	-	-	-

**Total ash content of the graphite is 0.3%. Ash composition analysis has not been conducted for graphite.*

The porosity of the carbon materials was determined by Helium Pycnometry. The Helium Pycnometry has been done at UNSW. A caliper was used to measure the volume of the carbon substrate (disc shape) and having the mass of the substrate, the apparent density was calculated. The absolute density was determined using a Micromeritics Accupyc II 1340 Helium Pycnometer. The porosity is given by **Equation 3.1**:

$$\boldsymbol{Porosity} = \left(\mathbf{1} - \frac{\boldsymbol{apparent\ density}}{\boldsymbol{absolute\ density}}\right).\mathbf{100\%} \qquad \mathbf{3.1}$$

The porosity measured by Helium Pycnometry is shown in **Table 3.3.** Three replicates were done for each carbon materials. As **Table 3.3** shows, charcoal has the highest porosity and graphite has the lowest porosity. Among cokes, coke E has the highest porosity and coke C has the lowest porosity.

Table 3.3: The porosity of carbon materials measured by Helium pycnometry.

Carbon material	Absolute density (g/cm^3)	Apparent density (g/cm^3)	Porosity%
Graphite	2.05±3%	1.92±2%	6
Charcoal	1.86±8%	0.27±4%	85
Coke A	1.89±11%	0.94±12%	50
Coke B	1.90±15%	0.93±10%	51
Coke C	1.81±10%	1.01±15%	44
Coke D	1.85±18%	0.96±11%	48

Coke E	1.93±12%	0.85±12%	55
Coke F	1.87±11%	1.009±9%	46

The specific surface area was determined by BET analysis, which is a widely used and established method for solid materials. This method is based on adsorption of a gas on a solid surface at a given pressure. The amount of adsorbate gas corresponding to the monomolecular layer on the surface is then calculated. The physical adsorption is from weak van der Waals forces between gas molecules and the adsorbent solid sample. By a volumetric or continuous flow procedure, the amount of gas adsorbed can be measured. The BET equation as in **Equation 3.2** calculates the specific surface area.

$$\frac{\mathbf{1}}{\boldsymbol{W}\left(\left(\frac{\boldsymbol{P}}{\boldsymbol{P_0}}\right)-\mathbf{1}\right)}=\frac{\mathbf{1}}{\boldsymbol{W_m C}}+\frac{\boldsymbol{c}-\mathbf{1}}{\boldsymbol{W_m C}}\left(\frac{\boldsymbol{p}}{\boldsymbol{p_0}}\right) \qquad \mathbf{3.2}$$

Where W is the weight of gas adsorbed at relative pressure, P/P_0, and W_m is the weight of adsorbate constituting a monolayer of surface coverage. C is the BET constant and is related to the energy of adsorption in the first absorbed layer and its value is an indication the magnitude of the adsorbent/adsorbate interactions [26]. A Micromeritics Tristar 3000 performing BET analyses was used at NTNU to measure the specific surface area of cokes and graphite and charcoal. This apparatus measures surface areas as low as 0.01 m^2/g using nitrogen as the adsorbate. A Micromeritics Tristar 3030 was used at UNSW to measure the specific surface area of cokes and graphite and charcoal. The technique used was nitrogen physisorption with the specific surface area determined using the BET model. Prior to analysis the samples were degassed under vacuum at 150ºC for 3hrs.

The results from BET surface area analysis of all carbon materials are given in **Table 3.4** average values are given from two measurements and show a standard deviation of 7% and less. It can be seen from that charcoal has the highest surface area and graphite has the lowest surface area. There is quite good correlation between the two equipment at NTNU (Run 1) and UNSW (Run 2).

Table 3.4: The BET surface area results for different carbon materials. Means (M) and standard deviation (SD) are also given.

Carbon material	Surface area(m^2/g)		M	SD	SD
	Run1	Run2	(m^2/g)	(m^2/g)	(%)
Coke A	3	3.2	3.1	0.1	3
Coke B	3.4	4	3.7	0.3	7
Coke C	2	2.2	2.1	0.1	4.5
Coke D	3	2.9	2.95	0.05	1.6
Coke E	4.28	5	4.64	0.36	7
Coke F	2.8	3	2.9	0.1	3.3
Graphite	0.33	0.55	0.44	0.35	7
Charcoal	258	265	261.5	3.5	1

Alicona infinite focus 3D optical microscope (**Figure 3.1**) was used at NTNU to measure the surface roughness of carbon materials. The optical system can create three-dimensional surface images which capture color and topographical information and is used to analyze roughness parameters. Keyence VK-X250 Laser Microscope was used at UNSW to measure the surface roughness of carbon materials. The laser system can create three-dimensional surface images.

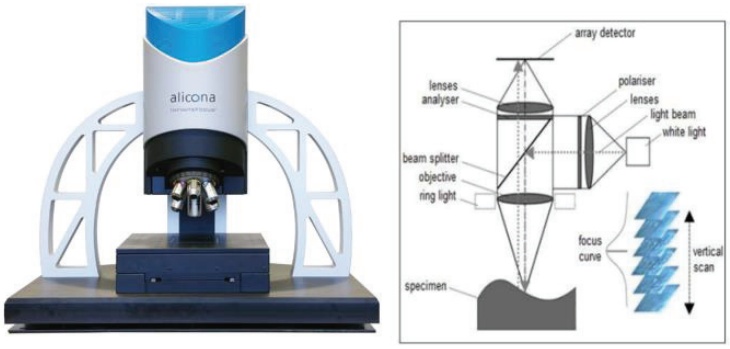

Figure 3.1: Optical focus variation surface measurement instrument (Alicona).

The average roughness is the main height as calculated over the entire measured area, R_a. The average surface roughness (R_a) was measured three times for each carbon material at NTNU. Run 4 was done for some of the samples at UNSW. **Table 3.5** shows R_a for all carbon materials. The average values are given from three measurements and for some samples from four measurements and show a standard deviation of 16% or less. As **Table 3.5** shows, coke E has the roughest surface and graphite has the smoothest surface.

Table 3.5: The measured R_a values for the carbon materials. Means (M) and standard deviation (SD) are also given.

Carbon material	R_a(µm)				M	SD	SD
	Run 1	Run2	Run3	Run4	(µm)	(µm)	(%)
Graphite	9	10	6	7	8	1.58	16
Charcoal	15	12.11	11	-	12.7	1.68	11
Coke A	82	75	83	-	80	3.56	4
Coke B	85	83	77	88	83.3	4.02	4.6
Coke C	65	62	63	-	63	1.29	2
Coke D	71	69	79	-	73	4.32	5.5
Coke E	97	95	98	100	97	1.87	2
Coke F	67	66	68	66	67	0.86	1.2

Figure 3.2 shows an example of a three-dimensional image of the surface of graphite and coke C.

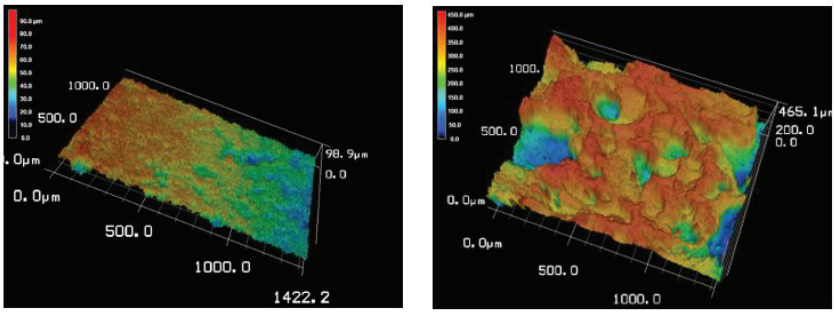

Figure 3.2: Three-dimensional topographic image of the surface of graphite (left) and coke C (right).

Coke samples and graphite and charcoal were analyzed using Xray diffraction (XRD) before and after annealing experiments. Cokes A and B and charcoal and graphite were analyzed at NTNU. Cokes C, D, E and F were analyzed at UNSW.

The carbon materials were first ground using a mortar and pestle and sieved passing a 150 mesh sieve. The powders were transferred to a backloading sample holder. The sample diameter was 25 mm and the depth was approximately 1 mm. The diffraction profile was collected between 10 and 40 deg of 2θ with a step of 0.02 deg with a Bruker AXS D8 Focus at NTNU and Philips X'Pert multipurpose X-ray diffraction system (MPD) at UNSW. The goniometer radius was 217.5 mm, and the divergence slit width was 0.1 degree. The wavelength of the incident X-ray was 1.5409 Å for copper Kα radiation.

The XRD pattern of coke C is depicted in **Figure 3.3**. The main feature of the spectra is the prominent carbon peak observed around 25 degree. This peak was used to determine the L_c parameter. The calculated L_c values are listed in **Table 3.6**.

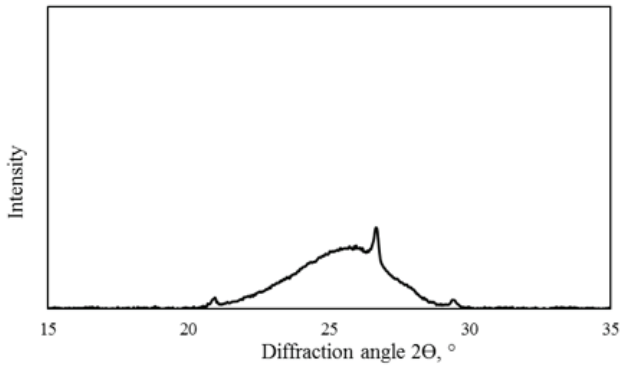

Figure 3.3: XRD pattern for coke C.

Table 3.6: Crystallite size, L_c, for different carbon materials.

Carbonaceous material	Crystallite height, L_c,Å NTNU	Crystallite height, L_c,Å UNSW
Graphite	389	
Charcoal	10	
Coke A	31	
Coke B	24	
Coke C		21.6
Coke D		22.8
Coke E		28.7
Coke F		24.6

Cokes C, D, E and F and graphite were analyzed using a Renishaw in Via Raman microscope with a 523 nm excitation wavelength. The beam size was 1.5 to 2 μm. Raman spectra were scanned from 800 to 2000 cm^{-1} with 25 mW laser power for an exposure time of 15 seconds. At least ten measurements in different zones were taken for each sample. In the

present work, overlapped G and D bands were deconvoluted into five peaks with Lorentzian band fitting. **Figure 3.4** shows a typical first order Raman profile of a coke F annealed at high temperature. The results of the spectrum decomposition are also presented, indicating excellent agreement.

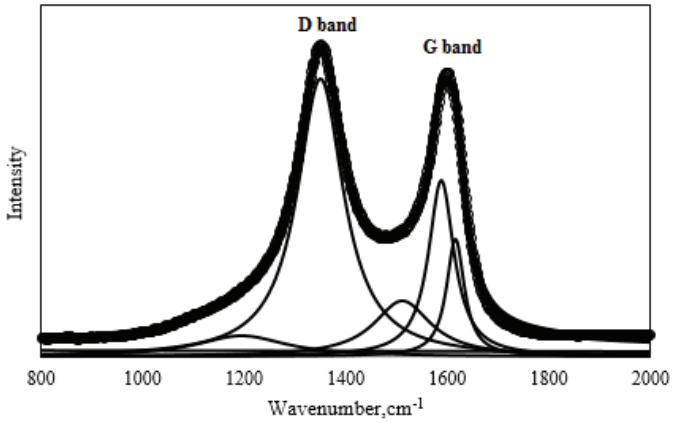

Figure 3.4: Typical Raman profile for metallurgical coke F annealed at 1450°C.

Raman spectra of coke has two peaks around 1360 cm^{-1} and 1580 cm^{-1}. The former and the latter peaks are known as D band and G band, respectively. D band is originated from defect structure of graphite and G band is related to normal graphite structure. In general, intensity ratios of these two bands I_D/I_G are used to evaluate an imperfection of carbon structure, where I_D is D band intensity and I_G is G band. The G fraction which characterizes coke graphitization was calculated as ratio of area under the G peak to the total area. **Table 3.7** shows the G fraction and ID/IG of raw carbon materials and the standard deviation.

Table 3.7: G fraction and I_D/I_G for carbon materials, means (M) and standard deviation (SD). 10 measurements were done for each sample.

Carbon material	G fraction		I_D/I_G	
	M	SD	M	SD
Graphite	59	12.5	0.29	0.008
Coke C	16	1.19	1.65	0.033
Coke D	15.33	0.74	1.7	0.031
Coke E	15.2	0.4	1.7	0.06
Coke F	16.6	0.92	1.69	0.04

3.2 Dissolution experiments

A vertical tube furnace was used for the dissolution reactions, which enables heating of samples in an inert gas atmosphere as shown in **Figure 3.5a**. The heat is supplied by a resistance graphite element and the furnace can hold the samples at temperatures up to 1700ºC. The furnace was evacuated before it was filled with Argon gas. All the experiments were run under an atmosphere of argon gas of grade 4.0 which has a minimum purity of 99.9% with a gas flow of 2.5 dm^3/min.

An alumina crucible was used for all melting experiments (**Figure 3.5c**). It had an outer diameter of 40 mm and outer height of 60 mm. Two thermocouples, one B-type for controlling the furnace and the C-type for temperature measurement were used during experiment. The control thermocouple was placed inside the alumina crucible right above metal and was connected to a PID temperature controller. Pilot heating sequences were run in order to find the appropriate temperature settings.

Experiments were conducted at two temperatures, 1450 and 1550°C. The furnace was heated to the desired temperature at a rate of 20°C/min under continuous argon purging. After the metal melt down, time was allowed for thermal stabilization of the bath for 30 minutes before any carbon addition. Carbon samples were then immersed in the liquid metal for specified times. The carbon rods were fixed to an alumina tube with a Mo-wire to be able to move it vertically (**Figure 3.5b**). The carbon materials were preheated before dipping in the melt by holding them over the bath for the whole process. Doing this, we can be sure that excessive bath boiling due to the immersion of cold sample will not happen. Carbon samples were subtracted from the bath after specific holding times. The crucible with the molten metal was pulled to the button part of the furnace and cooled to room temperature. After the experiments was finished, the amount of carbon as a function of time was determined by chemical analysis of the metal samples using LECO carbon analyzer.

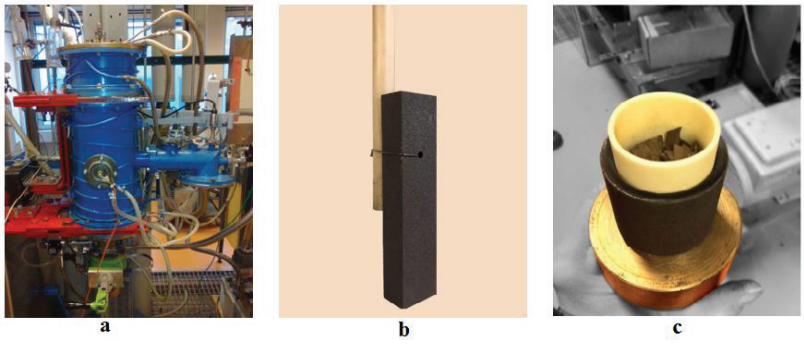

Figure 3.5: a) Resistance furnace b) Graphite rod attached to an alumina tube c) Alumina crucible including Fe-Mn chips.

Figure 3.6 shows temperature profile of the furnace. With this figure as a reference, the inner bottom of the crucible was put at 41 cm while the thermocouple tip was placed at 39.6 cm.

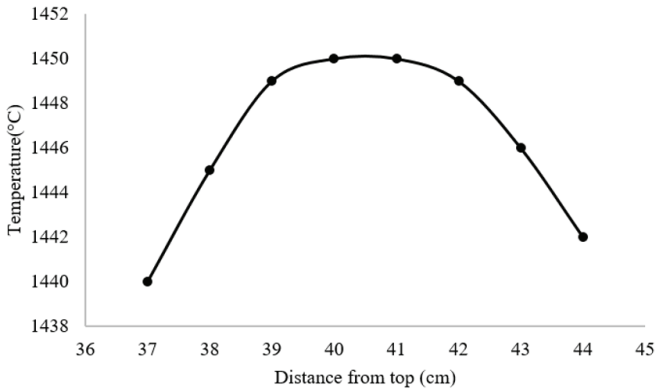

Figure 3.6: Temperature profile of the furnace.

A schematic illustration for measurement of carbon dissolution rate into molten Fe-Mn alloy carbon materials is shown in **Figure 3.7**.

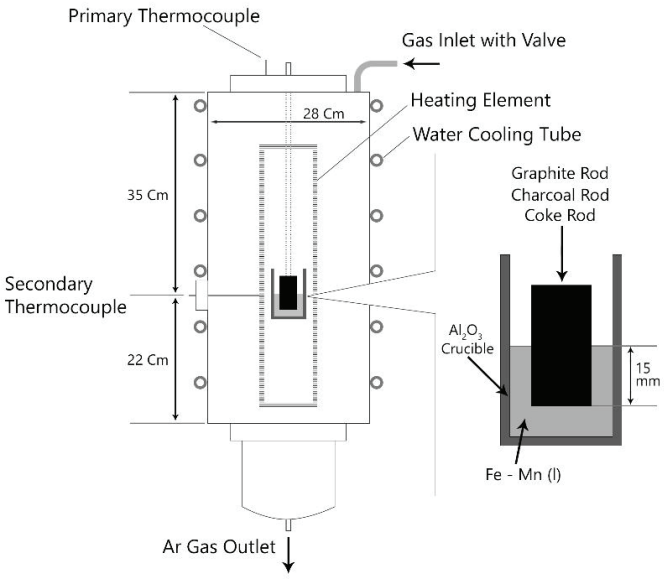

Figure 3.7: Apparatus for carbon dissolution rate measurement using graphite sample rods.

A summary of the experiments conducted in the resistance furnace is listed in **Table 3.8**. some defined experiments were conducted twice.

Table 3.8: List of experiments using resistance furnace.

Experiment No.	Temperature	Metal	Carbon material	Immersion time(s)	Note
1	1450	Fe-85%Mn	Graphite	30	
2	1450	Fe-85%Mn	Graphite	90	
3	1450	Fe-85%Mn	Graphite	120	
4	1450	Fe-85%Mn	Graphite	150	
5	1550	Fe-85%Mn	Graphite	0	
6	1550	Fe-85%Mn	Graphite	30	Replicate(No.69)
7	1550	Fe-85%Mn	Graphite	60	Replicate(No.70)
8	1550	Fe-85%Mn	Graphite	90	Replicate(No.71)
9	1550	Fe-85%Mn	Graphite	120	Replicate(No.72)
10	1450	Fe-60%Mn	Graphite	30	
11	1450	Fe-60%Mn	Graphite	120	
12	1450	Fe-60%Mn	Graphite	150	
13	1550	Fe-60%Mn	Graphite	60	
14	1550	Fe-60%Mn	Graphite	90	
15	1550	Fe-60%Mn	Graphite	120	
16	1450	Fe-85%Mn	Small graphite	60	
17	1450	Fe-85%Mn	Small graphite	120	
18	1550	Fe-85%Mn	Small graphite	30	
19	1550	Fe-85%Mn	Small graphite	60	
20	1450	Fe-60%Mn	Small graphite	60	

21	1450	Fe-60%Mn	Small graphite	120	
22	1550	Fe-60%Mn	Small graphite	30	
23	1550	Fe-60%Mn	Small graphite	60	
24	1450	Fe-85%Mn	Charcoal	0	
25	1450	Fe-85%Mn	Charcoal	15	
26	1450	Fe-85%Mn	Charcoal	30	
27	1550	Fe-85%Mn	Charcoal	0	
28	1550	Fe-85%Mn	Charcoal	15	Replicate(No.73)
29	1550	Fe-85%Mn	Charcoal	30	Replicate(No.74)
30	1450	Fe-60%Mn	Charcoal	0	
31	1450	Fe-60%Mn	Charcoal	15	
32	1450	Fe-60%Mn	Charcoal	60	
33	1550	Fe-60%Mn	Charcoal	0	
34	1550	Fe-60%Mn	Charcoal	30	
35	1550	Fe-60%Mn	Charcoal	60	
36	1450	Fe-85%Mn	Coke A	0	
37	1450	Fe-85%Mn	Coke A	15	
38	1450	Fe-85%Mn	Coke A	30	
39	1550	Fe-85%Mn	Coke A	0	
40	1550	Fe-85%Mn	Coke A	15	Replicate(No.75)
41	1550	Fe-85%Mn	Coke A	30	Replicate(No.76)
42	1450	Fe-85%Mn	Coke B	0	
43	1450	Fe-85%Mn	Coke B	15	
44	1450	Fe-85%Mn	Coke B	30	
45	1550	Fe-85%Mn	Coke B	0	

46	1550	Fe-85%Mn	Coke B	15	Replicate(No.77)
47	1550	Fe-85%Mn	Coke B	30	Replicate(No.78)
48	1550	Fe-85%Mn	Coke C	15	Replicate(No.79)
49	1550	Fe-85%Mn	Coke C	30	Replicate(No.80)
50	1550	Fe-85%Mn	Coke D	15	Replicate(No.81)
51	1550	Fe-85%Mn	Coke D	30	Replicate(No.82)
52	1550	Fe-85%Mn	Coke E	10	Replicate(No.83)
53	1550	Fe-85%Mn	Coke E	20	Replicate(No.84)
54	1550	Fe-85%Mn	Coke F	10	Replicate(No.85)
55	1550	Fe-85%Mn	Coke F	20	Replicate(No.86)
56	1550	Fe-10%Mn	Graphite	60	
57	1550	Fe-10%Mn	Graphite	90	
58	1550	Fe-10%Mn	Graphite	120	
59	1550	Fe-40%Mn	Graphite	60	
60	1550	Fe-40%Mn	Graphite	90	
61	1550	Fe-40%Mn	Graphite	120	
62	1550	Fe	Graphite	0	
63	1550	Fe	Graphite	120	Replicate(No.87)
64	1550	Fe	Graphite	300	
65	1550	Fe	Graphite	600	
66	1550	Fe-Mn-S	Graphite	0	
67	1550	Fe-Mn-S	Graphite	15	Replicate(No.88)
68	1550	Fe-Mn-S	Graphite	30	Replicate(No.89)

3.3 Wettability experiments

Sessile drop technique has been extensively used to study the interfacial phenomena occurring between graphite and liquid iron [69] and also between different carbonaceous materials and slag [92]. In this study the sessile drop technique was used to investigate the wettability and the interfacial phenomena occurring between Fe-Mn and different carbon materials. **Figure 3.8** shows schematically the experimental arrangement. (θ is the contact angle).

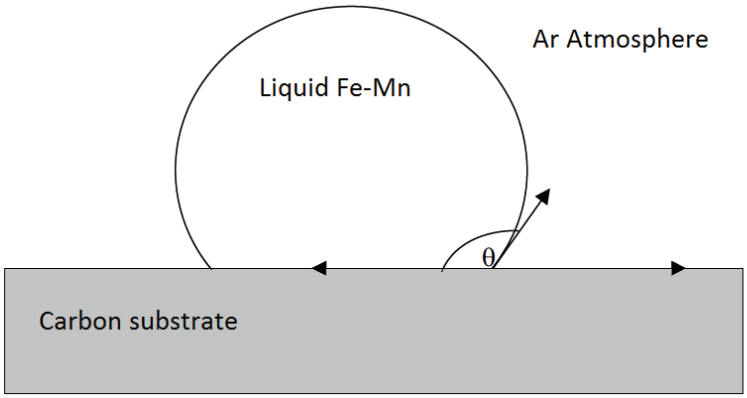

Figure 3.8: Schematic diagram of a sessile drop arrangement.

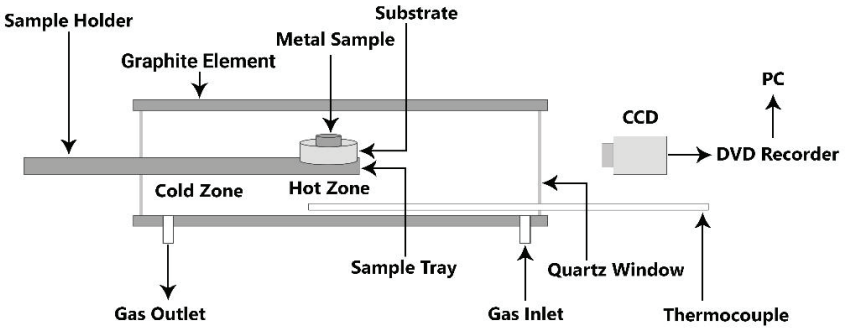

Figure 3.9: A schematic representation of sessile drop setup used at NTNU.

A horizontal tube furnace was used in order to study the wetting properties in the sessile drop method. **Figure 3.9** shows a schematic representation of the sessile drop setup with the heating element in the center, the sample holder sitting in the middle of the furnace is mounted to the left and the camera lens to the right. The sample is heated by the graphite element and surrounded by graphite shield. It is possible to heat the sample to 1600˚C in 1 minute in either a vacuum, inert or in a reducing gas. The maximum temperature of the furnace is 2400˚C and it is controlled by Keller PZ40 two color pyrometer, operating from 900 to 2400˚C focused on the graphite sample holder. A fire-wire digital video camera (Sony XCD-SX910CR) with a tele-centericlens (Navitar 1-50993D) is used to record images from the sample at 960×1280 pixels. The tele-centric lens is especially suitable for this type of measurement, with a 12× zoom allowing an image size from 50 to 4 mm across the frame, where the maximum magnification is equivalent to 3μm per pixel. The contact angles and linear dimensions of the images were measured directly from the image of the drop using Video Drop Shape Analysis software (First Ten Angstroms, Inc., Portsmouth, VA).

The furnace was designed to study the contact properties and the interaction between a small sample with a substrate with the maximum size of 10 mm in diameter and 2 to 5 mm height. The liquid droplet must be small enough to sit on top of the substrate without touching the edges, and a typical sample weight is varying from 0.35-0.37 g.

For wetting experiments, the substrate was located in the graphite holder and a metal particle was placed on the substrate. The furnace chamber was evacuated initially, and then backfilled with Ar with a flow rate of 0.1 NL/min (normal liter) until the end of the test. The metal/carbon assembly was held in the cold zone of the furnace until the desired temperature (1550°C) was attained. The heating rate was 100 ºC/min to 1450ºC and the 15 ºC/min to 1550ºC and kept for 30 min to make the isothermal condition. The assembly was then inserted into the hot zone. This eliminated any reaction that could occur at lower temperatures and possibly influence the phenomena to be studied at the temperature of interest. The melting of metal was marked as the beginning of contact time.

For carbon pickup from substrate, the assembly of metal and substrate was held in the hot zone of the furnace for defined periods of time, and then rapidly moved to the cold zone for quenching. The furnace was cooled by cutting the furnace power. The wetting images of the metal/carbon materials were recorded. Specially designed computer software was used to

determine the contact angle from the captured images, on the basis of a curve-fitting exercise. A typical photo was shown in **Figure 3.10**.

Figure 3.10: A typical photo captured during the wetting experiments.

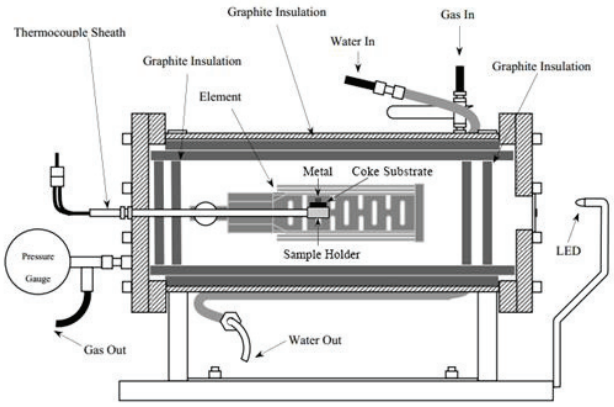

Figure 3.11: A schematic representation of sessile drop setup used at UNSW.

The wettability of cokes C, D, E and F with Fe-85wt%Mn was determined in a graphite furnace shown in **Figure 3.11** at UNSW. The furnace was designed with high cooling rate which allowed the samples to be quenched to the temperature below the melting point quickly after experiments (within 5 sec.). The metal/carbon assembly were placed on a graphite stage to slide into the hot zone of the furnace. Weights of the substrate (~0.2 g) and metal (~0.37 g) were recorded prior to experiment. The furnace chamber was evacuated

initially, and then backfilled with the Ar with a flow rate of 1.5 NL/min (normal liter) until the end of the test. The temperature increased with the heating rate 25°C/min to 1550°C and then kept for 30 min to make the isothermal condition. The melting of metal marked the beginning of contact time. A Sony DCR-TRV18E digital video camera was used to record image sequences during the wettability experiments. This camera gives images at a resolution of 720 x 576 pixels. A pair of Vivitar zoom lenses (one 4 x, one 1 x) are screwed onto the camera lens to provide the correct focal length for viewing within the furnace. ImageJ software was used to determine the contact angle by an average of the two sides as the difference is within acceptable limits for the method used (**Figure 3.12**).

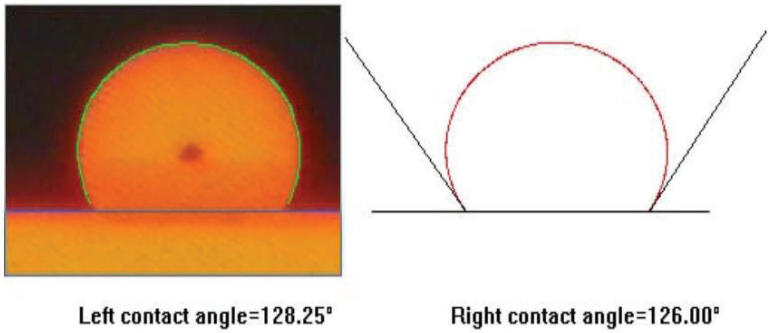

Figure 3.12: Sample program output for captured image angle analysis.

Table 3.9 presents the conditions under which the experiments were conducted.

Table 3.9: Wettability experiments at NTNU (90-91,99,102,103,96-98) and at UNSW (92-95,99-101).

Experiments No.	Temperature(°C)	Substrate	Metal	Note
90	1550	Graphite	Fe-85%Mn	
91	1550	Charcoal	Fe-85%Mn	Replicate(No.99)
92	1550	Coke C	Fe-85%Mn	Replicate(No.100)
93	1550	Coke D	Fe-85%Mn	
94	1550	Coke E	Fe-85%Mn	Replicate(No.101)
95	1550	Coke F	Fe-85%Mn	
96	1550	Coke C	Fe	Replicate(No.102)
97	1550	Graphite	Fe	
98	1550	Charcoal	Fe	Replicate(No.103)

3.4 Thermal treatment of carbon materials

The purpose of conducting annealing experiments was to investigate the effect of annealing temperature on the microstructure of the carbonaceous materials. **Table 3.10** summarizes the carbonaceous materials selected for thermal annealing experiments. Three lumps of each material with the size of approximately 20 mm in diameter were heat treated in a resistance furnace under argon atmosphere. The temperature increased to 400°C with the rate of 25ºC min^{-1} and then held for one minute. It was then increased to 1250°C, 1450°C and 1550°C, with the same heating rate and held for 30 minutes. The samples were contained in an alumina crucible, into which 2.5 dm^3/min of argon gas (99.9% pct) was continuously blown. Two thermocouples, one B-type for controlling the furnace and the C-type for temperature

measurement were used during experiment. The control thermocouple was placed inside the alumina crucible and was connected to a PID temperature controller.

Table 3.10: Thermal annealing of carbonaceous materials.

Experiment No.	Temperature(°C)	Carbon materials
104	1250	Graphite
105	1450	Graphite
106	1550	Graphite
107	1250	Charcoal
108	1450	Charcoal
109	1550	Charcoal
110	1250	Coke A
111	1450	Coke A
112	1550	Coke A
113	1250	Coke B
114	1450	Coke B
115	1550	Coke B
116	1250	Coke C
117	1450	Coke C
118	1550	Coke C
119	1250	Coke D
120	1450	Coke D
121	1550	Coke D
122	1250	Coke E
123	1450	Coke E

124	1550	Coke E
125	1250	Coke F
126	1450	Coke F
127	1550	Coke F

3.5 Kinetic calculations

The rate model of carbon dissolution from **Equation 2.5** was used to calculate and estimate the kinetic parameters in this work. According to **Equation 2.5**, kinetic parameters determining the rate is rate constant, reaction interface area, the volume and the driving force (Note that **Equation 2.5** is shown again for convenience). When rate and area are measured, volume is constant and driving force is chemically analyzed, the rate constant can be calculated.

$$\frac{dC}{dt} = \frac{kA}{V}(C_s - C_t) \qquad \textbf{2.5}$$

For C_s value, Tuset and Sandvik [28] equation was used as described in Chapter 2 . For convenience, the equation is shown below again.

$$Log\%Cs = \left(1.005 - 478/T(K)\right) + 0.147\ \%Mn/(\%Mn + \%Fe) \qquad \textbf{2.4}$$

Which gives a saturation level of 7.24 wt %C and 7.58 wt%C at 1450ºC and 1550ºC for the given alloy. The rate constant, k is determined from the negative slope of a V/A ln[(C_s-C_t)/(C_s-C_0)] versus time plot.

Area (A) was calculated from the carbon materials area, which was in contact with the metal in different times. **Figure 3.13** and **Equation 3.3** shows how the surface area of graphite

was calculated. **Figure 3.14** and **Equation 3.4** indicates the calculation of cokes and charcoal surface area during dissolution.

$$\boldsymbol{A = (m \times n) + 2(m \times l) + 2(n \times l)} \qquad \textbf{3.3}$$

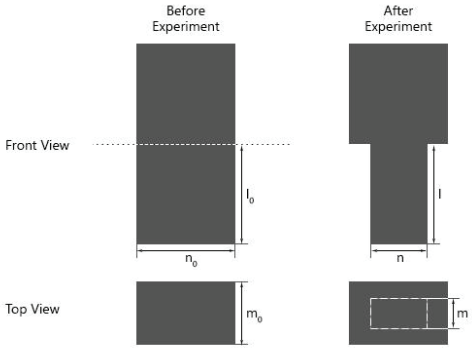

Figure 3.13: Schematic illustration about dissolution behavior of graphite in metal.

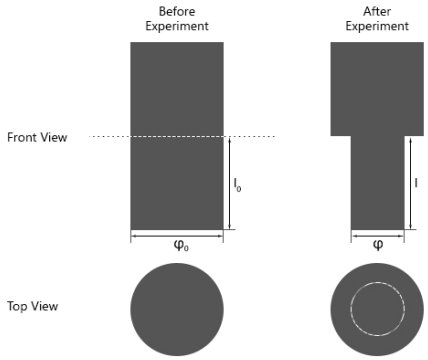

Figure 3.14: Schematic illustration about dissolution behavior of cokes and charcoal in metal.

$$\boldsymbol{A = (\pi \times \varphi) \times l + \pi(\frac{\varphi}{2})^2} \qquad \textbf{3.4}$$

Figure 3.15 shows an example of the surface area reduction of graphite during dissolution in Fe-85wt%Mn at 1550°C. It can be seen from this figure that the goodness of the fit of the data was best described by an exponential decrease in surface area with time.

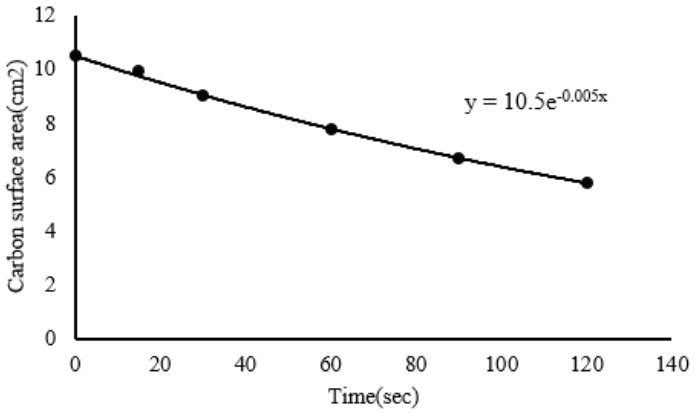

Figure 3.15: Surface area reduction during dissolution of graphite in Fe-85wt%Mn at 1550°C.

To determine the volume (V) of molten metal, the mass divided by the density of the metal. For example, for Fe-85wt%Mn:

$$\rho_{Fe_l} = 5.95\ gr/cm^3 \quad \textbf{3.5}$$

$$\rho_{Mn_l} = 6.98\ gr/cm^3 \quad \textbf{3.6}$$

$$\rho_t = (0.85 \times \rho_{Fe_l}) + (0.15 \times \rho_{Mn_l}) = 6.1\ gr/cm^3 \quad \textbf{3.7}$$

And the mass (m) of the metal is 100 g, so the volume is:

$$V = \frac{m}{\rho_t} = \frac{100}{6.1} = 16.4\ cm^3 \quad \textbf{3.8}$$

To verify the model, some dissolution experiments were done using a graphite with a 40% reduced surface area.

3.6 Other characterization methods used

3.6.1 XRF

The Mn and Fe contents of the samples were analyzed by an X-ray fluorescence (XRF) spectrometer (SPECTRO XEPOS, Kleve, Germany) at SINTEF MOLAB AS. X-ray fluorescence 1 (XRF) is widely used as an important tool in analytic materials research. XRF is the re-radiation (fluorescence) of atoms in the x-ray part of the spectrum following excitation. Atoms that are bombarded with primary x-rays or charged particles of sufficient energy can have inner shell electrons knocked out. When one of the atom's other electrons drops into the shell vacancy, it emits a (secondary) x-ray photon with an energy characteristic of the element. In this way the spectrum (number of photons as a function of energy) of the emitting atom can be used to identify it. In the case of manganese and iron there are primarily two x-ray energies that can be used for identification, the so-called Kα and Kβ x-rays at 5.90 kev and 6.49 kev, respectively. **Figure 3.16** is a Photograph of the XRF head unit showing the x-ray source and detector mounted on an XY translation stage and boom.

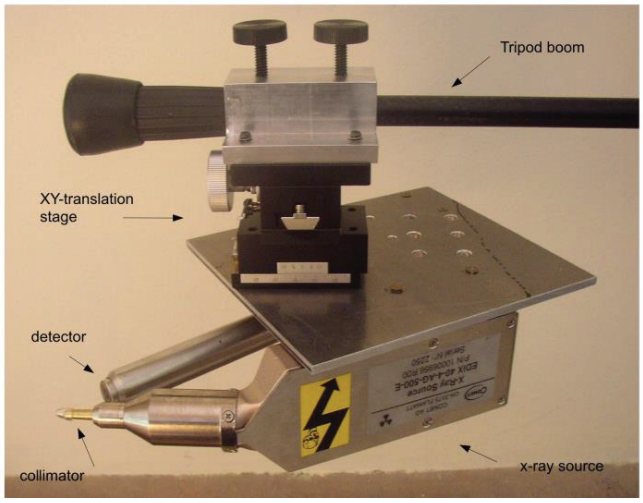

Figure 3.16: Photograph of the XRF head unit showing the x-ray source and detector mounted on an XY-translation stage and boom[93].

3.6.2 Carbon and sulfur percentage analysis using LECO.

The carbon and sulfur contents in the metal samples were analyzed by combustion-IR (LECO CS-200, St. Joseph, USA) at SINTEF MOLAB AS. A weighed sample was placed into a ceramic crucible. The system was closed and purged with oxygen. The LECO CS-200 uses a high frequency (HF) induction heated furnace. To get good coupling with the electric field, iron chips are added to the crucible together with the accelerator (tungsten). The purpose of the accelerators is to hasten the combustion as well as making a fluid melt in the crucible. The crucible was heated in a resistance furnace with fixed temperature of 1213 K (940°C) in oxygen atmosphere. Free carbon and sulfur from the sample react with oxygen to form CO and CO_2 and SO_2 which were analyzed by infrared detectors. The instrument is in theory calibrated from 0-100% for most elements. The XRF-Standard less method uses precalibrated lines set up by the instrument manufacturer. It can be used for quantification of almost any kind of sample, and by supplying the software with additional information it can't get by measuring, like carbon, the method is very useful. This LECO machine was used to determine carbon and sulfur content of metals with different compositions in different times.

3.6.3 SEM studies

A scanning Electron Microscope (SEM), Hitachi S-3400, equipped with a field emission gun was used within this research at UNSW. This equipment with secondary imaging mode (SE) was used to study all surfaces of different carbon materials before and after reaction in both sessile drop experiments and dissolution experiments.

A semi-quantitative microchemical analysis of the sample can be conducted with SEM analyzer and elements with atomic numbers as low as Boron can be detected. This energy dispersive spectroscopy (EDS) can produce spot microchemical analysis or image maps on a sample. The depth of analysis is limited to the interaction volume of the electron beam and is typically around 2-3 µm. In this study, EDS technique was also applied to make

quantitative analysis of some components in SEM. Details on sample preparation for SEM analysis can be found in Appendix A.

In sessile drop and dissolution experiments, SEM was used to investigate the carbon/metal contact area after the experiments on both metals and substrates. With regard to the fact that the metal drop does not stick to the coke substrates, SEM was also used to investigate the metal/carbon contact area after the wetting experiment on some coke substrates. In dissolution experiments, SEM was used to investigate the carbon/metal interface after immersion in metal. A representative SEM image is presented in **Figure 3.17**.

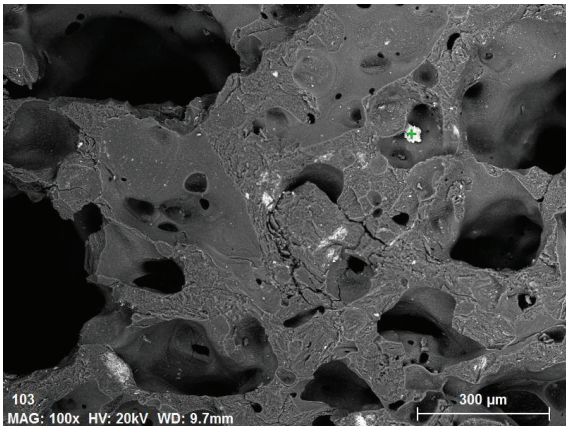

Figure 3.17: SEM image of raw coke D at 100x magnification.

4 Results

4.1 Results of dissolution studies

Carbon dissolution investigations were conducted on industrial carbon materials. One charcoal, six types of metallurgical cokes and charcoal were used. In addition, graphite was used as a reference material since it contains very little inorganic impurities and is highly structured. The experimental results, including dissolution rate constants are presented in this section.

4.1.1 Carbon materials

The resistance furnace was used to conduct the carbon dissolution experiments at two different temperatures 1450ºC and 1550ºC. The carbonaceous material rods were pushed down into the melt and this marked the reaction start time. Then after different times, the carbon rods were pulled out of the melt and the molten metal was also pulled down to the bottom of the furnace and cooled down. All of the metal samples were analyzed for carbon and some of them for sulfur by infrared combustion analyses.

The measured carbon dissolved in Fe-85wt%Mn over time, the plots of $-kt=V/A \ln[(C_s-C_t)/(C_s-C_0)]$ versus time for six cokes, one charcoal and graphite (small and big carbon samples) at 1550°C and replicates are depicted in **Figure 4.1** to **Figure 4.9**. Solid lines are derived from the modelling and will be described in detail in discussion chapter. The changes of different carbon materials surface area with time showed that the goodness of the fit of the data was best described by an exponential decrease in surface area with time. Figures of changes in surface area are presented in Appendix B. It is worth mentioning again that the initial surface areas of carbon materials are different because of the

difficulty of finding big samples of coke and charcoal. The initial surface areas of all cokes are the same.

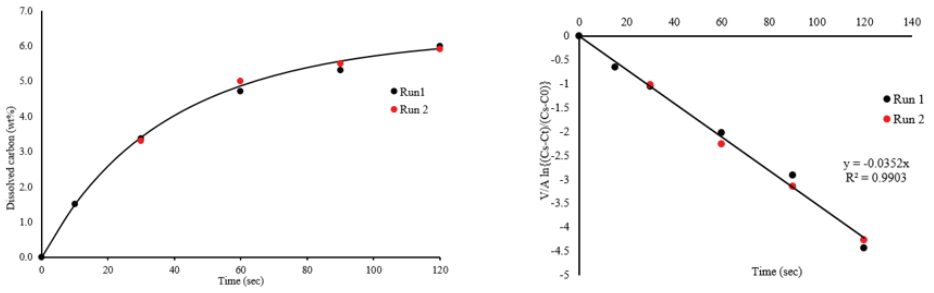

Figure 4.1: a) Carbon dissolved from graphite in Fe-85wt%Mn at 1550°C versus time (Exp.5-9 and Replicate 69-72) b) $-kt=V/A \ln[(C_s-C_t)/(C_s-C_0)]$ versus time plot.

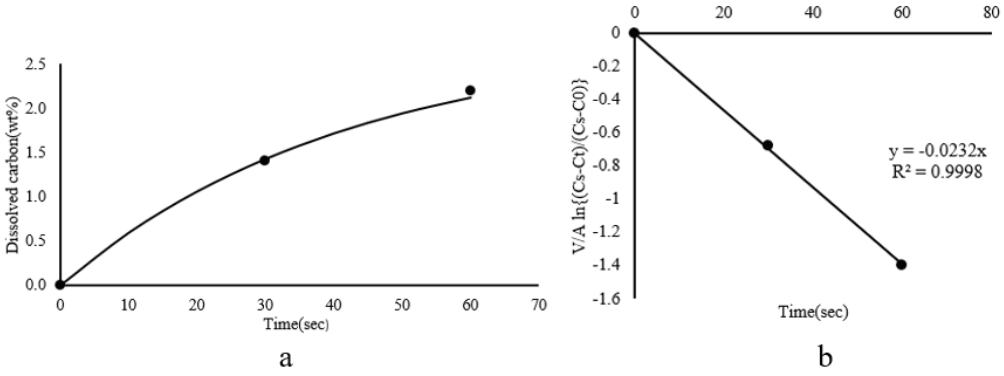

Figure 4.2: a) Carbon dissolved from small graphite in Fe-85wt%Mn at 1550°C versus time (Exp.18-19) b) $-kt=V/A \ln[(C_s-C_t)/(C_s-C_0)]$ versus time plot.

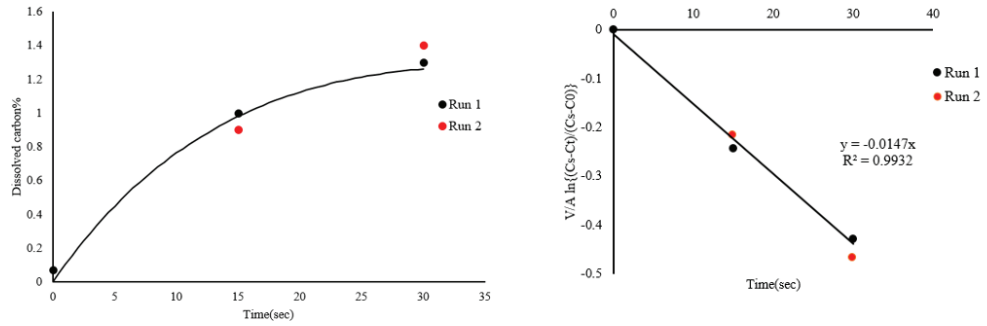

a b

Figure 4.3: a) Carbon dissolved from charcoal in Fe-85wt%Mn at 1550°C versus time (Exp.27-29 and Replicate 73-74) b) $-kt = V/A \ln[(C_s-C_t)/(C_s-C_0)]$ versus time plot.

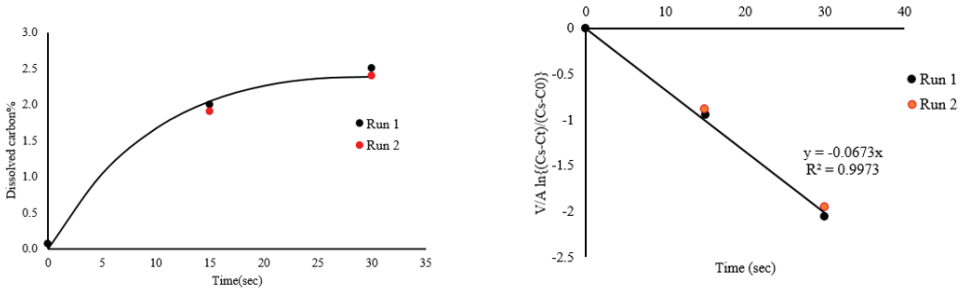

a b

Figure 4.4: a) Carbon dissolved from coke A in Fe-85wt%Mn at 1550°C versus time (Exp.39-41 and Replicate 75-76) b) $-kt = V/A \ln[(C_s-C_t)/(C_s-C_0)]$ versus time plot.

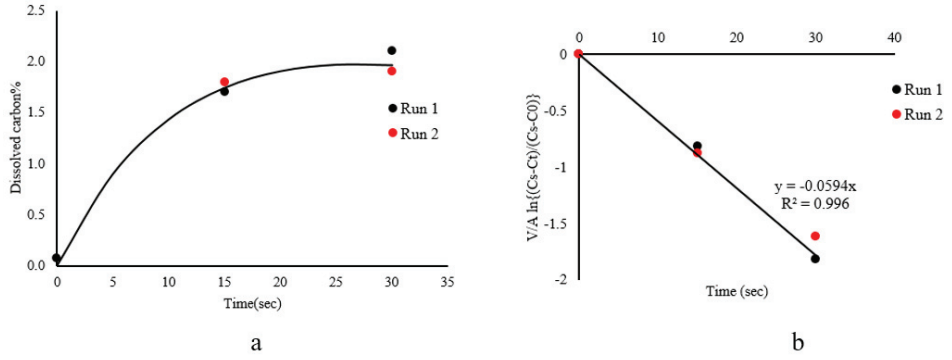

Figure 4.5: a) Carbon dissolved from coke B in Fe-85wt%Mn at 1550°C versus time (Exp.45-47 and Replicate 77-78) b) $-kt = V/A \ln[(C_s-C_t)/(C_s-C_0)]$ versus time plot.

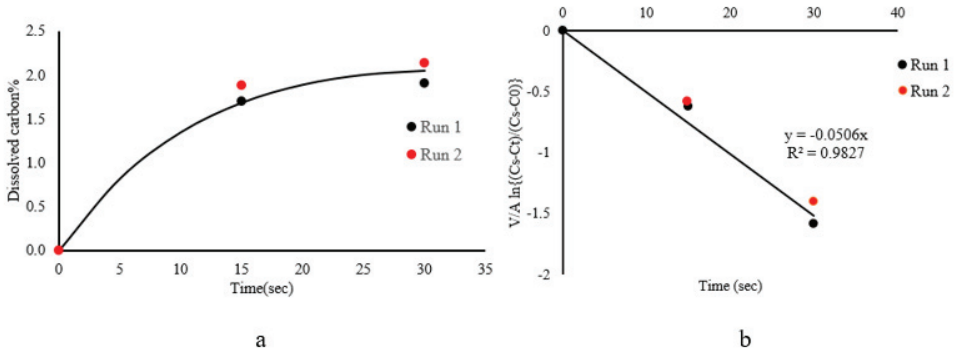

Figure 4.6: a) Carbon dissolved from coke C in Fe-85wt%Mn at 1550°C versus time (Exp.48-49 and Replicate 79-80) b) $-kt = V/A \ln[(C_s-C_t)/(C_s-C_0)]$ versus time plot.

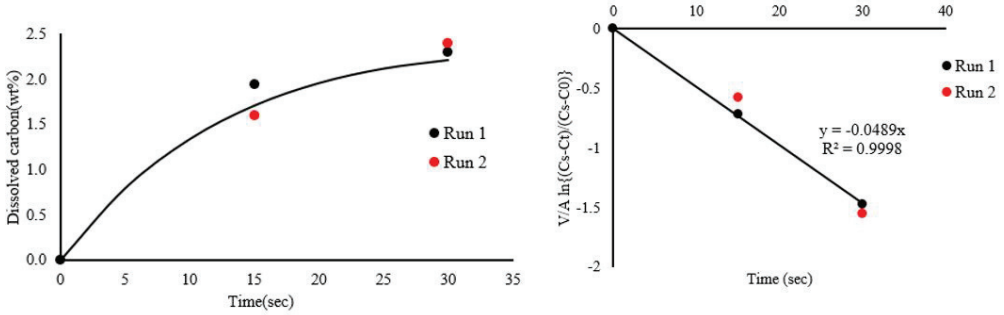

a b

Figure 4.7: a) Carbon dissolved from coke D in Fe-85wt%Mn at 1550°C versus time (Exp.50-51 and Replicate 81-82) b) $-kt = V/A \ln[(C_s-C_t)/(C_s-C_0)]$ versus time plot.

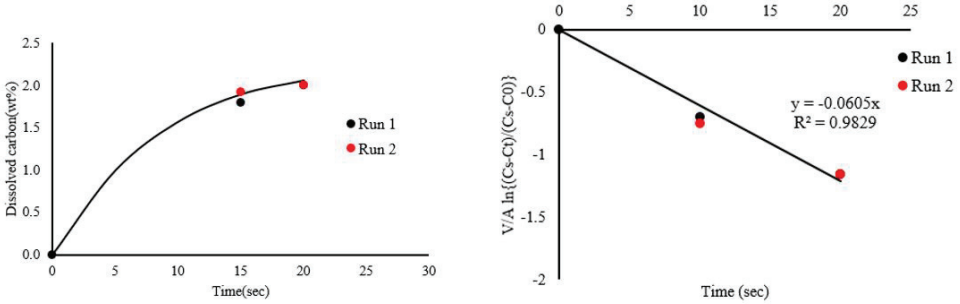

a b

Figure 4.8: a) Carbon dissolved from coke E in Fe-85wt%Mn at 1550°C versus time (Exp.52-53 and Replicate 83-84) b) $-kt = V/A \ln[(C_s-C_t)/(C_s-C_0)]$ versus time plot.

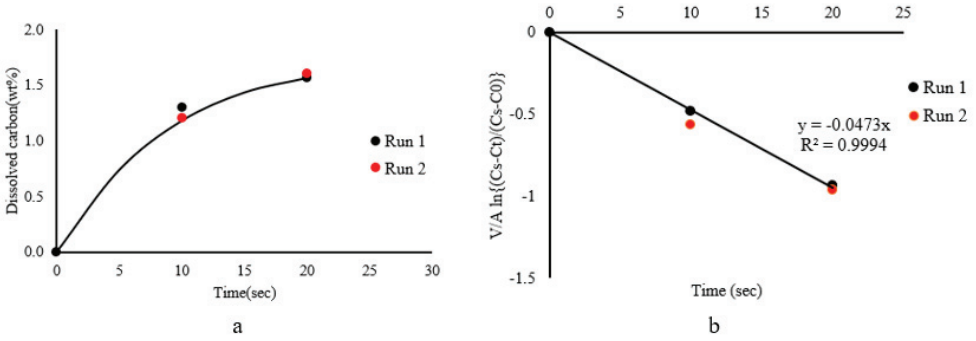

Figure 4.9: a) Carbon dissolved from coke F in Fe-85wt%Mn at 1550°C versus time (Exp.54-55 and Replicate 85-86) b) $-kt = V/A \ln[(C_s-C_t)/(C_s-C_0)]$ versus time plot.

It can be seen from **Figure 4.1** to **Figure 4.9** that the reproducibility of replicas is quite good. The first order reaction equation is quite good within the area investigated and it can be seen that R^2 are above 98% for all samples. It is also worth mentioning that as the carbon samples are quite small, they are more or less consumed when the carbon dissolved reaches 2.5 wt% for cokes and 1.4 wt% for charcoal. This means that even if we are far from saturation which is more than 7wt %, the rate will go toward zero as the area approaches zero. This explains that the curves are flattening out even if one is far from the saturation limit.

Corresponding overall rate constants, k_t, for different carbon materials in Fe-85 wt%Mn at 1550°C were determined and shown in **Figure 4.10** and were listed in **Table 4.1**.

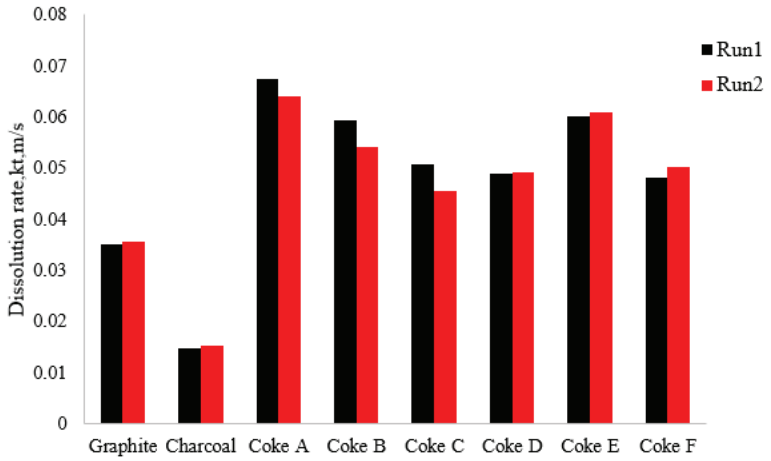

Figure 4.10: Overall rate constant, k_t, for various carbonaceous materials in Fe-85 wt%Mn at 1550°C.

Table 4.1: Rate constant, k_t, for different carbon materials in Fe-85 wt%Mn at 1550°C.

Carbonaceous material	$k_t \times 10^3 \pm 0.3^*$(cm/s)
Graphite	35.2
Charcoal	14.7
Coke A	67.3
Coke B	59.4
Coke C	50.6
Coke D	48.9
Coke E	60.5
Coke F	47.3

**0.3 is the standard deviation obtained for the duplicate runs of all samples*

It can be seen from **Figure 4.10** that there was a wide variation in dissolution rate constants amongst carbon materials. The dissolution rate constants for all cokes were higher than

graphite and charcoal. Charcoal has the lowest rate constant and coke A has the highest rate constant. There is some difference between the dissolution rate constant between two particles, that is two runs, of the same materials. The difference between the various carbon particles is however much lower than the difference between different types.

4.1.2 Temperature

To investigate the temperature dependence of carbon dissolution, cokes A, coke B, charcoal and big and small samples of graphite were chosen for further dissolution experiments at two different temperatures. Again, first order reaction rate was used to determine the rate constant at each experimental temperature. The measured carbon content and the plots of $-kt=V/A \ln[(C_s-C_t)/(C_s-C_0)]$ versus time at two different temperatures 1450°C and 1550°C for the carbonaceous materials are shown in **Figure 4.11** through to **Figure 4.17**.

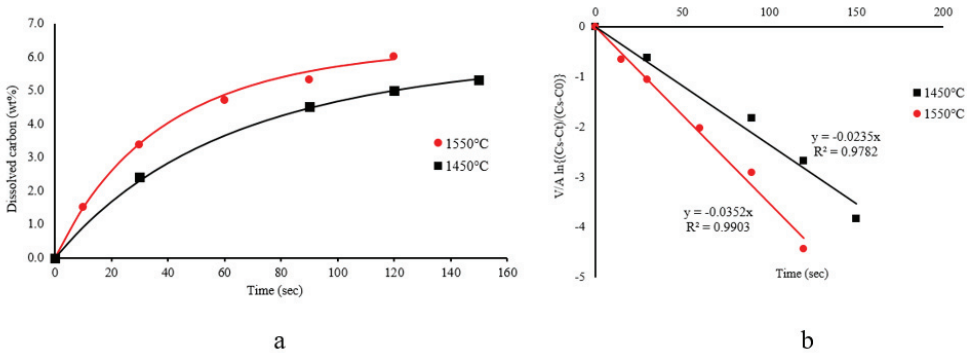

Figure 4.11: a) Carbon dissolved from graphite in Fe-85wt%Mn at 1550°C(Exp.5-9) and 1450°C(Exp.1-4) versus time b) $V/A \ln[(C_s-C_t)/(C_s-C_0)]$ versus time plot.

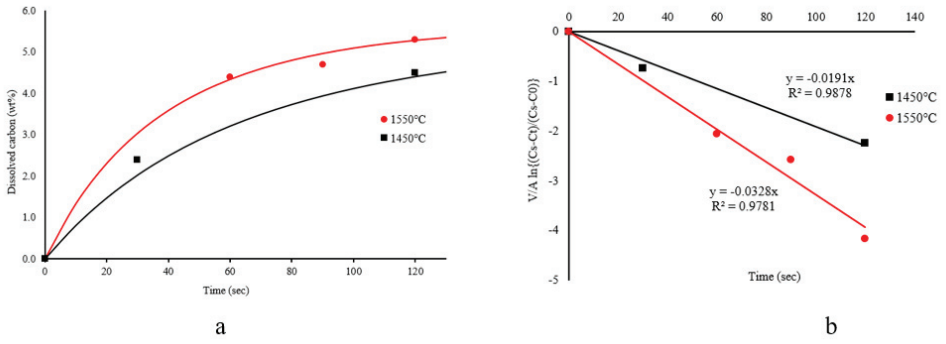

Figure 4.12: a) Carbon dissolved from graphite in Fe-60wt%Mn at 1550°C(Exp.13-15) and 1450°C(Exp.10-12) versus time b) V/A $\ln[(C_s-C_t)/(C_s-C_0)]$ versus time plot.

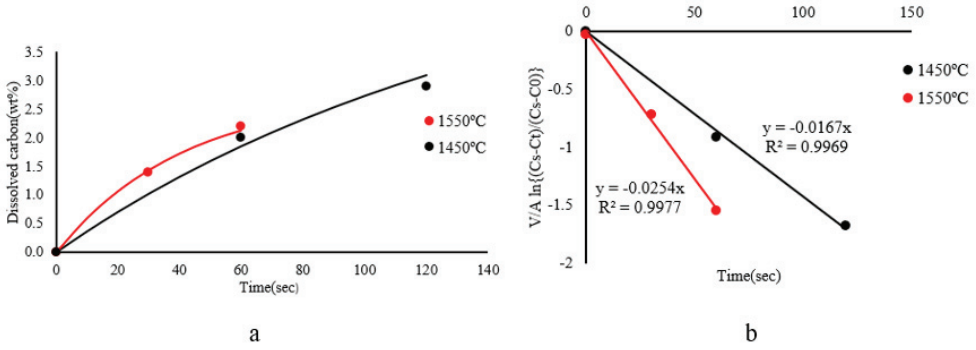

Figure 4.13: a) Carbon dissolved from small graphite in Fe-85wt%Mn at 1550°C(Exp.18-19) and 1450°C(Exp.16-17) versus time b) V/A $\ln[(C_s-C_t)/(C_s-C_0)]$ versus time plot.

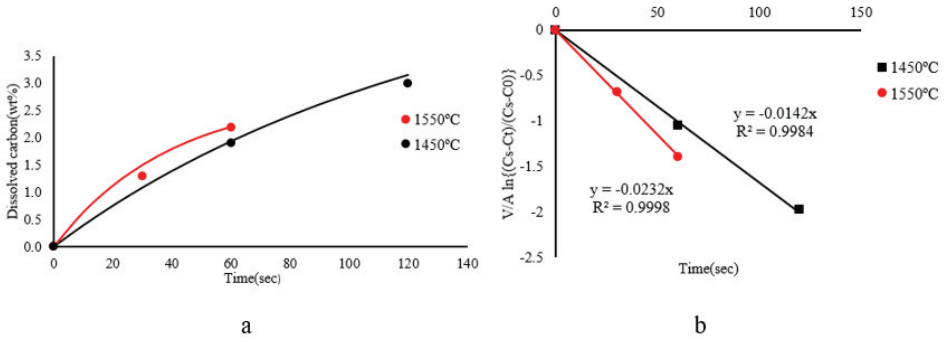

Figure 4.14: a) Carbon dissolved from small graphite in Fe-60wt%Mn at 1550°C(Exp.22-23) and 1450°C(Exp.20-21) versus time b) V/A $\ln[(C_s-C_t)/(C_s-C_0)]$ versus time plot.

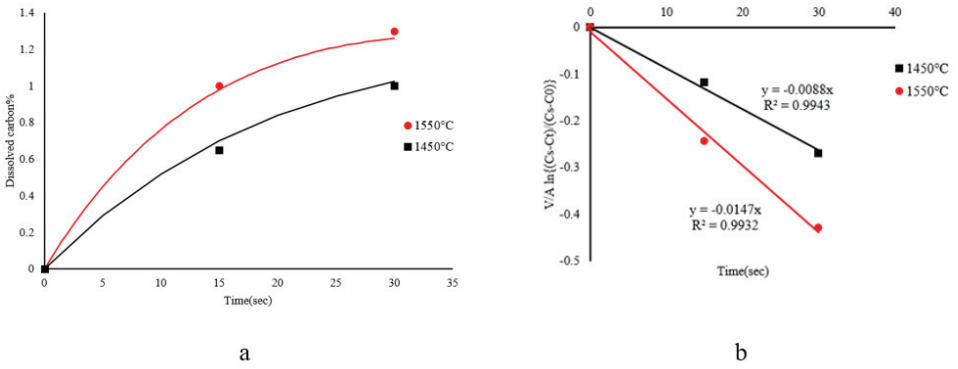

Figure 4.15: a) Carbon dissolved from charcoal in Fe-85wt%Mn at 1550°C(Exp.27-29) and 1450°C(Exp.24-26) versus time b) V/A $\ln[(C_s-C_t)/(C_s-C_0)]$ versus time plot.

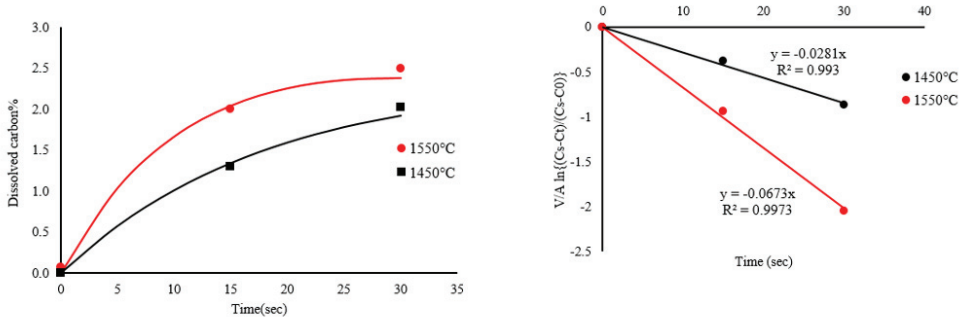

a b

Figure 4.16: a) Carbon dissolved from coke A in Fe-85wt%Mn at 1550°C(Exp.39-41) and 1450°C(Exp.36-38) versus time b) V/A $\ln[(C_s-C_t)/(C_s-C_0)]$ versus time plot.

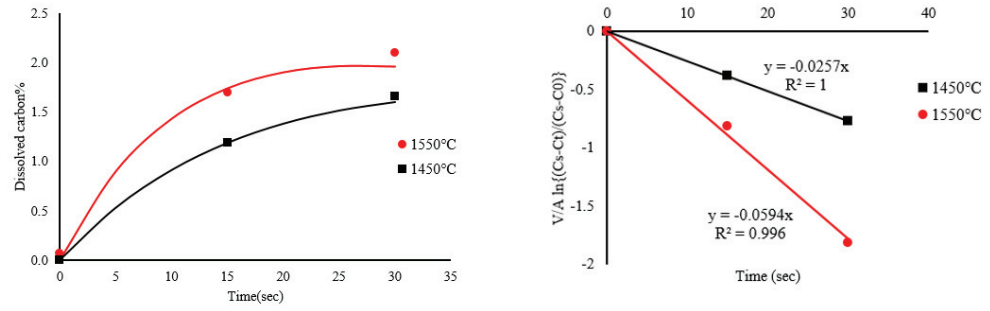

a b

Figure 4.17: a) Carbon dissolved from coke B in Fe-85wt%Mn at 1550°C(Exp.45-47) and 1450°C(Exp.42-44) versus time b) V/A $\ln[(C_s-C_t)/(C_s-C_0)]$ versus time plot.

A comparison of the plots in **Figure 4.11** to **Figure 4.17** shows that temperature had influence on the rate constant for all carbon materials tested, as expected. This influence was lower for graphite and larger for cokes and charcoal. It was also interesting to note that the dissolution rate of coke A > coke B > graphite > charcoal at both temperatures.

Table 4.2 lists the overall dissolution rate constant, k_t, for two different temperatures for each carbon source. From this table it was observed that k increased as temperature increased and that temperature had a greater effect on cokes than on graphite and charcoal.

Using an Arrhenius type equation (**Equation 2.8**), the activation energy, E_a, for carbon dissolution was obtained.

Table 4.2: Dissolution constant, k ($\times 10^3$) cm/s, for graphite (small and big), charcoal and cokes A and B at two different temperatures.

T(ºC)	Source of carbon	Metal composition	k(cm/s)-Run1	k(cm/s)-Run2
1450	Graphite	Fe-85%Mn	23.5	-
1550	Graphite	Fe-85%Mn	34.8	35.6
1450	Graphite	Fe-60%Mn	19	-
1550	Graphite	Fe-60%Mn	32	-
1450	Small graphite	Fe-85%Mn	16.7	-
1550	Small graphite	Fe-85%Mn	25.4	-
1450	Small graphite	Fe-60%Mn	14.2	-
1550	Small graphite	Fe-60%Mn	23.2	-
1450	Charcoal	Fe-85%Mn	8.8	-
1550	Charcoal	Fe-85%Mn	14.1	15.3
1450	Coke A	Fe-85%Mn	28.1	-
1550	Coke A	Fe-85%Mn	70.7	63.9
1450	Coke B	Fe-85%Mn	25.7	-
1550	Coke B	Fe-85%Mn	64.8	54

The Arrhenius plots for graphite (small and big samples) and charcoal and cokes A and B in Fe-85wt%Mn are shown in **Figure 4.18**. The Arrhenius plots for big and small graphite samples in Fe-60%Mn are shown in **Figure 4.19**. The calculated E_a values are presented in **Table 4.3.**

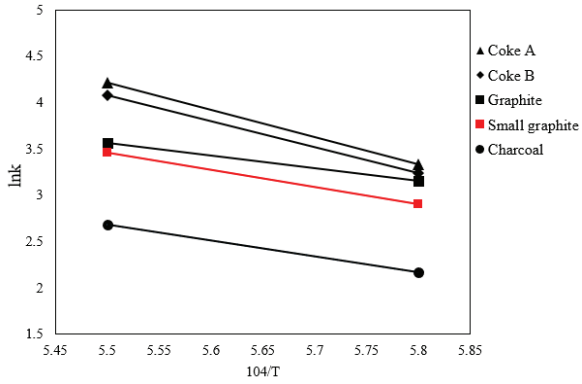

Figure 4.18: Arrhenius plot for carbon dissolution from different types of carbon in Fe-85wt%Mn.

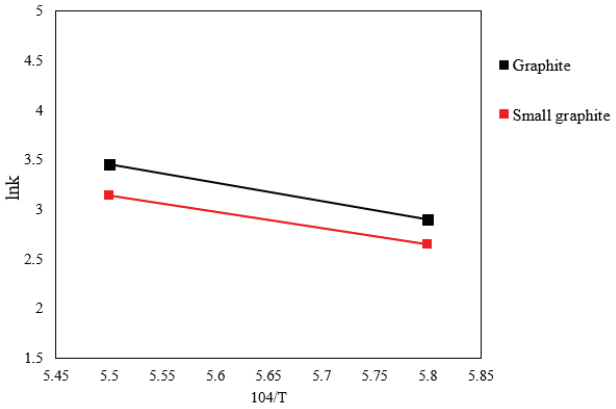

Figure 4.19: Arrhenius plot for carbon dissolution from big and small graphite in Fe-60wt%Mn.

Table 4.3: Calculated activation energy values for carbon dissolution from four carbon sources.

Carbonaceous material	Metal composition	Activation Energy, E_a (kJ/mol)
Graphite	Fe-85wt%Mn	105
Small graphite	Fe-85wt%Mn	109
Charcoal	Fe-85wt%Mn	134
Coke A	Fe-85wt%Mn	228
Coke B	Fe-85wt%Mn	219
Graphite	Fe-60wt%Mn	136
Small graphite	Fe-60wt%Mn	128

4.1.3 Metal composition

The dissolution experiments were conducted at 1550°C with liquid Fe-Mn alloy containing different manganese concentration ranging from 0 to 85wt% manganese. This was done to investigate the influence of manganese content in the Fe-Mn alloy on the dissolution rate of graphite. Dissolved carbon from graphite versus time, plots of $-kt=V/A \ln[(C_s-C_t)/(C_s-C_0)]$ versus time and the change of surface area of graphite over time for Fe, Fe-10wt%Mn, Fe-40wt%Mn and Fe-60wt%Mn are depicted in **Figure 4.20** to **Figure 4.23** respectively. The same information for dissolution of graphite in Fe-85wt%Mn was shown earlier in **Figure 4.1**.

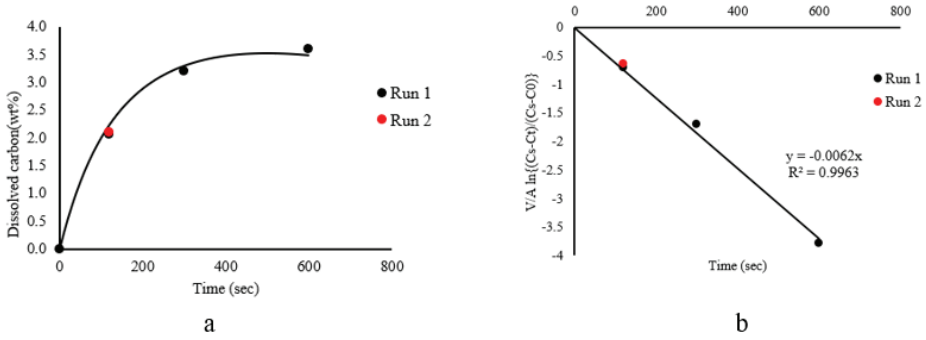

Figure 4.20: a) Carbon dissolved from graphite in Fe at 1550°C versus time (Exp.62-65 and Replicate 88) b) $-kt=V/A\ \ln[(C_s-C_t)/(C_s-C_0)]$ versus time plot.

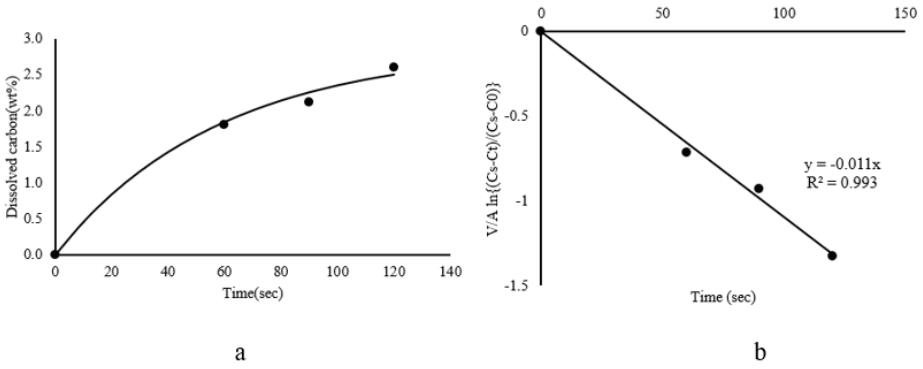

Figure 4.21: a) Carbon dissolved from graphite in Fe-10wt%Mn at 1550°C versus time (Exp.56-58) b) $-kt=V/A\ \ln[(C_s-C_t)/(C_s-C_0)]$ versus time plot.

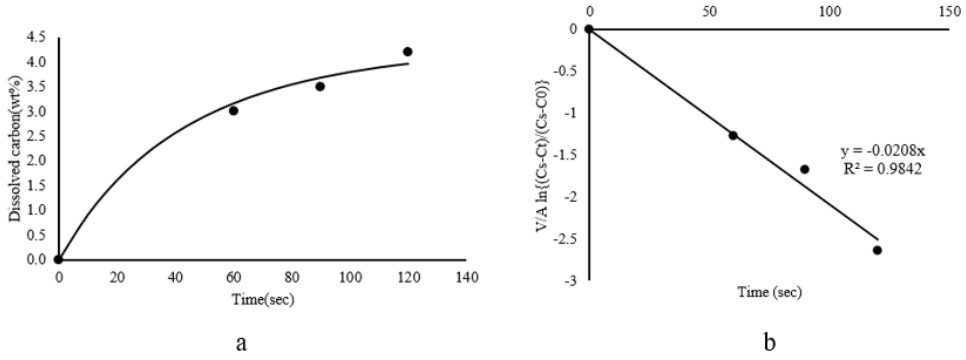

Figure 4.22: a) Carbon dissolved from graphite in Fe-40wt%Mn at 1550°C versus time (Exp.59-61) b) $-kt=V/A \ln[(C_s-C_t)/(C_s-C_0)]$ versus time plot.

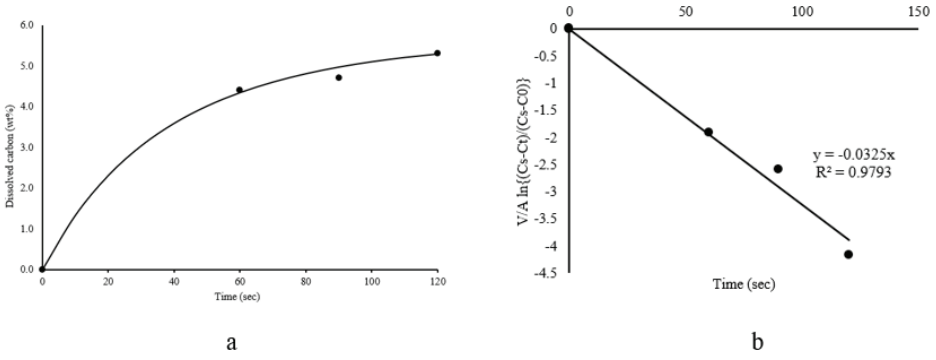

Figure 4.23: a) Carbon dissolved from graphite in Fe-60wt%Mn at 1550°C versus time (Exp.13-15) b) $-kt=V/A \ln[(C_s-C_t)/(C_s-C_0)]$ versus time plot.

Table 4.4 shows the graphite dissolution rate constant in five different composition and as it shows, with increasing manganese content in the alloy, the dissolution rate increased.

Table 4.4: The rate constant for different compositions.

Composition	Fe	Fe-10%Mn	Fe-40%Mn	Fe-60%Mn	Fe-85%Mn
Rate constant(cm/s)	0.0062	0.011	0.0208	0.0325	0.0352

Some dissolution experiments were done to verify the application of rate models. Dissolution rate of graphite with a 40% reduced surface area in Fe-60wt%Mn and Fe-85wt%Mn was investigated. **Figure 4.24** shows the dissolved carbon from graphite versus time and the plots of $-kt=V/A \ln[(C_s-C_t)/(C_s-C_0)]$ versus time for two different compositions. This figure indicates that the dissolution rate of small graphite in the metal with higher manganese content is higher that a metal with lower amount of manganese. However, the difference is not significant.

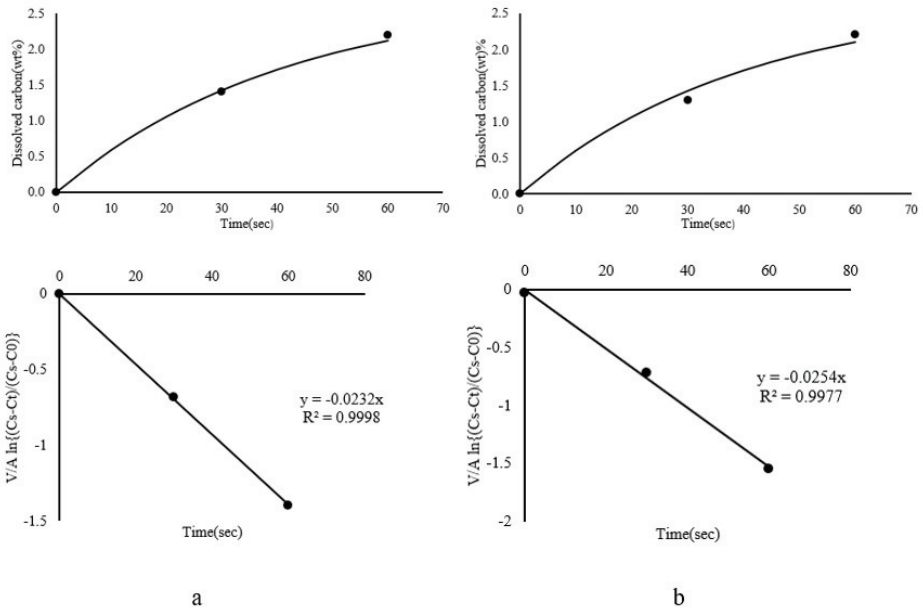

Figure 4.24: a) Carbon dissolved from small graphite in Fe-60wt%Mn at 1550°C versus time and $-kt=V/A \ln[(C_s-C_t)/(C_s-C_0)]$ versus time plot. b) Carbon dissolved from small graphite in Fe-85wt%Mn at 1550°C versus time and $-kt=V/A \ln[(C_s-C_t)/(C_s-C_0)]$ versus time plot.

4.1.4 Sulfur content in bath

To see the effect of sulfur content in the metal, on the dissolution rate of graphite, 1.69wt% sulfur was added to the metal. **Figure 4.25a** shows the amount of dissolved carbon from

graphite versus time for both metals with and without sulfur. A -kt=V/A ln[$(C_s-C_t)/(C_s-C_0)$] versus time plot for Fe-85%Mn and Fe-85w%Mn-1.69wt%S at 1550°C are depicted in **Figure 4.25 b**. It can be seen that the dissolution rate of graphite decreased slightly with adding sulfur to the metal. the k values with and without sulfur is 0.34 cm/s and 0.352 cm/s respectively.

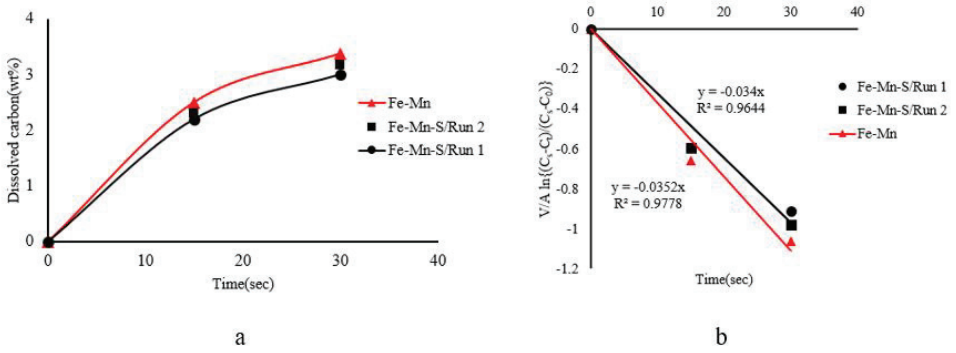

Figure 4.25: a) Carbon dissolved from graphite in Fe-85wt%Mn (Exp. and Fe-85wt%Mn-1.69wt%S (Exp.66-68, Replicate 88-89) at 1550°C versus time b) V/A ln[$(C_s-C_t)/(C_s-C_0)$] versus time plot.

Figure 4.26 shows the SEM image of the interface between graphite and metal adding sulfur at the graphite side. A thin layer which is composed mostly of MnS is seen on the graphite surface. Some sulfur was also detected in the metal bulk phase as shown in **Figure 4.27**. This can indicate that sulfur prefers to accumulate at the interface rather than distribute in the bulk metal.

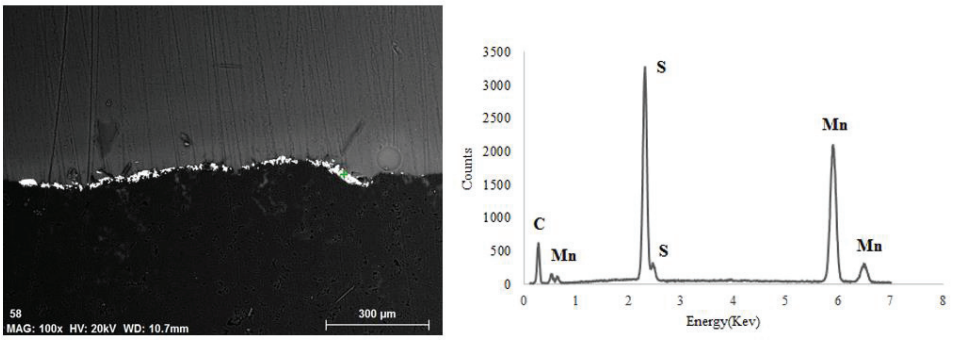

Figure 4.26: SEM image and EDS analyses of graphite side of the interface between Mn-Fe-S/graphite.

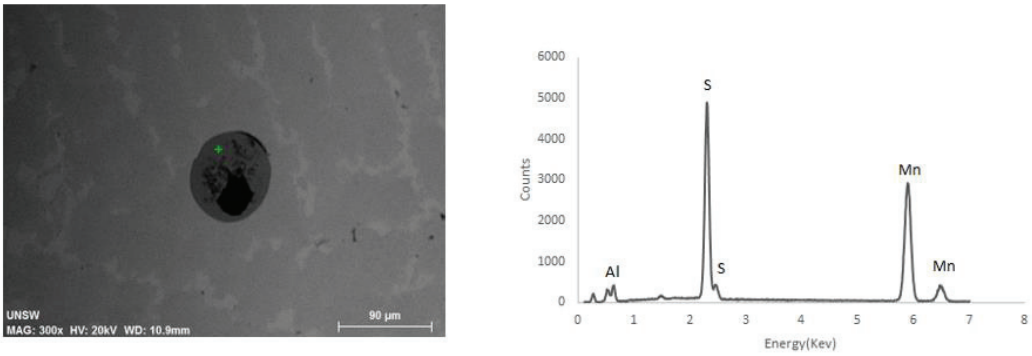

Figure 4.27: EM image and EDS analyses of MnS in the metal phase after immersion of graphite for 30 seconds at 1550°C.

4.1.5 Interfacial products

The interfacial products that form between the metal and carbonaceous materials are of great interest to further understand what is occurring during carbon dissolution. In this study, since the immersion time of carbon materials is limited to less than one minute for cokes and charcoal, it is interesting to see what is happening in such a short time. Coke E with highest amount of ash (13.68%) and coke D with the lowest amount of ash (9.61%) were chosen for investigating the interfacial products at initial stage of dissolution reaction using SEM with EDS analyses.

Figure 4.28 and **Figure 4.29** show the coke side of the interface and metal side of the interface respectively using coke E. It can be seen that after 30 seconds immersion in metal, there is no sign of ash layer at the interface which can block the surface and retard the dissolution reaction. There are some slag globes at the interface, but it is difficult to distinguish between the mineral matters which was available in the coke ash before reaction and the ash which formed after dissolution reaction. As it can be seen in the pictures, there were globes and discrete interfacial products mainly composed of alumina and silica.

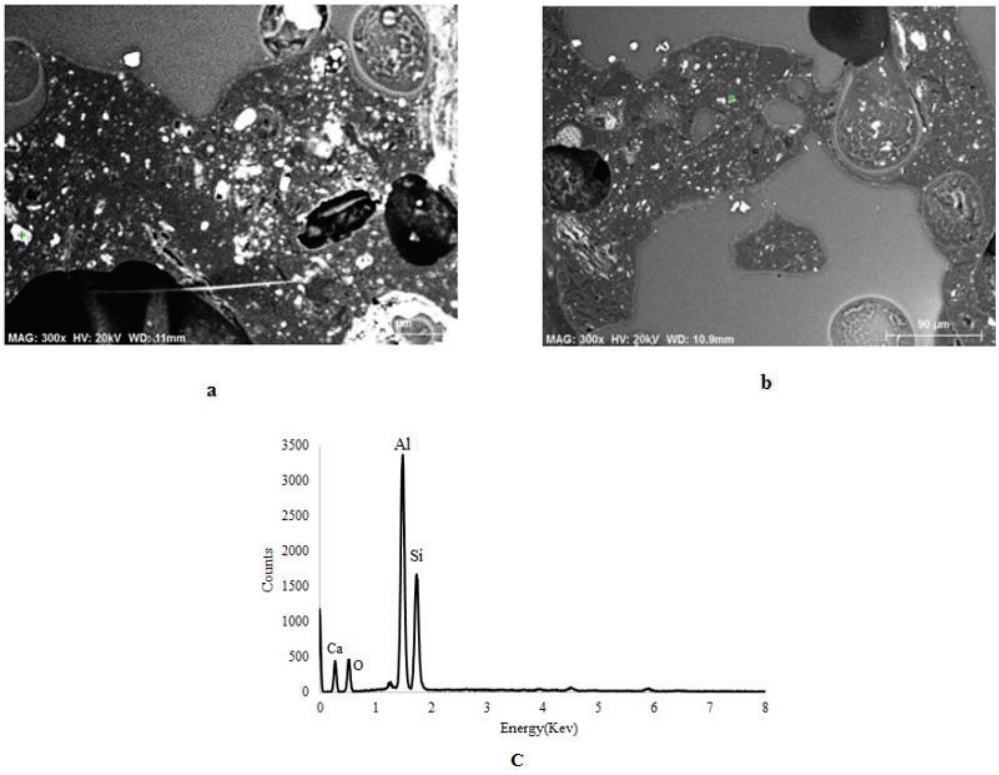

Figure 4.28: SEM image of coke E after a)15 sec and b)30 sec immersion in Fe-85%wt Mn and c) EDS analysis of a white globe.

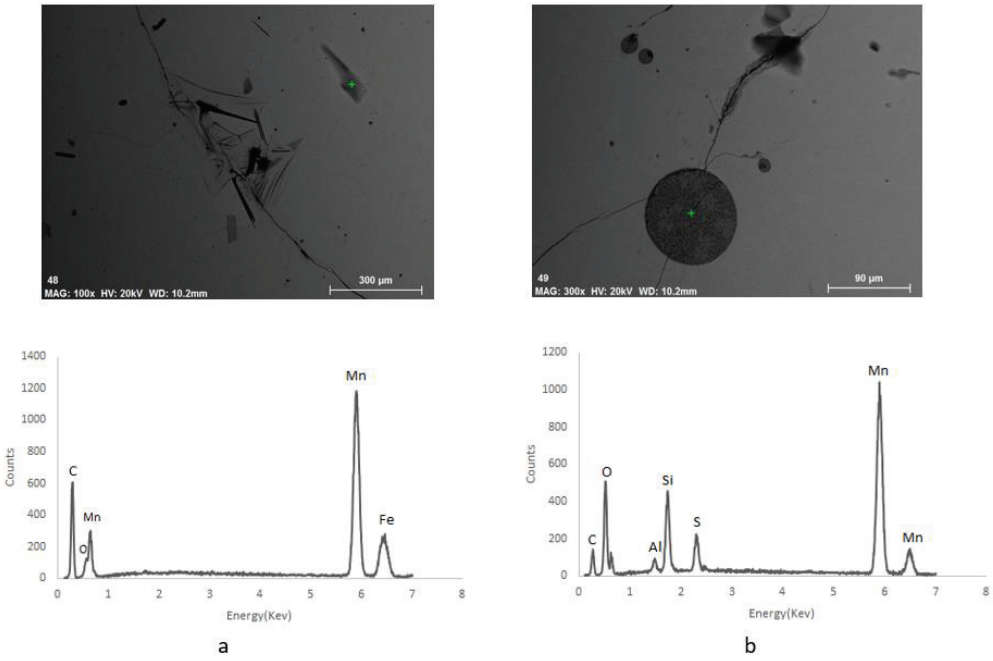

Figure 4.29: SEM image and EDS analyses of Fe-85%Mn that was in contact with coke E for 30 seconds.

Figure 4.30 and **Figure 4.31** show the coke D side of the interface and metal side of the interface after 30 seconds immersion in metal. Some products composed of alumina and silica are seen at the coke side of the interface and again in the metal side, there are some small particles including MnS and alumina and silica. It is worth mentioning that as **Figure 4.31** shows, there is no sign of carbide in the metal.

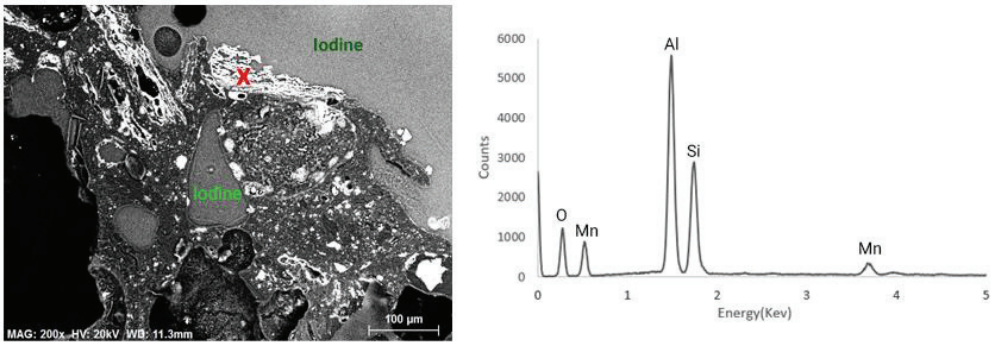

Figure 4.30: SEM images and EDS analyses of Fe-85%wt Mn and coke D interface carbon side after immersion for 30 seconds.

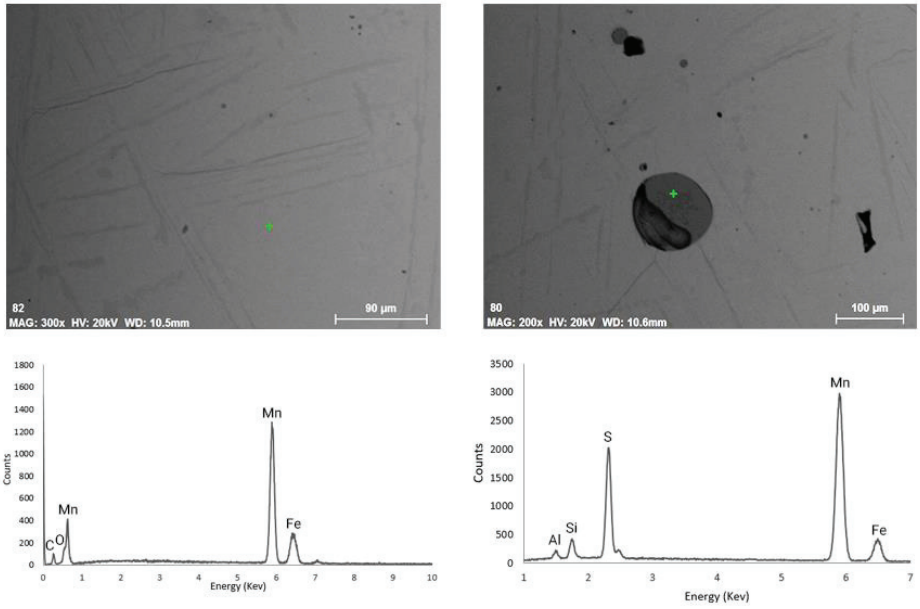

Figure 4.31: SEM images and EDS analyses of Fe-85%wt Mn and coke D close to the interface in metal after immersion for 30 seconds. a) bulk metal b) MnS particle in metal.

4.1.6 Sulfur dissolution

Some of the metal samples which were analyzed for carbon content were also analyzed for their sulfur content. The sulfur dissolution in the Fe-85%Mn over time for cokes C, D, E and F are shown in **Figure 4.32**. It can be seen that sulfur content followed a pattern similar to carbon dissolution rate and as the time is increasing, the sulfur dissolved in metal is also increasing. While cokes C, D and F show similar results, coke E dissolve more sulfur. This fits with the initial sulfur content shown in **Table 3.2** where it is seen that coke E has a higher sulfur content of 0.63%, while C, D and F have respectively 0.44, 0.50 and 0.50%S.

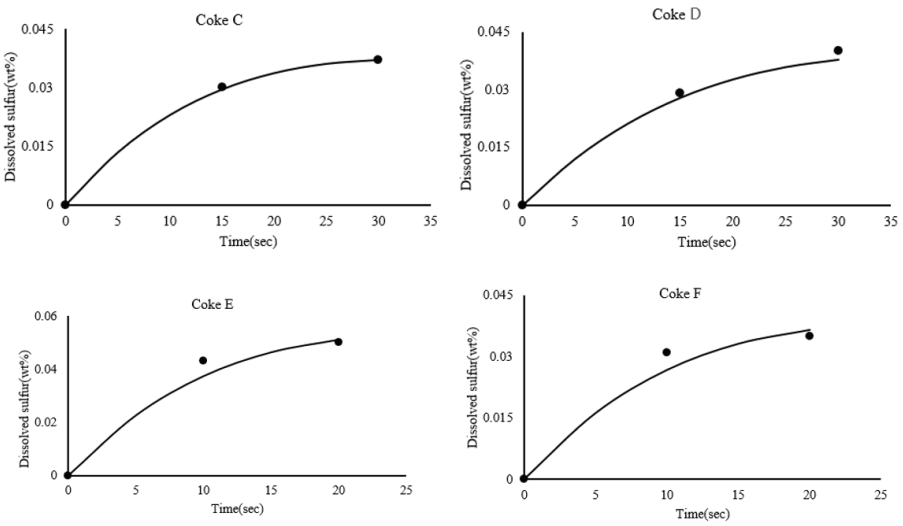

Figure 4.32: Sulfur pick-up content in the Fe-85 wt%Mn bath for coke C through coke F dissolution runs at 1550ºC.

4.2 Results of the wettability

Carbon dissolution is a two-phase interaction involving solid and liquid. Since mass transfer and heat transfer are the basic reactions involved in the process, wetting is therefore, the

first step towards carbon dissolution. A number of experiments were done to establish some of the interfacial phenomena between carbon materials and Fe and Fe-Mn alloy. The sessile drop technique was used to determine the dynamic wettability of cokes C, D, E and F, graphite and charcoal at 1550°C by Fe-85%Mn and also graphite, charcoal and coke C with pure iron. In this study, different types of carbon materials were cut in tablets with 10 mm diameter and 2-3 mm height. The wettability experiments were conducted under high purity argon gas in a horizontal tube furnace. Fe/Mn and Fe droplets weighed 0.4 g.

4.2.1 Wettability of carbonaceous materials with Fe-85wt%Mn

Wettability was measured as a function of time. The images were taken every three minutes after droplet started to melt. The wetting images of the cokes and graphite with Fe-85wt%Mn are shown in **Figure 4.33** to **Figure 4.38**. It is clear from the pictures that for coke, the initial contact angles are much lower that the final ones. For graphite and charcoal, a big difference cannot be seen between the initial contact angles and the final contact angles.

Figure 4.33: Sessile drop assembly for coke C. Initial (left) and final (right) contact angle images at 1550°C(Exp.92).

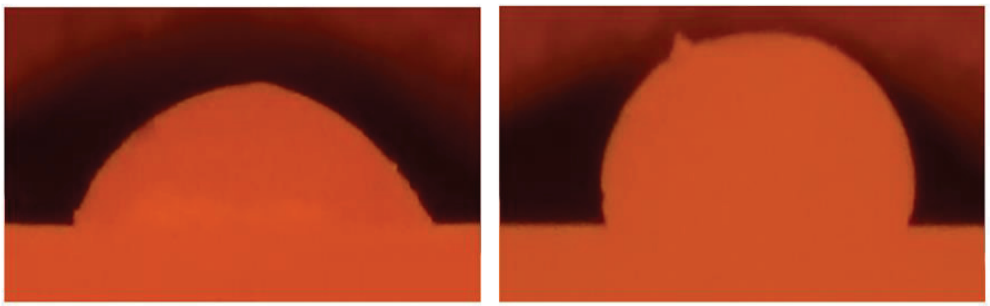

Figure 4.34: Sessile drop assembly for coke D. Initial (left) and final (right) contact angle images at 1550°C(Exp.93).

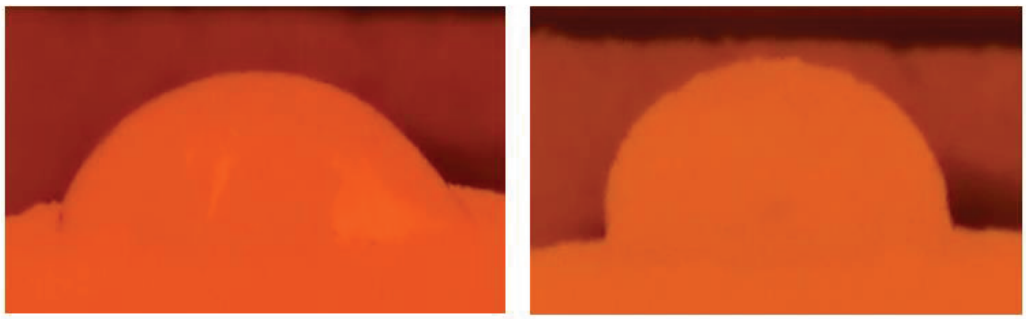

Figure 4.35: Sessile drop assembly for coke E. Initial (left) and final (right) contact angle images at 1550°C (Exp.94).

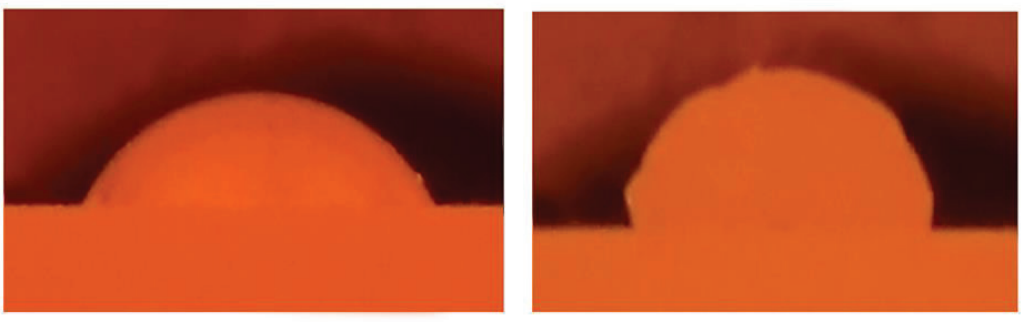

Figure 4.36: Sessile drop assembly for coke F. Initial (left) and final (right) contact angle images at 1550°C (Exp.95).

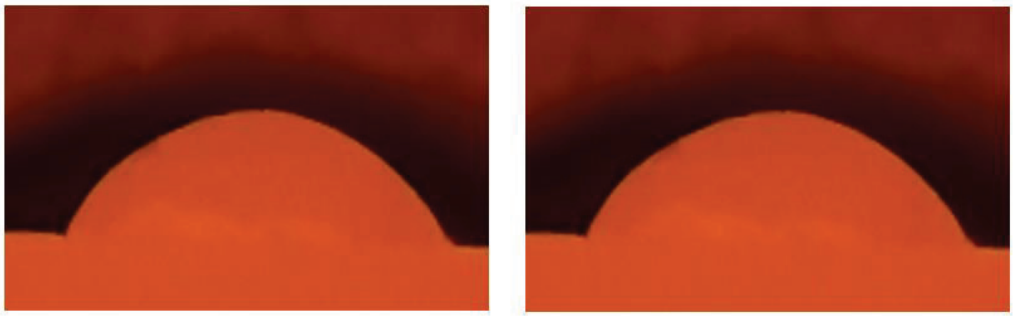

Figure 4.37: Sessile drop assembly for graphite. Initial (left) and final (right) contact angle images at 1550°C (Exp.90).

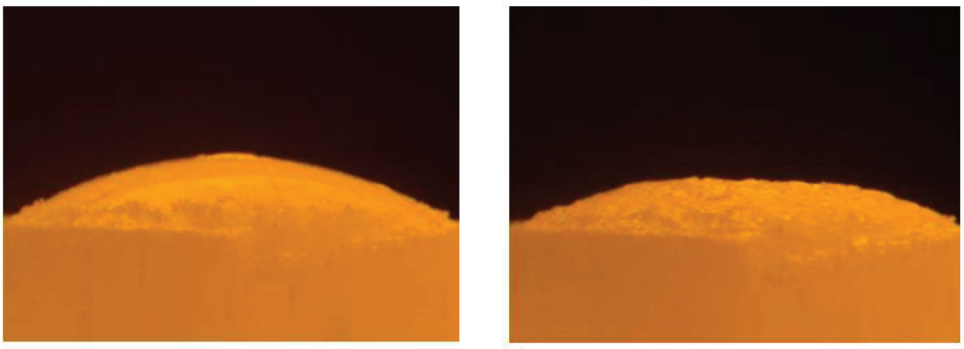

Figure 4.38: Sessile drop assembly for charcoal. Initial (left) and final (right) contact angle images at 1550°(Exp.91).

Results of the wettability studies on four cokes, graphite and charcoal with Fe-85wt%Mn and the replicates are summarized in **Figure 4.39**. It can be seen from **Figure 4.39**, that the contact angles for all four cokes were greater than 90° throughout the reaction period: The molten Fe-85wt%Mn was generally non-wetting coke substrates while it was wetting graphite and charcoal. Charcoal showed better wetting behavior compared to graphite and the contact angles were 30° and 65° for charcoal and graphite respectively.

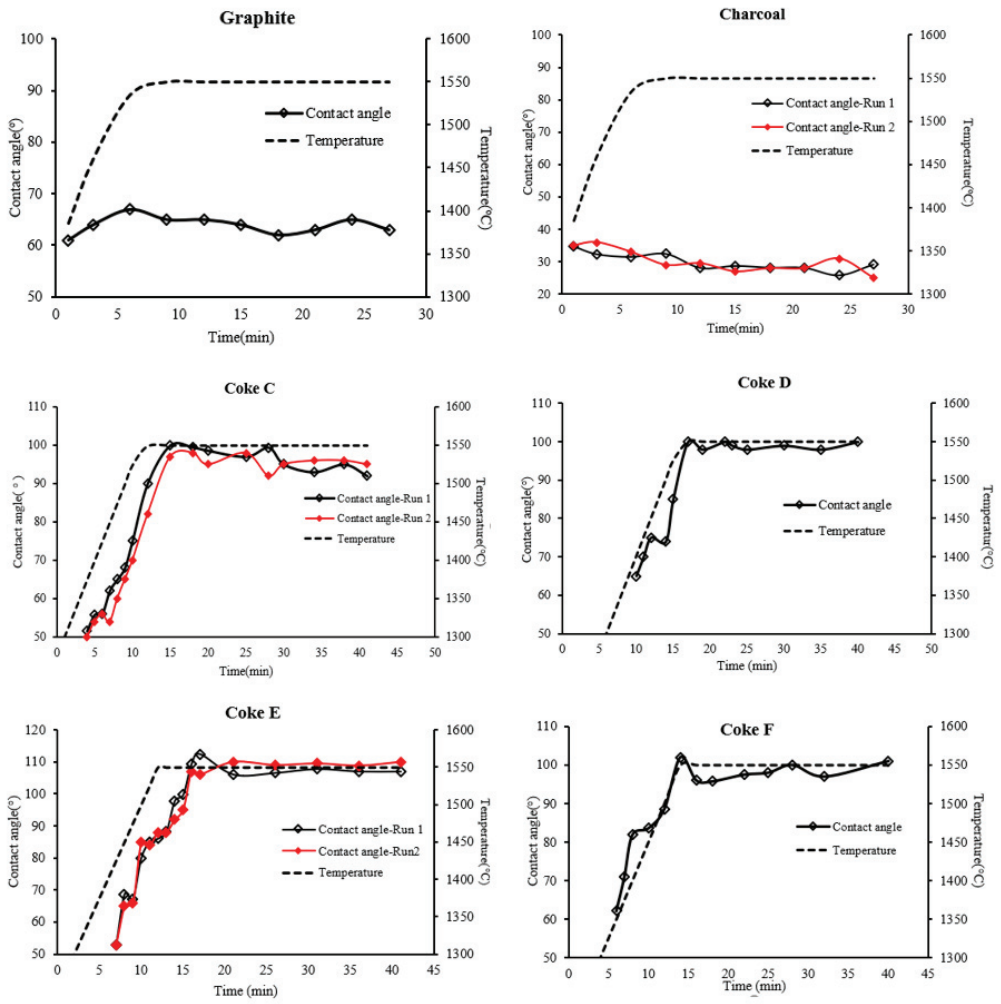

Figure 4.39: Dynamic contact angle measurements for coke D (Exp.93) coke C (Exp.92, Replicate100) coke E(Exp.94, Replicate 101) coke F(Exp.95) graphite(Exp.90) and charcoal(Exp.91, Replicate99) with Fe-85wt%Mn at 1550°C.

4.2.2 Wettability of carbonaceous materials with Fe

To be able to compare the wetting behavior of Fe-85wt%Mn and Fe with different carbon materials, three carbonaceous materials namely coke C, graphite and charcoal were chosen for wetting experiments with iron. The wetting images of coke C, charcoal and graphite with iron are shown in **Figure 4.40** to **Figure 4.42**. The same sample analysis of contact angle was used to measure the contact angle between carbonaceous materials and iron. From the pictures, the non-wetting behavior of coke and charcoal at final stage is visible while graphite showed wetting behavior.

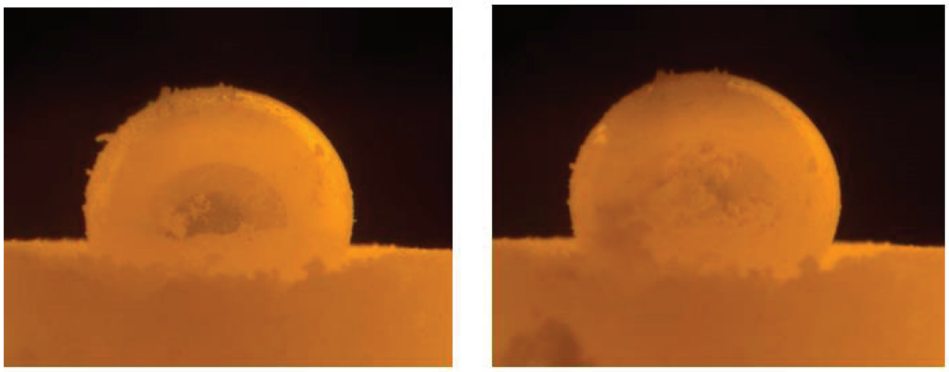

Figure 4.40: Sessile drop assembly for coke C. Initial (left) and final (right) contact angle images at 1550°C (Exp.96).

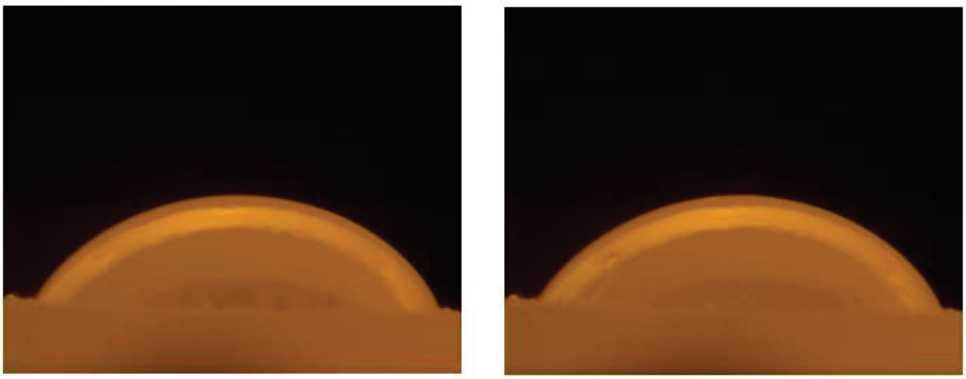

Figure 4.41: Sessile drop assembly for graphite. Initial (left) and final (right) contact angle images at 1550°C (Exp.97).

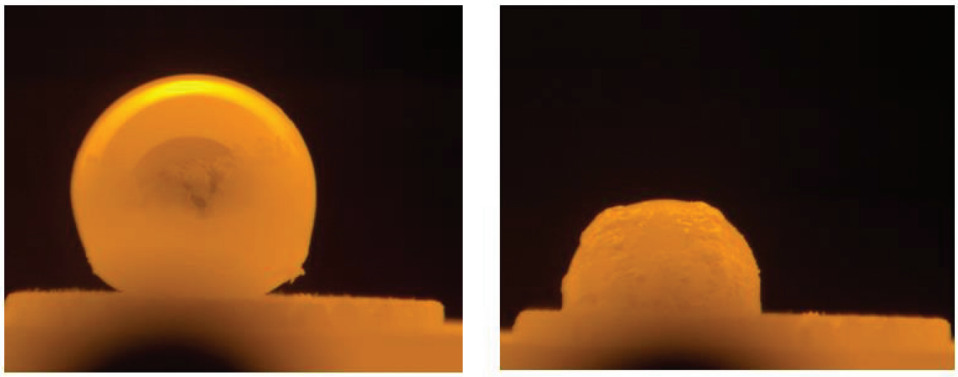

Figure 4.42: Sessile drop assembly for charcoal. Initial (left) and final (right) contact angle images at 1550°C (Exp.98).

Figure 4.42 shows that the volume of iron droplet decreased significantly. **Figure 4.43** shows the volume change of Fe droplet versus time for three different carbon materials. It can be seen that the greatest volume reduction was obtained for the case of charcoal substrate and smallest for coke. The iron has more or less penetrated the charcoal sample, which indicates a much better wetting than the measured wetting angle indicates.

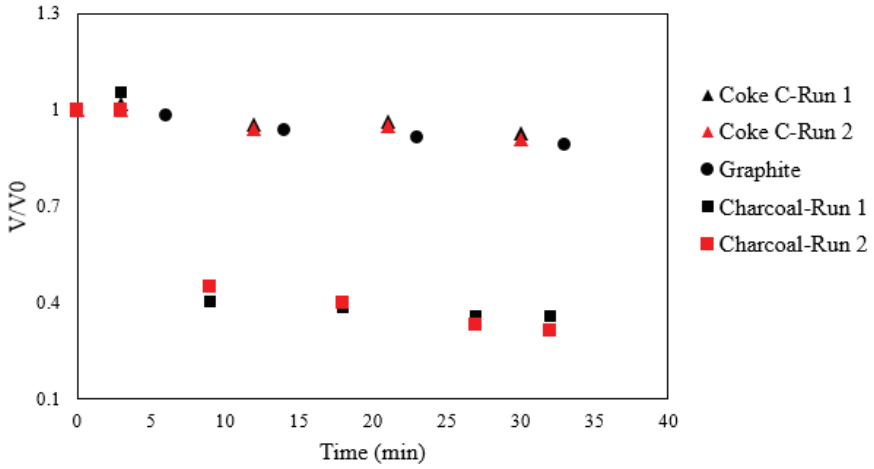

Figure 4.43: The changes in the V/V_0 ratio of Fe drop during wetting with three carbonic-eous material at 1550°C.

Results of the wettability studies on three carbonaceous materials with liquid iron and replicates are illustrated in **Figure 4.44**. In this figure, time zero was set at when the sample was at isothermal 1550°C. It can be seen from this figure that the contact angle for coke and charcoal were greater than 90° throughout the reaction, the molten iron was generally non-wetting coke and charcoal while was wetting graphite. Non-wetting behavior of coke and charcoal with iron might be related to the ash composition.

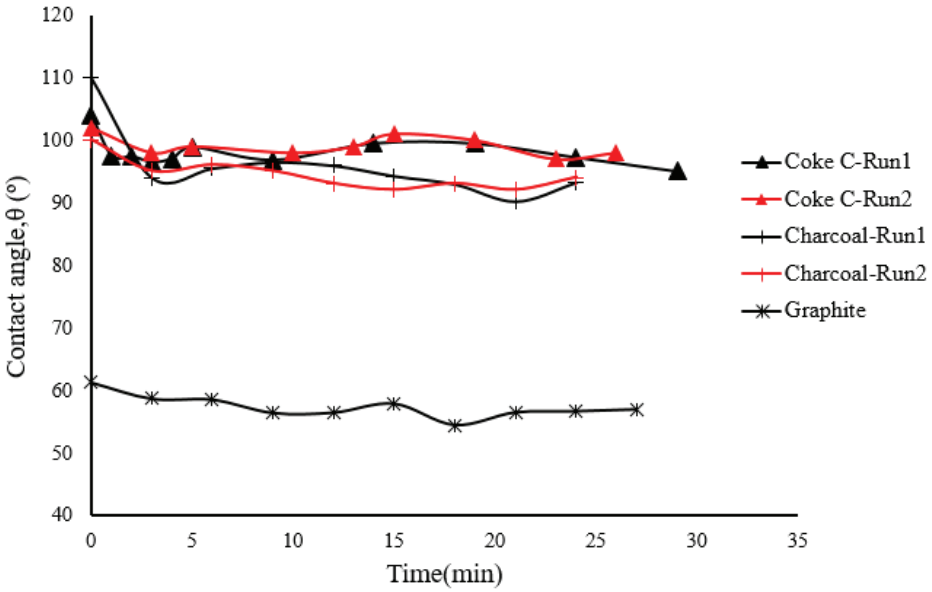

Figure 4.44: Dynamic contact angle measurements for coke C (Exp.96, Replicate102) graphite (Exp.97) and charcoal (Exp.98, Replicate103) with Fe at 1550°C.

4.2.3 Interfacial products

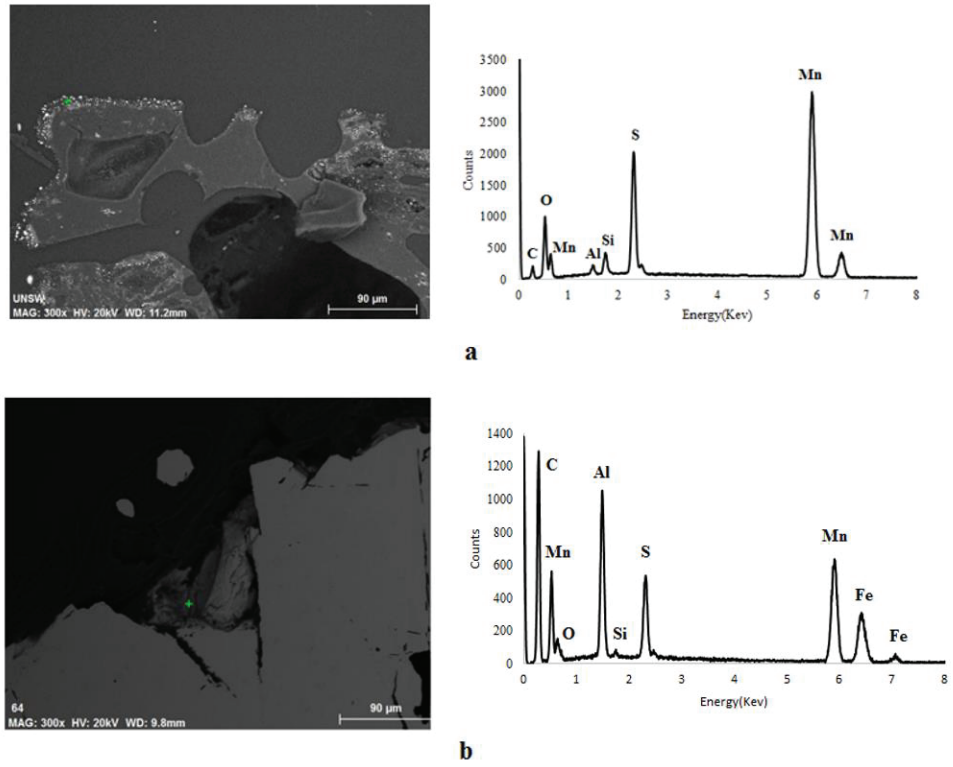

Figure 4.45: Ash layer including MnS particle in the a) coke side b) metal side of the coke E/metal interface after wetting experiment at 1550°C.

For investigation interfacial products using SEM and EDS after wetting reaction, coke E with the highest amount of sulfur and coke C with the lowest amount of sulfur were chosen. Presence of MnS, was verified by scanning electron microscopy accompanied with energy dispersive spectroscopy of the both sides of the interface of coke E as shown in **Figure 4.45**. **Figure 4.45a** shows the coke E side of the interface and it can be seen that an ash layer including mostly MnS covers the surface. **Figure 4.45b** shows the metal side of the interface and MnS was also detected in this part. Presence of alumina and SiC was also verified at the interface.

Figure 4.46 shows the metal which was in contact with coke E for 30 minutes at 1550°C. Carbide is visible in the bulk which means that metal probably was saturated with carbon and then the carbon will precipitate as graphite during cooling.

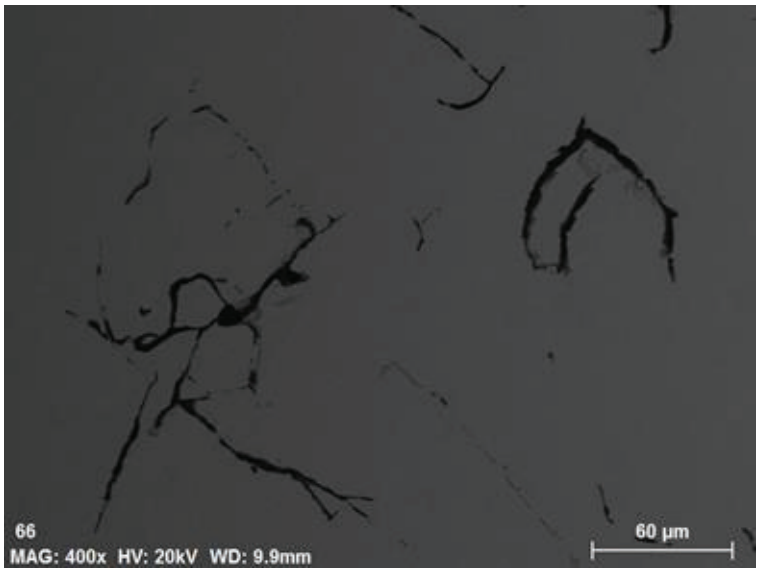

Figure 4.46: Interfacial products in the coke C side of the interface after wetting experiment at 1550°C.

Figure 4.47 shows the SEM image and EDS analysis of the interface of coke C and metal at coke side after wetting reaction at 1550°C. Some slag globes were detected at the interface and they are mostly composed of alumina and silica. The analyses also show Mn and Fe present, and it is believed that one has analyzed a mixture of oxide and metal phase.

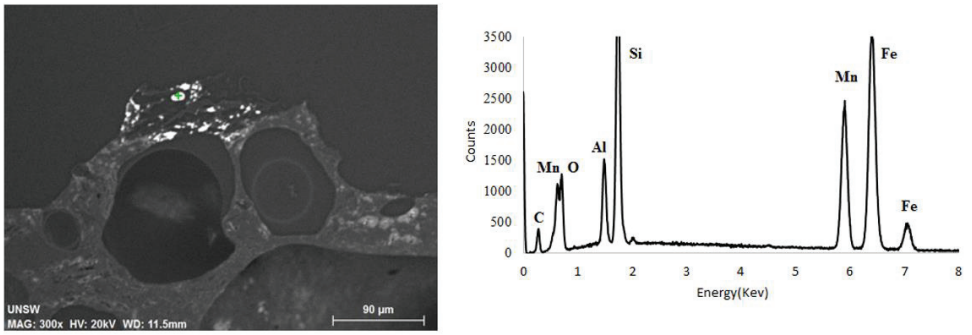

Figure 4.47: Fe-85wt%Mn metal bulk after wetting with coke C at 1550°C.

Figure 4.48 shows the SEM image of the bulk metal after wetting with coke C. It can be seen from SEM image and EDS analyses that the probably was saturated with carbon and then the carbon will precipitate as graphite during cooling. There is again a discussion if it is graphite mixed with the alloy phase or if it is (Mn,Fe)-carbide phases that has participated.

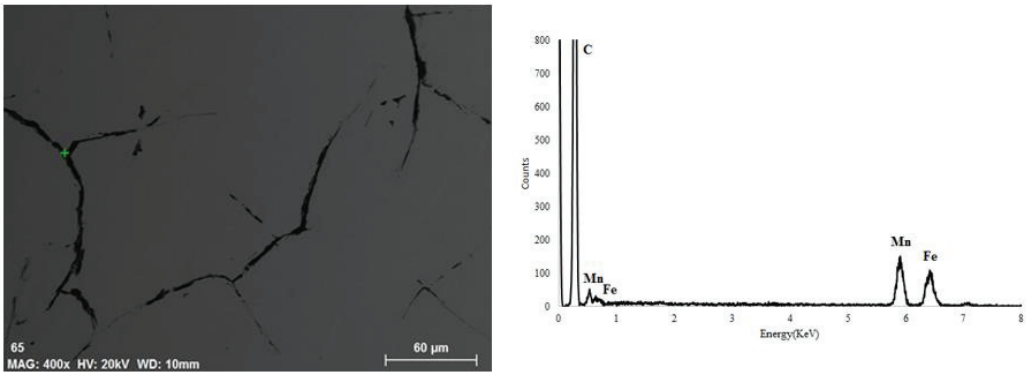

Figure 4.48: Fe-85wt%Mn metal bulk after wetting with coke C at 1550°C.

4.3 Results of carbon characterization

An important part of this research is investigating differences within and between groups of carbon materials. To be able to do so, the materials have to be characterized in a variety of ways. In this study, microstructure of carbonaceous materials at an atomic level has been

extensively studied using X-ray diffraction (XRD) and Raman spectroscopy as shown in Chapter 3. Effect of annealing temperature on the microstructure of different carbon materials was also studied and will be presented here. Additionally, macrostructure properties such as porosity, surface roughness and specific surface area of carbon materials were measured.

4.3.1 X-Ray Diffraction

Figure 4.49 presents XRD spectra and profiles of the 002 carbon peaks of original cokes A to F, charcoal and graphite. In the same figure the spectra is shown for the annealed carbon materials at 1250-1550°C as well. The shape of the 002 peak can be used as a qualitative indication of carbon structure crystallinity; carbon samples with narrower 002 peaks have a greater degree of ordering of carbon. A comparison of XRD profiles of samples treated at different annealing temperatures shows that the 002 carbon peak became sharper with increasing annealing temperature, indicating that the ordering of carbon increased with increasing annealing temperature.

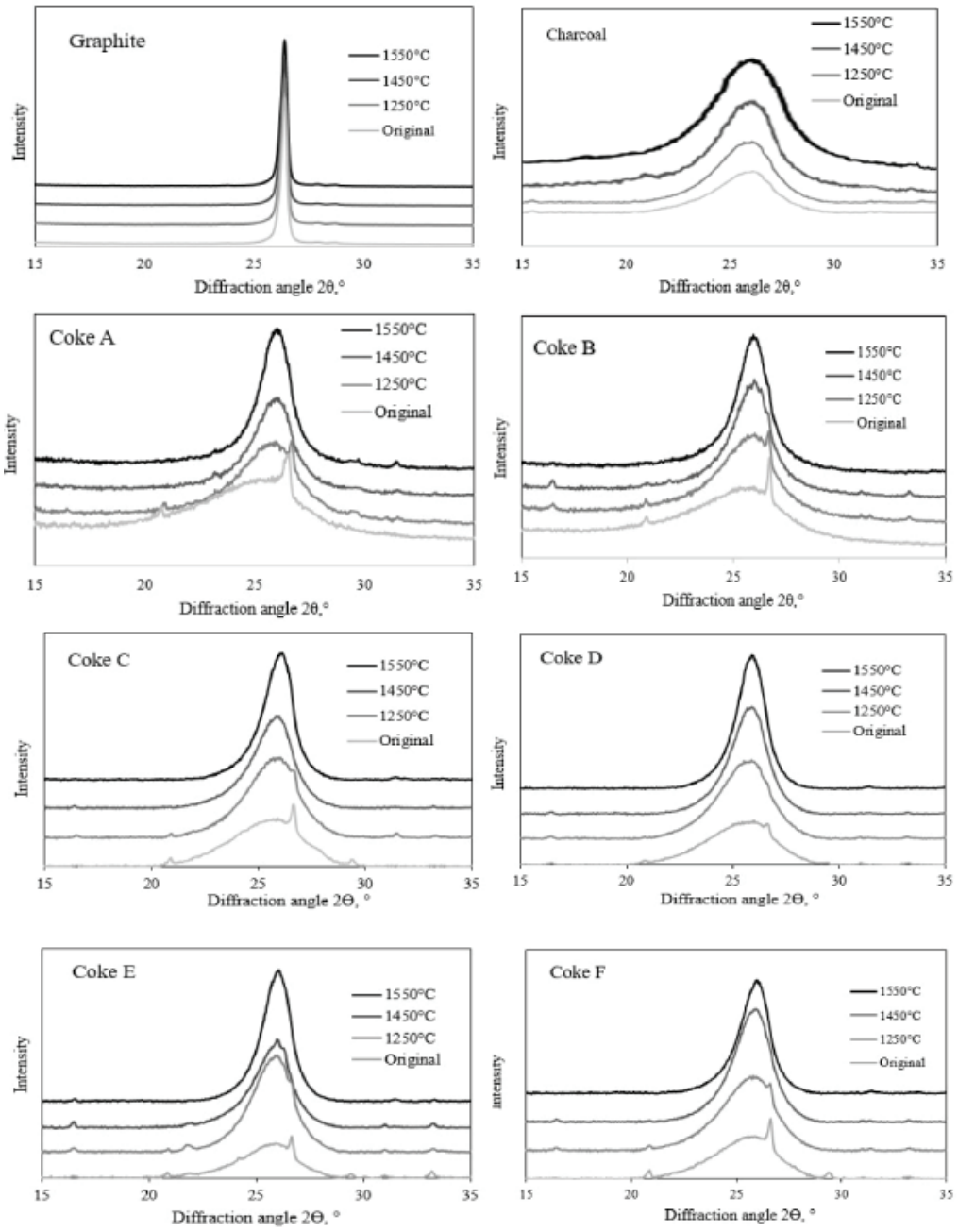

Figure 4.49: Profiles of 002 carbon peaks in XRD spectra of original coke A to coke F, charcoal and graphite and after annealing at different temperatures.

As it is shown in **Figure 4.49**, the peaks at 26 deg. in original coke samples was assigned to quartz in the coke ash. At higher temperature the SiO_2 would dissolve with other oxides, and the quartz peak cannot be seen. They were substantially removed in annealing above 1450°C. As it was expected, graphite with high ordered structure, did not change with increasing annealing temperature. The crystallite size of graphite remained constant (389 Å) during annealing.

The X-ray diffraction patterns of the charcoal is also shown in **Figure 4.49.** The diffraction profiles attributed to the 2θ = 26 deg. appear to be very informative. Narrowing of this peak, with increasing temperature is seen and this indicates developing atomic order of charcoal.

The effects of annealing on the carbon crystallite size L_c and interlayer spacing d_{002} for six cokes and charcoal subjected to different annealing temperature are presented in **Figure 4.50** to **Figure 4.56**. The crystallite size L_c of all carbonaceous materials increased with increasing heat treatment temperature. The growth of L_c is a reflection of the graphitization that occurs when the temperature rose over 1100°C[2]. As it is shown in the figures, cokes showed higher L_c compared to charcoal. Interlayer spacing d_{002} was also strongly affected by the annealing temperature. Increasing annealing temperature resulted in a denser structure and decreased d_{002} value. However, the minimum d_{002} value among all carbonaceous materials tested was higher than that of graphite (3.35Å). Cokes had a lower interlayer spacing than charcoal.

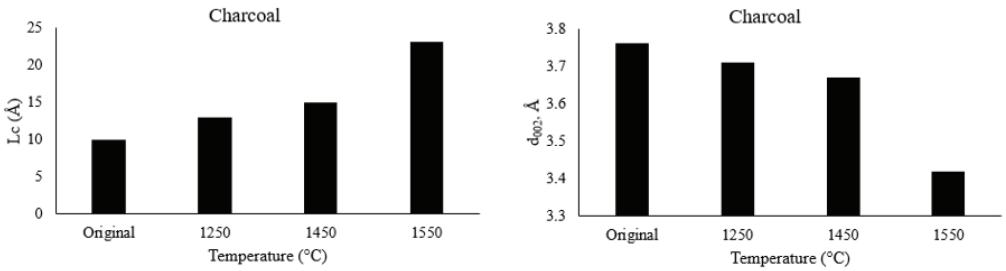

Figure 4.50: Crystallite size (L_c) and interlayer spacing(d_{002}) of charcoal annealed atg different temperatures(Exp.107-109).

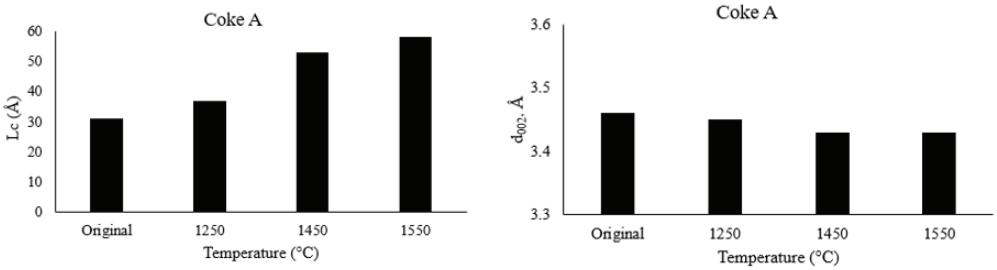

Figure 4.51: Crystallite size (L_c) and interlayer spacing(d_{002}) of coke A annealed at different temperatures(Exp.110-112).

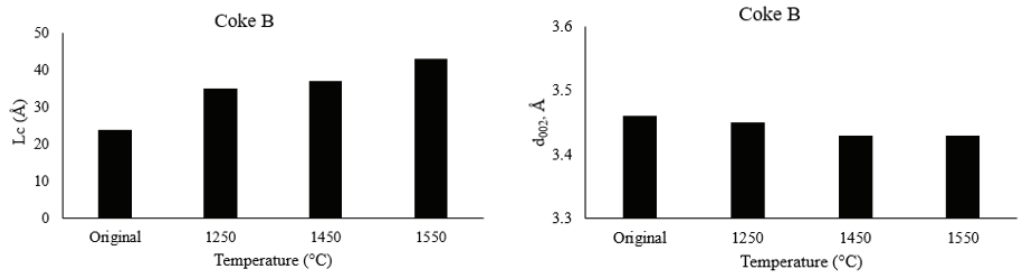

Figure 4.52: Crystallite size (L_c) and interlayer spacing(d_{002}) of coke B annealed at different temperatures(Exp.113-115).

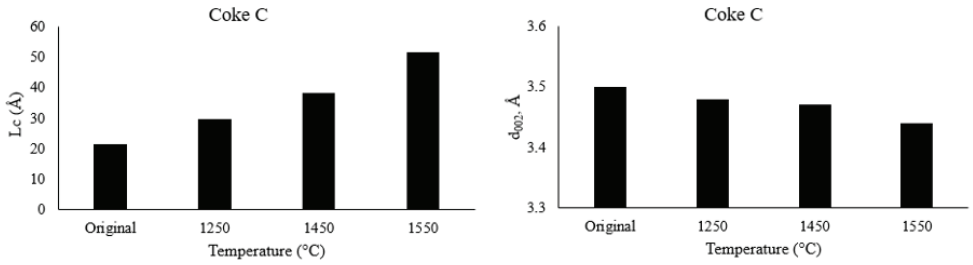

Figure 4.53: Crystallite size (L_c) and interlayer spacing(d_{002}) of coke C annealed at different temperatures(Exp.116-118).

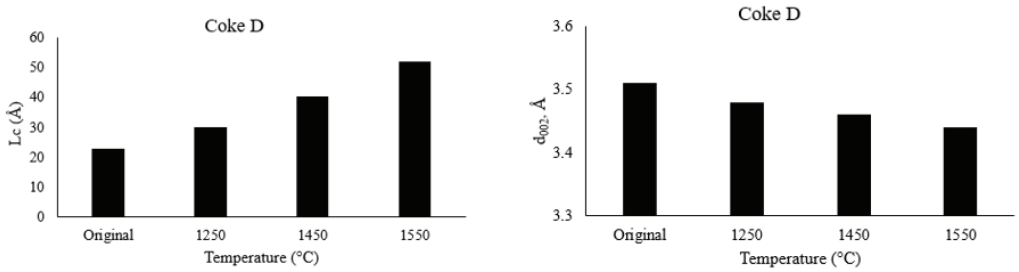

Figure 4.54: Crystallite size (L_c) and interlayer spacing(d_{002}) of coke D annealed at different temperatures(Exp.119-121).

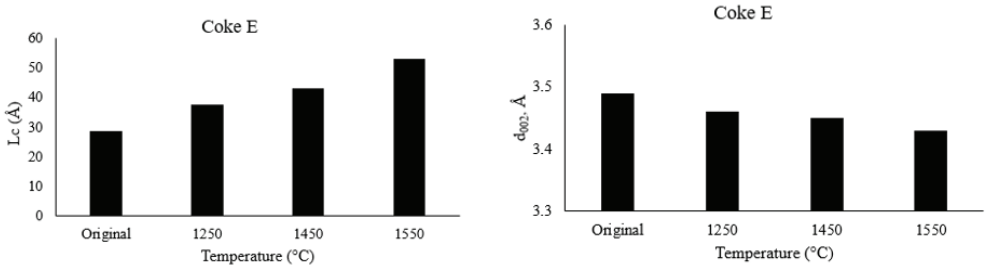

Figure 4.55: Crystallite size (L_c) and interlayer spacing(d_{002}) of coke E annealed at different temperatures(Exp.122-124).

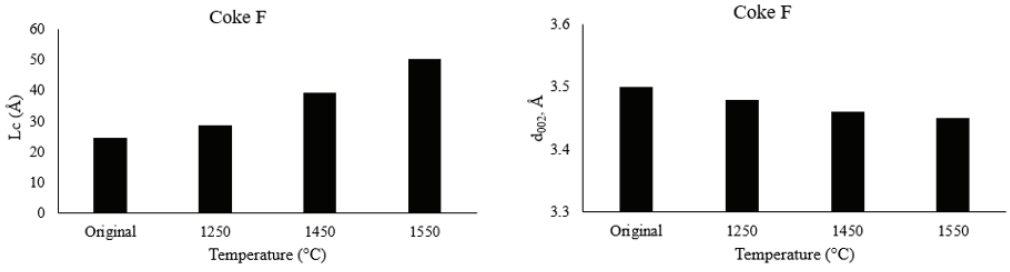

Figure 4.56: Crystallite size (L_c) and interlayer spacing(d_{002}) of coke F annealed at different temperatures(Exp.125-127).

Figure 4.57 and **Figure 4.58** compare the crystallite size and interlayer spacing of different carbon materials at different temperatures. Cokes had larger L_c values and crystallite size compared to charcoal. Cokes had lower interlayer spacing compared to charcoal demonstrating more complete graphitization.

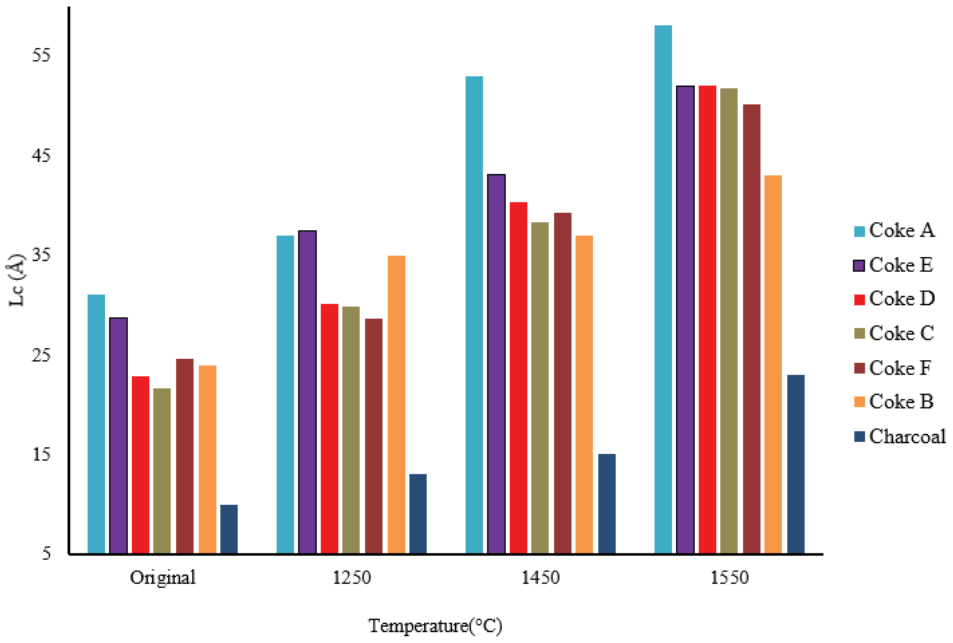

Figure 4.57: Crystallite size (L_c) of different carbon materials annealed at different temperatures.

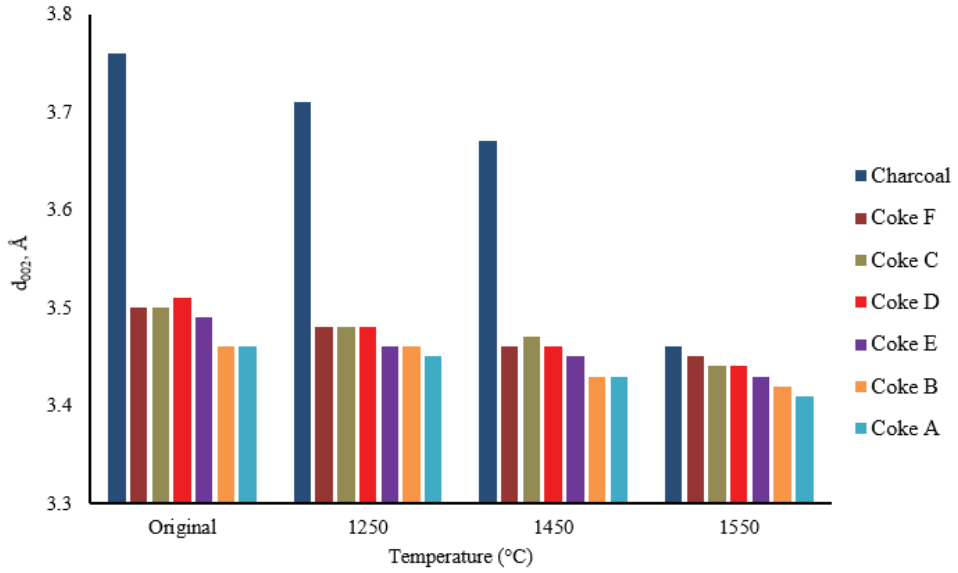

Figure 4.58: Interlayer spacing (d_{002}) ofdifferent carbon materials annealed at different temperatures.

4.3.2 Raman spectroscopy analysis

For investigating the microstructure of different carbon materials, Raman spectroscopy was also done for four cokes and graphite to see if it validates the results of XRD.

Figure 4.59 shows the Raman spectra for all cokes. The figure also includes Raman spectrum of graphite. The Raman spectrum of original cokes contained two overlapping D and G bands centered at around 1360 and 1600 cm^{-1}, respectively. Both bands became sharper when the annealing temperature increased from 1250°C to 1550°C. Raman spectrum of graphite presented three individual peaks centered at 1355, 1580, and 1620 cm^{-1}. Comparison of the Raman spectra of metallurgical coke and graphite indicates that the structure of metallurgical coke transformed towards graphite with increasing annealing temperature. The relative height of the D band peak to the G band peak also increased as annealing temperature rose.

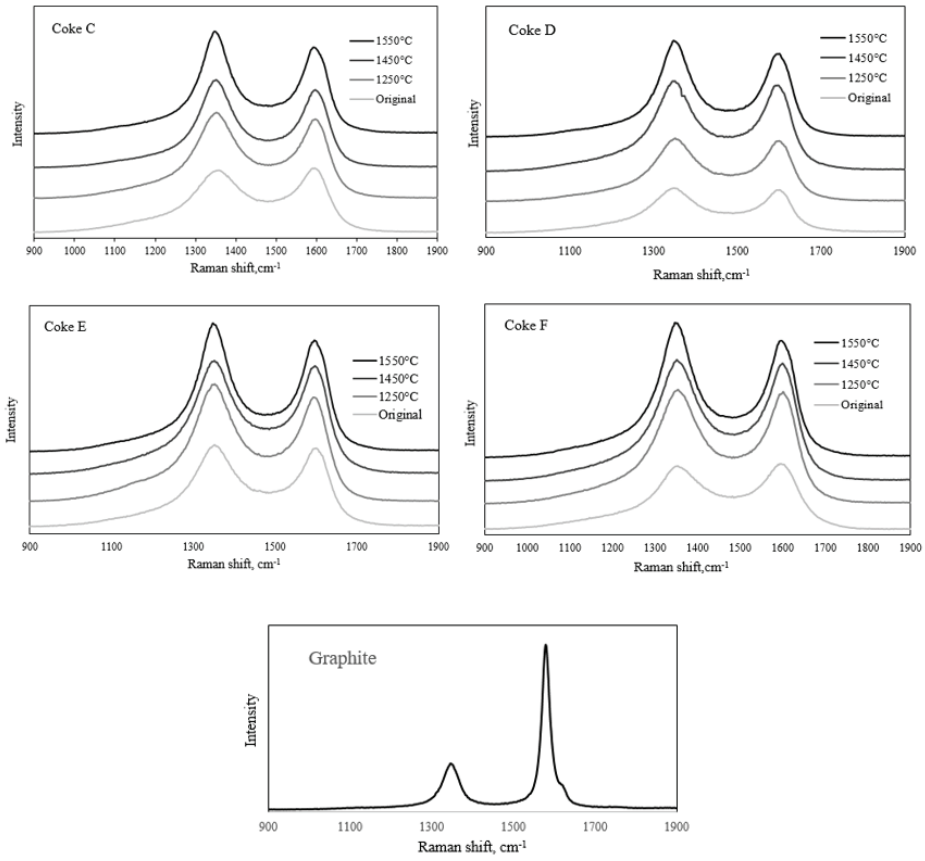

Figure 4.59: Change in Raman spectrum of cokes with annealing temperatures and graphite.

The G fraction of four types of cokes heat treated at different temperatures are presented in **Figure 4.60**. G fraction of all cokes increased as annealing temperature increased which indicates that the proportion of graphitic structure in cokes increased in the process of thermal annealing. The G fraction of tested graphite was approximately 58 pct which was higher that the G fraction of all cokes annealed at 1550°C.

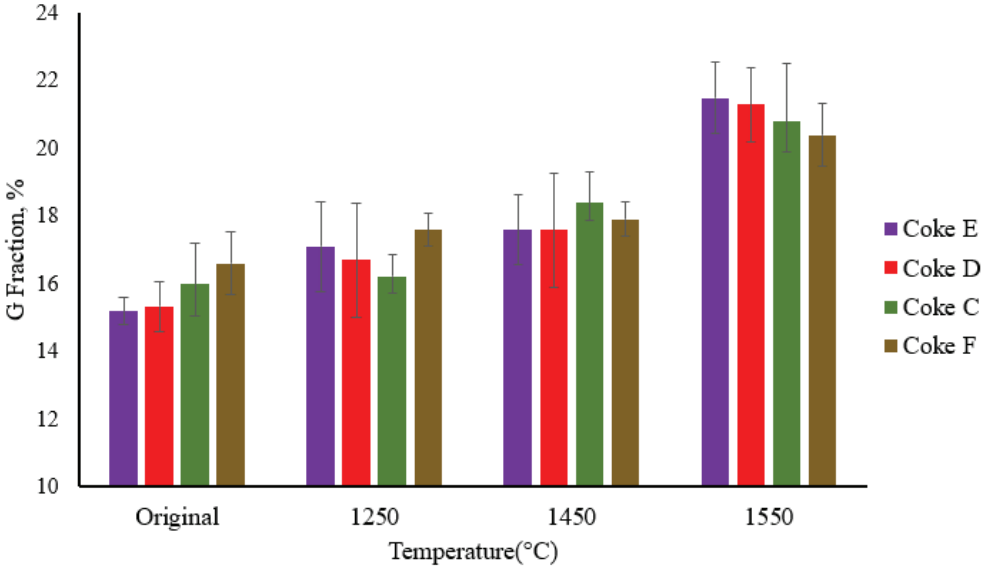

Figure 4.60: G fraction of different cokes annealed at different temperatures. The error bars show the standard deviations of the parameters for each sample.

The intensity ratio of the D band to the G band of different cokes with the treatment temperature are shown in **Figure 4.61**. General trends can be found that the peak intensity ratio of the D band to the G band decrease slightly for all four types of cokes. The decrease of I_D/I_G band ratios with the increase of the treatment temperature implied that structural defects and imperfections of the carbon crystallites were gradually eliminated during heat treatment.

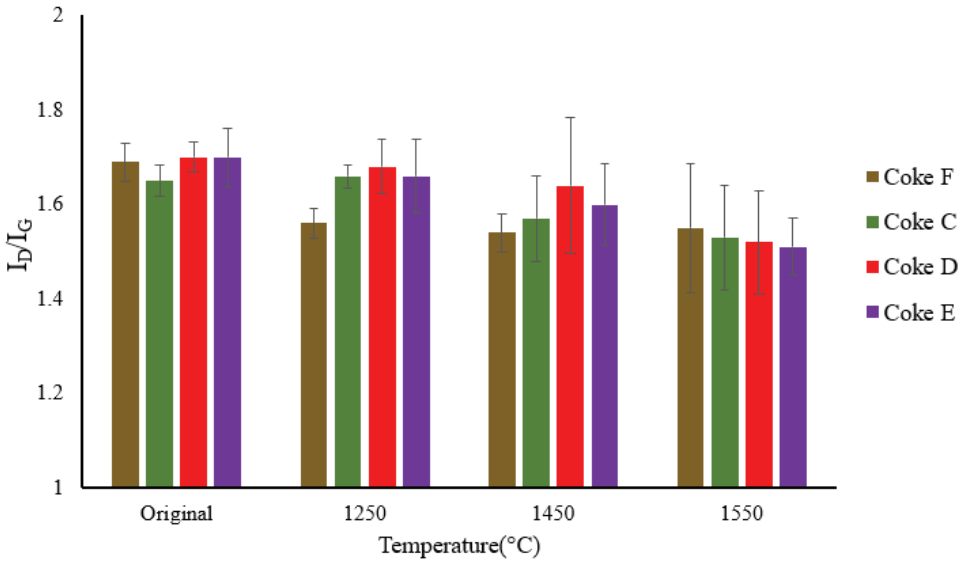

Figure 4.61: I_D/I_G for different cokes annealed at different temperatures. The error bars show the standard deviations of the parameters for each sample. The dashed lines show the trend.

As it is shown in **Figure 4.60** and **Figure 4.61**, at 1550°C, coke E has the highest G fraction followed by cokes D. Among these four cokes, coke F has the lowest G fraction and the highest I_D/I_G. It indicates that at 1550°C, coke E has the most ordered structure.

4.3.3 Surface roughness

The surface roughness of cokes A and B and graphite and charcoal were measured with an optical microscope. **Figure 4.62** and **Figure 4.63** show two-dimensional topographic map of these carbon materials. **Figure 4.62** shows that graphite and charcoal has quite uniform surfaces. The majority of graphite surface is green and yellow showing variances in height in the range of -10 to 15 µm and the majority of charcoal surface is blue and green showing height in the range of -30 to 5µm. **Figure 4.63** shows deeper pores for cokes compared to graphite and charcoal.

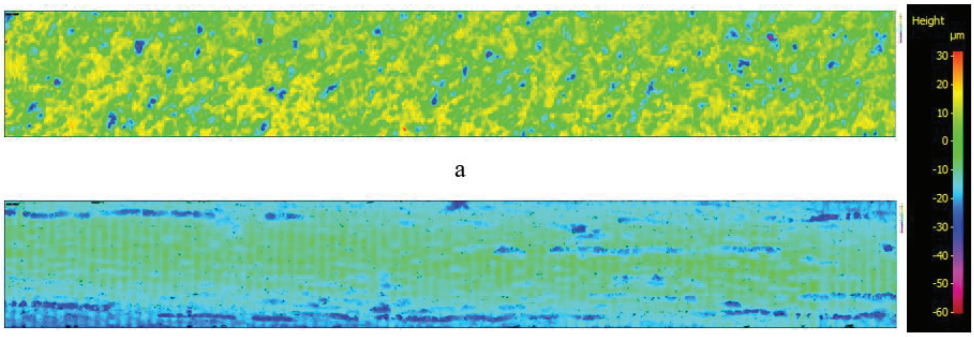

a

b

Figure 4.62: Two-dimensional topographic map of a) graphite b) charcoal at 20X magnification.

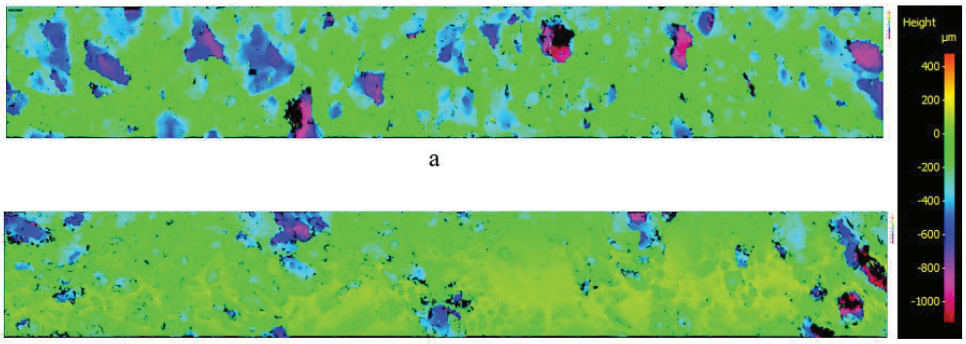

a

b

Figure 4.63: Two-dimensional topographic map of a) coke A b) coke B at 20X magnification.

Figure 4.64 shows three-dimensional topographic map of cokes C, D. E and F and also graphite which were measured with a laser microscope. **Figure 4.64a** shows that the graphite surface is smooth and is different than the cokes surfaces which have lots of pores. More topographic maps of different carbonaceous materials are shown in Appendix C.

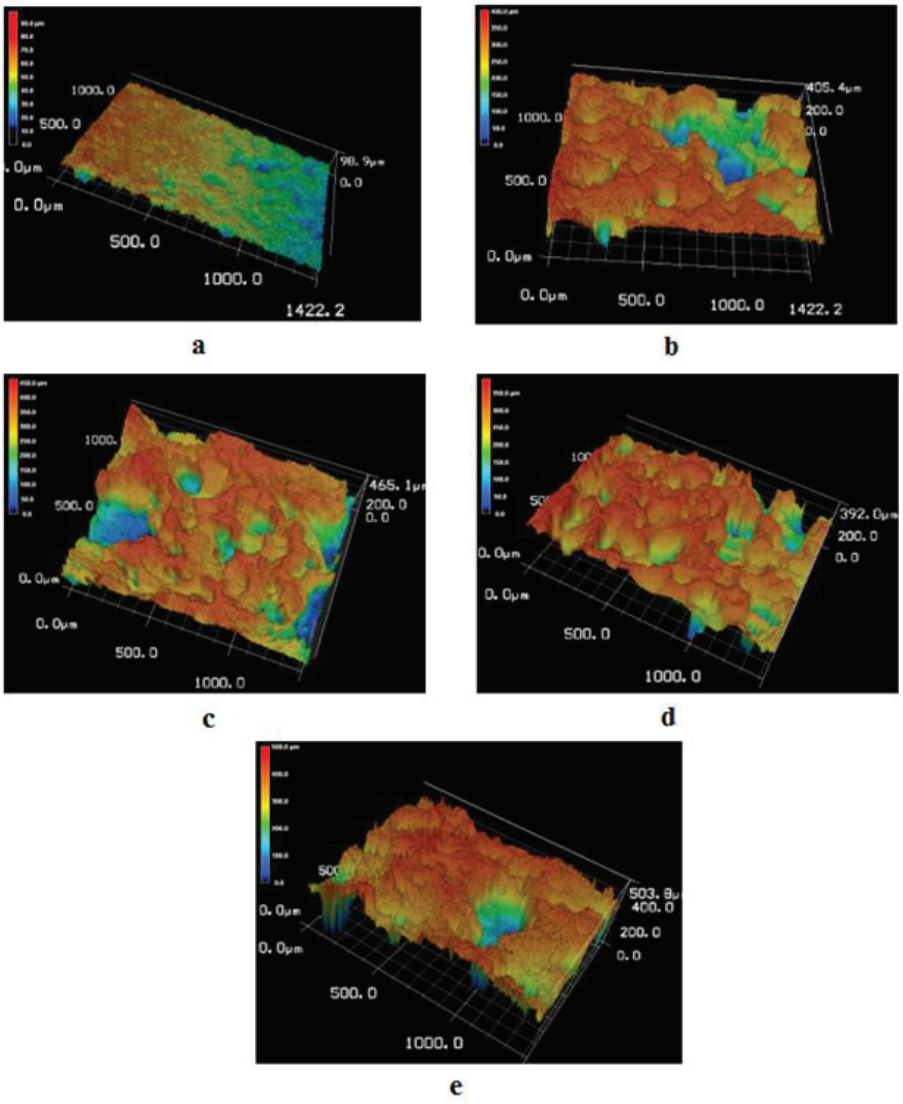

Figure 4.64: Three-dimensional topographic map of a) graphite b) coke C c) coke D d) coke E e) coke F at the same magnification.

5 Discussion

5.1 Dissolution mechanism

For carbon dissolution from solid carbon into Fe-Mn melts, the following steps could be rate determining:

Step 1. Dissociation of carbon atoms from its lattice site into the carbon/metal interface to establish a higher carbon concentration as shown in **Figure 5.1**.

Step 2. The diffusion or mass transfer of carbon atoms from the interface in the boundary layer(δ).

Step 3. The diffusion or mass transfer of carbon atoms into bulk liquid.

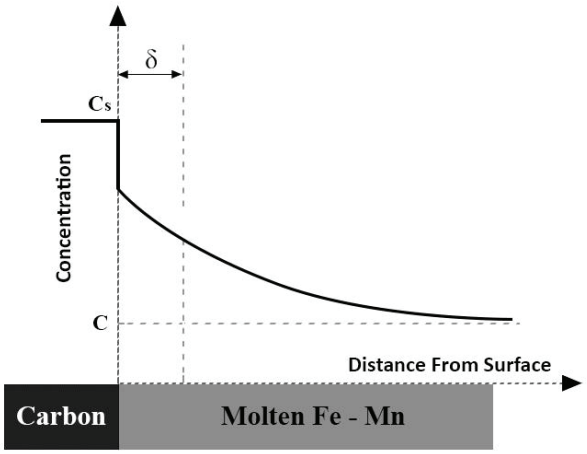

Figure 5.1: Schematic diagram of controlling steps in carbon dissolution from solid to molten metal (C is the bulk carbon concentration, C_s is the carbon saturation level at the interface and δ in the boundary layer).

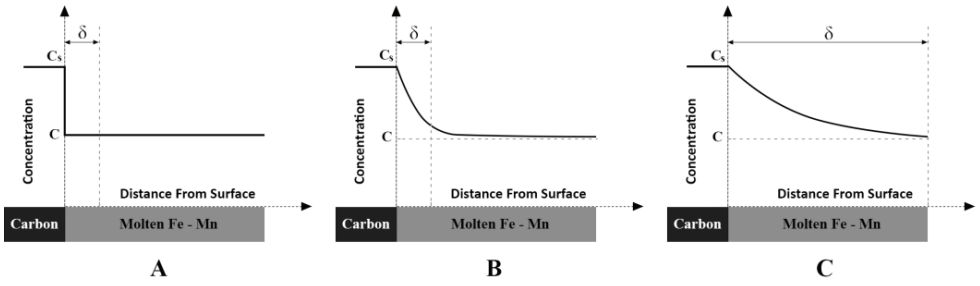

Figure 5.2: Three extreme cases of possible rate limiting steps.

Figure 5.2 shows the 3 extreme possible rate limiting steps. In Case A, the mass transfer in boundary layer and in the bulk are fast enough and the interfacial reaction is very important.

Carbon atoms are normally in vibration at the position on crystal sites. Existence of bonding energy between atoms prevents carbon atoms from escaping from the crystal site. However, the vibration will increase with increasing absorption of energy due to high temperature from the surroundings. Step 1 is concerned with dissociation of carbon atoms from their crystal sites by absorption of energy from high temperature molten metal. The rate of dissociation carbon atoms from crystal sites depends on many factors such as temperature, crystal microstructure and macrostructure of carbonaceous materials and the area of crystal surface opened for the interaction.

In Case B in **Figure 5.2**, the rate limiting step is the carbon diffusion in boundary layer. In this case, the dissociation of carbon from its crystal site and also the mass transfer of carbon in the metal bulk are fast. In Case C, only diffusion is determining the mass transfer and it also means that the boundary layer has an infinite thickness.

To evaluate the metal convection at higher temperature, heat transfer was modelled with COMSOL with the help of Trygve Storm Aarnæs. As it is shown in **Figure 5.3**, in the boundary layer, the velocity is the lowest and between 0 and 0.04 mm/s and will be about 0.4 mm thick. The highest velocity took place in the metal bulk and it is around 0.25-0.4 mm/s. However, the velocity of metal is fairly low compared to the velocity caused by rotating rods or induction furnace in comparing methods and can hence be a contributor to the rate in these experiments. The driving force of the velocity in the bulk metal will be the

temperature gradient shown in **Figure 5.4** from top to bottom. In the following discussion it is however assumed that the main part of the rate determining mechanism is a mixture of the chemical reaction and the mass transfer through the boundary layer.

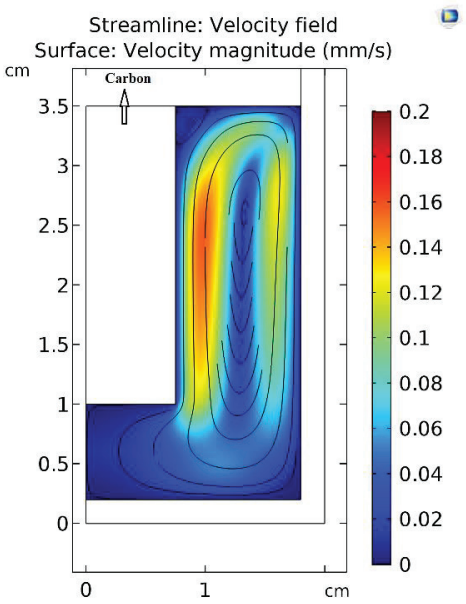

Figure 5.3: The Fe-85wt%Mn convection (mm/s) at 1550°C.

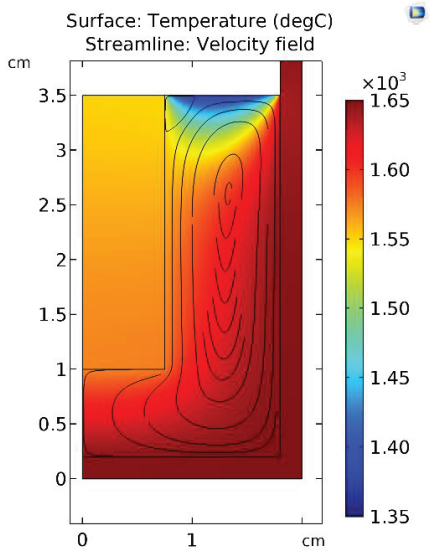

Figure 5.4: Temperature distribution in the crucible.

The rate of mass transfer depends on temperature, carbon saturation level and also stirring speed of metal. In this study we are not able to calculate k_r and k_m but we can investigate the factors influencing them and then evaluate the most probable dissolution mechanism. **Equation 2.22** is shown again in the following for convenience.

$$\frac{\mathbf{1}}{\boldsymbol{k_t}} = \frac{\mathbf{1}}{\boldsymbol{k_r}} + \frac{\mathbf{100}\boldsymbol{f}}{\boldsymbol{k_m \rho K_r}} \qquad \mathbf{2.22}$$

In previous studies [55, 58], the dissolution mechanism for dissolution of graphite in iron was determined to be mass transfer of carbon into molten iron. In this case, the dissolution coefficient k(1.48-2.93×10^{-4}m/s) is the maximum carbon mass transfer rate that could be established. A good agreement was seen in other studies that the dissolution rate of graphite is higher than non-graphitic carbon materials and the dissolution mechanism in this case, was determined to be interfacial reaction.

In our study, cokes have the highest dissolution rate (4.81-6.73×10^{-2} cm/s) following by graphite (3.52×10^{-2} cm/s) and the lowest dissolution rate constant of charcoal (1.47×10^{-2} cm/s). Thus, in this study, liquid side mass transport is not rate limitation for graphite dissolution and it means that the interfacial reaction will also be one of dominant rate

controlling steps during carbon dissolution even for graphite. As the method used in this investigation is a stagnant method, it is however in discrepancy with previous investigations that the present method should have a lower mass transfer rate.

Temperature will not directly affect the contact area, but temperature may indirectly affect the wettability between solid carbon and liquid, viscosity and fusion of the ash to affect the contact area. Temperature has a stronger impact on k_r than k_m because chemical reaction usually has larger activation energy. Temperature will affect C_{sat} and K_r. It can also affect k_r through solid carbon structure.

Structure of carbon may affect k_r, K_r and C_{sat}. This is because k_r describes the dissociation reaction rate of carbon atoms from solid lattice into the metal. The dissociation process includes the ruptures of atomic bonding type and the bonding strength are determined by the solid structure. K_r is related to the free energy change which depends on the solid structure. Different carbon materials such as graphite, charcoal and cokes are carbon of different structure and may have different K_r. C_{sat} is the equilibrium carbon content with the solid and varies with K_r and thus the solid structure. It is however expected that the K_r and C_{sat} is relatively close to the values for graphite.

Ash in carbonaceous materials would accumulate at the interface and become physical barriers at the interface which will reduce contact area available for further carbon dissolution.

Roughness, porosity and BET of different carbon materials may affect contact area between metal and carbon materials.

Sulfur is usually present in carbonaceous materials, either in carbon structure or in the ash phase. The sulfur dissolution from coke or coal occurs during carbon dissolution. The sulfur pickup will change carbon saturation content and k_r by sulfur adsorption blockage during carbon dissolution process. The major component in ash is silica, and the silica reduction will occur when fused ash contacts the liquid through the **Reaction 5.1**:

$$\boldsymbol{SiO_2 + 2C = Si + 2CO} \qquad \textbf{5.1}$$

This reaction will take a portion of carbon away from metal, increase silicon in the liquid and reduce silica in the ash. It will affect the carbon dissolution in metal and also the viscosity of the ash.

Sulfur can also react with CaO and MnO present in the system and consume dissolved carbon due to **Equations 5.2** and **5.3**. The product of these reactions, CaS and MnS, may remain at the interface to reduce contact area. CO generated from side reactions may contribute to the liquid phase agitation to increase k_m. When fluxing materials such as CaO present in the system, following reaction will occur to consume dissolved carbon and the product of this reaction, CaS may remain at the interface to reduce contact area.

$$\boldsymbol{S + C + CaO = CaS + CO} \qquad \textbf{5.2}$$

$$\boldsymbol{S + C + MnO = MnS + CO} \qquad \textbf{5.3}$$

CO generated from **Equations 5.1**, **5.2** and **5.3** may contribute to the liquid phase agitation to increase k_m[46]. On the other hand, the gas bubbles could be jammed at the interface to reduce the area available for carbon dissolution.

Interfacial active elements in the liquid, such as sulfur, would occupy the reaction sites to reduce k_r. Previous investigations on the sulfur effect showed that the dissolution rate was controlled by both mass transfer and interface reaction when sulfur was present in metal [39].

Alloy composition, that is Mn/Fe ratio, will affect the activity coefficient of carbon in liquid and therefore the carbon saturation content. Alloying elements will also affect k_m through affecting diffusivity of carbon in the liquid and the viscosity of the liquids [46].

In this study, the overall carbon dissolution rate (k_t) was calculated for all carbon materials and it includes the liquid mass transfer and interfacial reaction. The overall carbon dissolution rate constant was introduced in the first order kinetic equation and the integrated form. A good linear relationship was obtained by plotting $-k_t t = V/A \ln[(C_s-C_t)/(C_s-C_0)]$ versus time using experimental data even for cokes and charcoal as it is shown in **Figure 5.5**.

Contrary to other reported studies in this area[36, 39, 40, 54, 58, 60, 70] changing in surface area of carbon materials was considered. As it was mentioned Chapter 3, the volume was calculated from the melt mass and density.

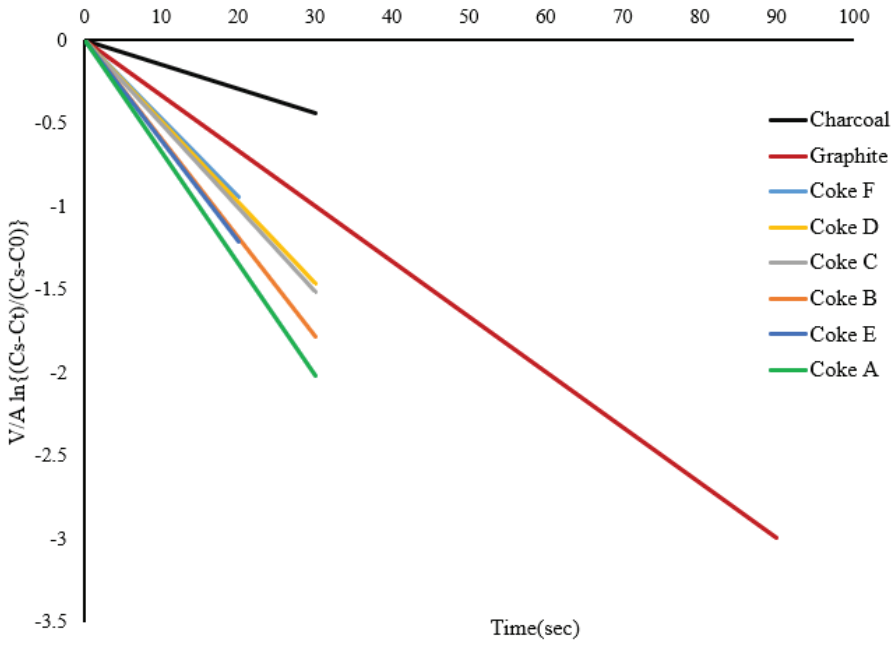

Figure 5.5: First order mass transfer coefficient plots for different carbon materials dissolution in Fe-85wt%Mn at 1550°C where the slope is k_t.

5.2 Effect of temperature on dissolution

To investigate the temperature dependence of carbon dissolution in this study, cokes A and B and charcoal and graphite (big and small samples) were chosen for further dissolution experiments at two different temperatures, 1450°C and 1550°C. A comparison of k_t value of different carbon materials at different temperatures, shows that temperature had influence on the dissolution rate constant of all carbon materials. This effect was lower on graphite and higher on cokes and charcoal.

It is worth mentioning that in this study, experiments were done just at two temperatures, thus the activation energy results may not be accurate enough. Results of **Table 4.3** are further discussed below in terms of individual characteristics.

The activation energy for graphite in this study, was 105kJ/mol in Mn-Fe alloys. This was a bit higher compared to the values from literatures. For example Bandyopadhyay[41] and Cham [16] reported that the activation energy for the dissolution of graphite in iron were 42kJ/mol and 52kJ/mol respectively. Olivares[56] and Orsten and Oeters[58] reported the activation energy to be 78.9 and 78 kJ/mol respectively for dissolution of graphite in iron. It has been reported that the rate limiting step in graphite dissolution in iron is the mass transfer of carbon atoms from the liquid boundary layer to bulk liquid.[32, 35]. The slightly higher k value in this investigation may indicate that the dissolution reaction is more important when it comes to the Mn-Fe alloys.

The dissolution activation energy obtained for coke A (228kJ/mol) and coke B (219kJ/mol) are two times larger than graphite which is consistent with other studies [16, 44]. The difference in activation energy between cokes and graphite can be explained on the basis of difference in structure and inorganic matter content. As Monte Carlo simulations[50] on graphite showed that carbon atoms dissociate easily from graphitic structure. Cokes have a much lower L_c value compared to graphite and thus contain more disordered carbon regions and less graphite like layers. It is therefore quite likely that more energy is required to dissociate the carbon atoms from the coke matrix. The high E_a values calculated for cokes may reflect the relative difficulty of atomic dissociation and suggest that the rate of carbon dissociation may play a significant role in the overall carbon dissolution process.

As mentioned before, the inorganic matter content can lead to a significantly higher E_a value[39, 52, 94]. The authors suggested that the inorganic matter in coke retards carbon dissolution by forming an ash layer covering the coke/iron interface and decreases the effective interfacial area, A, for carbon dissolution. However, in this study, because of the low immersion time, the ash blocking layer did not have time to form. Thus, the higher activation energy of cokes, compared to graphite, cannot be explained on the basis of inorganic matter. Not having enough time to generate the ash blocking layer, might be the reason that we got lower activation energies (219kJ/mol,228kJ/mol) for cokes compared to what others [39, 52, 94] obtained (300-479kJ/mol).

The activation energy of dissolution reaction was also calculated in the case when the reduction in carbonaceous materials surface area is ignored. As it is shown in **Table 5.1**, the calculation of activation energies were much lower when the reduction in surface area was ignored. Difference of activation energies considering and ignoring is higher for cokes compared to graphite and charcoal.

Table 5.1: Dissolution activation energy for different carbon materials (E_a^* is the activation energy which was obtained based on ignoring the surface area reduction of carbon during dissolution).

Carbonaceous material	Activation Energy, E_a (kJ/mol)	Activation Energy, E^*_a (kJ/mol) *
Graphite	105	52
Charcoal	134	80
Coke A	228	67
Coke B	219	65

In this study, the surface area reduction of carbonaceous materials during dissolution was influenced by factors such as temperature, initial surface area of carbonaceous materials and the density of carbon materials. At higher temperature, the surface area reduction was higher for all carbon materials. Charcoal with the lowest density and highest initial surface area showed higher surface area reduction. Graphite with higher density showed lower surface area reduction.

5.3 Carbon microstructure

Figure 5.6 shows the carbon crystallite size, L_c, as determined using Scherrer's equation, of all cokes and charcoal and their dissolution rate in Fe-85wt%Mn at 1550°C before contact with liquid metal. From **Figure 5.6**, it can be seen that there was little difference in L_c

between six coke samples and therefore the high overall dissolution of certain cokes, namely coke A, cannot be explained on the basis of crystallite size. It is in agreement with findings of Cham[16] who found no correlation between the carbon crystallite size of cokes (with similar crystallite sizes) and their dissolution rates in molten iron. Within poorly ordered carbon materials (charcoal and cokes), charcoal with lower crystallite size showed lower dissolution rate (**Figure 5.6**). The results were in agreement with previous studies [49, 55, 91] which have reported a link between structural ordering and dissolution rates of non-graphitic carbonaceous materials in liquid iron. It is worth mentioning that graphite has a very high L_c (389Å) and the rate constant is lower than cokes and higher than charcoal.

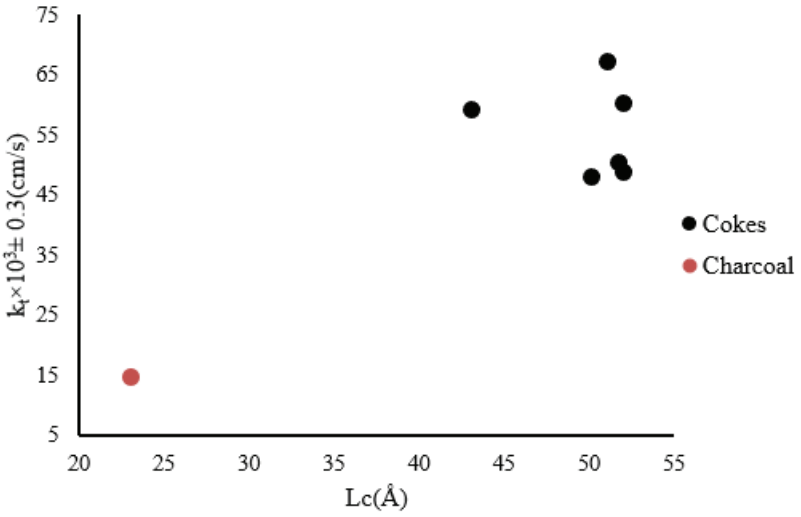

Figure 5.6: L_c values versus k_t at 1550°C for cokes and charcoal.

XRD and Raman analyses both characterize the microstructure of carbonaceous materials. The L_c parameter obtained by XRD measurement is related to the crystallite size, and the G fraction in Raman spectrum is assigned to graphitic structure of carbonaceous materials. Therefore, correlation is expected between parameters obtained in XRD and Raman analyses. In the temperature range 1250-1550°C, the L_c parameter marginally changed with temperature for all carbonaceous materials tested. The G fraction in the Raman spectra of cokes exhibited similar behavior, whereas G fraction of other carbonaceous materials

increased as temperature rose from 1250 to 1550°C which means that with increasing temperature, the structure of carbon materials become more ordered as expected.

The G fraction has previously been found to correlate with L_c for carbonaceous materials annealed in the temperature range 1100-1500°C[2]. In our study, graphitization by annealing simultaneously increased both the G fraction in the Raman spectra and the crystallite size of carbonaceous materials. **Figure 5.7** shows that with 10% increase in the G fraction, L_c increased from 21 to 55 Å. An increase in L_c can be caused by stacking of two or more graphitic units to form a larger graphite crystallite. In this study, the XRD results were confirmed by Raman results. (**Figure 5.7**).

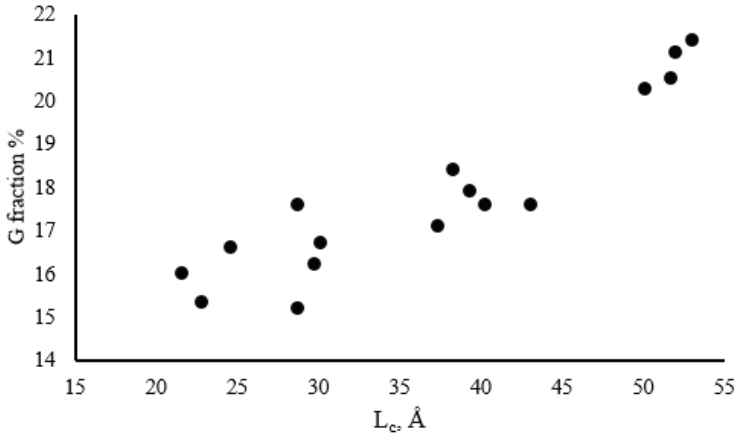

Figure 5.7: Correlations between L_c and G fraction for cokes subjected to heat treatment at 1250–1550 °C.

Figure 5.8 shows that the I_D/I_G is also correlated with d_{002} for cokes in the temperature range 1250-1550°C. Graphitization by annealing simultaneously decreased both I_D/I_G in the Raman spectra and also interlayer spacing between aromatic planes, d_{002}.

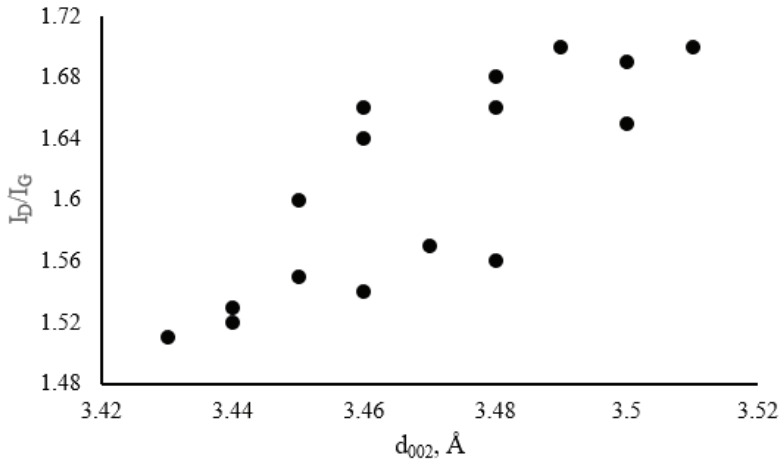

Figure 5.8: Correlations between d_{002} and I_D/I_G fraction for cokes subjected to heat treatment at 1250–1550°C.

5.4 Carbon macrostructure

In this study, Roughness, porosity and BET of carbon materials follow the same trend except for charcoal (**Figure 5.9**). **Table 5.2** shows the results of roughness and porosity and BET of all carbon materials and also their dissolution rate constant in Fe-85wt%Mn at 1550°C. It can be seen that among cokes, coke E with the roughest surface and the highest porosity and BET did not show the highest dissolution rate. Charcoal has the highest porosity among all carbon materials while its surface is very smooth and the dissolution rate was the lowest.

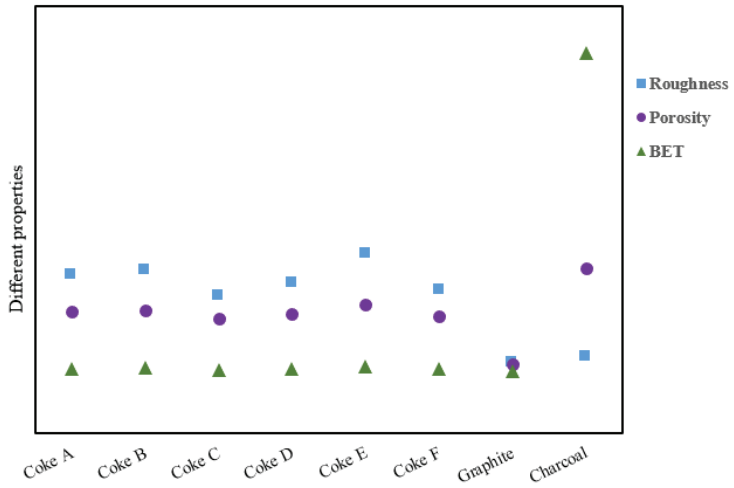

Figure 5.9: Roughness, porosity and BET of different carbon materials.

Table 5.2: Surface roughness, porosity and BET and dissolution rate of carbonaceous materials at 1550°C.

Carbon material	Roughness,R_a (µm)	Porosity (%)	BET(m^2/gr)	Dissolution rate constant, k_t(cm/s) in Fe-85 wt%Mn
Coke A	80	50	3.1	0.0673
Coke B	83.3	51	3.7	0.0594
Coke C	63	44	2.1	0.0509
Coke D	73	48	2.95	0.0489
Coke E	97	55	4.64	0.0605
Coke F	67	46	2.9	0.0481
Charcoal	12.7	85	261.5	0.0147
Graphite	8	6	0.44	0.0352

As **Figure 5.10** shows, among cokes, with increasing roughness and porosity and BET, the dissolution rate showed an increasing trend. Thus, a correlation can be seen between macrostructure of cokes and their overall dissolution rate in Fe-85wt%Mn. However, the R-

squared values are very low. Having correlation between porosity of cokes and their dissolution rate constant is in agreement with findings of Mourao et al.[39] who reported that cokes with high porosity exhibit higher dissolution rate and further suggested that higher porosity offers more surface area for reaction and its effect seems to be more significant in the initial stage because at the later stage, the liquid metal may get trapped in the pores and tend to get saturated by carbon. As it was mentioned earlier, the dissolution rate can be influenced by contact area in the case of both two mechanisms. If we add the results for graphite and charcoal to **Figure 5.10**, we will get **Figure 5.11**. This figure shows that the roughness, porosity and BET of charcoal are very different with other carbon materials and do not follow the same trend as others.

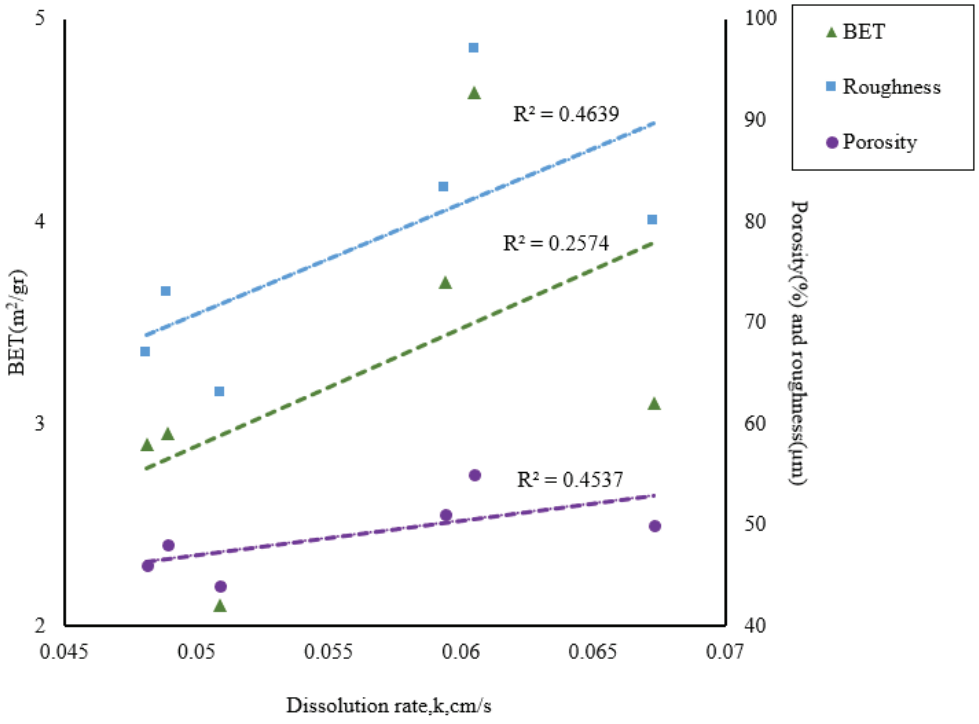

Figure 5.10: Relationship between roughness, porosity and BET of cokes and their overall dissolution rate in Fe-85wt%Mn at 1550°C. Trendlines are also shown.

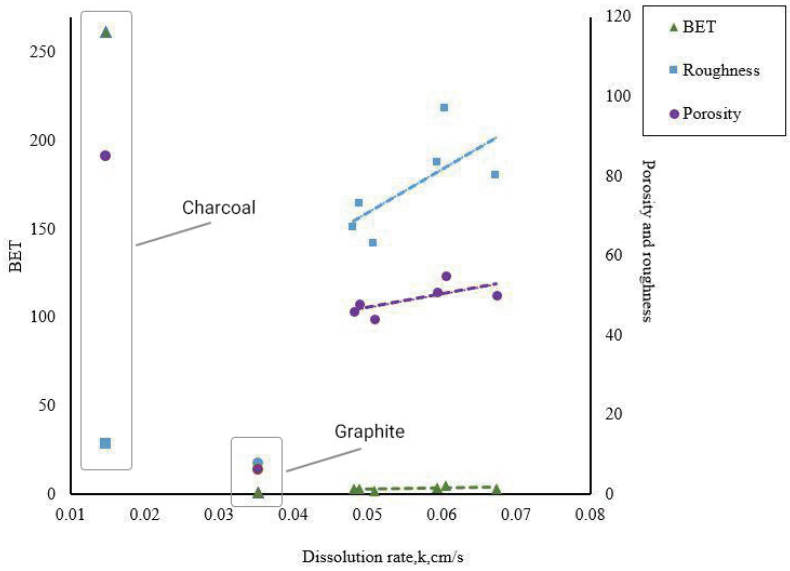

Figure 5.11: Relationship between roughness, porosity and BET of cokes, graphite and charcoal and their overall dissolution rate in Fe-85wt%Mn at 1550°C.

5.5 Ash in the coke

In this study, cokes E and D were chosen for further investigating the interfacial products after dissolution experiments. No ash layer was found at the interface and it might be because the immersion time was less than one minute for all cokes and the ash layer did not have enough time to be formed. It was in agreement with several literature studies which found that in the absence of a mineral layer, carbon dissolution into iron is fast and it considered to be a first order liquid phase mass transfer process [40, 52, 54, 69]. Some researchers [36, 44, 45], in a study of non-graphitic carbon material dissolution in liquid iron divided the data into two periods covering the initial period of carbon dissolution and a latter period. In their study, there was a significant change in the value of k_m in Fe-C melt, after a period of time. In all the mentioned studies, the transition from higher to lower dissolution rate occurs after approximately 30 minutes. A possible explanation for the apparent change in the rate constant was attributed to the formation of ash layer at the metal/coke interface which can block the surface and decrease the dissolution rate.

All experimental data in this study are in the initial period since all the experiments have been done for less than 30 seconds for cokes and charcoal and less than 2 minutes for graphite. Inspection of **Table 5.3** and **Figure 5.12** shows that the difference in reaction rates among cokes was not due to the differences in ash content since coke E has higher ash yield than other cokes, and the dissolution rate is also high.

Table 5.3: Ash content of different cokes and their dissolution rate in Fe-85wt%Mn at 1550°C.

Carbon materials	Ash content%	Dissolution rate constant, k_t(cm/s) in Fe-85wt%Mn
Coke A	10.39	0.0673
Coke B	11.25	0.0594
Coke C	11.82	0.0509
Coke D	9.61	0.0489
Coke E	13.68	0.0605
Coke F	11.42	0.0481

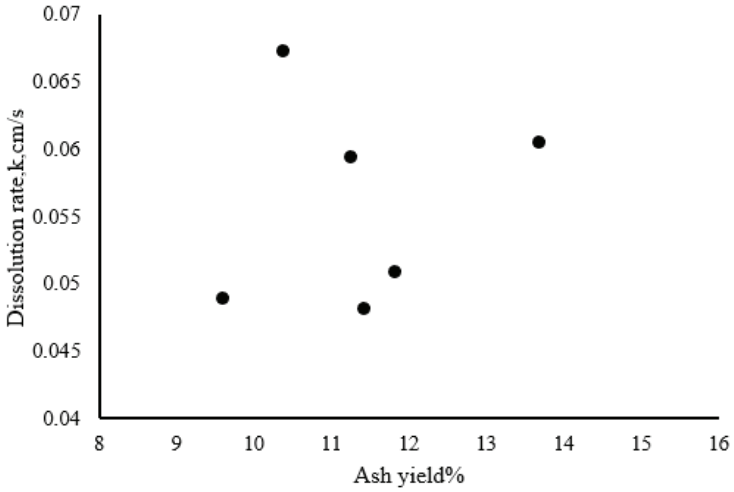

Figure 5.12: Relationship between ash yield of the cokes and their dissolution rates in Fe-85wt%Mn at 1550°C.

5.6 Side reactions

Sulfur is usually present in carbonaceous materials, either in the carbon structure or in the ash phase [46]. The sulfur dissolution from four cokes was investigated in this study. It was shown that sulfur content of the metal followed a pattern similar to carbon dissolution. As it is shown in **Figure 5.13,** it was found that there was a direct correlation between carbon and sulfur pick up from the coke, i.e. the dissolution of sulfur occurs simultaneously with carbon dissolution. This pattern was also observed by Cham[16] and Jones[54] who conducted an investigation on the kinetics of carbon dissolution in molten iron at 1550°C using different types of cokes. They concluded that the pick-up of sulfur by the molten iron increased proportionally to the dissolution of carbon.

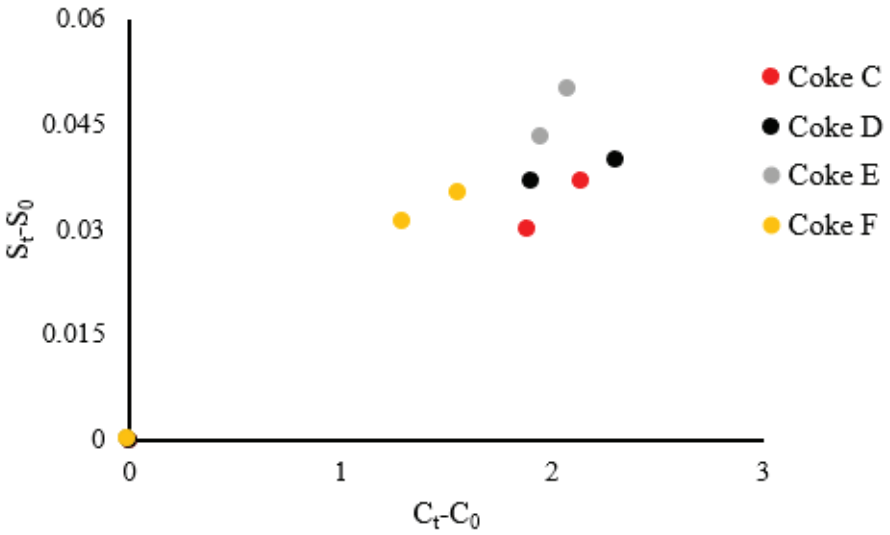

Figure 5.13: Change in S and C content in Fe-85wt%Mn bath for cokes C to F at 1550°C.

Ash components provide reactants for most of the side reactions occurring at the interface[16]. The side reactions will not directly affect the carbon dissolution rate, but they will indirectly affect carbon dissolution rate by changing compositions of the liquid and the ash[46]. The main difference between cokes was in the amount of Al_2O_3, SiO_2 and Fe_2O_3 in the bulk ash chemistry. As **Table 5.4** shows, coke E contained more silicon dioxide, iron oxide and aluminum oxide compared to other cokes, therefore the differences in reaction rates cannot be explained of the amount of the inorganic compositions of cokes. **Figure 5.14** shows the relationship between SiO_2/Al_2O_3 ration of different cokes and their dissolution rate in Fe-85wt%Mn. No correlation can be found between the SiO_2/Al_2O_3 ratio of different cokes and their dissolution rate in Fe-85wt%Mn at 1550°C.

Table 5.4: Major constitutes in the ash of the cokes.

Carbon materials	Coke composition		
	SiO_2	Al_2O_3	Fe_2O_3
Coke A	6.38	3.18	0.8
Coke B	5.6	2.79	0.6
Coke C	6.97	3.07	0.87
Coke D	4.22	2.84	0.83
Coke E	7.35	3.96	0.95
Coke F	6.29	2.87	0.68

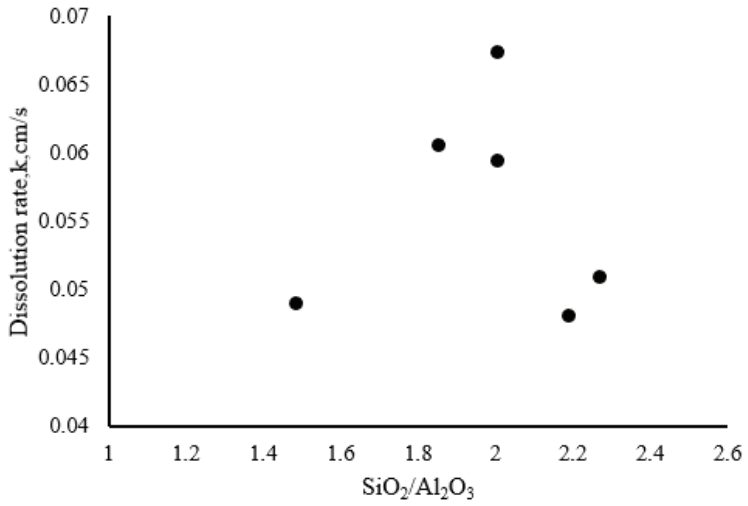

Figure 5.14: Relationship between SiO_2/Al_2O_3 ration and dissolution rate.

5.7 Sulfur content

When adding 1.69 wt% sulfur to Fe-Mn metal, no significant difference was seen on the overall dissolution rate of graphite. The dissolution rate decreased slightly from 0.035 cm/s to 0.034 cm/s which is within the uncertainty range. It is however in agreement with findings of Wu[55] who found that with adding sulfur to iron more than 1.2 wt%, the dissolution rate constant of graphite into iron would be constant.

SEM image of the surface of the graphite showed a thin layer which is composed mostly of MnS at the graphite surface. Using FactSage, it was shown that most of solid MnS was formed at high temperature and not participated in the cooling process. As **Figure 5.15** shows, at 1550°C, the system consists of a liquid phase (LIQU) and a solid MnS phase. As it is cooled, more MnS will participate. The main part of the metal starts solidifying at 1200°C and as it can be seen in more detail in **Figure 5.16**, there is bump in the MnS generation at this temperature. Thus, it might be the interface of the graphite acts as a nucleation point of MnS formation.

A layer containing MnS at the surface can indicate that sulfur prefers to accumulate at carbon surface. Sulfur is a known surface active element and can lower the surface tension of liquid iron[16]. This was in agreement with findings of Khanna et al.[95] who used the Monte Carlo simulations to investigate the effects of sulfur during decarburization of molten iron-carbon alloys. It was found that sulfur atoms were found to preferentially concentrate in the top few layers, with the second layer showing the highest amounts of sulfur; very little sulfur was observed in the bulk liquid. In our study, however, some sulfur was also detected in bulk phase of the metal as well. Other researchers [55, 56, 58, 96] also believed that presence of sulfur in the metal, would retard the graphite dissolution rate in iron and the reason was that the carbon diffusion coefficient (k_m) decreased with increasing sulfur in the melt. However, this was not found in this study.

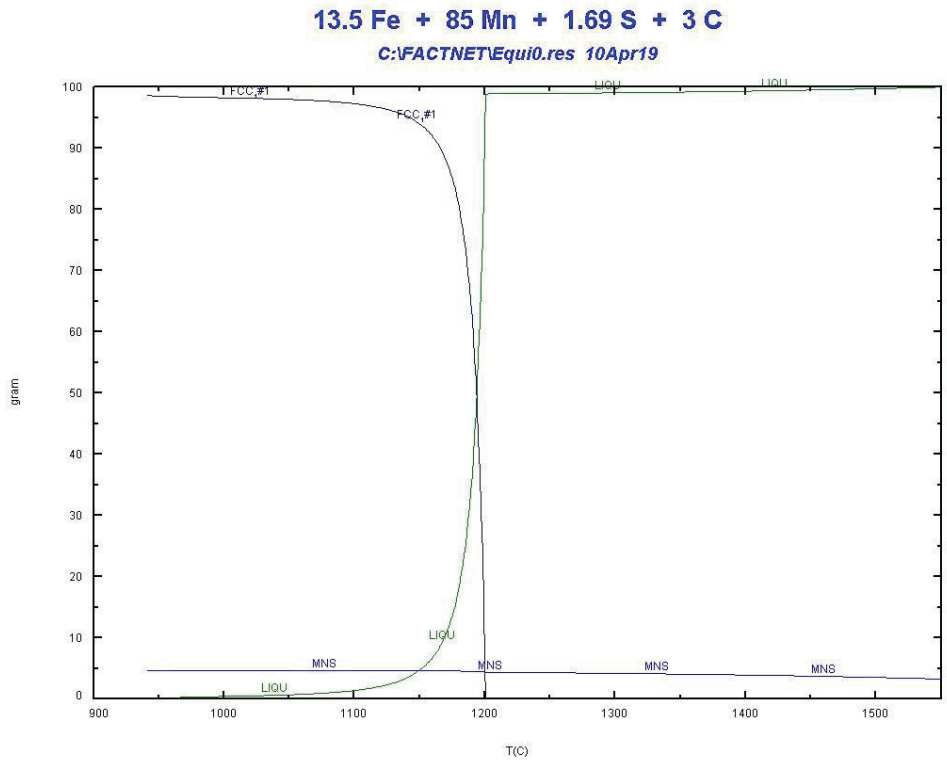

Figure 5.15: Amount of phases versus temperature.

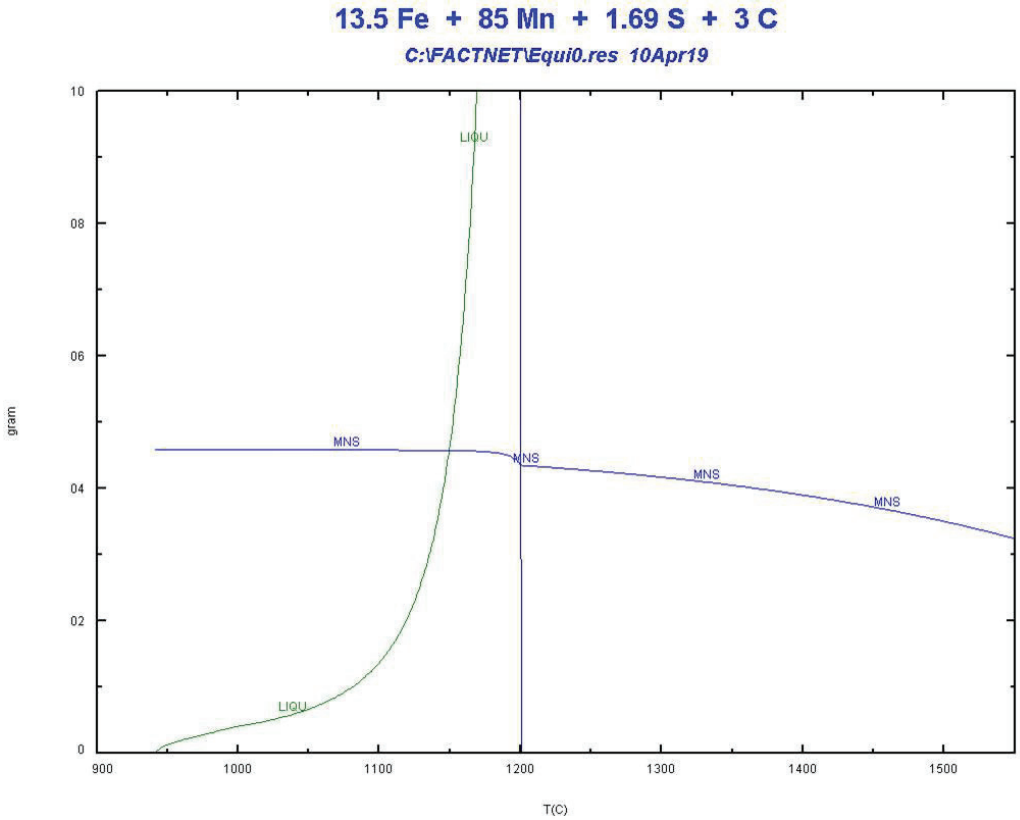

Figure 5.16: Close up of Figure 5.15 showing changes in MnS amount during cooling.

5.8 Metal composition

It is apparent from the data presented in **Figure 5.17** that with increasing amount of manganese in the alloy, the graphite dissolution rate constant increased. As it was mentioned earlier, manganese has higher carbon saturation level compared to iron. The carbon saturation level in pure manganese at 1550ºC is around 7.8 % while in pure iron at the same temperature is around 5.5 wt%. In the case of Mn addition to the iron manganese alloy, the driving force should be higher, thus, our experiments results meet the expectations. Adding alloying elements such as Si, Mn and S will also affect the diffusivity of carbon in the liquid and affect the viscosity of the liquid [46].

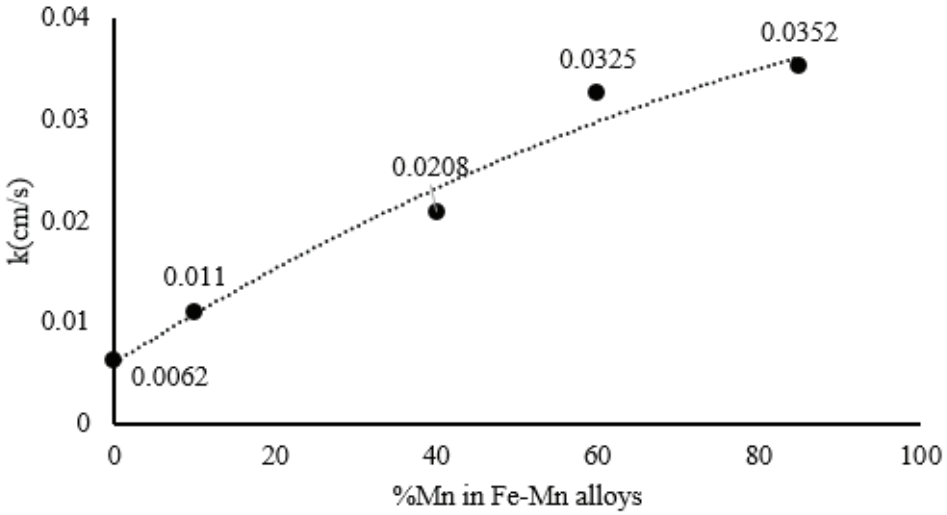

Figure 5.17: Influence of manganese amount on the dissolution rate of graphite in Mn ferroalloys.

It may be noted from the values stated in **Figure 5.17** that the value of k for pure iron is 6.2×10^{-3} cm/s (considering the surface area reduction). The dissolution rate of graphite in pure iron in the present study appear to be close to the values reported by others. For example, Kosaka and Minowa[33] reported a value of k to be 8.1×10^{-3} cm/s at 1548ºC and Bandyopadhyay [41] reported the value to be 4.5×10^{-3} cm/s at 1550ºC (ignoring the surface area reduction). If we ignore the reduction in surface area of graphite and use the initial surface area of graphite in dissolution reaction (as it is calculated and showed in **Table 5.5**), as other investigators did, the dissolution rate of graphite in pure iron would be 2.4×10^{-3} which is in the lower area.

Table 5.5: Dissolution constant, k_t ($\times 10^3$) cm/s, for graphite, charcoal and cokes at 1550°C (k* is the rate constant when the reduction in surface area was ignored).

Composition	k_t(cm/s)	k_t*(cm/s)
Fe	0.0062	0.0024
Fe-10wt%Mn	0.011	0.0075
Fe-40wt%Mn	0.0208	0.013
Fe-60wt%Mn	0.0325	0.018
Fe-85wt%Mn	0.0352	0.021

5.9 Wettability and dissolution rate

Four types of cokes, graphite and charcoal were chosen to investigate their behavior when they initially came in contact with molten Fe-85wt%Mn droplets. As **Table 5.6** shows, all carbon materials including cokes show wetting behavior at the time of melting. The melting point for Fe-85wt%Mn is around 1300°C and the contact angles for all cokes are between 60-65°. The high dissolution rate of cokes at the initial stage might be because of the good wettability of them with metal at the initial stage of dissolution. Charcoal and graphite contact angles did not change significantly over time and remained more or less constant. **Figure 5.18** shows the relationship between initial and final contact angle of different cokes and their dissolution rate in Fe-85wt%Mn at 1550°C. An increasing trend can be seen between final and initial contact angles of cokes and their dissolution rate. However, within the cokes investigated, the trend is opposite to the expectations since it is expected that better wettability concludes to higher dissolution rate. It is also worth mentioning that the initial contact angles are quite close (between 60-65°) and dissolution rate might not be explained on the basis of contact angles. **Figure 5.19** shows the same relationship for charcoal and graphite in addition to different cokes. It can be indicated that although charcoal and graphite have lower initial and final contact angles (good wetting) compared to cokes, but they have

lower dissolution rate. Thus, for charcoal and graphite, dissolution rate is not influenced by wettability.

Table 5.6: Initial and final contact angles for different substrates at 1550°C.

Carbon material	Initial contact angle (°)	Final contact angle (°)
Graphite	61	60
Charcoal	35	30
Coke C	60	95
Coke D	62	100
Coke E	65	110
Coke F	62	98

NB. Initial contact angle was taken in the melting point of droplet and the final contact angle was taken at the end of wetting experiments.

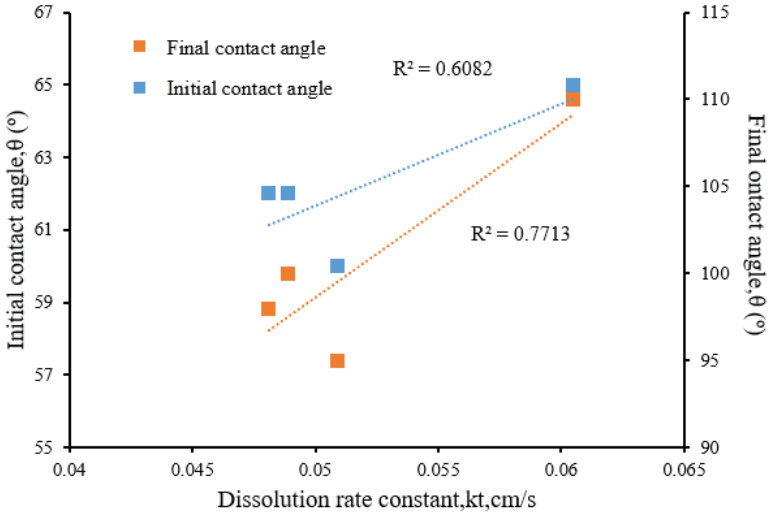

Figure 5.18: Relationship between initial and final contact angles and dissolution rate for different coke samples and the dissolution rates in Fe-85wt%Mn at 1550°C.

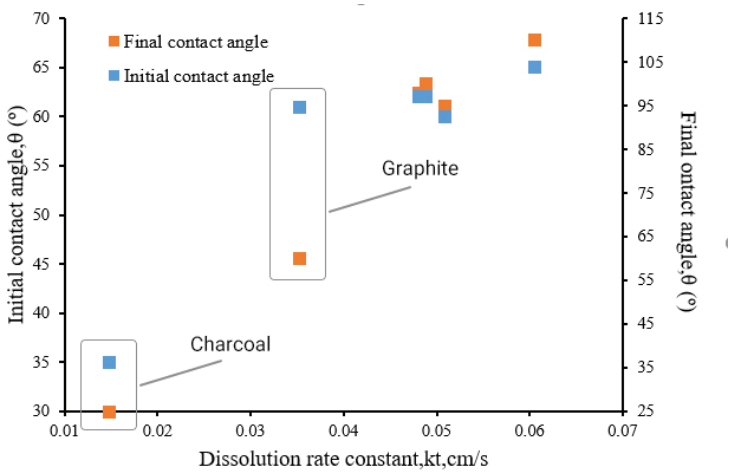

Figure 5.19: Relationship between initial and final contact angles and dissolution rate for different carbon materials and the dissolution rates in Fe-85wt%Mn at 1550°C.

5.10 Kinetic modelling of carbon dissolution in Fe-Mn

The rate model of dissolution of carbon materials are discussed in this section. For convenience, the rate model and the Arrhenius equation are reproduced below.

$$\frac{dC}{dt} = \frac{kA}{V}(C_s - C_t) \quad \textbf{2.5}$$

$$ln\, k = ln\, k_0 - E_a / RT \quad \textbf{2.8}$$

Based on k_0 and activation energy calculated from Arrhenius equation, the dissolution rates can be described by using the rate models. The rate model, was able to describe all of the dissolution rates of all carbon materials at experimental temperatures. This was observed from using two different Fe/Mn compositions. Note that the parameters which describes the best fit were applied to the rate models. The solid lines which describe the amount of carbon in metal from the rate models (in results part) showed good match with the measured amount. These results confirm the validity of using first order reaction for cokes and charcoal and graphite. To verify the application of the rate models, experiments with lower surface area of graphite, were done and as it was mentioned earlier the activation energy and k_0 was quite close, the model was still applicable. The rate modelling validated using the first order reaction rate for the dissolution of all carbon materials tested in this study in both Fe-85wt%Mn and Fe-60wt%Mn. Since the carbon material is affecting the rate, the interfacial reaction must be important. However, the mass transfer may also affect the rate but that is not known from our experiments. However, previous investigations suggest that it is also important.

Table 5.7 shows that the mass transfer limitations is supported by some number of evidences and interfacial reaction limitations is also supported by some of the evidences, so we can conclude that the overall dissolution mechanism is both mass transfer of carbon into the metal and interfacial reactions at the metal/carbon interface. The main evidence regarding chemical reaction limitations is due to the fact that different carbon materials gives different rates. Initially before any S dissolution and any possible ash layer is formed, all carbon materials should give the same rate constant and same activation energy if only mass transfer was limiting. The activation energy is quite low, and this may indicate a contribution from mass transfer as well. As previous literature stresses the contribution from the mass transfer, as well as using a stagnant method in our case, it is believed that mass transfer is also one of the contributing factors. This can however not be evidenced by the factors investigated, as the study of reaction mechanism was not focused in this thesis.

Table 5.7: Kinetic analysis of observed carbon dissolution rates.

Answered by experiments & modelling	Rate limiting step is:		
	Mass transfer	Interfacial reaction	Mixed
Observed rates fit well with modelling	yes	yes	yes
Size of activation energy of rate constants	yes	no	yes
Rate affected by carbon microstructure	no	yes	yes
Rate affected by carbon macrostructure	no	yes	yes
Rate affected by wettability	no	yes	yes
Rate affected by sulfur in metal	yes	yes	yes
Rate affected by alloying element (Mn)	yes	yes	yes
Rate affected by ash content	yes	no	yes

5.11 Wettability of Mn-Fe alloy on carbon materials

Wettability between carbonaceous materials and Fe-Mn alloy was believed to affect the dissolution rate. In our study however, it was shown that in the initial stage of dissolution, wettability did not affect the dissolution rate directly, but it might have some indirect effects. In complex heterogeneous materials such as chars and cokes, several factors can influence the wettability of these carbonaceous sources [16, 55]. These factors include manganese level in the alloy, inorganic matter yield and chemical composition in the coke, carbon microstructure and macrostructure and formation of phases at the interface due to reaction taking place at the interface.

Three carbon materials as substrates were used to investigate the wettability with pure iron and Fe-85%wt Mn. **Figure 5.20** shows the contact angle versus time for Fe and Fe-

85wt%Mn which were in contact with three different carbon materials at 1550°C. As **Table 5.8** shows, for all three carbon materials, the contact angle decreased with adding manganese to the pure iron. The biggest reduction of contact angle was seen for charcoal, however for coke and graphite it was hardly any difference.

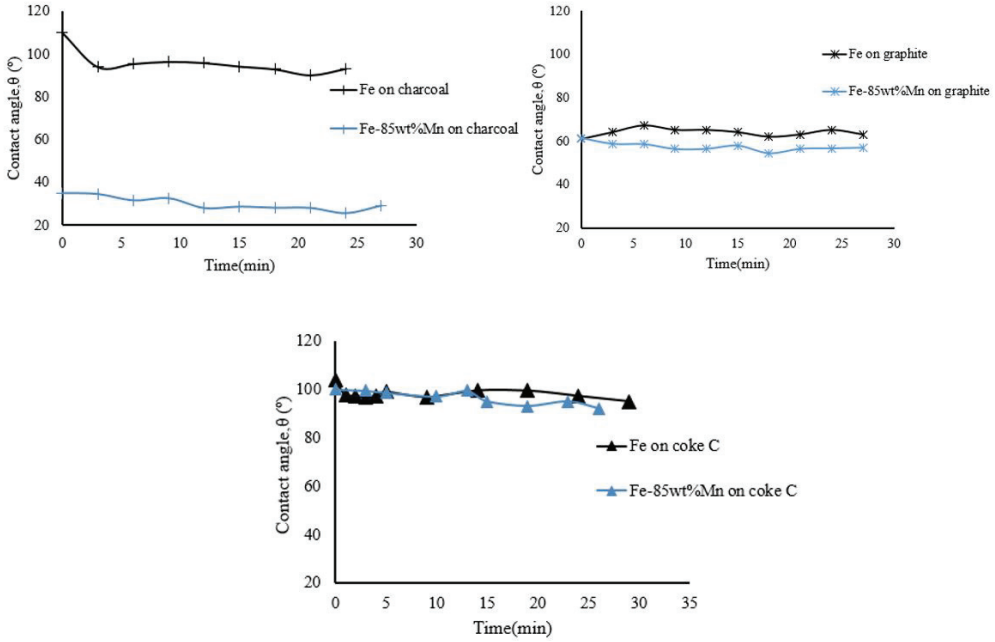

Figure 5.20: Contact angle versus time for Fe and Fe-85wt% on different carbon materials

Table 5.8 summarizes the contact angle for both compositions on three different carbon materials.

Table 5.8: Contact angle between two metal compositions and three carbon materials.

Carbon material	Contact angle with Fe	Contact angle with Fe-85wt%Mn
Coke C	100	92
Charcoal	95	30
Graphite	65	60

As indicated in **Table 5.8** and **Figure 5.20**, the largest difference between the two different metal compositions can be seen for charcoal. Charcoal was non-wetting with iron but showed a very good wetting behavior with Fe-85wt%Mn. However, because of the high amount of pores in charcoal and metal penetration into the pores, the contact angle is between metal and metal instead of metal and charcoal. Thus, the contact angle we measured, cannot be accurate. **Figure 5.21** shows the wetting image of Fe/charcoal and Fe-85wt%Mn/charcoal.

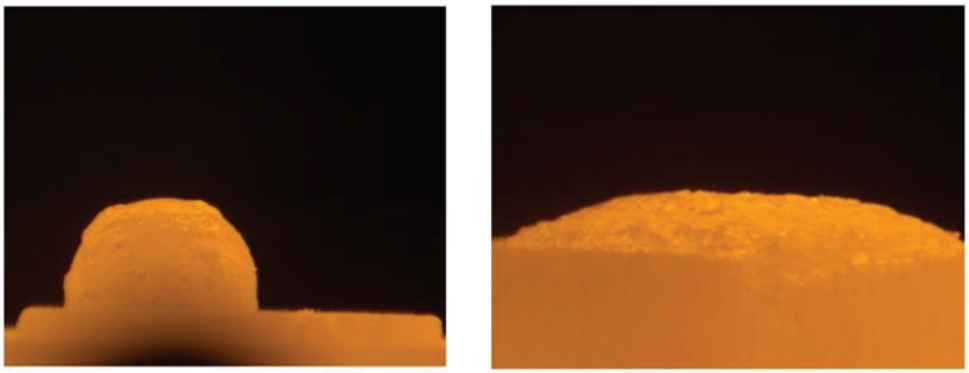

Figure 5.21: Sessile drop assembly for charcoal with Fe (left) and Fe-85wt%Mn (right) at the end of experiment at 1550°C.

The other observed evidence was that iron passed through the substrate in both two runs while iron manganese did not show this behavior as it is shown in **Figure 5.22**.

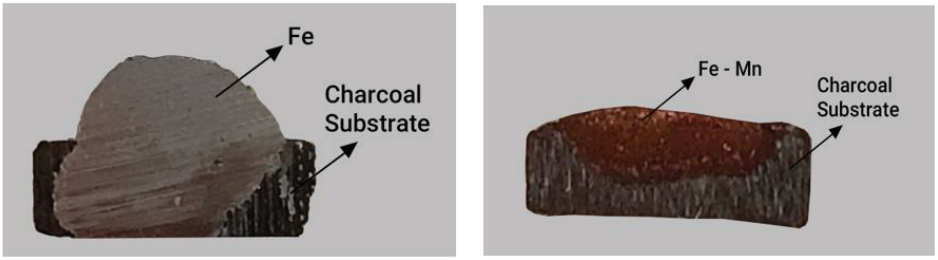

Figure 5.22: Different behavior of Fe droplet (left) and Fe-85wt%Mn droplet (right) on charcoal substrate at the end of wetting experiment at 1550°C.

The possible explanation for the different behavior of iron on charcoal might be because of the different macrostructure such as different porosity and different pore sizes of different charcoal samples. The reason for different behavior of Fe and Fe-85wt%Mn on charcoal cannot be due to the direction of pores in charcoal substrates, since in both cases, the pores are vertical as shown in **Figure 5.23**.

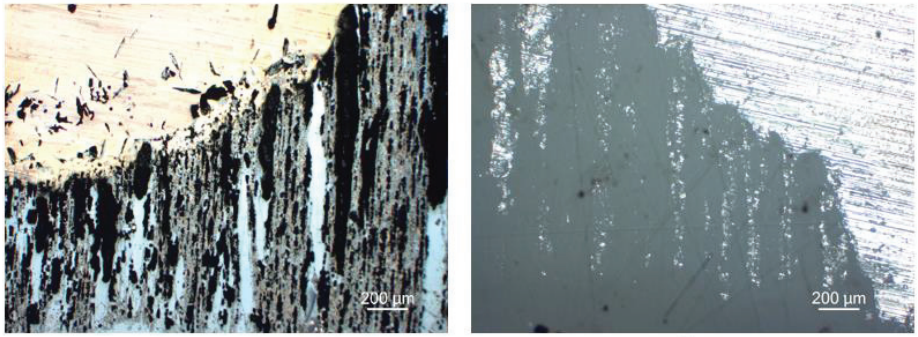

Figure 5.23: a) Charcoal substrate in contact with Fe-85wt% Mn b) charcoal substrate in contact with Fe.

Non-wetting behavior of charcoal with iron might be because of the ash composition of charcoal. As it was indicated in the experimental chapter, charcoal ash composed mostly of MgO, CaO and K_2O. It was indicated in previous literatures [16, 94] that some inorganic matter in the ash namely CaO and MgO and alkali oxide like K_2O can reduce the wettability by forming an adhering slag layer between carbon materials and iron. Ohno et al.[63] also confirmed that existence of ash in charcoal decrease the contact between iron and charcoal.

The other reason for the higher wettability of Fe-85wt%Mn with all three carbon materials compared to Fe might be the lower surface tension of Fe-85wt%Mn. It was also confirmed by previous investigations[81, 82] that with adding manganese to iron, the surface tension decreases which resulted in greater wettability and a smaller contact angle.

Effect of microstructure of carbon materials on the wettability is limited to two studies; Cham[16] did not find any correlation between crystallite size of different cokes and their wettability with iron. The crystallite size of cokes in study of Cham[16] was close and this might be the reason that the difference in their wettability with iron could not be explained

by their difference in crystallite size. Contrary to Cham[16], Olivares[56] found that the contact angle between iron and carbonaceous substrates increased with decreasing crystallinity. It was concluded that the decrease in dissolution rate, attributed to carbon structure, may be the result of decrease in real contact between the liquid and carbon. In our study, a big difference was not seen in the crystallite size of different cokes at 1550°C, but it can be noted that within poorly ordered carbonaceous materials (coke and charcoal) with increasing crystallite size (increasing crystallinity), contact angle increased (**Figure 5.24** and **Figure 5.25**). Graphite has very high crystallite size (389Å) and the contact angle with Fe-85wt% is 45° and with Fe is 60°did not fit this correlation. Within each group, e.g. within the cokes no correlation was seen between crystallite size and wettability.

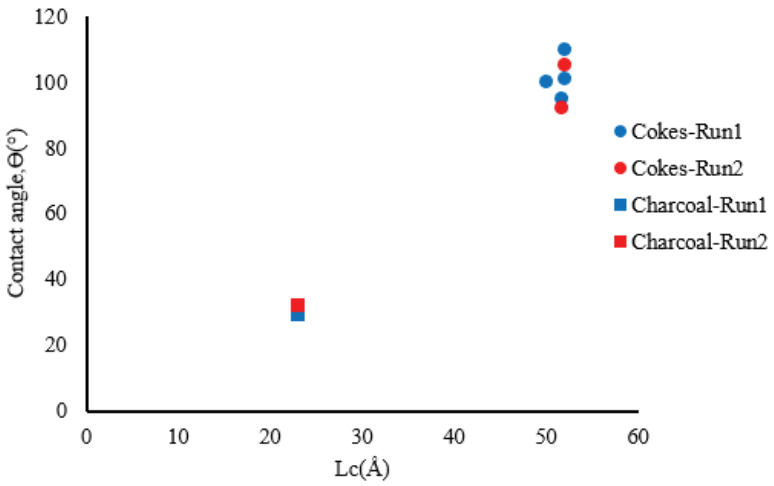

Figure 5.24: Contact angle between Fe-85wt%Mn and carbonaceous materials versus crystallite size at 1550°C.

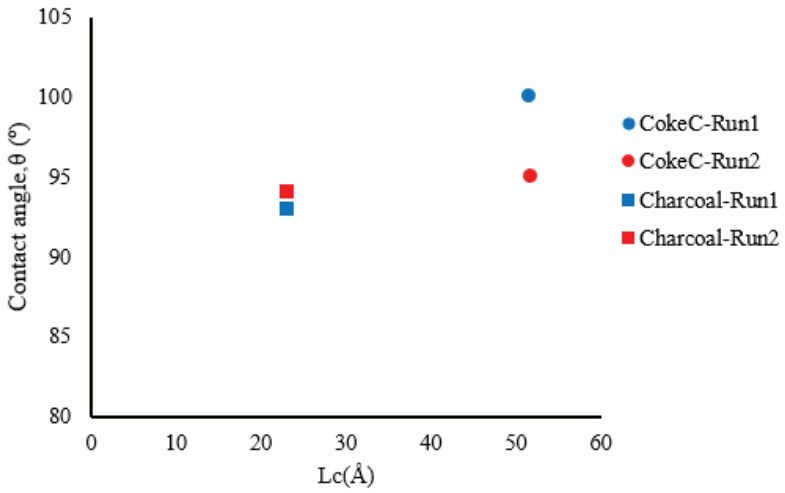

Figure 5.25: Contact angle between Fe and carbonaceous materials versus crystallite size at 1550°C.

As mentioned in chapter 2, the Young equation describes the balance at the three-phase contact with the assumption that the surface is topographically smooth (**Figure 5.26a**). This is however not true in the case of real surfaces such as cokes which instead of having one equilibrium contact angle value exhibit a range of contact angles between the advancing and receding ones. In Wenzel state, the droplet penetrates between the peaks and wets the complete surface while in Cassie-Baxter model, the droplet remains suspended over the peaks without wetting the bottom of the surface. (**Figure 5.26b** and **Figure 5.27c**).

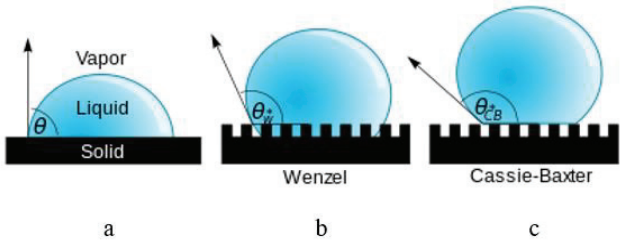

Figure 5.26: Representation of (a) Young (b) Wenzel and (c) Cassie-Baxter models.

The correlation between wettability and surface roughness of carbonaceous materials are shown in **Figure 5.27**. As it can be seen in **Figure 5.27** and **Figure 5.28** for cokes, which are non-wetting systems, with increasing roughness, the wettability decreased. Both charcoal and graphite showed wetting behavior with metal. Charcoal with rougher surface and higher porosity showed much better wettability than graphite. This result is in agreement with the findings of Wenzel[83] which says that for wetting systems, with increasing roughness, the wettability increases and for non-wetting systems, with increasing roughness the wettability decreases. It is also in agreement with finding of Ciftja[22] who found that among graphites with different roughness, the one which was rougher, had better wettability with silicon. However, for cokes, using the Wenzel model does not seem suitable, in principle because the surface is a non-wetting one, in which the mechanical structuration has produced many pores and thus many air pockets. The right way in this case would be to apply the Cassie-Baxter model[85]. However, for this purpose it is necessary to know the values of the solid fraction (fraction of solid phase in contact with liquid phase), in order to calculate the apparent contact angles. As these values are unknown, the model is unable to predict contact angles.

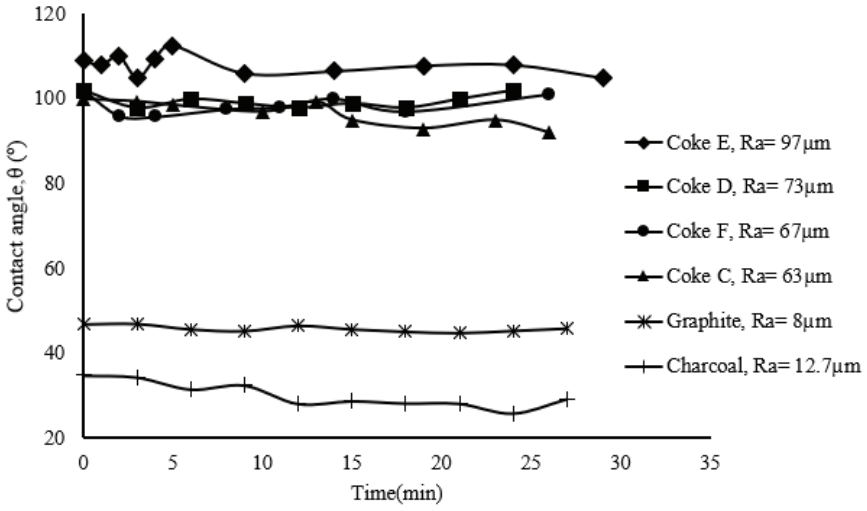

Figure 5.27: Contact angles of Fe-85wt%Mn versus time for different carbon materials with different roughness.

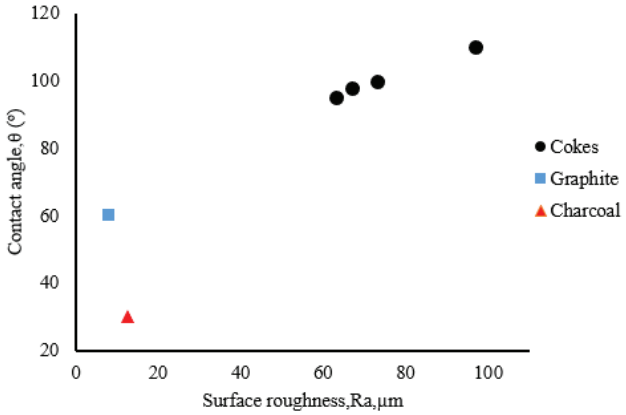

Figure 5.28: Relationship between contact angle and surface roughness of different carbon materials.

Table 5.9 and **Figure 5.29** show the correlation between porosity of different carbonaceous materials with their contact angle with Fe-85wt%Mn. Charcoal with the highest porosity showed the lowest contact angle and cokes with lower porosity showed higher contact angle. Graphite showed the lowest porosity and the contact angle is still low. In non-wetting system, the coke with higher porosity, showed higher contact angle and in wetting systems, with increasing porosity, the contact angle decreased. In this study, we can correlate the porosity of carbon materials to the roughness. Pores at the surface, affect the roughness which means that surfaces with higher amount of pores, are rougher. For wetting systems (charcoal and graphite) with increasing porosity (roughness) the wettability increased, but for non-wetting systems, with increasing porosity (roughness) the wettability decreased. There is no studies on the effect of porosity of carbon materials on the wettability, but since in our study, porosity and roughness follow the same trend, we can conclude that it is in agreement with Wenzel[83] model.

Table 5.9: Porosity and contact angle for different carbon materials

Carbon material	Porosity%	Contact angle, θ, °
Graphite	6	45
Charcoal	85	35
Coke C	44	95
Coke D	48	100
Coke E	55	110
Coke F	46	98

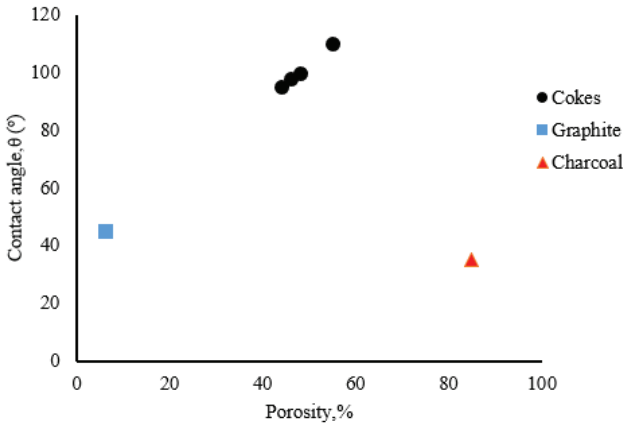

Figure 5.29: Relationship between contact angle and porosity of different carbon materials.

The interfacial products produced by the chemical reactions taking place at the interface during wetting, will affect the wetting properties. Among cokes, coke E and coke C with the highest and the lowest amount of sulfur respectively, were chosen to investigate the interfacial products. A comparison of the interfacial product formed after 30 minutes from coke E and coke C highlights the initial difference. The interfacial product formed with coke E had a network structure. Lower wettability of coke E could be caused to some extent by

this network structure, which block liquid metal from coming into contact with coke. The interfacial product formed with coke C lacked the network structure. Instead, there were discrete interfacial products which has globe shape and would allow liquid metal to come into contact with coke. It is worth mentioning that coke C contained less sulfur and after wetting reaction, no sulfur was detected at the interface.

These results were in agreement with other studies: The non-wetting behavior of the coke with iron, might be because of the interfacial products which can block the surface and decrease the contact area [35]. In this study, sulfur is present in mineral phases and as part of the organic component of the coke. Although sulfur is not a major component of the coke inorganic matter, it is an important element to consider. MnS was detected at the interface between coke E and metal and may block the surface and decrease the contact between coke and metal. This is in agreement with findings of Cham[16] who found that the interfacial products containing sulfides, such as MnS, can act as a physical barrier blocking coke/iron contact, thus reducing the contact area.

Alumina, silica and SiC were also detected at the interface of both cokes but since EDX cannot give us a quantitative analysis, it is difficult to compare two cokes. In previous studies, existence of alumina and silica and SiC were found to decrease the wettability by decreasing the contact between coke substrates and iron [87, 88]. In this study, however, coke E has the highest amount of alumina and silica but also has the lowest wettability in contradiction to previous studies. As **Table 5.10** and **Figure 5.30** show, no correlation can be found between SiO_2/Al_2O_3 ratio and the wettability of different carbon materials with Fe-85wt%Mn.

Table 5.10: SiO_2/Al_2O_3 ratio of different cokes and their wettability with Fe-85wt% Mn at 1550°C.

Carbon material	SiO_2/Al_2O_3	Contact angle, θ, °
Coke C	2.27	95
Coke D	1.49	100
Coke E	1.86	110
Coke F	2.19	98

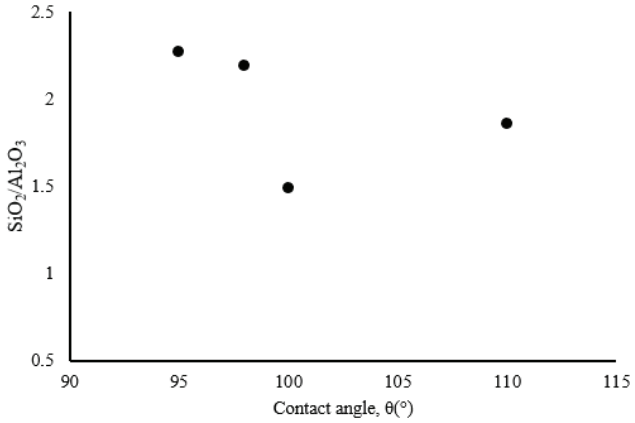

Figure 5.30: Relationship between SiO_2/Al_2O_3 ratio and contact angle for cokes.

6 Conclusions and future work

6.1 Conclusions

An in-depth investigation was conduct on the dissolution behavior of six cokes and one charcoal and graphite in liquid Fe-Mn metal at initial stage. A range of experimental techniques were used to identify the main factors affecting the kinetics of carbon dissolution and the role of carbon microstructure, macrostructure and liquid/solid wettability. Factors influencing liquid/solid wettability were also investigated. The main conclusions obtained from this project were:

1. Different carbon materials dissolve in molten Fe-Mn metal at different rates. The dissolution rate constant was calculated using first order reaction rate. It was found that k value for cokes was higher than graphite and charcoal. However, there is larger difference between the different carbon groups than within different cokes.
2. With increasing manganese content of metal, dissolution rate increased. Fe-85wt%Mn dissolves graphite 5 times faster than Fe. However, at high Mn content of 60-85wt%Mn, there is not much difference in dissolution rate.
3. Dissolution of sulfur from cokes into metal was found to be in direct correlation with carbon dissolution from cokes.
4. Increasing melt sulfur content, did not seem to be a significant factor influencing dissolution rate of graphite in metal.
5. Thermal annealing of the carbon materials above 1250°C significantly increased the degree of graphitization. Crystallite size (L_c) increased, interlayer spacing (d_{002}) decreased and G fraction also increased.
6. The crystallite sizes of the cokes were similar and therefore the effect of L_c could not be established. Within poorly ordered carbon materials (charcoal and cokes) with increasing crystallinity, dissolution rate increased and in this case, the crystallite size (L_c) could play an important role in determining the carbon dissolution behavior.
7. No correlation can be found between ash content of the coke and their dissolution rate.

8. The effect of temperature was observed to be stronger for dissolution of cokes and charcoal than for graphite. In this study, interfacial products have not been formed in the initial stage of dissolution reaction and that might be the reason that the activation energies of cokes are less than previous studies. The activation energies of charcoal and graphite are less compared to cokes. That might be because of the complicated carbon structure in cokes which make it difficult for carbon to dissociate from coke structures.
9. Roughness and porosity and BET of the carbon materials follow the same trend except for charcoal. Among cokes, with increasing porosity, roughness and BET, the dissolution rate slightly increased although R^2 is very low (lower than 0.5).
10. At the initial stage of wetting, all cokes showed wetting behavior with Fe-85wt%Mn and that might be one of the reasons of high dissolution rates of cokes at the initial stage. However, one cannot find any correlation between wetting, initial and final contact angles and dissolution rate.
11. The dissolution mechanism for all carbon materials found to be both interfacial reactions at the carbon/metal interface and mass transfer of carbon in the metal.
12. Cokes showed non-wetting behavior with contact angles ranging from 95-110° after 30 minutes of contact while charcoal and graphite showed wetting behavior with Fe-Mn. That might be because of the oxide layer on the cokes surface.
13. Macrostructure of carbonaceous materials, porosity and surface roughness, were found to have significant effect on the wettability. Wenzel model[83] found to be applicable in this study. Thus, in non-wetting systems, with increasing roughness and porosity, the wettability decreased. Consequently, roughness and porosity cokeE>cokeD >cokeF >cokeC and the contact angle for cokeE> cokeD > cokeF > cokeC. While in wetting system which includes graphite and charcoal, roughness and porosity of charcoal> graphite and contact angle for graphite> charcoal.
14. Charcoal showed a very different wetting behavior both with Fe and Fe-Mn. High amount of metal penetrates into the charcoal due to the high porosity and thus the contact angle would be between metal and metal instead of metal and charcoal. Thus, the contact angles cannot be correctly established.
15. Formation of interfacial products and their physical properties can affect the wettability. The enriched mineral matter (ash) layer can form a barrier at the

coke/metal interface, reducing the wettability. The initial differences observed in the interfacial products of coke C and coke E provide an explanation to the differences seen in wettability between coke C and coke E. As discussed earlier, the network like interfacial product formed with coke E can act as a physical barrier and therefore decrease the wettability. The barrier can also inhibit other interfacial reactions from occurring. Whereas, for coke C, the globe shape interfacial products, would not hinder wettability.

16. The difference was not only in the morphology of the interfacial product, it was also in the chemical composition. For coke E, MnS was detected at the interface and presence of MnS is known to lower the liquidus temperature of the interfacial product. This maybe an important aspect to consider since interfacial products that contain less MnS (coke C) may have a higher liquidus temperature, which in turn can affect the overall viscosity of the interfacial layer.
17. Solid microstructure and macrostructure, ash content of cokes had effects on wettability and thus on dissolution rates. Since wettability between metal and carbonaceous materials would affect the contact area between them, it confirms that the interfacial reactions are also important.

6.2 Future work

Based on the results of this research work, some recommendations are pointed out for the future work:

1. In current study, the carbon dissolution from stationary carbon rod was investigated. However, investigating the dynamic carbon dissolution measurements with rotating carbon with different rotation speed in order to better understand the effect of mass transport is of importance.
2. In the present study, charcoal showed a very different and unique behavior. Thus, investigating the nature of charcoal using different characterization techniques seem to be necessary. Using different types of charcoal with different porosities and different surface roughness in dissolution experiments is recommended. Making briquettes out of charcoal with higher density by crushing and pressing could be

very helpful to see if it is the charcoal microstructure or macrostructure that is giving the low dissolution rate.

3. In this study, the dissolution kinetics of carbon materials in metal was studied in just two different temperatures. Thus, the activation energy results cannot be accurate. Doing the same experiments in other temperatures are necessary to lower the uncertainty of the model as well as the activation energy.
4. It is recommended to find the reduction rate of slags with dissolved carbon in metal as well as with solid carbon to see the difference as it was the first motivation of this study. This is of a great importance from the industrial point of view. Because, it will be a starting point for developing the present processes or stablishing new processes for manganese ferroalloys production which are more independent of solid carbon materials.
5. As it was observed in this study, with adding a defined amount of sulfur which was higher that saturation in metal, the dissolution rate did not change significantly. Adding different amount of sulfur below saturation level to metal is necessary to see how it affects the dissolution rate.

References

[1] J. Safarian, "Kinetics and mechanisms of reduction of MnO-containing silicate slags by selected forms of carbonaceous materials," PhD, Department of materials science and engineering, Norwegian university of science and technology, Norway, 2007.

[2] X. Xing, "Effect of heat treatment on properties of carbonaceous materials," PhD, Department of materials science and engineering, The university of new south wales, Sydney, Australia, 2012.

[3] L. Kolbinsen and A. Holmelid, "Production of syngas by metallurgic conversion," in Eurogas 90, Norway, Trondheim, 1990, pp. 81-98.

[4] Skjervheim.T.A and Olsen.E.S, "Kinetics and mechanisms related to the manganese process," in Electric Furnace Conference Proceedings, 1993, pp. 137-144.

[5] Y. Lee and L. Kolbinsen, "Kinetics of oxygen refining process for ferromanganese alloys," ISIJ International, vol. 45, no. 9, pp. 1282-1290, 2005.

[6] E. Olsen, M. Tangstad, and T. Lindstad, Production of manganese ferroalloys. Trondheim,Norway: Tapir academic press, 2007.

[7] V. Sahajwalla, M. Dubikova, and R. Khanna, "Reductant characterisation and selection: Implications for ferroalloys processing," presented at the INFACON 10, South africa, Cape town, 1-4 February, 2004.

[8] F. Vasko, D. Newhart, and A. Strauss, "Coal blending models for optimum cokemaking and blast furnace operation," Journal of the Operational Research Society, vol. 56, no. 3, pp. 235-243, 2005.

[9] L. Lu, V. Sahajwalla, C. Kong, and D. Harris, "Quantitative X-ray diffraction analysis and its application to various coals," carbon, vol. 39, pp. 1821-1833, 2001.

[10] X. Xing, G. Zhang, H. Rogers, P. Zulli, and O. Ostrovski, "Effects of annealing on microstructure and microstrength of metallurgical coke," Metallurgical and Materials Transactions B, vol. 45, no. 1, pp. 106-112, 2014.

[11] M. Kawakami et al., "Characterization of thermal annealing effects on the evolution of coke carbon structure using raman spectroscopy and x-ray diffraction," ISIJ International, vol. 46, no. 8, pp. 1165-1170, 2006.

[12] M. Kawakami, T. Karato, T. Takenaka, and S. Ykoyama, "Structure analysis of coke, wood charcoal and bamboo charcoal by raman spectroscopy and their reaction rate with CO2," ISIJ International, vol. 45, no. 7, 2005.

[13] A. Guedes, B. Valentim, A. C. Prieto, S. Rodrigues, and F. Noronha, "Micro-Raman spectroscopy of collotelinite, fusinite and macrinite," International Journal of Coal Geology, vol. 83, no. 4, pp. 415-422, 2010.

[14] M. Legin-Kolar, D. Radenovic, and U. D., "Changes in structural parameters of different cokes during heat treatment to 2400," Fuel, vol. 78, pp. 1599-1605, 1999.

[15] H. Pierson, Handbook of carbon, graphite,diamond and fullerenes: properties, processing and applications. USA: Noyes, 1993.

[16] S. Cham, "Investigating factors that Influence carbon dissolution from coke into molten Iron," PhD., School of Materials Science and Engineering, The university of new south wales, Austrlia, 2007.

[17] T. Gruber, T. Waldek zerda, and M. Gerspacher, "Raman studies of heat-treated carbon blacks," carbon, vol. 32, no. 7, pp. 1377-1382, 1994.
[18] M. Grant, A. Chaklader, and J. Price, "Factors affecting the strength of blast furnace coke " Fuel, vol. 70, no. 2, pp. 181-188, 1991.
[19] V. Gomez, J. Villegas, D. Valle, and C. Calahorro, "Heat treatment of rockrose char in air, effect of surface chemistry and porous texture.," Carbon, vol. 34, no. 4, pp. 533-538, 1996.
[20] S. Tsai, Fundamentals of coal benenefication and utilization. The Netherlands: Elsevier Science Publishing Company, 1982.
[21] X. Xing, G. Zhang, M. Amico, G. Ciezki, Q. Meng, and O. Ostrovski, "Effect of annealing on properties of carbonaceous materials. Part II: Porosity and pore geometry," Metallurgical and materials transactions B, vol. 44B, pp. 862-869, 2013.
[22] A. Ciftja, "Solar silicon refining; Inclusions, settling, filtration, wetting " PhD, Norwegian university of science and technology, 2009.
[23] J. Tomeczek and S. Gill, "Volatiles release and porosity evolution during high pressure coal pyrolysis," Fuel, vol. 82, pp. 285-292, 2003.
[24] D. Ramos, "Quality of eucalyptus charcoal for use in silicon production," PhD., Federal University of Viçosa, MINAS GERAIS - BRAZIL, 2018.
[25] B. Nadir, "Mn alloys production with the use of natural gas," MSC., Norwegian university of science and technology, Trondheim, Norway, 2015.
[26] J. Chipman et al., "The solubility of carbon in molten iron and in iron-silicon and iron-manganese alloys," Transactions of the American society for metals, vol. 44, pp. 1215-1232, 1952.
[27] E. Turkdogan, R. Hancock, S. Herlitz, and J. Dentan, "Thermodynamics of carbon dissolved in Iron alooys," Journal of the Iron and steel institute, vol. 183, pp. 69-72, 1955.
[28] J. Sandvik and j. K. Tuset, "The solubility of carbon in Ferrosilicomanganese at 1330-1360C," SINTEF, Trondheim, Norway, 1970.
[29] M. Tangstad, "The high carbon ferromanganese process coke bed relations," PhD, Department of Metallurgy The Norwegian Institute of Technology, 1996.
[30] R. Ni, Z. Ma, and S. Wei, "Thermodynamics of Mn–Fe–C and Mn–Si–C system," Steel research, vol. 61, no. 3, pp. 113-116, 1990.
[31] E. Turkdogan, R. Hancock, and S. Herlitz, "The solubility of graphite in manganese, cobalt and nickel," Journal of the Iron and steel institute, vol. 182, pp. 274-277, 1956.
[32] R. Olsson, V. koump, and T. Perzak, "Rate of dissolution of carbon in molten Fe-C alloys," Transactions of the metallurgical society of alme, vol. 236, pp. 426-429, 1966.
[33] M. Kosaka and S. Minowa, "Dissolution of steel cylinder into liquid Fe-C alloy," Iron and steel, vol. 53, no. 8, pp. 983-997, 1967.
[34] J. Wright and I. Taylor, "Multiparticle dissolution kinetics of carbon in iron-carbon-sulphur melts," ISIJ International, vol. 33, no. 5, pp. 529-538, 1993.
[35] C. Wu and V. Sahajwalla, "Dissolution rates of coals and graphite in Fe-C-S in direct ironmaking: Influence of melt carbon and sulfur on carbon dissolution," Metallurgical and materials transactions B, vol. 31B, pp. 243-251, 2000.

[36] R. Khanna, F. McCarthy, H. Sun, N. Simento, and V. Sahajwalla, "Dissolution of carbon from coal-chars into liquid iron at 1550 °C," Metallurgical and materials transactions B, vol. 36B, pp. 719-729, 2005.
[37] V. Dahlke and O. Knacke, "Die auflosung von kohlenstoff in flussigem eisen," vol. 26, ed: Steel research international, 1955, pp. 365-425.
[38] Y. Shigeno, M. Tokuda, and M. Ohtani, "The dissolution rate of graphite into Fe-C melt containing sulphur or phosphorus," Transactions of the Japan Institute of Metals, vol. 26, pp. 33-43, 1985.
[39] M. Mourao, G. Krishna Murthy, and J. Elliott, "Experimental investigation of dissolution rates of carbonaceous materials in liquid iron-carbon melts," Metallurgical and materials transactions B, vol. 24B, pp. 629-637, 1993.
[40] S. Cham, R. Sakurovs, H. Sun, and V. Sahajwalla, "Influence of temperature on carbon dissolution of cokes in molten iron," ISIJ International, vol. 46, pp. 652-659, 2006.
[41] D. Bandyopadhyay, S. Singh, D. Sanyal, K. Singh, and K. Singh, "A study on dissolution kinetics of carbon in liquid iron bath," Chemical Engineering Journal, vol. 94, no. 2, pp. 79-92, 2003.
[42] H. Sun, "Factores influencing dissolution of carbonaceous materials in liquid iron," Metallurgical and Materials Transactions B, vol. 36, pp. 893-894, 2005.
[43] Z. Zhang, J. Zhang, K. Jiao, H. Song, and Z. Liu, "Influence of sulfur on dissolution of graphite in molten iron," in The minerals, metals and materials society, USA, 2015.
[44] D. Jang, Y. Kim, M. Shin, and J. Lee, "Kinetics of Carbon Dissolution of Coke in Molten Iron," Metallurgical and Materials Transactions B, vol. 43, no. 6, pp. 1308-1314, 2012.
[45] M. Chapman, "Insoluble oxide product formation and its effect on coke dissolution in liquid iron," PhD., University of Wollongong, Austrlia, 2009.
[46] H. Sun, "Analysis of reaction rate between solid carbon and molten iron by mathematical models," ISIJ International, vol. 45, no. 10, pp. 1482-1488, 2005.
[47] J. Wright and B. Baldock, "Dissolution kinetics of particulate graphite injected into iron/carbon melts," Metallurgical and Materials Transactions B, vol. 19B, pp. 375-382, 1988.
[48] V. Grigoryan and V. Karshin, "Influence of surfactants on the dissolution kinetics of Graphite in liquid iron," Russian metallurgy, pp. 1313-1328, 1972.
[49] C. Wu and V. Sahajwalla, "Dissolution rates of coals and graphite in Fe-C-S melts in direct ironmaking: dependence of carbon dissolution rate on carbon structure," Metallurgical and Materials Transactions B, vol. 31B, pp. 215-216, 2000.
[50] V. Sahajwalla and R. Khanna, "A Monte Carlo simulation study of dissolution of graphite in iron-carbon melts," Metallurgical and materials transations B, vol. 31B, pp. 1517-1525, 2000.
[51] H. Sun, K. Mori, V. Sahajwalla, and R. D. Pehlke, "Carbon solution in liquid iron and iron alloys," High temperature materials and processes, vol. 17, no. 4, 1998.
[52] H. Gudenau, J. Mulanza, and D. Sharma, "Carburization of hot metal by industrial and special cokes," Steel research, vol. 61, no. 3, pp. 97-104, 1990.
[53] S. Ericsson and P. Mellberg, "Influence of sulphur on the rate of carbon dissolution in liquid iron," Scandinavian journal of metallurgy, vol. 10, no. 1, pp. 15-18, 1981.

[54] N. Jones, "Kinetics of carbon dissolution in Fe-C alloy at 1550C," Ironmaking and Steelmaking, vol. 25, no. 6, pp. 460-465, 1998.
[55] C. Wu, "Fundamental investigation of molten iron/carbon interactions in direct ironmaking," PhD, School of materials science and engineering, University of new south wales, Australia, 1998.
[56] R. Olivares, "The effect of sulfur on the dissolution of graphite and carbons in liquid iron-carbon alloys," PhD, Material science and engineering, University of New castle, New castle, Australia, 1996.
[57] J. Wright and W. Denholm, "Dissolution of particulate carbon in a turbulent iron bath," presented at the The AusIMM Melbourne Branch Symposium, Melbourne, 1984.
[58] S. Orsten and F. Oeters, "Dissolution of carbon in liquid iron," in 5th International Iron and Steel Congress, Philadelphia, PA, 1986: Proceedings of the 6th Process Technology Conference, pp. 143-155.
[59] V. Sahajwalla, I. Taylor, and J. Wright, "Rates of carbon transfer from sources injected into Fe-C-S melts," in Ironmaking Conference Proceedings, United states, 1993, pp. 355-365.
[60] S. Cham, V. Sahajwalla, R. Sakurovs, H. Sun, and M. Dubikova, "Factors influencing carbon dissolution from cokes into liquid Iron," ISIJ International, vol. 44, no. 11, pp. 1835-1841, 2004.
[61] S. Cham, V. Sahajwalla, and R. Sakurovs, "The dissolution of cokes in molten iron," presented at the 21st annual international Pittsburgh coal conference, Osaka,Japan, 2004.
[62] K. Ohno, T. Maeda, K. Nishioka, and M. Shimizu, "Effect of carbon structure crystallinity on initial stage of iron carburization," ISIJ International, vol. 50, no. 1, pp. 53-58, 2010.
[63] K. Ohno et al., "Effects of charcoal carbon crystallinity and ash content on carbon dissolution in molten iron and carburization reaction in iron-charcoal composite," ISIJ International, vol. 52, no. 8, pp. 1482-1488, 2012.
[64] P. Pistorius, "Reductant selection in ferro-alloy production: The case for the importance of dissolution in the metal," The Journal of The South African Institute of Mining and Metallurgy, pp. 33-36, 2002.
[65] N. Kayama and O. Ishikawa, Imonology, vol. 37, no. 4, 1965.
[66] M. Rahman, "Fundamental investigation of slag/carbon interactions in Electric Arc Furnace steelmaking process," PhD, School of materials science and engineering, The university of New South Wales, Sydney, Australia, 2010.
[67] M. Chapman, B. Monaghan, S. Nightingale, J. Mathieson, and R. Nightingale, "Formation of a mineral layer during coke dissolution into liquid iron and its influence on the kinetics of coke dissolution rate," Metallurgical and Materials Transactions B, vol. 39, no. 3, pp. 418-430, 2008.
[68] H. Gudenau, D. Senk, A. Babich, and C. Froehling, "Coke behaviour in the lower part of BF with high injection rate " presented at the International BF lower zone symposium, Wollongong, 2002.
[69] C. Wu, R. Wiblen, and V. Sahajwalla, "Influence of ash on mass transfer and interfacial reaction between natural graphite and liquid Iron," Metallurgical and Materials Transactions B, vol. 31B, pp. 1099-1104, 2000.

[70] F. McCarthy, V. Sahajwalla, J. hart, and N. Saha-chauhury, "Influence of ash on interfacial reactions between coke and liquid iron," Metallurgical and Materials Transactions B, vol. 34B, pp. 573-580, 2003.
[71] S. Cham, R. Khanna, V. Sahajwalla, R. Sakurovs, and D. French, "Influence of mineral matter on carbon dissolution from metallurgical coke into molten iron: Interfacial phenomena," ISIJ International, vol. 49, no. 12, pp. 1860-1867, 2009.
[72] J. Li, "Wetting of ceramic materials by liquid silicon, aluminium and metallic melts containing titanium and other reactive elements: A review " Ceramics International, vol. 20, pp. 391-412, 1994.
[73] M. Dekker, Wettability (Surfactant science series). New york: TD Blake, 1993.
[74] B. Keene, Slag atlas. Germany: Verlag Stahleisen GmbH, 1995.
[75] I. Aksay, C. Hoge, and J. Pask, "Wetting under chemical equilibrium and nonequilibrium conditions," The journal of physical chemistry, vol. 78, no. 12, 1974.
[76] B. Keene, "Review of data for the surface tension of iron and Its binary alloys," International Materials Reviews, vol. 33, no. 1, 1988.
[77] Y. Chung and A. Cramb, "Dynamic and equilibrium interfacial phenomena in liquid steel–slag systems," Metallurgical and materials transactions B, vol. 31B, pp. 957-971, 2000.
[78] K. Nakashima and K. Mori, "Interfacial properties of liquid iron alloys and liquid slags relating to iron-and steel-making processes," ISIJ International, vol. 32, no. 1, pp. 11-18, 1992.
[79] N. Takiuchi, N. Shinozaki, T. Taniguchi , K. Mukai , and Y. Tanaka "Effects of oxygen and temperature on the surface tension of liquid iron and Its wettability of alumina," Journal of the Japan Institute of Metals, vol. 55, no. 2, pp. 180-185, 1991.
[80] I. Jimbo, A. Sharan, and A. Cramb, "Recent measurement of surface and interfacial tension in steel related systems," presented at the 76th steelmaking conference, Dellas,Texas, 1993.
[81] J. Lee, L. Hoai, and M. Shin, "Density and surface tension of liquid Fe-Mn alloys," Metallurgical and materials transactions B, vol. 42B, pp. 546-549, 2011.
[82] T. Lida and R. Guthrie, The physical properties of liquid metals. New York: Oxford University Press Inc, 1993.
[83] R. Wenzel, "Resistance of solid surfaces to wetting by water," Industrial and engineering chemistry, vol. 28, no. 8, 1936.
[84] A. Calvimontes, Thermodynamic equilibrium in the wetting of rough surfaces. Germany: Lulu Press, Inc., 2014.
[85] A. Cassie and S. Baxter, "Wettability of porous surfaces," Transactions of the faraday society, vol. 40, pp. 546-551, 1944.
[86] R. Khanna, I. Mansuri, and V. Sahajwalla, Wettability of carbonaceous materials with molten iron at 1550°C. 2015.
[87] K. Ohno, T. Miyake, S. Yano, C. Nguyen, T. Maeda, and K. Kunitomo, "Effect of carbon dissolution reaction on wetting behavior between liquid iron and carbonaceous material," ISIJ International, vol. 55, no. 6, pp. 1252-1258, 2015.
[88] L. Zhao and V. Sahajwalla, "Interfacial phenomena during wetting of graphite/alumina mixtures by liquid iron," ISIJ International, vol. 43, no. 1, pp. 1-6, 2003.

[89] B. Monaghan, M. W. Chapman, and S. Nightingale, "The wetting of liquid iron carbon on aluminate minerals formed during coke dissolution in iron," presented at the 5th International Congress on the Science and Technology of Ironmaking, Shanghai, China, 19-23 October, 2009.
[90] C. Wu and V. Sahajwalla, "Influence of melt carbon and sulfur on the wetting of solid graphite by Fe-C-S melts," Metallurgical and Materials Transactions B, vol. 29B, pp. 471-477, April 1998 1998.
[91] R. Wiblen and V. Sahajwalla, "Influence of properties of carbonaceous materials on carbon dissolution into iron," in 84 th Steelmaking Conference, Warrendale, PA, 2001.
[92] A. Mehta and V. Sahajwalla, "Coal-char/slag interactions during pulverised coal injection in a blast furnace: Reaction kinetics and wetting investigations," ISIJ International, vol. 43, no. 10, pp. 1512-1518, 2003.
[93] J. Mcneil and F. Cecil, "X-ray fluorescence measurements of manganese in petroglyphs and graffiti in the Bluff, Utah Area," C. s. o. Mines, Ed., ed.
[94] M. Peters, H. Gudenau, M. Scheiwe, and R. Sieger, "17 Stresses exerted on coke in the lower region of a blast furnace," presented at the Second European Ironmaking Congress, Glasgow, 1991.
[95] R. Khanna, V. Sahajwalla, N. Simento, and S. Seetharaman, "Atomistic Monte Carlo simulations on the influence of sulphur during high-temperature decarburization of molten iron–carbon alloys," Acta material, vol. 58, no. 6, pp. 2225-2236, 2010.
[96] F. Heisterkamp and K. Lohberg, "Diffusion des Kohlenstoffs in flüssigen Eisen-Kohlenstoff-Silizium- und Eisen-Kohlenstoff-Schwefel-Legierungen," Arch.Eisenhuttenwes, vol. 37, 1999.
[97] C. Gomez, D. Strickler, and L. Austin, "An iodized mounting medium for coal particles," Journal of electron microscopy technique vol. 1, pp. 285-287, 1984.

Appendix A: Sample preparation for SEM analysis

Mounting and cutting the sample

1. Samples from wetting experiments and dissolution experiment were set in a silicone rubber mould.
2. Epoxy resin was prepared by mixing EpoFix resin with EpoFix hardener in a 25 to 3 ratio.
3. The sample was the labelled and placed under pressure again.
4. Some of the samples were cut using Struers Accutom-5 after mounting to have both cross section and surface view and the they were mounted again.

Grinding and Polishing

The samples were automatic ground using Struers RotoForce-4 grinder/polisher with silicon carbide paper (grades ranging from P500 to P1200) at 150 rpm

After grinding, the samples were polished at 3 stages:

1. Using a Struers Tegramin-30 and 9µ DiaPro on a rotating wheel at approximately 150rpm for 90 seconds.
2. Then using a 3µ DP-Mol3 on a rotating wheel at approximately 150rpm for 90 seconds
3. Finally, 1µ DP-NapB1 on a rotating wheel at approximately 150rpm for 90 seconds

N.B. Samples were ultrasonically cleaned and spray rinsed by Struers Lavamin after grinding and between each subsequent polishing stage.

Epoxy preparation for some of the carbon samples

Finally, some samples were mounted in a iodoform-containing epoxy that grants higher contrast for carbon-containing materials. The recipe was revised after Gomez [97]. For the creation of this resin, 10% wt. iodoform is dissolved at room temperature into a resin, after stirring thoroughly. Then, the solution is cooled down to 10°C, and the hardener is added in the proportions specified by the resin producer. The application of a 10 nm thick carbon coating grants the conductivity of the epoxy, which is necessary for SEM analysis.

Appendix B: Surface area changes

In this study, the reduction of carbon surface area during dissolution was considered. **Figure B-1** shows the surface area reduction versus time for different carbon materials dissolved in Fe-85wt%Mn at 1550°C. As it can be seen from these figures, the changes of different carbon materials surface area with time showed that the goodness of the fit of the data was best described by an exponential decrease in surface area with time.

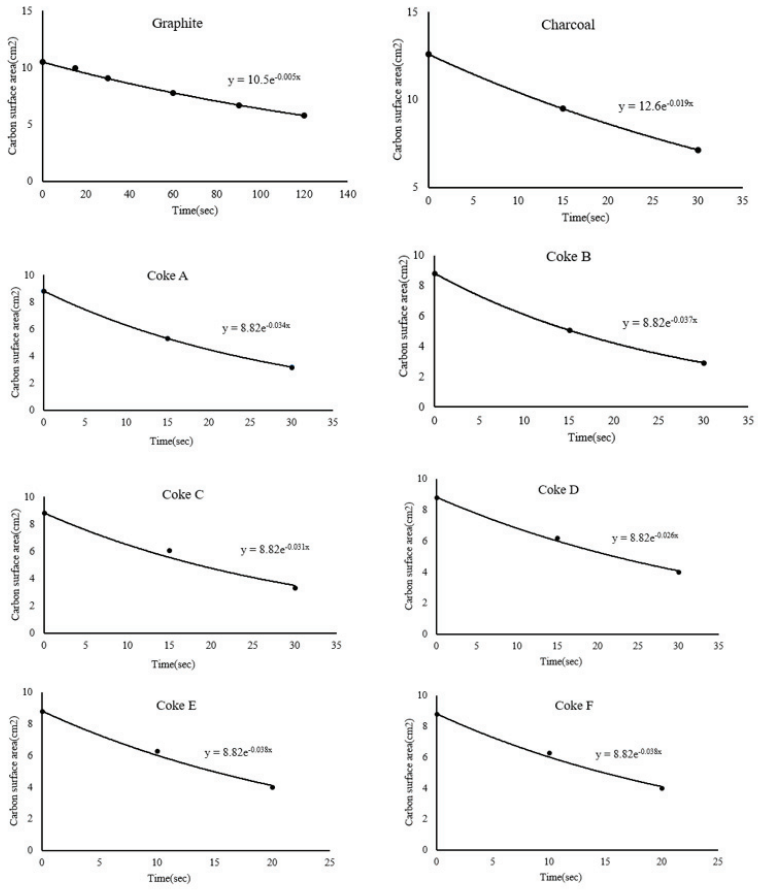

Figure B-1: Carbon surface area changes during dissolution in Fe-85wt%Mn at 1550°C.

Figure B-2 shows the reduction in surface area of different carbon materials in Fe-85wt%Mn at 1450°C. **Figure B-3** shows the reduction of graphite surface area during dissolution in Fe-60wt%Mn at 1450°C.

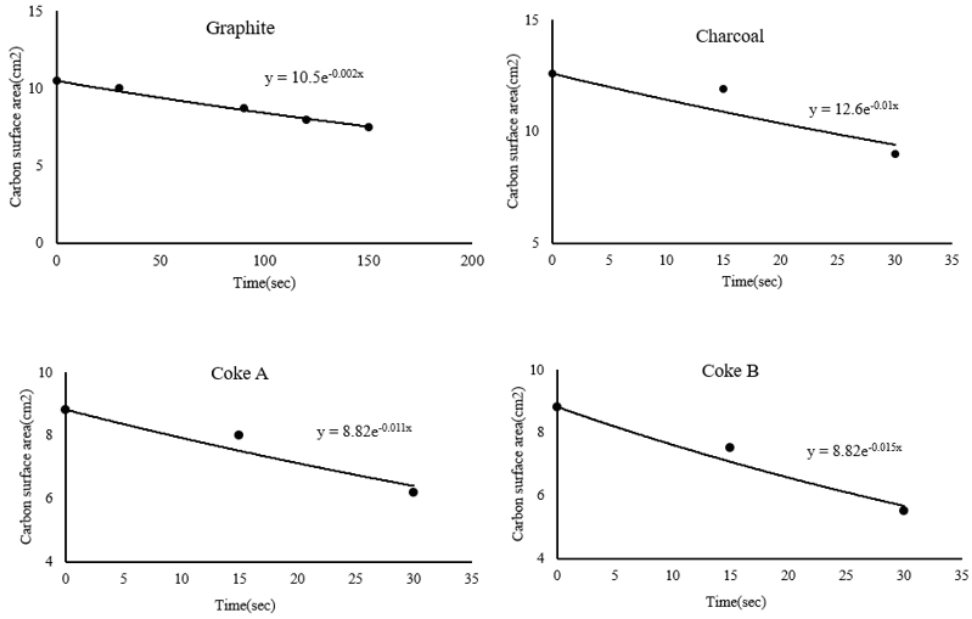

Figure B-2: Carbon surface area changes during dissolution in Fe-85wt%Mn at 1450°C.

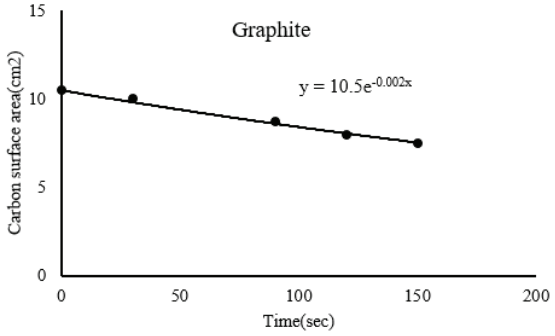

Figure B-3: Carbon surface area changes during dissolution in Fe-60wt%Mn at 1450°C.

The surface area reduction of graphite in different metal compositions are shown in **Figure B-4.**

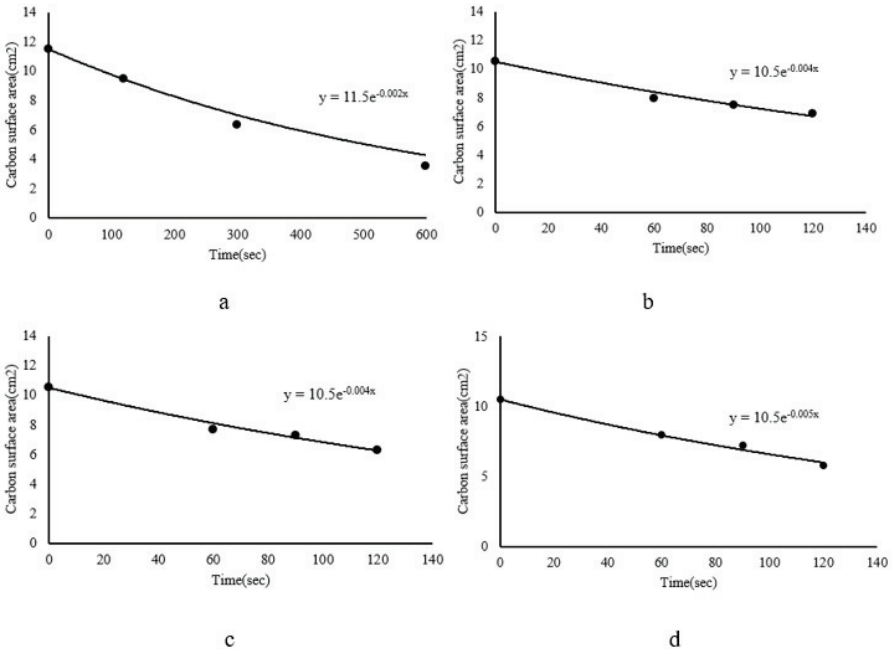

Figure B-4: Graphite surface area reduction during dissolution in a)Fe, b)Fe-10wt%Mn c)Fe-40wt%Mn and d)Fe-60wt%Mn at 1550°C.

Figure B-5 shows surface area reduction of small graphite during dissolution in two different compositions at two different temperatures. It can be indicated that the reduction in surface area is higher at higher temperature.

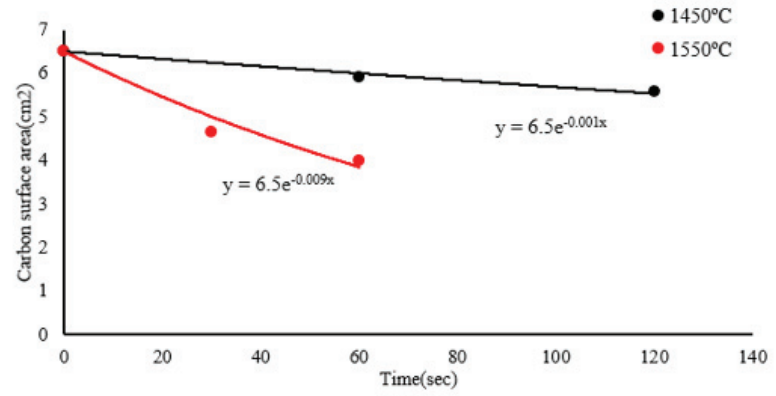

a

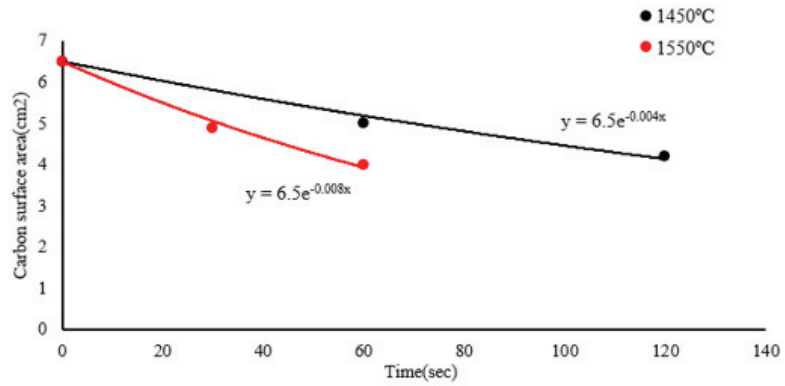

b

Figure B-5: Small graphite surface area reduction during dissolution in a) Fe-60wt%Mn and b) Fe-85wt%Mn at 1450 and 1550°C.

Appendix C: Surface roughness pictures

Figures C-1 to **Figure C-4** show the surface image, three-dimensional and two-dimensional topographic map and also one-dimensional topographic profile along one or two axis for different carbon materials which were done at UNSW. **Figures C-5** and **Figure C-6** show three-dimensional topographic map of 4 carbonaceous materials which were done at NTNU.

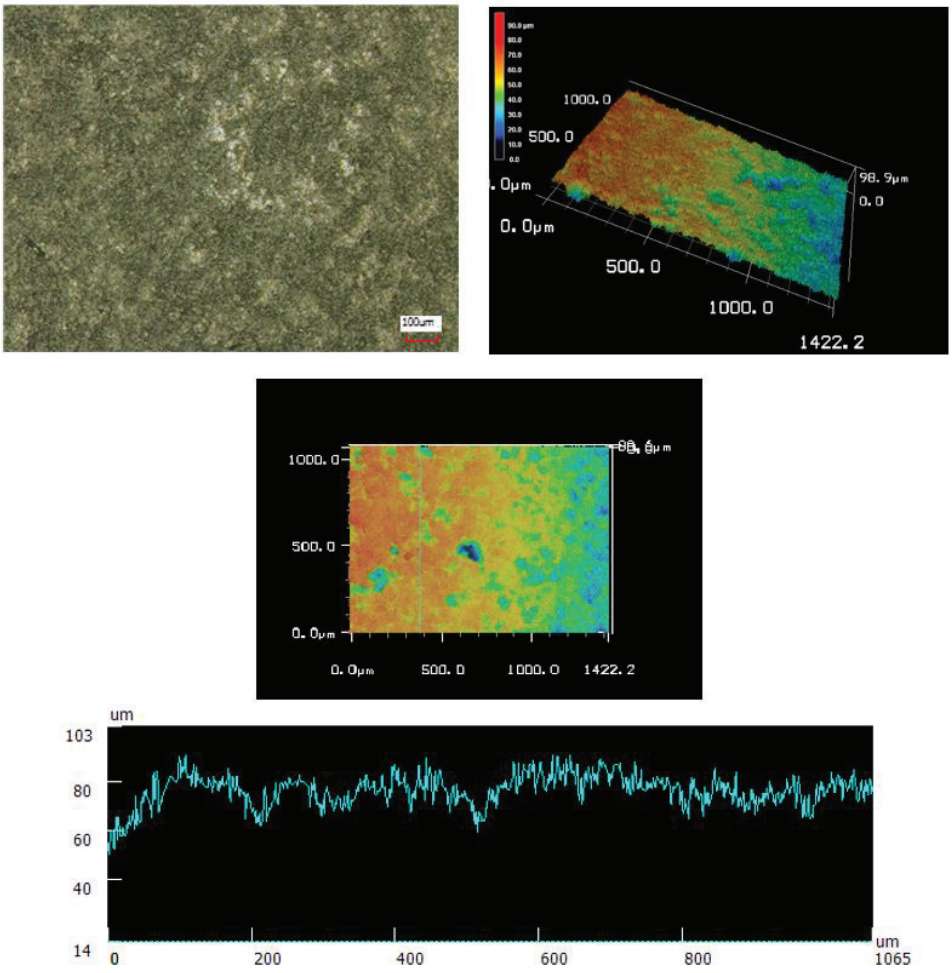

Figure C-1: Three-dimensional topographic map of graphite and its profile along Y axis (was done at UNSW).

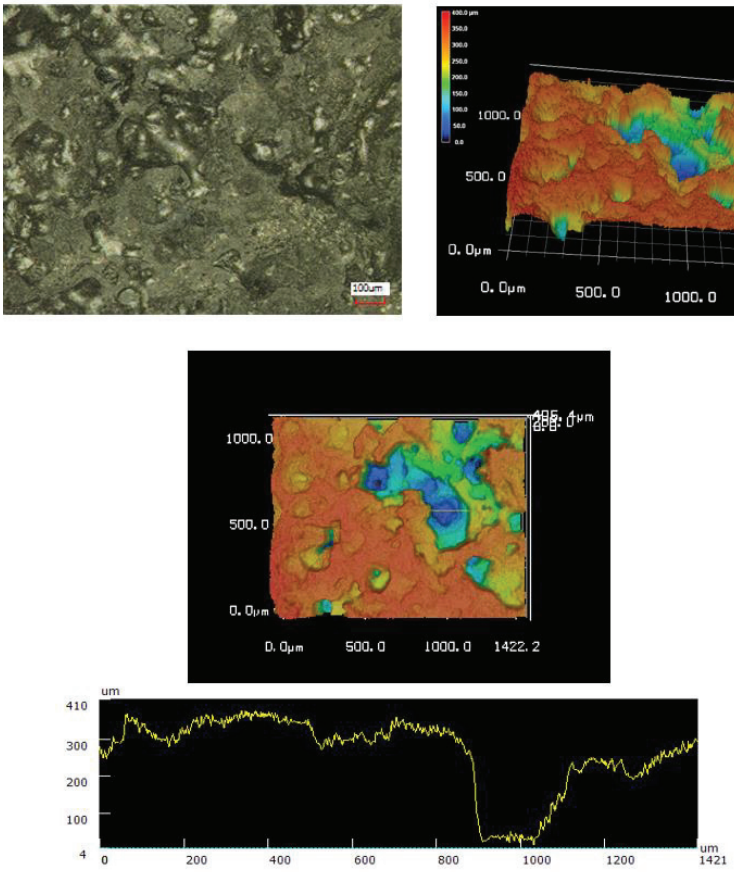

Figure C-2: Three-dimensional topographic map of coke B and its profile along X axis (Was done at UNSW).

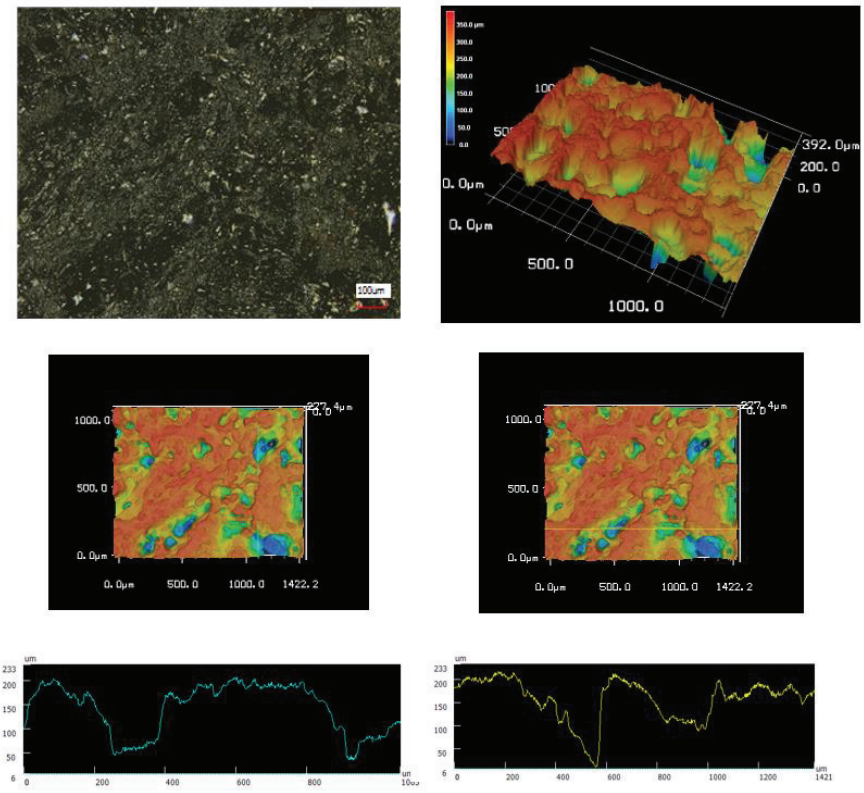

Figure C-3: Three-dimensional topographic map of coke E and its profile along X axis (yellow line) and Y axis (blue line).(was done at UNSW).

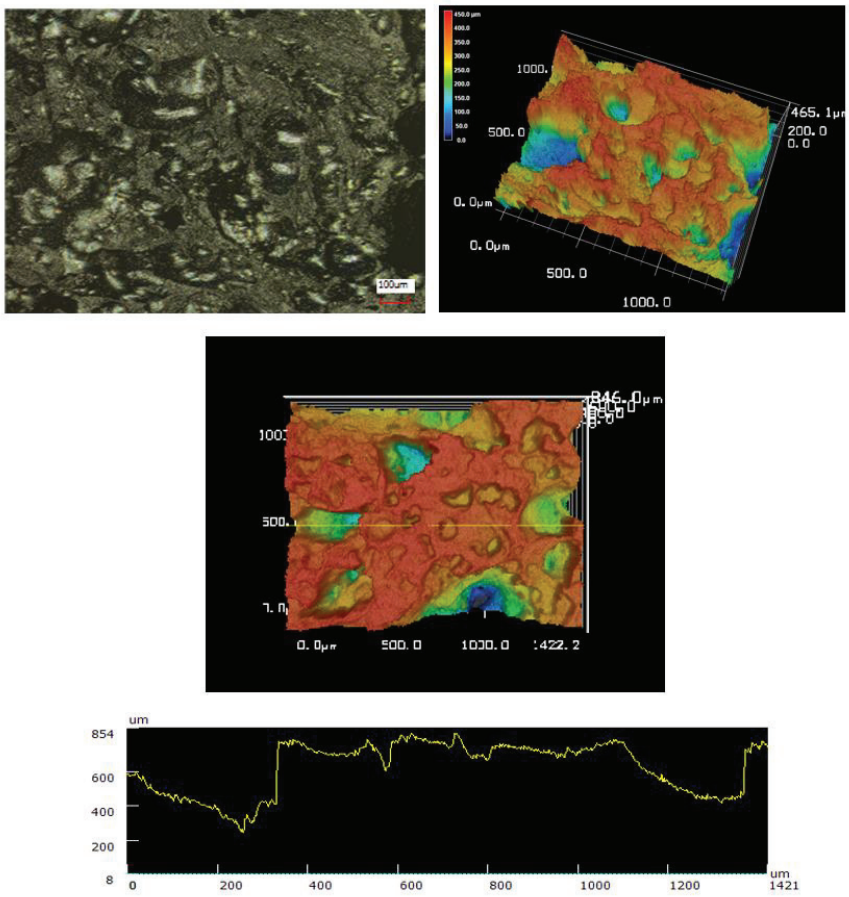

Figure C-4: Three-dimensional topographic map of coke D and its profile along X axis(was done at UNSW).

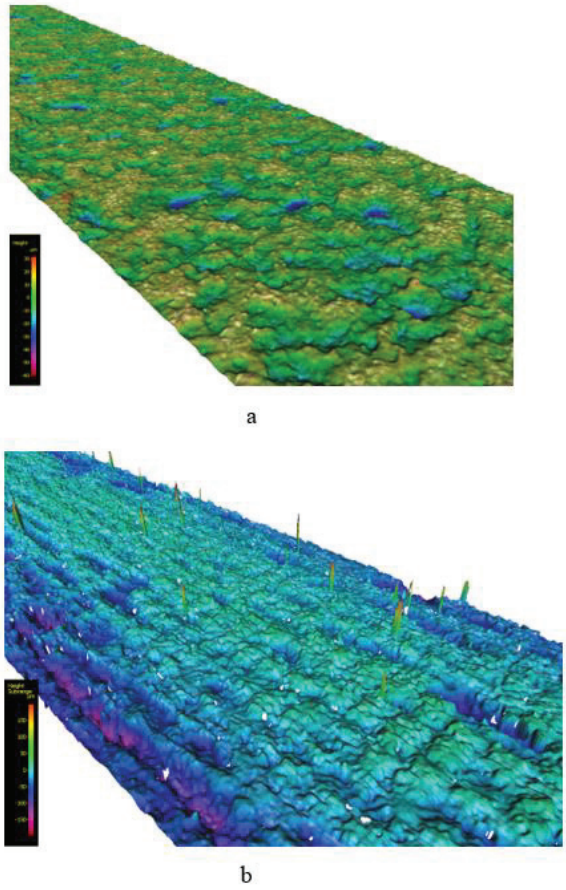

Figure C-5: Three-dimensional topographic map of a) graphite b) charcoal (was done at NTNU).

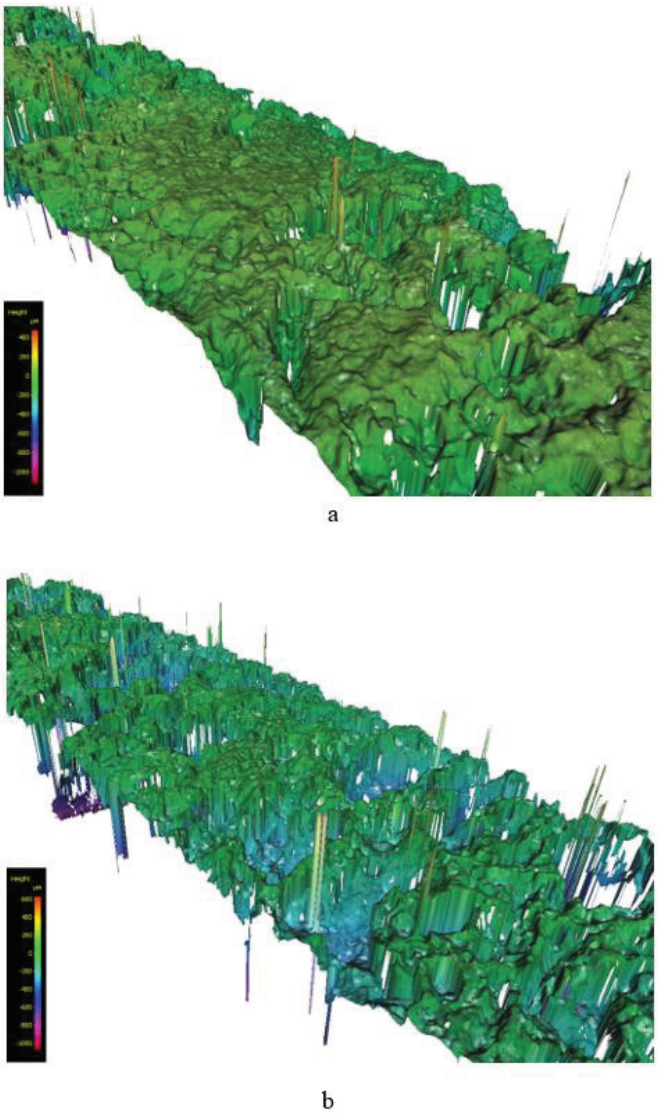

Figure C-6: Three-dimensional topographic map of a) coke A b) coke B (was done at NTNU).